

**Development of a Novel Non-invasive Digital Clinical  
Assessment Tool and its 3D Measurable Parameters  
for the Orthotic Treatment of Adolescent Idiopathic  
Scoliosis**

A thesis submitted to  
The Department of Biomedical Engineering  
University of Strathclyde  
for the degree of  
Doctor of Philosophy

by

**Sun Hae Jang**  
**BSc, MSc, CO, FAAOP**

March 2019

“We delight in the beauty of the butterfly, but rarely admit the changes it has gone through to achieve that beauty.”  
- Maya Angelou

## Declaration of Author's Rights

This thesis is the result of the author's original research. It has been composed by the author and has not been previously submitted for examination which has led to the award of a degree.

The copyright of this thesis belongs to the author under the terms of the United Kingdom Copyright Acts as qualified by University of Strathclyde Regulation 3.50. Due acknowledgement must always be made of the use of any material contained in, or derived from, this thesis.

Signed:  Sun Hae Jang

Date: 4th March 2019

## **Declaration of Source of Funds**

- Provost's New Faculty Award (2014 – 2015), Eastern Michigan University (MI, USA) for the project "Radiographic Spinal Alignment Parameters System and Radiographic Spinal Misalignment Analyses for Adolescent Idiopathic Scoliosis"
- Faculty Research Fellowship Award (2015 – 2016), Eastern Michigan University (MI, USA) for the projects "Concurrent Validity of 3D Skin Level Spinal Alignment Parameters for Adolescent Idiopathic Scoliosis" and "Normal Values and Reference Ranges of 3D Spinal Alignment Parameter System for Adolescent Idiopathic Scoliosis"
- CHHS-Sponsored Research Award (2015 – 2016), Eastern Michigan University (MI, USA) for the projects "Concurrent Validity of 3D Skin Level Spinal Alignment Parameters for Adolescent Idiopathic Scoliosis" and "Normal Values and Reference Ranges of 3D Spinal Alignment Parameter System for Adolescent Idiopathic Scoliosis"
- CHHS-Sponsored Research Award (2017 – 2018), Eastern Michigan University (MI, USA) for the project "Pilot Study: Optimal Corrective Force Placements of Spinal Orthoses in Treating AIS"

## Acknowledgements

I would like to thank my family and especially my husband, Jong Han and my daughter, Nicole, who have been always loving me and constantly supportive of all I have pursued.

I would also like to thank Prof. Philip Rowe for accepting me as a long-distance part-time student to the PhD program at Strathclyde. Since then he has been thoroughly supportive and very understanding of my full-time working and part-time schooling between the USA and UK. He has been exceptional in his efforts to accommodate my schedule and provide as many meetings as possible when I visited Strathclyde for my studies. He provided helpful guidance throughout my research period. During the last year he set up Skype meetings every two weeks to provide detailed comments and feedback on each of the research studies performed.

I owe gratitude to Dr. Steven Koop and Gillette Children's Specialty Healthcare (Minnesota, USA) where I have been working for 15 years. It has been a great place to work and gain the clinical experiences for orthotic treatment of adolescent idiopathic scoliosis and also gave me an opportunity to conduct the radiographic analysis study. I wish to thank Dr. Eun-Seok Son and Keimyung University Dongsan Medical Center (Daegu, South Korea) where the concurrent validly test was performed for the newly developed measurable parameters. I also want to thank Ms. Janet Olafson, who is a friend and former colleague. Her knowledge and understanding in treating adolescent idiopathic scoliosis as a certified orthotist, contributed to her reviewing of the contents of this thesis. I would also like to thank my colleagues, school director, and college dean and associate dean of Eastern Michigan University (Michigan, USA) where I am currently teaching as a full-time faculty. They have always been supportive of my part time PhD study and the university provided some internal research funding necessary for the research studies. Without any help from all of them, this thesis would not have been able to have been completed.

Finally, I dedicate this thesis to my lovely and unforgettable son, Alex, who led me to my career as an orthotist and piqued my initial interest in the subject of rehabilitation but moved to Heaven just before starting my PhD study.

## **Abstract**

Adolescent Idiopathic Scoliosis (AIS) is the most common of the types of idiopathic scoliosis (IS), which has three-dimensional (3D) deformities which occur in the vertebrae, spine and rib cage during the adolescent period. The aetiology is still unknown but it is hypothesized to be multi-factorial. Orthotic treatment is the most commonly used conservative treatment for AIS to prevent curve progression and surgical intervention. Among the three pathological features of AIS, the coronal misalignment pattern is the most studied area because the two-dimensional (2D) coronal PA radiographic image is the most utilized as the primary clinical assessment tool and employed for both diagnosis and outcome measurement of AIS deformities in scoliosis clinics. The sagittal misalignment patterns have been the most unknown area of study. Lack of available comprehensive knowledge about the deformities of AIS in 3D space may leave clinicians to make assumptions in treating AIS. This may influence the success rates of orthotic treatment which have been inconsistent and found to vary considerably. The literature review and the survey project of this thesis also showed that there are not enough universally agreed-upon principles to guide orthotists in the 3D orthotic treatment of AIS, which may also induce significant quality deviations for each scoliosis orthotic device system.

To address this clinical gap, it was necessary to develop new effective 3D surface level measurable parameters to quantify the 3D AIS deformities and spinal misalignment, and to build a new suitable 3D non-invasive digital assessment tool that can be used with the parameters to evaluate and improve 3D spinal biomechanical knowledge and correction for effective orthotic treatment.

For this thesis, two spinal alignment measurable parameter systems were developed. First, a radiographic spinal alignment parameters (RSAPs) system was developed based on the 3D osseous structural characteristics of a human's erect spine and the unique features in each spinal bony structural segment. The newly developed RSAPs were studied to determine if they are useful in quantifying coronal and sagittal AIS misalignment, especially for sagittal misalignment patterns, which had not been clearly defined prior to this study. Then the skin level spinal alignment parameters

(SSAPs) were developed based on the previously established radiographic parameters (RSAPs), and validated by defining whether SSAPs correspond to RSAPs for the same subject and identifying if the skin profile of SSAPs accurately reflects the structural characteristics of a human's erect spine. The 3D concept of skin level parameters (3DSPs) was developed by adding six key non-spinal alignment parameters to comprehensively quantify not only 3D global spinal misalignments of AIS but also detect other major skeletal scoliosis deformities from the skin surface level. In addition, the reference range of 3DSPs were defined and its discriminative validity was examined by comparing the values between the AIS group and the non-scoliosis group.

This thesis introduced the development of a non-invasive digital calculating and visualisation assessment application by utilizing motion capture technology. This application can measure the corrective forces applied by corrective pads and provide immediate visual feedback on the computer screen by displaying the spinal misalignment and deformities numerically and visually, appearing in one of two colours depending on whether each value of 3DSPs is within the non-scoliotic reference range for that parameter while applying corrective forces. The feasibility of the newly developed assessment tool and measurable parameters was evaluated by showing their capability in quantifying 3D misalignment and deformities of AIS, by identifying the unclear 3D characteristics of AIS deformity, and by finding answers for some of the long-term unsolved biomechanical questions and current existing disagreements among the professional community involved in the orthotic treatment of AIS.

In conclusion, this thesis demonstrated that these combined application tools can help clinicians and researchers to have a better understanding of the 3D misalignment and deformity patterns of idiopathic scoliosis, can contribute in establishing a unified and comprehensive 3D biomechanical corrective theory in orthotic treatment, and can lead to the improvement of orthotic clinical assessment and treatment outcomes in AIS.

## List of Publications and Podium Presentations at Peer Reviewed Journals and Conferences

- Jang, S. H., Davis, K. L., & Thach, S. D. (2019). Current Practice in Orthotic Treatment of AIS. *JPO: Journal of Prosthetics and Orthotics*, 31(1), 23.
- Jang, S. H., Koop, S., & Rowe, P. (2015). Radiographic Analysis of Sagittal Misalignment patterns in Adolescent Idiopathic Scoliosis. Oral Presentation at *10th International SOSORT Annual Meeting of International Conference on Conservative Management of Spinal Deformities*, Katowice, Poland. May 2015.
- Jang, S. H., Davis, K. L., & Thach, S. D. (2017). Current Practice in Orthotic Treatment of Adolescent Idiopathic Scoliosis. Oral Presentation at *43<sup>rd</sup> Academy Annual Meeting & Scientific Symposium of American Academy of Orthotists & Prosthetists*, Chicago, IL, USA. March 2017.
- Jang, S. H., Koop, S., & Rowe, P. (2017). Sagittal Misalignment Patterns and Pathogenesis of Adolescent Idiopathic Scoliosis (Newer Findings), Oral Presentation at *16<sup>th</sup> World Congress of International Society for Prosthetics and Orthotics*, Cape Town, South Africa. May 2017.
- Jang, S. H., Son, E., & Rowe, P. (2018). Concurrent Validity of 3D Skin Level Spinal Alignment Parameters for Adolescent Idiopathic Scoliosis (Vol. 30, Issue 2S, p. 55). Presented at the American Academy of Orthotists & Prosthetists, 44th Academic Annual Meeting & Scientific Symposium, New Orleans, LA, USA: *Journal of Prosthetics and Orthotics*.
- Jang, S. H., Rowe, P. (2019). Reference Ranges of 3D Spinal Alignment Parameter System for Adolescent Idiopathic Scoliosis. Oral Presentation at *14th International SOSORT Annual Meeting of International Conference on Conservative Management of Spinal Deformities*, San Francisco, USA. May 2019.

# Contents

Declaration of Author's Rights.....	i
Declaration of Source of Funds .....	ii
Acknowledgements.....	iii
Abstract.....	v
List of Publications and Podium Presentations at Peer Reviewed Conferences.....	vii
Contents .....	viii
List of Figures .....	xii
List of Tables .....	xv
List of Abbreviations and Symbols.....	xvii
Chapter 1. Introduction.....	1
1.1 Introduction.....	2
1.2 Pathological Features of Adolescent Idiopathic Scoliosis .....	2
1.3 Curve Progression Mechanism of AIS.....	4
1.4 Orthotic Treatment for AIS.....	5
1.5 General Outline of This Thesis .....	7
Chapter 2. Aims, Objectives, and Thesis Outlines .....	8
2.1 Introduction.....	9
2.2 Clinical Rationales of the Thesis.....	9
2.3 Thesis Outline and Scope.....	10
2.4 Aims and Objectives of the Thesis.....	12
Chapter 3. Literature Review .....	14
3.1 Introduction.....	15
3.2 Literature Review 1: Measurable Parameters That Influence Biomechanical Success in Orthotic Treatment of AIS .....	15
3.2.1 Background .....	15
3.2.2 Methods.....	16
3.2.3 Findings.....	16
3.2.4 Discussion .....	19
3.2.5 Summary .....	23
3.3 Literature Review 2: Non-Invasive Technological Tools that Can Assess the 3D Deformity of AIS.....	23
3.3.1 Methods.....	23
3.3.2 Findings.....	25
3.3.3 Discussion .....	27
3.3.4 Summary .....	30
3.4 Literature Review 3: 3D Biomechanical Correction Concept of AIS...	30
3.4.1 Methods.....	30
3.4.2 Findings and Discussion.....	31

3.5	Conclusion.....	32
Chapter 4.	Survey Project - Current Practice in Orthotic Treatment of AIS .....	33
4.1	Introduction .....	34
4.2	Processes Used to Develop the Survey Questionnaire.....	35
4.3	The Original Manuscript of the Survey Project Submitted to JPO.....	44
4.4	Discussion and Conclusion .....	67
Chapter 5.	Radiographic Spinal Alignment Parameters System and Radiographic Spinal Misalignment Analyses for Adolescent Idiopathic Scoliosis ....	71
5.1	Introduction .....	72
5.2	Design Rationale of The Spinal Alignment Parameters for AIS .....	72
5.2.1	Functions and Neural Alignment of Spine.....	72
5.2.2	Radiographic Spinal Alignment Parameters .....	75
5.3	Materials and Methods .....	77
5.3.1	Subjects .....	77
5.3.2	Outcome Measures .....	78
5.3.3	Deformity Classification .....	80
5.3.4	Data Analysis .....	80
5.4	Results .....	81
5.5	Discussion and Conclusion .....	83
5.5.1	Scopes of RSAPs in Quantifying 2D AIS Spinal Misalignment .....	83
5.5.2	Limitations of Using RSAPs for Defining 3D AIS Misalignment.....	86
Chapter 6.	Skin Level Spinal Alignment Parameters System and Concurrent Validity Test.....	88
6.1	Introduction .....	89
6.2	Materials and Methods .....	89
6.2.1	Subjects .....	89
6.2.2	Outcome Measures .....	90
6.2.3	Procedures .....	93
6.3	Data Analysis .....	93
6.4	Results .....	94
6.5	Discussion and Conclusion .....	95
Chapter 7.	Development of a Non-Invasive Digital Calculating and Visualisation Assessment Application .....	100
7.1	Introduction .....	101
7.2	Development of 3D Skin Level Parameters.....	102
7.2.1	Measurements of 3D Skin Level Parameters .....	102
7.2.2	Examples of Calculation Methods for Parameters .....	107

7.3	Development of Non-Invasive Digital Calculating and Visualisation Assessment Application .....	108
7.3.1	Overview of Application Concept.....	108
7.3.2	Application Setting for Data Collection.....	111
7.3.3	Application for the Calculation of Parameter Values .....	112
7.3.4	Application for Visualisation of Parameter Values and Colour Indicators.....	119
7.3.5	Application for Visualisation of Spinal Alignment and Colour Indicators.....	122
7.3.6	Application for Applied Force Measurements and Visualisation .....	125
7.4	Discussion and Conclusion .....	132
Chapter 8.	Normal Values and Reference Ranges of the Surface Level Spinal Alignment Parameters System .....	133
8.1	Introduction .....	134
8.2	Materials and Methods .....	134
8.2.1	Subjects .....	134
8.2.2	Outcome Measures and Procedures .....	135
8.3	Data Analysis .....	137
8.4	Results .....	138
8.5	Discussion and Conclusion .....	140
Chapter 9.	Discriminative Validity Study for the 3D Surface Level Parameters System Between Non-Scoliosis Group and Scoliosis Group.....	142
9.1	Introduction .....	143
9.2	Methods and Data Analysis .....	143
9.3	Results .....	144
9.4	Discussion and Conclusion .....	147
Chapter 10.	Evaluation of The Digital Calculating and Visualisation Assessment Application; Pilot Study Results: Optimal Corrective Force Placements of Spinal Orthoses in Treating AIS .....	149
10.1	Introduction .....	150
10.2	Methods.....	151
10.2.1	Subjects .....	151
10.2.2	Apparatus .....	152
10.2.3	Procedure.....	156
10.2.4	Primary and Secondary Outcome Measures .....	158
10.2.5	Data Analysis .....	159
10.3	Results for Demographic Characteristics.....	159
10.4	Case Study for Subject 1 .....	161
10.4.1	Methods.....	161
10.4.2	Findings .....	162
10.5	Case Study for Subject 2 .....	164

10.5.1 Methods .....	164
10.5.2 Findings .....	164
10.6 Case Study for Subject 3 .....	166
10.6.1 Methods and Findings .....	166
10.7 Case Study for Subject 4 .....	168
10.7.1 Methods .....	168
10.7.2 Findings .....	170
10.8 Case Study for Subject 5 .....	170
10.8.1 Methods and Findings .....	170
10.9 Discussion and Conclusion .....	173
Chapter 11. Summary, General Discussion, and Recommendations .....	176
11.1 Introduction .....	177
11.2 Answers to the Research Questions Posed.....	177
11.3 General Discussion: General Overview of the Important Contributions ..	184
11.3.1 Quantification of the Misalignment and Deformities of AIS and Better Knowledge of 3D Characteristics of AIS Deformity.....	184
11.3.2 Clarification of the Existing Disagreement: Biomechanical Elements in the Orthotic Treatment of AIS .....	189
11.3.3 Uses of 3D Non-Invasive Digital Assessment Tool and Measurable Parameters for Scoliosis Clinics and Future Studies .....	192
11.4 Limitations and Recommendations for Further Study .....	193
References	196
Appendices	206

## List of Figures

Figure 1.1 - Images for Various Types of Corrective Orthoses for AIS: (a) CTLSO (Milwaukee Orthosis), (b) High or Mid Profile TLSO, and (c) Low Profile TLSO.....	6
Figure 3.1 - Keywords Flow Chart 1 .....	17
Figure 3.2 - Measuring Method for Cobb Angle .....	20
Figure 3.3 - Keywords Flow Chart 2 .....	25
Figure 5.1 - Four Spinal Regions of Non-scoliotic Spine in Sagittal View with their Kyphosis or Lordosis Shapes .....	74
Figure 5.2 - The Measurement Method for Five Coronal Segmental Alignment to Horizontal Angles on the Posterior-Anterior Full-Spine Radiograph of an AIS Spine with the Anatomical Landmarks of 6 Coronal RSAPs. ..	76
Figure 5.3 - The Measurement Method for Five Sagittal Segmental Alignment to Horizontal Angles on the Lateral View Full-Spine Radiograph of an AIS Spine with the Anatomical Landmarks of 6 Sagittal RSAPs. ....	77
Figure 5.4 - The Location of Each Anatomical Landmark of the Three Sagittal Deviational Angles.....	79
Figure 5.5 - Illustrations and Radiographic Examples of the Seven Proposed Sagittal Misalignment Patterns with Sagittal Central Sacral Lines.....	85
Figure 6.1 - The Measurement method and 6 Key Surface Level Anatomical Landmarks of SSAPs on the Radiographic Lateral View of the AIS Spine. ....	91
Figure 6.2 - Measurement Methods and 10 Anatomical Landmarks of Each System .....	92
Figure 6.3 - Visual Comparison Between Both (a) Coronal and (b) Sagittal Spinal Alignment of RSAPs and SSAPs.....	96
Figure 6.4 - Comparison between SLTA and 3LTA-S by Each Subject.....	97
Figure 6.5 - Comparison between SCEA and 3CEA-S by Each Subject .....	97
Figure 6.6 - An Example of the Difference in Anatomical Landmark between RSAPs and SSAPs in the Coronal Curvature Area .....	98
Figure 7.1 - “How to Measure 3UTA” as an Example .....	102
Figure 7.2 - TRA and LRA .....	103
Figure 7.3 - C5A and SSA .....	104
Figure 7.4 - PTA and SCA.....	105
Figure 7.5 - An Example for How to Calculate the Parameter Values of 3UTA, CUTA, and SUTA.....	107
Figure 7.6 - The D-flow Application .....	109
Figure 7.7 - Motion Capture Technology .....	109

Figure 7.8 - The Design Process Flowchart of the Digital Calculating and Visualisation Application.....	110
Figure 7.9 - (a) The Application Setting Part for Data Collection in the Design Process Flowchart of the Digital Calculating and Visualisation Application, (b) Programmed Modules of the Application Setting Part for Data Collection in the D-Flow Application .....	111
Figure 7.10 - (a) The Application Parameter Module (Runtime Console), (b) A Pointer with a Reflective Marker, and (c) the Maker Matcher Module in the D-Flow Application .....	112
Figure 7.11 - The Application Setting Part for the Calculation and Visualisation of Parameter Values in the Design Process Flowchart of the Digital Calculating and Visualisation Application .....	113
Figure 7.12 - Programmed Modules of the Application Setting Part for the Calculation of the 3DSP Parameter Values.....	113
Figure 7.13 - Programmed Script, Billboard, and Object Modules for Visualisation of the 3DSP Parameter Values and Colour Indicators.....	119
Figure 7.14 - Visualisation of Parameters and Spinal Alignment with Colour Indicators in the DRS Window.....	120
Figure 7.15 - The Application Setting Part for the Visualisation of Spinal Alignment and Colour Indicator for Each Segment in the Design Process Flowchart of the Digital Calculating and Visualisation Application	123
Figure 7.16 - Programmed Script and Event Modules for Visualisation of Spinal Alignment.....	123
Figure 7.17 - Programmed (a) Force Data and Calibration Script Modules for Measuring Applied Forces and (b) 3D text Modules for Visualisation of the Applied Force Values in the D-Flow Application .....	125
Figure 7.18 - Visualisation of Applied Force Values in the DRS Window.....	126
Figure 7.19 - The Application Setting Part for the Applied Force Measurements and Visualisation in the Design Process Flowchart of the Digital Calculating and Visualisation Application .....	126
Figure 7.20 - Apparatus and Materials I .....	127
Figure 7.21 - Apparatus and Materials II.....	128
Figure 7.22 - Apparatus and Materials III: .....	128
Figure 8.1 - The Placements of Reflective Markers on the Key Skin Level Anatomical Landmarks .....	136
Figure 8.2 - Motek (D-flow) DRS Window.....	137
Figure 8.3 - Coronal and Sagittal Spinal Alignments of the Non-scoliotic Spines .	140
Figure 9.1 - Comparing the Boxplots of Each SSAP Between the Two Groups.....	145
Figure 9.2 - Comparing the Boxplots of Each SNSP Between Two Groups.....	146

Figure 10.1 - Setup and Connection with All Equipment and Apparatus .....	153
Figure 10.2 - Posterior, Lateral, and Anterior Views of a Subject in the Scolio-Corrective Frame while Corrective Forces are Applied.....	155
Figure 10.3 - Forces in Transverse view at Thoracic Apex Level for a Right Thoracic Curve .....	156
Figure 10.4 - Different Forces Applied on the Coronal View of Subject 1 .....	161
Figure 10.5 - Different Forces Applied on Subject 2.....	165
Figure 10.6 - The PA, Full Spine Radiograph of Subject 3.....	166
Figure 10.7 - The PA, Full Spine Radiograph of Subject 4.....	168
Figure 10.8 - Different Forces Applied on Subject 5.....	171

## List of Tables

Table 1.1 - General Orthotic Design Recommendations for AIS based on the Apical Level of a Curve .....	6
Table 3.1 - Characteristics of Studies and Findings of Literature Review 1 .....	18
Table 3.2 - Characteristics of Studies and Findings of Literature Review 2 .....	18
Table 5.1 - The Results of the Correlation Matrices between Sagittal and Coronal Spinal Alignment Parameters .....	82
Table 5.2 - Seven Sagittal Misalignment Patterns .....	82
Table 5.3 - (Upper) The 7 major sagittal misalignment patterns and their classification by the apex location of coronal curves. (Lower) The mean and the standard deviation of each sagittal segment to horizontal angle classified by each coronal curve type.....	83
Table 6.1 - Means and Standard Deviations of Parameter Values.....	94
Table 6.2 - The Pearson's Correlation Coefficient (r) with Each p-values of the Test of Significance.....	95
Table 7.1 - The List of 19 Key Surface Level Anatomical Landmarks of 3DSPs...	106
Table 8.1 - The Mean, Standard Deviation (SD), and 95% Confidence Interval (CI) for Each 3DSPs.....	139
Table 8.2 - The Reference Ranges of Each Parameter Classified by Three Different Categories .....	139
Table 9.1 - Subject Characteristics of the Scoliosis Group and Non-Scoliosis Group .....	143
Table 9.2 - The Mean, Standard Deviation (SD), and Result of the Nonparametric Independent Two Tailed T-test for Each Parameter Between the Non-scoliosis Group and Scoliosis Group.....	144
Table 10.1 - 3D skin level Parameters for Outcome Measures .....	158
Table 10.2 - Demographic Characteristics of the Study Subjects with Coronal and Sagittal Spinal Alignment Parameters Measured from the Skin Surface .....	160
Table 10.3 - The Values of 3DSPs of Each Subject .....	160
Table 10.4 - Subject 1: The Values of 3DSPs Measured by the Application with and without Applied Specific Forces .....	163
Table 10.5 - Subject 2: The Values of 3DSPs Measured by the Application with and without Applied Specific Forces .....	165
Table 10.6 - Subject 3: The Values of 3DSPs Measured by the Application with and without Applied Specific Forces .....	167
Table 10.7 - Subject 4: The Values of 3DSPs Measured by the Application with and without Applied Specific Forces. ....	169

Table 10.8 - Subject 5: The Values of 3DSPs Measured by the Application with and without Applied Specific Forces .....	172
Table 10.9 - Recorded Forces (N) When the Parameters were Most Improved in Each Case .....	174

## **List of Abbreviations and Symbols**

Adolescent Idiopathic Scoliosis (AIS)  
Idiopathic Scoliosis (IS)  
Three-Dimensional (3D)  
Scoliosis Research Society (SRS)  
Posterior–Anterior (PA)  
Two-Dimensional (2D)  
Thoracic-Lumbar-Sacral Orthoses (TLSOs)  
Cervical-Thoracic-Lumbar-Sacral Orthoses (CTLSOs)  
Radiographic Spinal Alignment Parameters (RSAPs)  
Skin Level Spinal Alignment Parameter System (SSAPs)  
3D Skin Level Measurable Parameters (3DSPs)  
International Society on Scoliosis Orthopaedic and Rehabilitation Treatment (SOSORT)  
Rib Vertebral Angle (RVA)  
Surface Topography (ST)  
Quantec Spinal Image System (QSI)  
Integrated Shape Imaging System (ISIS)  
Computed Scan (CT-Scan)  
Spinal Orthotic Scientific Society (SOS)  
American Academy of Orthotists and Prosthetists (AAOP)  
Journal of Prosthetics & Orthotics (JPO)  
United States of America (USA)  
Coronal Lower Cervical Alignment to Horizontal Angle (CCEA)  
Coronal Upper Thoracic Alignment to Horizontal Angle (CUTA)  
Coronal Lower Thoracic Alignment to Horizontal Angle (CLTA)  
Coronal Upper Lumbar Alignment to Horizontal Angle (CULA)  
Coronal Lower Lumbar Alignment to Horizontal Angle (CLLA)  
Sagittal Lower Cervical Alignment to Horizontal Angle (SCEA)  
Sagittal Upper Thoracic Alignment to Horizontal Angle (SUTA)  
Sagittal Lower Thoracic Alignment to Horizontal Angle (SLTA)  
Sagittal Upper Lumbar Alignment to Horizontal Angle (SULA)  
Sagittal Lower Lumbar Alignment to Horizontal Angle (SLLA)  
Carestream Picture Archiving and Communication System (PACS)

Sagittal Central Sacral Line (SCSL)  
Line of Gravity (LoG)  
Sagittal Angle of C4 (SAC4)  
Sagittal Angle of T7 (SAT7)  
Sagittal Angle of L3 (SAL3)  
3D Lower Cervical Alignment to Horizontal Angle (3CEA)  
3D Upper Thoracic Alignment to Horizontal Angle (3UTA)  
3D Lower Thoracic Alignment to Horizontal Angle (3LTA)  
3D Upper Lumbar Alignment to Horizontal Angle (3ULA)  
3D Lower Lumbar Alignment to Horizontal Angle (3LLA)  
Pearson's Correlation Coefficient (r)  
Any parameter measured from the coronal view (-C)  
Any parameter measured from the sagittal view (-S)  
Thoracic Rotation Angle (TRA)  
Lumbar Rotation Angle (LRA)  
C5 Balance Angle (C5A)  
Sternal Angle (SSA)  
Pelvic Tilt Angle (PTA)  
Upper Sacral Angle / Sacral Alignment to Horizontal Angle (SCA)  
Standard Deviation (SD)  
Confidence Interval (CI)  
Skin Level Non-Spinal Alignment Parameters (SNSPs)  
DOB (Date of Birth)  
Skin Level Pelvic Incidence (SPI)  
Newton Unit (N)

## **Chapter 1. Introduction**

## **1.1 Introduction**

Adolescent Idiopathic Scoliosis (AIS) is the most common of the types of idiopathic scoliosis (IS) that occurs during the adolescent period. The prevalence of AIS is approximately 2% to 2.5% of most populations, affecting up to 0.15–4% of schoolchildren (Kane, 1977; Reamy and Slakey, 2001). AIS is a three-dimensional (3D) deformity of the vertebrae, spine, and rib cage that produces asymmetries of the trunk (Lowe et al., 2000). While the etiopathogenesis is still unknown, it is hypothesized to be multi-factorial (Lowe et al., 2000).

## **1.2 Pathological Features of Adolescent Idiopathic Scoliosis**

According to the Scoliosis Research Society (SRS) definition, AIS is diagnosed when the spine has more than 10 degrees of coronal curvature with some evidence of rotation as seen on a posterior–anterior (PA) radiograph (Richards et al., 2005). Furthermore, it is generally accepted that an AIS scoliotic spine has three main pathological and biomechanical characters. First, in the transverse plane, if there is a scoliotic deformity in a certain spinal segment, the spinal column including the individual vertebrae in the segment, are rotated toward the convex side of the curve. The abnormal rotations of the spinal column and the vertebrae in the scoliotic spinal segment produce an asymmetric shape of the rib cage, including rib prominence (Adam et al., 2008), (Stokes, 1989; Jaremko et al., 2002; Parent et al., 2005; Gum et al., 2007; Kotwicki and Cheneau, 2008). In addition, its closest spinal segments have a tendency to rotate in the opposite direction to the segment that has a scoliotic deformity, including pelvic rotation (Gum et al., 2007).

Secondly, the spinal column in the segment that has a scoliotic deformity not only rotates to the convex side of the curve but also moves away from the spinal midline to the convex side of the curve. Thus, the lateral displacement of the spinal column (also called the coronal curve) can be seen in the coronal plane. The coronal curve patterns can be simply classified depending on whether the convexity of the curve is located on the right or left, and on where the apical vertebra of the curve is located. For example, there is a cervicothoracic curve if the apex is at the level of C7/T1; a thoracic

curve if the apex is between T2 and T11; a thoracolumbar curve if it is at T12/L1; and a lumbar curve if it is between L2 and L4 (Kotwicki and Cheneau, 2008). The curve can also be classified based on the number of an existing structural coronal curve such as a single, a double, or a triple structural curve (Lonstein, 1996). In addition, there are established coronal curve classifications such as the “King” classification and “Lenke” classification (Lenke et al., 2001; King et al., 1983). Other deformities such as spinal imbalance (C7 decompensation), trunk asymmetry, pelvic rotation, shoulder height difference, trunk height difference, and pelvic obliquity can be also observed in coronal plane.

Finally, in the sagittal plane, the only known deformity is a loss of thoracic kyphosis (thoracic hypo-kyphosis or flattening) if a structural curve is seen coronally in the thoracic segment. Dickson et al. (1984) reported that the hypo-kyphosis in the thoracic segment causes a tightening of the posterior structure in the spinal column on the lower region of the structural curve (Dickson et al., 1984). However, this does not always explain all sagittal misalignment patterns and deformities. In addition, the sagittal aspect has been relatively uninvestigated when compared to the deformities of the coronal plane and transverse plane. While several studies have already classified AIS coronal deformities and misalignment patterns as mentioned above, sagittal deformities and misalignment patterns have not yet been defined or established. Although the Lenke classification introduced three possible sagittal structural criteria (Smith et al, 2008), it failed to categorize sagittal misalignment patterns enough to develop a clear comprehensive classification (Ovadia, 2013). The scarcity of research into the sagittal plane may be attributed to the absence of measurable parameters that can quantify sagittal spinal misalignment.

Among the three pathological features of AIS, the coronal misalignment pattern is the most studied area because the two-dimensional (2D) coronal PA radiographic image is the most utilized as the primary clinical assessment tool and used for both diagnosis and outcome measurement of AIS deformities in scoliosis clinics. This may be due to the limitations of the 2D PA radiographic assessment tool. Several experts

(Dickson, 2010) have stated that 3D deformities cannot be adequately described by merely assessing deformities in only one plane.

Therefore, the current standard practice which only assesses curvature in one or two planes, and leaves clinicians to make assumptions regarding misalignment and deformities in 3D space, is a critical deficiency in the field (Dickson, 2010).

### **1.3 Curve Progression Mechanism of AIS**

It is generally known that there is a high risk of curve progression during adolescence, which is a period of rapid skeletal growth (Weinstein and Ponseti, 1983; Dickson and Weinstein, 1999; Richards et al., 2005). Richards et al., (2005) mentioned in their article that there is also a high risk of curve progression if the patient's gender is female (5.2 times more frequent in girls than in boys), the initial curve magnitude is between 20 and 29 degrees, or the skeletal maturity (Risser sign) is between 0 and 1 (Richards et al., 2005; Rogala et al, 1978). The Risser sign presents the degree of skeletal maturity by measuring the state of ossification of the iliac apophysis on the pelvis on the PA radiograph: 0 - no evidence of ossification of the apophysis; 1 - 25% excursion; 2 - 50% excursion; 3 - 75% excursion; 4 - 100% excursion; 5 - fusion of the apophysis to the iliac crest.

The Hueter–Volkmann Effect, which is one of the hypotheses for the pathogenesis of AIS, proposes an explanation of the curvature-progression mechanism (Burwell, 2003, Weiss and Hawes, 2004). Asymmetric mechanical loading at the epiphyseal plates of the skeletally immature spine makes for asymmetric growth of the vertebral bodies and discs, and this then causes wedging on the vertebral bodies and discs. The wedging of vertebrae and discs produces curvature of the spine. The spinal curvature, once established, creates more asymmetric loading at the epiphyseal plates. Thus, the curvature progresses through this repetitive cycle, as described above (Burwell, 2003; Stokes et al., 2006; Stokes, 2007) .

## 1.4 Orthotic Treatment for AIS

Orthotic treatment is the most commonly used conservative treatment for AIS (Richards et al., 2005; Danielsson et al., 2007; Yrjönen et al., 2007; Katz, 2010; Schiller et al., 2010). The purpose of the orthotic treatment is to limit the extent of curve progression while awaiting skeletal maturation and reducing the need for surgical intervention (Richards et al., 2005). An orthotic device should provide mechanical corrective forces to the scoliotic spine, rib cage, and trunk of an AIS patient. The corrective forces are generated through the shape of the orthosis itself and by additional pads which apply forces by controlling the tension of the straps. The orthosis attempts to restore the spinal column and trunk to a neutral anatomical position in all three planes (Lou et al., 2008). Most clinics in the United States follow the clinical treatment guideline written by Rowe (2003). In this manual, three treatment options are recommended: (a) observation only if the patient has a Risser sign of 0 or 1 and a Cobb angle of less than 20°, or if the patient has a Risser sign of 2 or 3 and a Cobb angle of less than 30°; (b) orthotic treatment if the patient has a Risser sign of 0 or 1 and a Cobb angle of 20–40°, or if the patient has a Risser sign of 2 or 3 and a Cobb angle of 30–40°; and (c) surgery if the patient has a Cobb angle of greater than 50° while curves between 40° and 50° fall into a grey area.

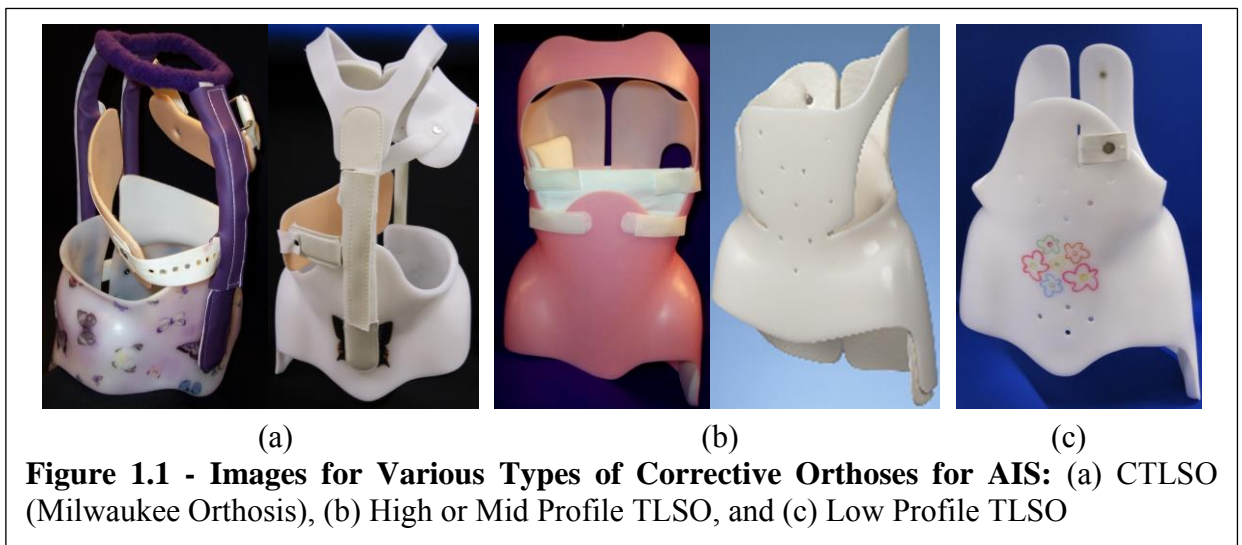
Numerous orthotic device systems and designs have been used for AIS, and the choice of orthosis depends on factors such as the apical level of curvature, geographical location, cosmetic and aesthetic specifications, preference for day-time or night-time use and the popularity of a given orthosis (Patwardhan et al., 1996). Table 1 introduces general orthotic design recommendations for AIS according to the apical level of a coronal curve among low, mid, high-profile thoracic-lumbar-sacral orthoses (TLSOs) and cervical-thoracic-lumbar-sacral orthoses (CTLTOs), which is called a Milwaukee orthosis (Table 1.1) (Jang et al., 2019). In addition, Figure 1.2 presents images for various types of orthotic devices used for treating AIS.

Success rates for orthotic treatment have been found to vary considerably. Several studies reported that the rates of surgical intervention, which are considered as orthotic treatment failure rates, range anywhere from 1% to 43% after orthotic treatment

(Dolan and Weinstein, 2007; Lonstein & Winter, 1994). However, the recently published BrAIST (Bracing in Adolescent Idiopathic Scoliosis Trial) study, which is a multi-centre randomized controlled trial involving twenty-five institutions in the United States and Canada, found the overall success rate with orthotic treatment to be 75% or a 25% failure rate (Weinstein et al., 2013). Many factors may account for these inconsistencies in the success rates of orthotic treatment. The facts that there are no universally agreed-upon principles to guide the orthotic treatment of AIS and that orthotists lack a fundamental understanding of 3D misalignment and deformity patterns, may induce significant quality deviations for each scoliosis orthotic device system (Rigo et al., 2006; Bagnall et al., 2009). Thus, to maximize the effectiveness of orthotic treatment, it is necessary to identify key biomechanical principles and to be able to quantify and report them. Orthotists should know exactly how the corrective forces induced by the orthosis act on the trunk, rib cage, and spine as well as how to improve the patient's comfort level while maintaining the appropriate degree of corrective force (Simith, 2003; Lou et al., 2008). This can only be achieved by improved orthotic metrology.

<b>Orthotic Design Options</b>	<b>Curve Types</b>
CTLISO (Milwaukee Orthosis)	Curves with the apex above T7/8 or Curves with T1 tilt
High or Mid Profile TLSO	Curves with the apex on and below T7/8
Low Profile TLSO	Curves with the apex below T12

**Table 1.1 - General Orthotic Design Recommendations for AIS based on the Apical Level of a Curve**



## **1.5 General Outline of This Thesis**

Hence, in an effort to further clarify the little-known 3D misalignment patterns and deformities of AIS and the unclear biomechanical corrective principles in the orthotic treatment of AIS, a new 3D spinal measurement system is needed. It is also necessary to develop a new AIS assessment tool that can be used in conjunction with the new 3D spinal measurement parameters. This thesis reports the development, validation, and implementation of these two systems. The next chapter describes the detailed thesis outline and the aims and objectives for the thesis.

## **Chapter 2. Aims, Objectives, and Thesis Outlines**

## **2.1 Introduction**

This chapter sets out the clinical rationale for the thesis and the development of both the 3D spinal alignment measurable parameters and the non-invasive digital assessment tool mentioned in the previous chapter. It also gives the thesis aims and objectives.

## **2.2 Clinical Rationales of the Thesis**

The current clinical understandings for treating AIS are summarized as follows:

1. AIS is a three-dimensional (3D) deformity of the spinal column, vertebrae, rib cage, and trunk. There is still a lack of understanding for the 3D misalignment and deformities of AIS, especially in relation to the sagittal plane.
2. A 2D posterior-anterior (PA) view radiographic image is the most commonly utilized primary assessment tool for AIS deformities in scoliosis clinics. However, PA radiographs detect only the coronal deformities of the curve.
3. Orthotic treatment is the most commonly used conservative treatment for AIS to prevent further curve progression and reduce risk of surgical intervention by providing mechanical corrective forces on the scoliotic spine, rib cage, and trunk. However, the inability to assess and treat the condition in 3D has the potential to lead to inconsistent outcomes in the orthotic treatment. This likely accounts for the widely variable orthotic treatment success rates in the literature.
4. The biomechanical principles employed during orthotic treatment of AIS are not fully defined. Clinicians are left to rely on inaccurate assumptions regarding misalignment and deformities in 3D space.

To address this clinical gap, it was necessary to develop a new measurable spinal alignment parameter system that is capable of quantifying the 3D misalignment patterns and deformities of AIS. Secondly, developing a new 3D non-invasive digital assessment tool that can be used in conjunction with these parameters was required.

### 2.3 Thesis Outline and Scop

The next chapter, **Chapter 3**, presents the findings of three different literature reviews. The literature reviews were performed (a) to identify whether there are any *commonly used* measurable parameters that are capable of quantifying the 3D misalignment and deformity of AIS and can biomechanically influence the success of the orthotic treatment; (b) to define whether there are any non-invasive assessment tools or technological systems that can assess the 3D deformity of AIS; and (c) to find if there are any studies which already defined the 3D biomechanical orthotic correction of AIS. The rationale for the necessity of developing new systems is confirmed in this chapter.

**Chapter 4** introduces the survey project “Current Practice in Orthotic Treatment of AIS”, which was conducted to identify major biomechanical corrective elements that raised disagreement between clinicians that treat AIS.

**Chapter 5** shows the development process and rationale for the radiographic spinal alignment parameters (RSAPs) that can be used for radiographic assessment. Through radiographic analyses of 100 AIS patients, this chapter describes an experiment that determines whether the RSAPs are useful in defining sagittal AIS misalignment patterns that have not been clearly defined before this study.

**Chapter 6:** The validated 2D concept for RSAPs was modified for use in 3D skin level assessment, called the skin level spinal alignment parameter system (SSAPs). The key osseous anatomical landmarks for the RSAPs were transferred to the closest anatomical locations on the skin surface. This chapter then presents a concurrent validity test conducted to validate the 3D concept of the SSAPs. This was performed by examining whether there exists any relationship between values measured on the skin level anatomical landmarks from the SSAPs and corresponding values measured on the original osseous radiographic landmarks from the RASPs taken at the same time using the same AIS subject.

**Chapter 7** describes the development of a non-invasive digital calculation and visualisation assessment tool that can be used with the 3D skin level measurable parameters (3DSPs) including SSAPs. This chapter also introduces computer applications built with motion capture technology for the development of the assessment tool. The chapter presents the development of a *Scoli Corrective Standing Frame* built to measure the forces applied to the torso during orthotic fitting.

**Chapter 8** presents a study which was conducted to examine the reference ranges of all 3DSPs by measuring each value from the anatomically neutral spine and trunk of non-scoliotic adolescents in the same age range as the AIS group. This chapter also shows that SSAPs measured from non-scoliotic spines reflect the structural characteristics of a natural human spine. The reference ranges found for each measurement can be used to identify the optimal locations for 3D corrective forces in the assessment tool on the basis of whether the parameters are within the reference ranges of the non-scoliotic subjects.

**Chapter 9** introduces an analysis of the discriminative validity of the 3DSPs by comparing the values collected from the similar age ranges of the scoliosis and non-scoliosis groups.

**Chapter 10:** Finally, a pilot study performed to test the implementation of the developed digital assessment tool with the 3DSPs is presented. The implementation was evaluated on five AIS patients by investigating whether the tool can find answers for the biomechanical questions identified from the survey project, “Current Practice in Orthotic Treatment of AIS” (Chapter 4).

**Chapter 11** summarizes the development process of both the 3D spinal alignment measurable parameters and the non-invasive digital assessment tool. The advantages and limitations of the developed measurable parameters and assessment tool are also discussed and closing remarks about future work are given.

## 2.4 Aims and Objectives of the Thesis

The main aims of this thesis were to develop effective 3D surface level measurable parameters to quantify the 3D misalignment and deformities of AIS, and to build a suitable 3D non-invasive digital assessment tool that can be used with the 3D surface level spinal alignment parameters to clarify and improve the 3D biomechanical corrective theory in treating AIS.

To address and accomplish the goals of this thesis, several studies were conducted. The lists of objectives of those studies are described as follows:

1. To determine whether there are (a) any *commonly used* measurable parameters that can quantify the 3D misalignment and deformity of AIS and biomechanically influence success in orthotic treatment; (b) any assessment tools that can assess the 3D deformity of AIS; (c) any studies which have already defined the 3D biomechanical orthotic correction of AIS.
2. To identify major biomechanical corrective elements that have raised disagreement among clinicians that treat AIS.
3. To determine whether the newly developed RSAPs are useful in quantifying 2D AIS misalignment, especially for sagittal misalignment patterns which had not been clearly defined prior to this study.
4. To verify whether the validated RSAPs can be used on skin surface level landmarks to measure 3D spinal alignment by performing a concurrent validity test between the values measured from the skin level anatomical landmarks of SSAPs and corresponding values measured from the original osseous landmarks of RASPs.
5. To examine if SSAPs reflect the structural characteristics of a human's erect spine and the unique features in each spinal osseous structural segment.
6. To identify reference (normal) ranges for all 3DSPs including SSAPs to use in developing a digital assessment tool.
7. To investigate the discriminative validity (or contrast validity) of 3DSPs by comparing existing data collected from non-scoliosis and scoliosis groups.
8. To test if the developed digital assessment tool can identify the key elements of the 3D orthotic biomechanical corrective concepts with 3DSPs.

In general, the primary intention of this thesis was to help orthotists by providing a better understanding of the 3D misalignment and deformity patterns of AIS and to help resolve the existing disagreement among the professional community involved in the orthotic treatment of AIS. Future studies conducted using these two applications could then contribute to establishing a unified and comprehensive 3D biomechanical corrective theory in orthotic treatment, resulting in the improvement of treatment outcomes in AIS.

## **Chapter 3. Literature Review**

### **3.1 Introduction**

This chapter presents the findings of three different areas of literature directly related to this thesis. The first area reviewed was to discover literature evidence regarding the *commonly used* measurements or parameters that can fully quantify the 3D deformities and misalignment of AIS and can biomechanically influence the success of orthotic treatment. The second area reviewed was performed to identify whether there are any non-invasive assessment tools or technological systems that can assess the 3D deformity of AIS. The third area reviewed was conducted to ascertain if there are any studies which already defined the 3D biomechanical correction of AIS. The results of the three reviews are summarized at the end of this chapter.

### **3.2 Literature Review 1: Measurable Parameters That Influence Biomechanical Success in Orthotic Treatment of AIS**

#### **3.2.1 Background**

Finding measurable parameters that are capable of quantifying the 3D misalignment and deformity of AIS is necessary to research the little-studied 3D misalignment patterns and deformities of AIS, and ultimately help to define and solve the clinical problems associated with AIS. Thus, a literature review was performed to find out whether there exist any *commonly used* measurements or parameters that can fully quantify the 3D deformities and misalignment of AIS. Another aim was to establish whether the measurements or parameters identified through this review can biomechanically influence success of orthotic treatment.

This review sought out studies that focus on immediate in-orthosis correction rather than long term effects of orthotic use. However, the concept of the “immediate in-orthosis correction” is a widely used and well-known method for the prediction of long-term outcomes after orthotic treatment. It has been understood that there is a correlation between the immediate in-orthosis correction and the long-term biomechanical effectiveness of orthotic treatment (Clin et al., 2010). Thus, this method was adopted in the search for measurable parameters. The limitations of the current gold standard parameters used when assessing 3D AIS misalignment and deformities,

and the resulting necessity for new measurable parameters are discussed.

### 3.2.2 Methods

The literature search was performed through the PubMed database because it yields the most comprehensive search results for scoliosis. The PubMed database, which focuses on clinical and biomedical literature, is a free resource, of over 29-million citations (as of 2019) from MEDLINE, and a user-friendly search engine developed and maintained by the National Center for Biotechnology Information, at the U.S. National Library of Medicine, located at the U.S. National Institutes of Health (Lu, 2011; U.S. National Center for Biotechnology Information, 2019).”The following keywords or combination of keywords were used: *idiopathic scoliosis*, *orthosis*, *brace*, *biomechanics*, *correction*, *outcome*, *rib*, *effect*, *effectiveness*, *curve*, and *risk* (Figure 3.1). The search was limited to studies specifically related to AIS and English-language publications.

The following exclusion criteria were applied to study selection:

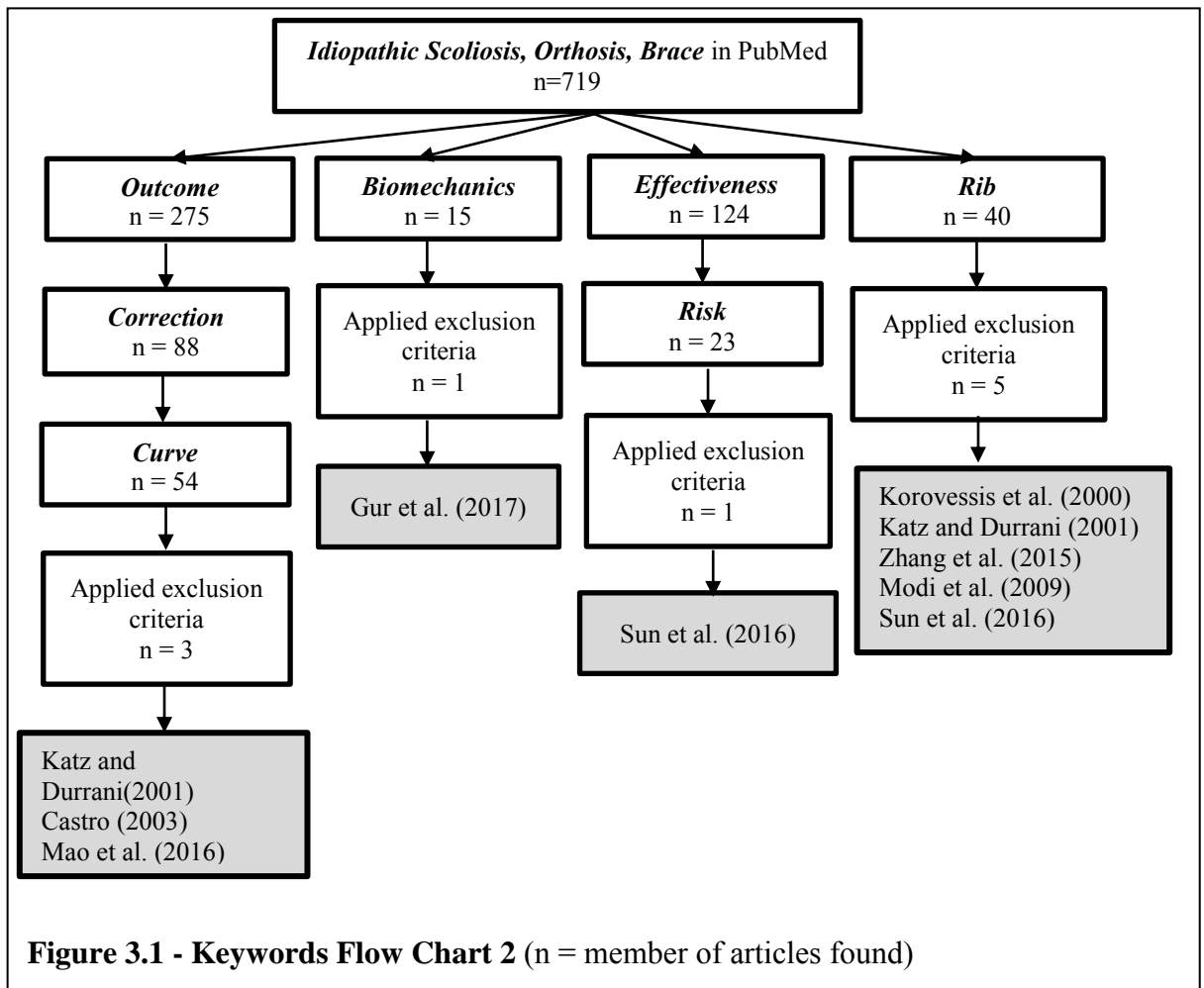
1. Studies related to other types of scoliosis were excluded.
2. Studies related to aetiology, operative treatment, or physical therapy were excluded.
3. Studies focusing on a specific orthotic system were excluded.
4. Studies using non-quantitative design method were excluded (The literature review of Chapter 4 covered all descriptive paper, education materials and textbooks).
5. All literature reviews, education materials, and oral presentations were excluded.
6. Studies published before the year 2000 were excluded (During the literature review for Chapter 4, no article related to this topic published between 1960 to 2000 could be found).
7. Studies for simulation or personalized computer modelling were excluded.

### 3.2.3 Findings

#### ***Study Selection***

A total of 719 articles were identified via the literature search using the following three keywords: *idiopathic scoliosis*, *orthosis*, and *brace*. Several other keywords and

the exclusion criteria mentioned above were applied to ensure the selection of appropriate studies that were related to measurable parameters that can quantify AIS misalignment and deformity and biomechanically influence orthotic treatment success for the review. Figure 3.1 presents a flow chart for the keywords. Of the 719 articles reviewed, 132 were deemed of sufficient fit to meet the application of the exclusion criteria, and when this was undertaken, only 8 remained.



### *Study Characteristics*

Table 3.1 presents a short description of each of the eight studies found via the search, including its purpose, design, participants, instrumentation, outcome measures, and findings. All studies focused on AIS and employed similar research methodologies and analysis techniques. Only one study used a non-radiographic analysis approach with a 3D electromagnetic tracking device.

Study	Purpose	Design	Participants	Instruments	Biomechanical Outcome Measures	Findings
Korovessis et al. (2000)	Effects of orthotic treatment	Prospective study	N=24, girls only; wearing orthosis		Cobb angle, convex and concave sides of rib-vertebral angle (RVVA) (T7-T12), coronal trunk balance, vertebral inclination, rotation, and translation (T7-L4)	Orthotic treatment is effective on reduction of curve progression and surgery
Katz and Durani (2001)		Retrospective review study	N=51 (girl:47, boy:4), wearing orthosis		Cobb angle, vertebral tilt angles, decompensation, apical translation and rotation, RVA, pelvic tilt, lumbar pelvic relationship (LPR)	In-orthosis correction for double curve of at least 25% and wearing time of >18h/day increased the successful outcome of the orthotic treatment
Castro (2003)		Prospective cohort and retrospective analysis	N=41, (girl:38, boy:3), wearing orthosis	Radiographic Analysis: before orthotic treatment, in-orthosis during orthotic treatment, and at final follow-up	Cobb angle, apical three vertebral body wedging (concave to convex height ratios)	Orthosis is effective on immediate derotations of the spine and is not effective if the curve is not corrected 20% in-orthosis
Modi et al. (2009)	Prognostic factors for outcome in orthotic treatment	Retrospective analysis	N=113 (girl:95, boy:18), wearing orthosis		Cobb angle, pelvic obliquity, convex and concave sides of RVVA and the difference of RVVA (RVVAD), the drooping value of convex rib	The curve will likely progress when the drooping of the convex apical rib along with RVVAD is noticed in-orthosis
Zhang et al. (2015)	Orthotic treatment in AIS	Prospective study	N=89, girls only; wearing orthosis		Apical vertebral rotation, Cobb angle, Risser sign	Cobb angle and apical vertebral rotation and spinal length increasing velocity are important factors to predict progression
Sun et al. (2016)		Retrospective analysis	N=48, girls only; wearing orthosis		Spinal length increasing velocity	
Mao et al. (2016)		Retrospective cohort study	N=95, girls only; wearing orthosis		Convex side of RVVA (CRVA) and RVAD	The initial RVAD $\geq 20^\circ$ and CRVA $\leq 68^\circ$ are valid factors in predicting the risk of curve progression during the orthotic treatment.
Gur et al. (2017)	Acute effects of orthotic treatment	Prospective study	N=26 (girl:23, boy:3), wearing orthosis	Analysis with 3D electromagnetic tracking device: in- and out-of-orthosis	Cobb angle: Initial correction rate (ICR) vs. Initial reduction velocity (ARV)	The ARV is a better predictor for curve progression than ICR in-orthosis.
					Scapular kinematics: internal/external rotation, upward/downward rotation, anterior/posterior tilt, and maximum humerothoracic elevation level	Orthotic treatment improves scapular kinematics and upper extremity function.

**Table 3.1- Characteristics of Studies and Findings of Literature Review 1**

Four of the eight studies used a prospective study design while the other four used a retrospective design. There were no studies found that utilized a randomized controlled trial design. The subject selection inclusion criteria of most studies matched or closely matched the Scoliosis Research Society (SRS) inclusion criteria (Cobb angle, 25–40°), which was introduced by Richards et al. (2005) as a methodological reference framework for orthotic treatment studies. Following the SRS subject inclusion recommendations, four studies recruited only females only. The SRS subject gender inclusion criteria for AIS related clinical studies was established based on the systematic literature review, and on long term follow-up clinical studies (Richards et al., 2005). The evidences confirmed that AIS is more than 10 times more common in girls than in boys, girls have a higher risk of curve progression, and that orthotic treatment can only help girls with AIS by preventing curve progression (Soucacos et al., 1998; Soucacos et al., 2000; Richards et al., 2005; Yrjönen et al., 2007; Sun et al., 2010).

#### 3.2.4 Discussion

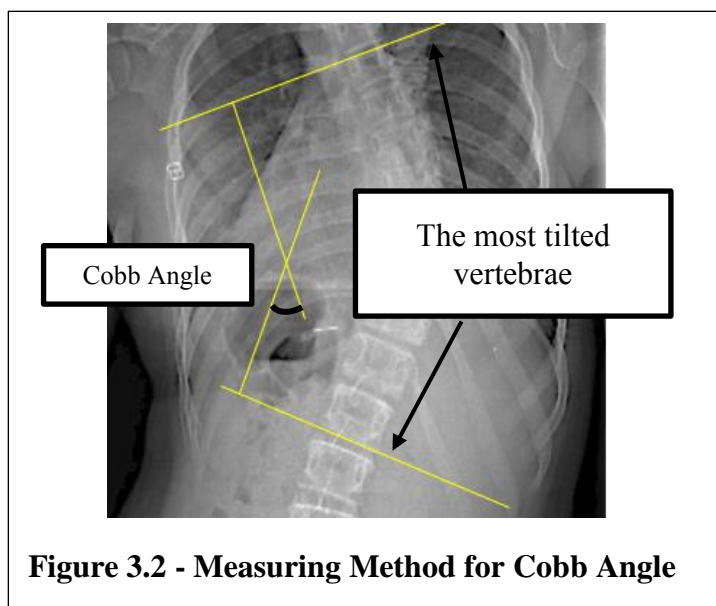
Through analysis of the data from the eight articles, four main measurements were identified as parameters that had been used to quantify the misalignment and deformities of AIS and possibly may influence the success of orthotic treatment. These four measurable parameters were:

1. Cobb angle measurement
2. Vertebral rotation measurement
3. Rib vertebral angle measurement
4. Scapular kinematics measurements

#### ***Association of Cobb Angle and Orthotic Treatment Outcome***

The Cobb angle method has been used as the gold standard for the diagnosis and treatment outcome assessment in AIS for many years. It involves measuring the magnitude of the coronal curvature angle on a posterior-anterior (PA) radiograph (Kotwicki and Cheneau, 2008). According to the *International Society on Scoliosis Orthopaedic and Rehabilitation Treatment (SOSORT) Terminology Consensus*

(SOSORT members et al., 2010), the definition of a Cobb angle is the angle between lines on the superior endplate of the upper cephalad end vertebra and on the inferior endplate of the lower caudal end vertebra (SOSORT members et al., 2010). These end vertebrae are defined as the most tilted vertebrae superiorly and inferiorly, which are angled maximally towards the concavity of the curve from the apex of the curve on the PA radiograph (Figure 3.2). The Cobb angle method can measure a curve occurred at various locations of the spine.



Cobb angle reduction when wearing the orthosis has frequently been used as a parameter to gauge successful orthotic treatment in AIS as shown in Table 3.1. Numerous studies, including the articles found through this search, have been published to show the correlation between the initial Cobb angle reduction in the orthosis and successful orthotic outcome (Bassett et al., 1986; Katz and Durrani, 2001; Castro, 2003; Simith, 2003; Clin et al., 2010; Korovessis et al., 2000; Zhang et al., 2015). In addition, two of the eight studies reviewed here provided a degree estimate for the optimal in-orthosis correction for the Cobb angle through PA radiographic analysis by comparing before orthotic treatment and initial in-orthosis correction (Katz and Durrani, 2001; Castro, 2003). It has been known since the 1970s that an initial reduction of the Cobb angle by 50% in-orthosis is generally accepted as a sign of successful orthotic treatment (Smith, 2003).

Castro's study in 2003 questioned the efficacy of orthotic treatment if Cobb angle values measured in the orthosis did not improve by at least 20% when compared to the angle before starting orthotic treatment (Castro, 2003). Katz and Durrani (2001) also reported that in double curve cases, Cobb angle reduction in-orthosis of 25% or more significantly increased optimal orthotic treatment outcome. It can be concluded that an initial reduction of the Cobb angle between 20% and 50%, depending on the curve type and the initial curve magnitude, may be an indication of optimal in-orthosis correction leading to successful orthotic outcomes.

However, several studies have found that there were limitations in utilizing the Cobb angle method to measure or quantify global spinal misalignment patterns (Kotwicki, 2008). Some studies discovered that the Cobb angle was not always proportional to severity for all 3D deformities of scoliosis (Dickson and Weinstein, 1999; Shufflebarger and King, 1987). Of particular note, Asher and Manna (1999) reported that surgical Cobb angle reduction does not always correlate with an improvement in global trunk symmetry.

In addition, the Cobb angle method has also been used in measuring the curvature angle magnitude of thoracic kyphosis and lumbar lordosis on the sagittal spine profile via a lateral view radiograph. However, the normal reference values for the thoracic kyphosis angle and lumbar lordosis angle measured by the Cobb angle method have never been clearly established. Several studies have been published regarding the normal ranges for the thoracic kyphosis angle and the lumbar lordosis angle, but their reported reference values had ranges that were too wide to be clinically suitable (Bernhardt & Bridwell, 1989; Bradford et al., 1974; Ghandhari et al., 2013; La Maida et al., 2013; Propst-Proctor and Bleck, 1983; Stagnara et al., 1982; Vialle et al., 2005). For example, one study found that there was no significant difference in thoracic kyphosis angle and lumbar lordosis angle between the scoliosis group and the non-scoliosis group (Propst-Proctor and Bleck, 1983).

### ***Association of Vertebral Rotation and Orthotic Treatment Outcome***

Vertebral rotation is one of the identifying characteristics of scoliosis. There are

four commonly used methods of describing vertebral-rotation measurement through radiographs: the Cobb, Nash–Moe, Perdriolle, and Stokes measures (Lam et al, 2008). Castro indicated that it is difficult to accurately measure vertebral rotation in standing PA radiographs because the measurement of vertebral rotation via this method is notoriously inaccurate and statistically unreliable (Castro, 2003). This article also reports that immediate de-rotations of the vertebral bodies are notable when an orthosis is applied (Castro, 2003), especially at the thoracic apical vertebrae (Castro, 2003; Korovessis et al., 2000). However, there are no studies confirming an association between vertebral rotation and successful orthotic outcomes.

#### ***Association of Rib Vertebral Angle (RVA) and Orthotic Treatment Outcome***

The RVA measurement method has been studied by numerous researchers. Significant RVA asymmetry between the concave and convex sides of the thoracic curve is observed in AIS (Grivas et al., 2002; Canavese et al., 2011). Two studies published the relationship between the outcome of orthotic treatment and RVAs. Korovessis et al. (2000) reported that orthotic treatment had no effect on the droop of the seven lower ribs because drooping of the ribs caused by an orthosis is not a permanent deformity. Later, studies by Modi et al. (2009) and Sun et al. (2016) reported that changes in RVAs were noticeable when an orthosis was applied and may indicate an association with curve progression. However, there was insufficient evidence to consider RVA improvement in-orthosis as a parameter for successful orthotic outcomes.

#### ***Association of Scapular Kinematics Measurements and Orthotic Treatment Outcome***

One of the AIS deformities is vertebral or spinal column rotation in the presence of structural curves. If the structural curve is located at the thoracic region, it produces an external rotation of the rib (or the rib rotates to the convex side of the curve), and an asymmetry between bilateral scapulae in the transverse plane (Gum et al., 2007). Gur et al. (2017) mentioned that orthotic treatment improves scapular kinematics and upper extremity function. However, no evidence was found to demonstrate that scapular kinematics measurements will indicate the success of orthotic treatment.

### 3.2.5 Summary

Eight articles were found and reviewed. The literature revealed four measurable parameters capable of quantifying the misalignment and deformity of AIS. The Cobb angle method was the only measure that could be described as a useful parameter that can biomechanically indicate a successful orthotic outcome. To achieve an optimal outcome in orthotic treatment, the orthosis should meet the criteria of at least a 20% initial reduction of the Cobb angle in-orthosis. However, there was insufficient evidence found regarding the relationship between other parameters (in-orthosis improvement of vertebral rotation, RVA, or scapular kinematics measurements) and successful orthotic outcomes.

Furthermore, this review also found that the Cobb angle method was limited in quantifying the 3D deformities and global misalignments of AIS. Thus, there exists a need to develop a new measurable parameter system to comprehensively quantify the AIS 3D deformities and global misalignment and yield a better understanding of 3D AIS misalignment and deformity. A new measurable parameter system can contribute to the creation of a unified and comprehensive set of biomechanical corrective principles in a complicated and not well understood area in orthotic treatment for AIS.

## **3.3 Literature Review 2: Non-Invasive Technological Tools that Can Assess the 3D Deformity of AIS**

### 3.3.1 Methods

Radiographic technology has been used as an assessment tool of diagnosis, progression, and as the outcome measure in treating AIS with the Cobb angle method. According to the current clinical guidelines for the treatment of AIS, each adolescent patient is recommended to visit their scoliosis clinic every 4-6 months during the treatment period until skeletal maturity (approximately 2-5 years); and at least one spine full radiograph (PA) should be taken per each visit to assess orthotic treatment progress by measuring the Cobb angle of each curve on the radiograph.

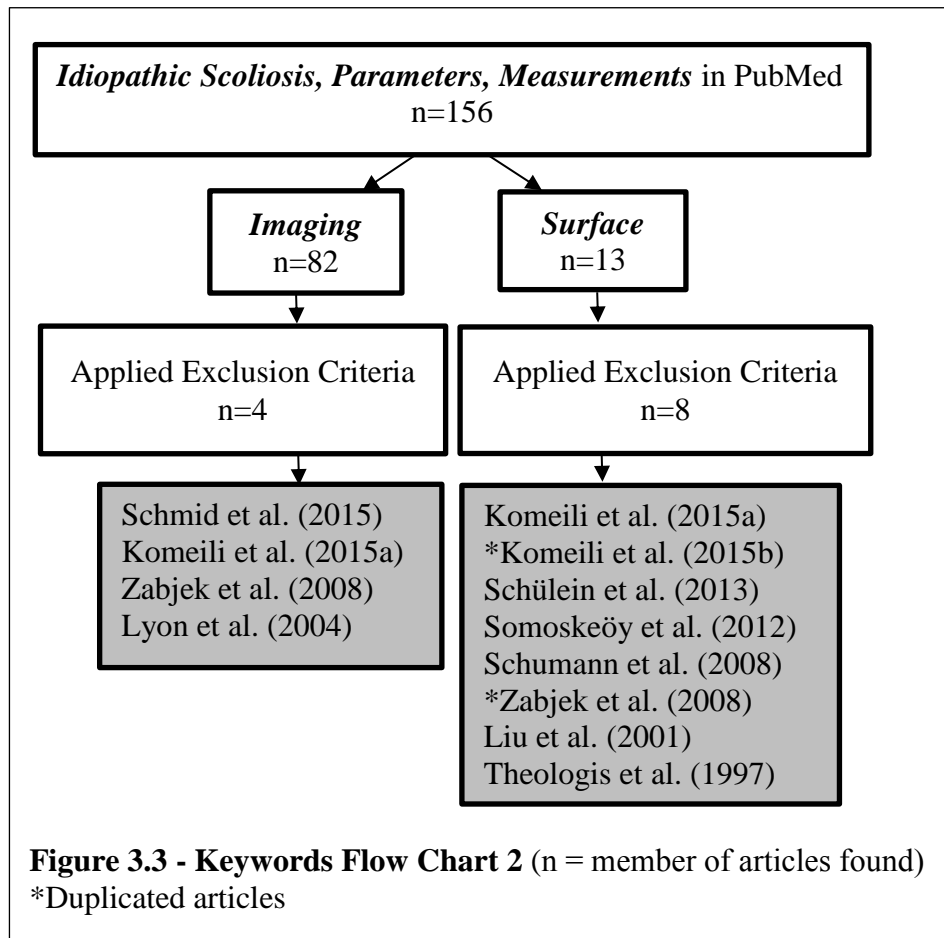
However, the awareness of the potential oncogenic effects of radiation exposure has increased, and several studies found that there is a higher risk of breast cancer in patients who had been exposed to radiation frequently (Ardran et al., 1980; Ronckers et al., 2010). For example, Ronckers et al. (2010) found that cancer mortality was 8 % higher than expected in patients who had repeated radiographs for scoliosis, and there was a four times greater relative risk of breast cancer in female patients with spinal disorders.

Thus, the purpose of this section of the literature review was to find whether there are any non-invasive assessment tools or technological systems that can assess the deformity of AIS, rather than using radiographic technology.

In PubMed, a literature search was performed using the following key words: *Idiopathic Scoliosis, Parameters, Measurements, Imaging, and Surface*. The search was limited to studies specifically related to AIS and English-language publications. The following exclusion criteria were applied to study selection:

1. Studies published before the year 1995 were excluded (Current available technologies were developed after 2000, except radiography).
2. Studies related to other types of scoliosis were excluded.
3. Non-English written articles were excluded.
4. All literature reviews, education materials, and oral presentations were excluded.
5. Studies related to the following conditions were excluded: gait, surgery, bone density, body composition, genetic test, breast asymmetry, spinal cord, pulmonary system, x-rays, skeletal growth

Of the 156 articles reviewed, 95 were deemed of sufficient fit to meet the application of the exclusion criteria and when this was undertaken only 10 remained (Figure 3.3).



### 3.3.2 Findings

#### *Study Selection*

The 10 found articles were divided and classified into three different types of assessment tools based on the tool that each study used while conducting their study.

1. Surface Topography: Komeili et al., 2015a; Komeili et al., 2015b; Liu et al., 2001; Lyon et al., 2004; Schumann et al., 2008; Theologis et al., 1997; Schülein et al., 2013
2. EOS Imaging System: Somoskeöy et al., 2012
3. Motion Capture Technology: Schmid et al., 2015; Zabjek et al., 2008

Instruments	Study	Purpose	Design	Participants	Biomechanical Outcome Measures	Findings
	Komeili et al. (2015a)	To determine the capability of the deviation color map (DCM) of the Surface Topography (ST) torso scans (Minolta laser scanner) to detect curve progression	Cross-sectional study	N=100 AIS patients	Asymmetry visual analysis on the DCM of the torso ST scans compared with Cobb angle, over 1-year follow-up interval.	The classification model detected 85.7% of the progression and 71.6% of the non-progression cases.
	Komeili et al. (2015b)	To investigate the correlation between the DCM of the torso ST scans and the spinal deformities presented on radiographs	Cross-sectional study	N=124 IS patients including 100 AIS cases	The number, direction, and locations of the curve(s) defined on the DCM of each full torso ST scan compared with Cobb angles	The average percentage of agreement was 62%, 66%, and 23% for single, double, and triple curves, respectively while curve direction was always correctly identified.
Surface Topography including Raster-stereophotography	Liu et al. (2001)	To provide functional classification of spinal deformity of mild idiopathic scoliosis using Quantec Spinal Image System (QSIS)	Prospective study	N=248 AIS patients	12 QSIS back surface metrics including other measurements (trunk height, pelvic tilt angle, Suzuki hump sum, axial surface rotation, kyphosis, and lordosis) measured on the back surface scans	The back surface image could provide a quantitative assessment of mild spinal deformity.
	Lyon et al. (2004)	To assess the intra-observer reproducibility of the OSIS metrics	Prospective study	N=200 AIS patients	12 QSIS back surface metrics including other measurements measured on the back surface scans	The reliability of the parameters was excellent.
	Schumann et al. (2008)	To estimate the technical errors of ST in three standardized postural positions.	Prospective study	N=100 IS patients	Two ST measurements (average lateral deviation and average surface rotation) in three different postures and three different age groups.	ST measurements can be influenced by artificial postures and therefore cannot be considered objective.
	Theologis et al. (1997)	To evaluate the reliability of the Integrated Shape Imaging System (ISIS) scans in detecting progression of scoliosis	Retrospective study	N=78 AIS subjects with a right thoracic curve	The ISIS parameters compared with the Cobb angle after subjects were divided into the spinal fusion, brace, and observation groups	The ISIS technique demonstrated significant changes in this group of patients with progressive scoliosis.
	Schulten et al. (2013)	To investigate the inter-observer and intra-observer reliability of raster-stereographic 3D back surface analysis (Formetric III 4D)	Prospective study	N=39 AIS post-op patients	The series of several measurements (trunk length, trunk inclination, trunk imbalance, kyphosis, and lordosis) of the raster-stereographs	The reliability of the raster-stereography in regard to the investigated parameters is excellent.
EOS Imaging System	Somoskeőy et al. (2012)	To compare accuracy, correlation of measurement values, intra-and inter-observer reliability of methods by the 2D EOS and 3D EOS	Retrospective study	N= EOS images of 201 subjects including 175 AIS cases	Cobb angles, kyphosis and lordosis angles measured from conventional manual 2D EOS and vertebra vector-based 3D EOS	3D EOS measurements could fully substitute 2D EOS measurements, with similar accuracy and higher intra-observer reliability and interrater reproducibility.
Motion Capture Technology	Schmid et al. (2015)	To examine the accuracy of a marker set for the static measurement of spinal curvatures	Prospective study	N=10 AIS patients with a thoracic curve	Curvature angles measured from the motion capture technology compared with the Cobb angles measured from the bi-planar radiographs	Curvature angles measured from the motion capture and lateral view radiograph were reasonably accurate while curvature angles measured from the motion capture and PA radiograph were systematically underestimated.
	Zabjek et al. (2008)	To compare the posture characteristics measured between motion capture technology and radiography	Prospective study	N=57 AIS patients	The parameters of the posture characteristics measured from motion capture technology compared with the curvature types defined from the radiography	There was a strong positive intraclass correlation between curvatures types (radiography) and the parameters of the posture characteristics (motion capture technology).

**Table 3.2 - Characteristics of Studies and Findings of Literature Review 2**

This literature review was conducted to find out whether there are any non-invasive assessment tools or technological systems currently available for assessing AIS deformity, and to also identify which system have been used in the studies. Thus, neither the strength and relevance, nor the methodology and statistics of each study were analysed. This review was only focused on the instrument or apparatus of each study found through the literature search.

### ***Study Characteristics***

Table 3.2 presents a short description of each of the 10 studies, including its purpose, design, participants, outcome measures, and findings with the three different assessment tool classifications. Most of studies focused on similar research methodologies and analysis techniques by performing either a validity test or a reliability test of outcomes measured using each assessment tool. The results of the review indicated that each assessment tool had pros and cons in detecting the spinal deformity of AIS. In the discussion section, the detailed analysis of each assessment tool is presented. The advantages and limitations to using current available systems including motion capture technology are also discussed.

### 3.3.3 Discussion

#### ***Surface Topography***

Of the 10 studies, seven were conducted for validating surface topography (ST) technology or by utilizing ST. ST is a non-invasive tool to capture an AIS patient's posterior torso surface and assess AIS external deformities from the shape of the posterior torso. Several topographic systems have been developed since the 1970s to eliminate the need of radiographs for adolescents, and Moiré topography was one of the first methods developed in 1970. Raster-stereography was developed in 1988 as an improved version of Moiré topography (Liu et al., 2013; Takasaki, 1971). Several different ST systems were discovered in the literature review such as: Quantec Spinal Image System (QSI), Formetric Rasterstereography System, and Integrated Shape Imaging System (ISIS). These systems were developed from different countries and groups but were very similar to each other. While ISIS captures the surface data of the

posterior torso using an optical scanner, plotter, camera and projector, QGIS is composed of an optical raster-stereography unit, project, a digital camera, and computer software (Liu et al. 2013). Both require markers to obtain the 3D coordinates from the marked anatomical landmarks of the back-surface shape. However, Formatertric is a markerless raster-stereography system and obtains surface data from raster lines and a biomechanical model (Liu et al. 2013). The recent version, Formatertric 4D has a very high inter- and intra-observer reliability (Schüle et al., 2013).

However, some of the studies concluded the ST system was not reliable in detecting the AIS deformity fully and could detect certain types of curves poorly (Theologis et al., 1997; Liu et al., 2001; Komeili et al., 2015a; Schumann et al., 2008). The biggest disadvantage in utilizing ST is that these systems can detect only the posterior part of the torso.

### ***EOS Imaging System***

To reduce radiation doses in medical imaging, a slot-scanning x-ray technique of the EOS imaging system has been developed (Hui et al., 2016). In addition to this minimum radiation dose radiograph technique, EOS added a 3D reconstruction spinal modeling concept obtained by bi-planar PA and lateral radiographs. Several studies already validated the 3D EOS reconstruction technology developed using bi-planar radiographs as a reliable 3D quantitative tool to assess the scoliotic deformity (Hayashi et al., 2009; Humbert et al., 2009). Thus, the usage of EOS has increased recently in some of hospital-based scoliosis clinics (Somoskeöy et al., 2012). However, this system is extremely expensive and not financially possible in most scoliosis clinics. Even though it uses a lower radiation dose compared with the standard digital radiography, the system still requires ionizing radiation exposure.

### ***Motion Capture Technology***

In the medical field, optoelectronic motion capture technology has been used to analyse various types of human motion as a 3D non-invasive assessment tool, especially for assessing and analysing gait. There are several different motion capture

systems on the market. Most have the capability of measuring and processing kinetic and kinematics data by tracking reflective markers attached to the body using multiple optical motion capture cameras.

Schmid et al. (2015) defined the relationship between markers attached on the surface level and the corresponding Cobb angle measured through radiographic analysis for AIS patients in their study. The paper concluded that skin marker-based motion capture techniques can be used as a non-invasive assessment of AIS. However, the techniques they developed were used to detect AIS posture changes rather than for the measurement of absolute spinal curvature angles (Schmid et al., 2015). Zabjek et al. (2008) also concluded the motion capture technology can identify the unique postural characteristics related to the types of spinal curvature.

Two more articles which were conducted using motion capture technology were found through an additional literature search. Skin marker-based measurements from the static analysis of motion capture technology was also verified by having high correlations with radiographic measurements in the master's thesis of Solomito (2011), which is titled "*The Use of Motion Analysis Technology as An Alternative Means of Assessing Spinal Deformity in Patients with Adolescent Idiopathic Scoliosis*". The thesis also reported that the static analysis of motion capture technology can replace a radiographic analysis method and also concluded that the static analysis can minimize radiographic radiation exposure (Solomito 2011). The other study, called "*Realistic Model of Spine Geometry in Human Skeleton in Vicon System*", introduced the process of creating a 3D computer model of the spine with 3D scanning and graphics software that can be inserted into the human skeleton models used in Vicon motion capture systems (Długosz et al., 2012). However, this model could not quantify any spinal deformities and the actual visualisation of the measurements and spine in real time.

Static analysis using motion capture technology to assess the scoliotic spine was validated in the first three studies. The fourth modeled the dynamic movement of the spine but was not used for quantifying spinal deformities in real time. These studies also mentioned that the currently available software still has difficulty in producing

kinetic and kinematic analysis of spinal movements. The other limitation in utilizing the technology was placing markers accurately on the skin surface, and the soft tissue movement artefact, because the spine is under movable skin and at a distance inside the torso.

### 3.3.4 Summary

In conclusion, there were 3 technological systems that can assess the 3D deformity of AIS spine in the literature. However, it was found that ST cannot detect a full torso and EOS has a poor accessibility for use in most scoliosis clinics. Furthermore, EOS could not completely eliminate the radiation exposure. Thus, this literature review indicated that motion capture technology may be one of the best options currently available to understand the 3D deformities of AIS and could accurately generate 3D Cartesian coordinated geometric data gained from reflective markers attached to the skin surface over anatomical landmarks of the AIS spine. However, there was no study verified that the motion capture technology can assess and quantify spinal deformities in real time.

## 3.4 Literature Review 3: 3D Biomechanical Correction Concept of AIS

### 3.4.1 Methods

As mentioned previously, the ultimate goal of this thesis is to develop an assessment tool and measurable parameters needed in clarifying 3D biomechanical corrective theory of AIS orthotic treatment. Thus, this literature review was performed to find whether there are any studies performed to define the 3D biomechanical orthotic correction of AIS, by reviewing 132 articles of the first literature review, which were found before applying the exclusion criteria (Figure 3.1). Nine studies conducted for the 3D biomechanical orthotic correction of AIS were found: Aubin et al., 1997; Chan et al., 2012; Clin et al., 2010; Desbiens-Blais et al., 2012; Gignac et al., 2000; Karimi et al., 2016; Krištof et al., 2010; Labelle et al., 2007; Wynarsky & Schultz, 1991.

### 3.4.2 Findings and Discussion

7 of the found 9 studies, were performed to assess optimal forces applied by orthosis by simulating the finite element model or 3D reconstruction model of the scoliotic trunk (Wynarsky and Schultz, 1991; Aubin et al., 1997; Gignac et al., 2000; Labelle et al., 2007; Clin et al., 2010a; Desbiens-Blais et al., 2012; Karimi et al., 2016). Especially, Gignac et al. (2000) defined the placements and magnitudes of optimal corrective forces, which should be achieved by an orthosis through the use of finite element models. Aubin et al. (1997) reported that an optimal way to achieve trunk correction is to apply loads on the lateral-anterior area at the convex side of the curve in the transverse plane. Furthermore, Karimi et al. (2016) evaluated the effect of various load configurations and magnitudes in correcting scoliotic curves by simulating on the 3D model of scoliotic spine. The 3D model was established using the computed scan (CT-scan) images of the spine of the subject. However, Desbiens-Blais et al. (2012) approached the finite element model using a 3D reconstruction of the trunk skeleton from the bi-planar radiographs and of the torso surface from the surface topography.

Two other studies used a force logging system (Chan et al., 2012) and a pressure distribution film method (Krištof et al., 2010). Both methods can record forces at multiple locations by placing it between the skin and an orthosis. However, these systems were only validated for future use in the optimization of orthotic treatment (Krištof et al., 2010; Chan et al., 2012). No clinical study yet existed which used these systems to define optimal 3D biomechanical orthotic correction by measuring in-orthosis pressure.

The results of this review indicated that most studies found used the 3D finite element or reconstruction model of a scoliotic spine instead of a real scoliotic spine in identifying the optimal biomechanical correction of orthotic treatment.

### **3.5 Conclusion**

The first reviews found that there is no measurable parameter system that can quantify the 3D deformities of AIS and that the Cobb angle method was limited in quantifying the 3D deformities and global misalignments of AIS. Through the second and third literature reviews, motion capture technology may be a choice to detect the 3D deformity of AIS. Eliminating radiographic radiation exposure for AIS patients was considered the most important benefit obtained by using motion capture technology to assess spinal deformities of the AIS spine. However, no assessment tool was found to provide the immediate or real-time feedback of orthotic correction by visualizing measurements and spine alignment in defining optimal orthotic correction performed on the real scoliotic spine.

Hence, the results of the three literature reviews indicated a need to develop a new measurable parameter system to comprehensively quantify the AIS 3D deformities and global misalignment and yield a better understanding of 3D AIS misalignment and deformity. In addition, these reviews discovered the necessity of developing a new suitable 3D non-invasive and radiation-free digital assessment tool that can be used with the 3D surface level spinal alignment parameters and provide immediate feedback of orthotic correction. Furthermore, the two systems developed through this thesis would contribute to the creation of a unified and comprehensive set of biomechanical corrective principles in a complicated and often ignored area in the orthotic treatment for AIS.

## **Chapter 4. Survey Project - Current Practice in Orthotic Treatment of AIS**

## 4.1 Introduction

This chapter introduces a survey project, “*Current Practice Standards in Orthotic Treatment of Adolescent Idiopathic Scoliosis*,” that the author conducted as the primary investigator while serving as the chair of the Spinal Orthotic Scientific Society (SOS) of the American Academy of Orthotists and Prosthetists (AAOP) with two other officers, *Kara L. Davis, MS, CPO, FAAOP* and *Scott D. Thach, MSPO, CO*. The manuscript was published in the *Journal of Prosthetics & Orthotics (JPO)* (Jang et al., 2019). In 2015-2016, this online survey was conducted to assess the current practice and status of orthotic treatment for adolescent idiopathic scoliosis (AIS) from spinal orthotic practitioners. There was no strong evidence in the literature to support clinical decision making in some of these treatment areas. In such circumstances, a poll of experts who agree on a statement can be used until a true scientific consensus can be reached. The results of these expert opinion studies can be used to encourage research scientists to perform studies that can affirm or reject such concepts.

Such consensus statements are an agreed-upon method to produce current best practice statements based on the available and scientifically valid outcomes-based evidence. However, as mentioned previously, the biomechanical correction principles in treating AIS are not clearly defined in practice or the literature. Therefore, this survey sought to identify the actual present biomechanical theories used by experienced spinal orthotists working in the United States of America (USA) in their clinical practice of orthotic treatment of AIS. The survey was also used to determine which areas of agreement or disagreement arise regarding the biomechanical correction theory used for orthotic treatment for AIS, based on the polled expert opinions of experienced spinal orthotists.

This chapter 4 explains the development processes of the survey questionnaires including the rationale for the survey questions selected. The final author manuscript that was submitted to JPO and published in January 2019 is included (Jang et al., 2019). At the end of this chapter, the findings of this study are summarized briefly, and the strengths and weaknesses of the methodology are discussed in the context of this thesis.

## **4.2 Processes Used to Develop the Survey Questionnaire**

As mentioned above, this survey's purpose was to identify current treatment beliefs within the USA on the orthotic treatment of AIS. This study also included the literature review results of all topics identified with 'significant disagreement' between spinal orthotist respondents in the survey. Thus, key biomechanical concepts were contained in the survey questions including the questionnaire which addressed some of the more controversial topics within the spinal orthotics community.

All three authors were involved in developing the survey questions. The questions for the general target concepts were selected initially from the clinical observations and experiences learned from their current practice in their clinical settings. The authors are all American board-certified orthotic practitioners, leaders of SOS, and have been working treating scoliosis for many years at the scoliosis clinics of major children's hospitals located throughout USA. The principal investigator, myself had 19 years of clinical orthotic experience in treating scoliosis as a certified orthotist, including more than 10 years working experience in the scoliosis clinic at Gillette Children's Specialty Healthcare (Saint Paul, Minnesota, USA), and teaches spinal orthotics clinical courses including scoliosis orthotic management and spinal biomechanical theories since August, 2013 as a tenured associate professor and researcher in the Orthotics-Prosthetics Master's Program at Eastern Michigan University (Ypsilanti, Michigan, USA). Kara L. Davis is also a scoliosis specialist and has been working at the scoliosis clinic of the Texas Scottish Rite Hospital for Children (Dallas, Texas, USA) for more than 10 years; and Scott D. Thach was trained at the scoliosis clinic of the Children's Healthcare of Atlanta (Atlanta, Georgia, USA) and continues to work there.

To develop the questions for the more specific controversial topics within the community, a preliminary consensus meeting was organised and held during the SOS Scientific Forum at the 40<sup>th</sup> AAOP Academy Annual Meeting and Scientific Symposium (February 27 2014, Chicago, Illinois, USA), to discuss the areas of agreement or disagreement regarding the current practice of orthotic treatment, and the key biomechanical elements used in treating AIS. The SOS invited experts in the field

of scoliosis treatment and other spinal deformities as panellists. The panellists gave a short presentation that covered key biomechanical elements of orthotic treatment for AIS, and then discussed the areas of agreement or disagreement regarding the current practice of orthotic treatment in treating AIS. These discussion points were used to develop the initial questions targeting the controversial topics reviewed in the survey. Later, the initially developed questions were sent to scoliosis specialists for review and finalized with minor changes subsequently.

The URL for the survey is:

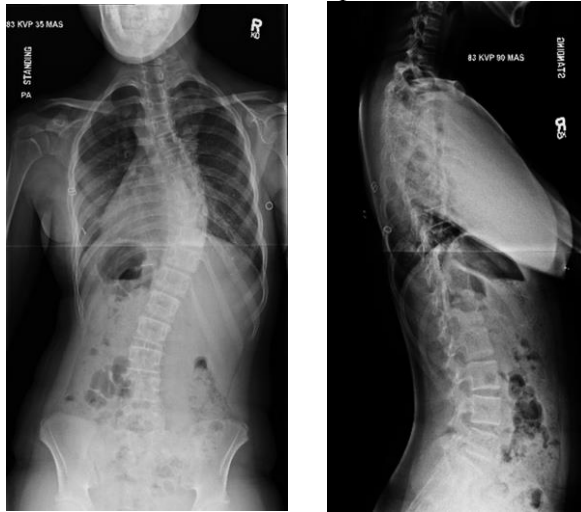
<https://docs.google.com/forms/d/e/1FAIpQLSdentGrDYM04asQgsVvs2Pr7W9zAozSoA9mjzMpuKuHYfkkgQ/viewform>. Here are the survey questions provided to the participants:

*Part 1: General Questions*

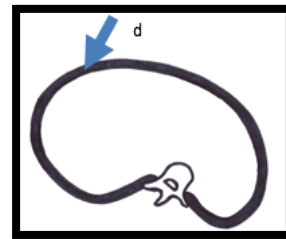
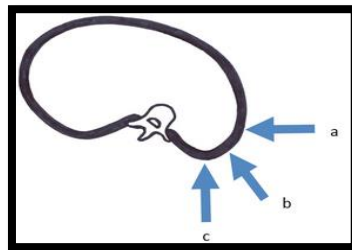
- 1) *Are you a credentialed orthotist or orthotist/prosthetist? (ABC certified, State licensed and/or BOC certified)*
  - a. *Yes*
  - b. *No*
  
- 2) *How many years have you been treating patients for AIS with a spinal orthosis?*
  - a. *Less than 2 years*
  - b. *2-5 years*
  - c. *5-10 years*
  - d. *10-15 years*
  - e. *Longer than 15 years*
  
- 3) *How many spinal corrective orthoses do you fit per year for AIS patients?*
  - a. *0-12 (less than one per month)*
  - b. *12-24 (approximately one or two per month)*
  - c. *24-48 (approximately two to four per month)*
  - d. *More than 48 (approximately more than one per week)*
  
- 4) *From the orthotist perspective, which of following is important when achieving an optimal orthotic outcome while treating AIS? (Choose all you believe to be true)*
  - a. *To reduce Cobb angle or coronal curvature in orthosis*
  - b. *To minimize spinal C7 decompensation in the coronal plane*
  - c. *To realign sagittal misalignment*
  - d. *To de-rotate rotational deformity in the transverse plane*
  - e. *To align to the neutral alignment of the spine and trunk in all three planes*
  
- 5) *In your clinic, what is the prescribed wear schedule for a daytime or fulltime orthosis?*
  - a. *12 hours*
  - b. *12-16 hours*
  - c. *16-18 hours*
  - d. *18-23 hours*

Part 2: Using the below radiographs (Case Example 1), please answer Q6-Q12.

Case Example 1



- 6) Where do you recommend applying a primary corrective force for the thoracic curve in transverse plane?
- Location a
  - Location b
  - Location c
  - Somewhere else \_\_\_\_\_



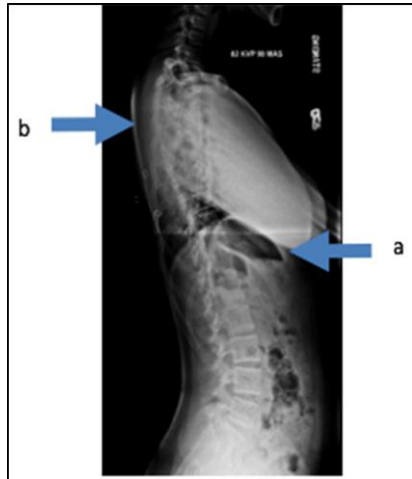
- 7) Do you usually consider to apply a coupled de-rotational corrective force “d” on the anterior part of the thoracic level as a secondary corrective force in the transverse plane?
- Yes
  - No
  - Yes, but somewhere else \_\_\_\_\_
- 8) Which of the following do you recommend on the level of a thoracic pad for the case example 1?
- The superior edge of a thoracic pad should be placed on the rib attached at the apex of the thoracic curve
  - The superior edge of a thoracic pad must extend to the apical VERTEBRAL level of the thoracic curve
  - The middle part of a thoracic pad should be placed on the apical VERTEBRAL level of the thoracic curve
  - Other \_\_\_\_\_

9) Which of the following do you recommend on the left axillary area for the case example 1?

- a. Building an axillary extension only without a pad or a minor thickness pad for comfort
- b. Building an axillary extension with an axillary pad
- c. Other \_\_\_\_\_

10) Where would you recommend applying a primary corrective force in the sagittal plane to address the thoracic hypokyphosis (thoracic flattening) in Case Example 1?

- a. Posteriorly directed force on the anterior part of rib cage
- b. Anterior directed force approximate to the level of the spine of scapula
- c. Both a+b
- d. Not needed for Case Example 1
- e. Somewhere else \_\_\_\_\_



11) In Case Example 1, would you recommend applying abdominal compression?

- a. Yes, always, not only in this case example 1, but in all patients.
- b. Yes, in this case example, but sometimes no abdominal compression is necessary.
- c. No, not in this case example, but sometimes abdominal compression is necessary.
- d. No, never. I do not apply abdominal compression.

12) If a patient has no hyper-lumbar lordosis in the sagittal plane as shown in Case Example 1, do you still reduce lumbar lordosis?

- a. Yes, always, not only in this case example 1, but also in all patients
- b. Yes, for this case example, and I sometimes reduce lumbar lordosis in other AIS cases
- c. No, for this case example, but I sometimes reduce lumbar lordosis in other AIS cases
- d. No, never

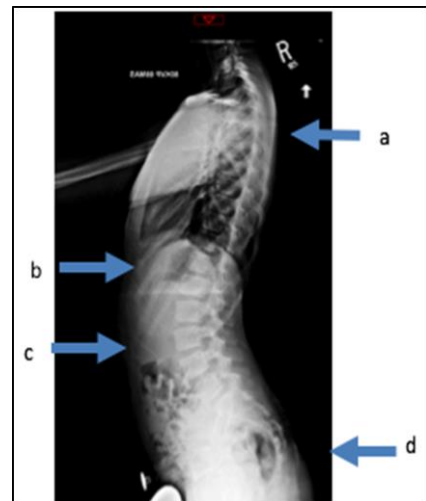
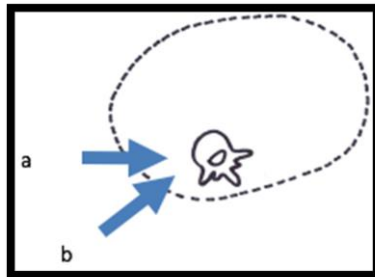
Part 3: Please answer Q13-14 based on the Case Example 2.

Case example 2



13) In the Case Example 2, where would you recommend applying a primary corrective force for the lumbar curve in the transverse plane?

- a. Medially directed force on the paraspinal muscles
- b. Antero-medially directed force along the paraspinal muscles
- c. Somewhere else \_\_\_\_\_



14) How do you address the sagittal deformities of the Case Example 2?

- a. Only provide forces on the "a" and "b" areas
- b. Only provide forces on the "c" and "d" areas
- c. Apply forces on the all "a", "b", "c", and "d" areas
- d. No force applied in the sagittal plane
- e. Somewhere else \_\_\_\_\_

Part 4: Please answer Q16-Q18 based on the Case Example 3.

Case example 3



- 15) In Case Example 3, where do you consider applying a corrective force in order to correct the lumbar curve?
- Along the paraspinal muscles in the lumbar region
  - Along the paraspinal muscles in the lumbar region, including the inferior margin of one or 2 ribs
- 16) What do you do when the C7 is decompensated to the left in the coronal plane as shown in Case Example 3?
- Build a trochanteric extension and pad on the right
  - Build a trochanteric extension and pad on the left
  - Apply more medially directed corrective force on the left axillary area with the counter-force on the right side of the thoracic area
  - Nothing, we are not treating C7 compensation
- 17) If a patient has a single primary curve, more than 35-degree Cobb angles, where the apex is located at or below T12/L1 such as Case Example 3, what is your orthotic recommendation?
- Provide TLSO with sternal bar
  - Provide TLSO without sternal bar
  - Nocturnal brace (Charleston or Providence)
  - Other \_\_\_\_\_

Part 5: Extra questions

- 18) If a patient has an upper thoracic curve (with at apex T2- T6) or cervico-thoracic curve (with at apex C7 -T1), what is your orthotic recommendation?
- Provide TLSO with sternal bar, without treating upper thoracic curve
  - Provide TLSO without sternal bar, without treating upper thoracic curve
  - Provide CTLSO, Milwaukee
  - Provide TLSO with some modification or TLSO attached with a trapezius sling
  - We cannot treat curves with a high thoracic apex in an orthosis

- 19) *If coronal balance is made worse (more decompensated) despite improved Cobb angle IN ORTHOSIS, is this acceptable?*
- No, it is a brace failure and must be addressed through adjustments or re-made*
  - Yes, it is OK as long as the Cobb angle is improved*
  - Sometimes, please explain: \_\_\_\_\_*
- 20) *When do you consider using a trochanter extension?*
- to address decompensation*
  - to accentuate leverage forces for lumbar curves*
  - Both a and b*
  - Other \_\_\_\_\_*
- 21) *What is your stance (or opinion) on pelvic obliquity, secondary to scoliosis, (and NOT a leg length difference)? (Choose all that apply)*
- It is often present but does not affect how I make my orthosis*
  - A good orthosis will level the hips when good biomechanical correction of the deformity is achieved*
  - A good orthosis will not necessarily level the hips, even when good biomechanical correction of the deformity is achieved*
  - Other (explain): \_\_\_\_\_*

The following section summarises the constructed survey questions. The first three questions (Q1-Q3) of the survey were for selecting the specific survey population and checking they were suitably qualified. For high-quality data, only certified orthotists or certified orthotists and prosthetists who had been treating AIS, full time for more than 2 years were selected, and considered as “experts”.

The next two (Q4 and Q5) were general questions related to orthotic treatment for AIS, rather than specific clinical cases. Q4 was for defining whether the orthotists had a 3-dimensional concept in the biomechanical orthotic treatment goals or not. The purpose of the Q5 was to obtain a consensus regarding the full time wearing hours of the orthosis recommended for the AIS patients of each scoliosis clinic where the qualified clinicians were working.

Three typical case examples were given for the next twelve questions. Case example 1, a typical right single thoracic curve, which is the most common curve type in AIS, was provided with its PA and lateral view radiographs for the next seven

questions (Q6 - Q12). Q6 and Q7 asked for the 3D placements of a primary corrective force and its coupled de-rotational corrective force for the transverse plane. Q8 and Q9 were questions for the coronal corrective forces. The purpose of these questions was to identify the level of a right thoracic pad and its counterforce on the left axillary area. Q10 was to examine the placement of optimal sagittal corrective forces applied to treat the thoracic hypo-kyphosis (thoracic flattening) which the case example 1 demonstrates. Q11 and Q12 asked about the necessity of an abdominal compression force and its counterforce in reducing lumbar lordosis such as the case example 1, which does not have any lumbar hyper-lordosis.

Q13 and Q14 were questions for another typical case example 2, which exhibits a double structure (right thoracic and left lumbar) curve with both thoracic hypokyphosis and lumbar hyper-lordosis. It's PA and lateral view radiographs were also provided. Q13 was especially designed to assess the 3D placements of a primary corrective force for the lumbar curve in transverse view. Q14 asked for the expert's opinion about how to address sagittal deformities in the thoracic and lumbar regions.

Case example 3, a single left lumbar curve was given with its PA and lateral view radiographs for Q15 to investigate the optimal placement of a primary corrective force for the lumbar curve. Q16 asked the expert's opinion for biomechanical design options for the case that has a C7 decompensation in the coronal view. Q17 asked for the design preference of experts for the case where the curve is more than 35 degrees.

The last four questions (Q18 - Q21) were chosen to examine the biomechanical corrective topics, which had not been covered in the previous specific case examples. Q18 asked for the experts' judgements and orthotic recommendations to treat a case of an upper thoracic curve (with at apex T2- T6) or cervico-thoracic curve (with at apex C7 -T1). Q19 asked experts treatment protocols regarding the importance of coronal balance in the orthosis for a case where coronal balance is made worse (more decompensated) despite an improved Cobb angle in orthosis. The survey also asked experts when they build a trochanteric extension into the orthosis(Q20). The last question, Q21, asked about the necessity for pelvic obliquity correction for a case that

a patient had pelvic obliquity due to secondary to AIS, but not from the leg length difference. As mentioned previously, all these questions were emerged from the initial consensus conference and also were validated by the selected scoliosis specialists before conducting the survey project.

### **4.3 The Original Manuscript of the Survey Project Submitted to JPO**

#### **CURRENT PRACTICE IN ORTHOTIC TREATMENT OF AIS**

Sun Hae Jang, MSc, CO, FAAOP, Kara L. Davis, MS, CPO, Scott D. Thach, MSPO,  
CO

#### **INTRODUCTION**

Adolescent Idiopathic Scoliosis (AIS) is the most common type of idiopathic scoliosis and a three-dimensional (3D) deformity of the vertebrae, spine, rib cage, and trunk.<sup>1,2</sup> Orthotic treatment is the most common conservative treatment for idiopathic scoliosis and provides 3D mechanical actions of corrective forces on the scoliotic vertebrae, spine, rib cage, and trunk in order to limit the extent of curve progression while awaiting skeletal maturation and to reduce the need for surgical intervention.<sup>3</sup>

What precisely constitutes an effective orthosis remains poorly understood, or at the very least, still elicits debates among orthotists regarding the best biomechanical principles. Some of these differences may be due to changing beliefs over time. Reducing the Cobb angle is generally still accepted as a gold standard of bracing success, though falls noticeably short of understanding the 3D component of scoliosis. Additionally, orthotic designs have changed through the decades, going from metal and leather, high profile designs, to more modern, under arm designs. There are also regional differences, where major scoliosis centers seem to bleed out general orthotic design beliefs on a proximity basis.

The current standard clinical practice and the biomechanical correction concepts of conservative treatment for AIS have not been clearly defined. Ongoing efforts to clarify and define both the orthotic terminology and biomechanics of adolescent idiopathic scoliosis have begun to lay the groundwork for what could eventually become best practice guidelines. In 2002, the American Academy of Orthotics and Prosthetics convened a State of the Science Conference which outlined basic understandings as well as identified shortcomings in current research regarding orthotic interventions.<sup>4</sup> While this served a great need and remains a gold standard,

thirteen years have passed and many advances have been made in the treatment of AIS. The SOSORT group has been a leader in the international community of the conservative treatment of scoliosis and has published several articles in the SOSORT journal that convey “expert” agreement in areas that cannot yet be defined by research.<sup>5-6</sup>

The purpose of this project was (1) to use a survey tool that polls expert opinions of experienced spinal orthotists to identify areas of agreement or disagreement regarding the current practice of orthotic treatment and the key biomechanical elements in treating AIS and (2) to share the literature review results of all topics identified with significant disagreement in the survey.

Several concepts were touched upon in the questionnaire that target some of the more controversial topics within the community. It is the belief of the authors that there is no strong evidence in the literature to support decision making in some of these areas, and so it would be of benefit to use popular belief of “experts” until more formal research can affirm or reject such concepts. The long-term goal would be to contribute towards a consensus statement on orthotic treatment of AIS. Consensus statements by definition are an agreed upon current best practice standard based upon scientific outcomes based evidence. Medicine in general does not always have the necessary scientific evidence to confirm a consensus and when such a situation arises, a poll of so-called “experts” that agree on a statement may be used.

## **METHODS**

This study used an online-based survey method. Twenty-one multiple choice style questions were developed for this study that focused on general concepts and typical radiographic case examples to target orthotic biomechanical concepts including some of the more controversial topics within the spinal orthotic community. The first three questions regarding experience and credentials were used to identify the subject’s qualification and to exclude those participants that did not fit the “expert” qualification. A total of 18 questions pertaining to the orthotic biomechanical corrective concepts in treating AIS were asked.

- Participant inclusion criteria: CO/CPO with scoliosis orthotic treatment experience of at least 2 years.
- Participant exclusion criteria: CO/CPO with no or less than 2 years of scoliosis orthotic treatment experience and/or non-CO/CPO or other healthcare professionals.

Participants for this survey project were recruited by sending a link for the online survey to the Spinal Orthotics Society (SOS) members of the American Academy of Orthotists and Prosthetists (AAOP) through a mass emailing system as a primary recruitment tool. The link was also posted on the SOS website. Other communities were also provided this link in order to invite other spinal orthotists in the spinal orthotic field who may not have been a part of the SOS mailing system. A consent form was attached to the first page of the online survey link. Before starting the survey, each participant gave their consent by selecting the “continue” button in the survey site. The survey was completed and the results were analyzed using Google Forms. The pie diagrams used in this paper were created through <https://www.meta-chart.com>.

If any participants provided their email address at the end of the survey to express their willingness to participate in a focus group meeting, the email address was removed from the data after receiving the survey response and prior to starting data analysis. Responses were then analyzed by quantifying how many people picked each multiple-choice option for the survey questions and identifying how many participants agreed or disagreed. Questions that had an agreement of 50% or more participants were classified as having reached general agreement. Those questions that had less than 50% agreement were selected to have a review of the literature conducted to fully analyze any knowledge published on the topic.

## **RESULTS**

A total of 50 people completed the survey. However, only 46 of the 50 participants qualified for participant inclusion criteria. Three contributors were not certified orthotists and one had less than 2 years of experience in orthotic treatment for AIS and were excluded.

A majority (67%) of the qualified participants had over 15 years of experience. 28% answered that they fit at least 2 corrective orthoses per month while 39% of participants fit more than one orthosis per week. In the clinics of 76% of the qualified participants, 18-23 hours was the prescribed wear schedule for a daytime or fulltime orthosis.

There was a clear consensus on 11 biomechanical orthotic correction topics where more than 50% of the participants chose a single answer. The results of this survey are presented in Figures 1-11.

Regarding the “choose all that apply” type question that asked for the biomechanical goals of the orthotic treatment, 63% of the participants chose “to reduce Cobb angle or coronal curvature in orthosis” as an important goal in achieving an optimal orthotic outcome while treating AIS. The second highest choice (61%) participants chose was “to align to the neutral alignment of the spine and trunk in all three planes”. “To realign sagittal misalignment” was picked by the least number of participants (41%). This data can be found in Table1.

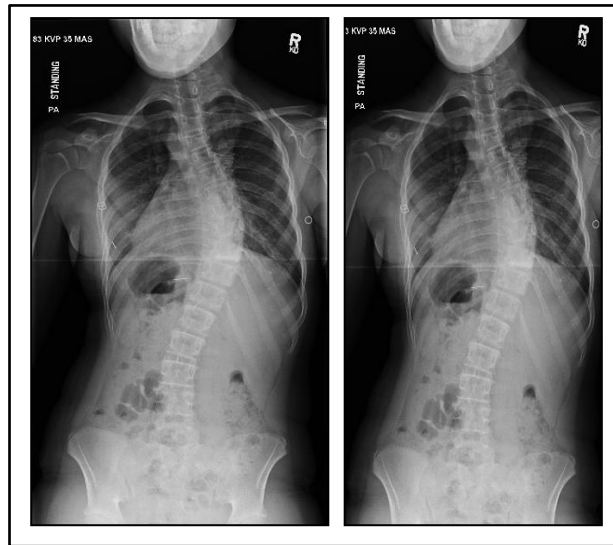
Biomechanical Goals of Orthotic Treatment	Agreement
To reduce Cobb angle or coronal curvature in orthosis	63%
To align to the neutral alignment of the spine and trunk in all three planes	61%
To de-rotate rotational deformity in the transverse plane	52%
To minimize spinal C7 decompensation in the coronal plane	50%
To realign sagittal misalignment	41%

**Table 1:** Results of choose all that apply question on biomechanical goals of orthotic treatment.

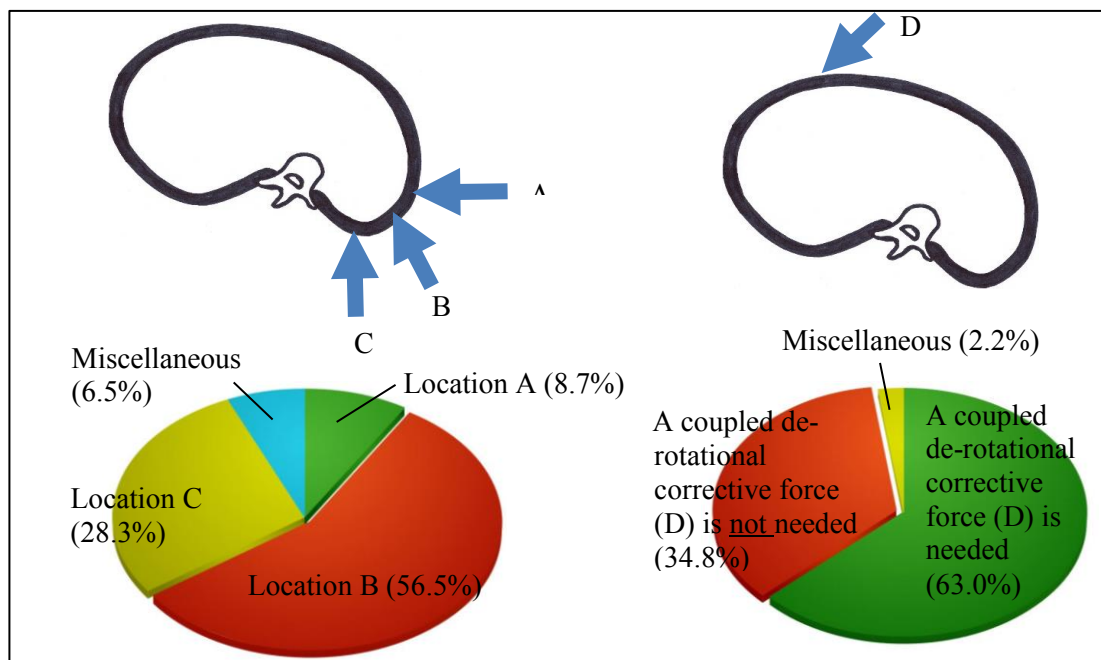
### Questions for Case Example 1: Single Thoracic Curve Type (Image 1)

Figure 1 shows the results of two survey questionnaires regarding the placement of a primary corrective force and its coupled de-rotation force for the thoracic curve in the transverse plane. 51% of the participants chose location “B” as the primary corrective force for Case Example 1 while 63% of the participants chose

to apply a coupled de-rotational corrective force “D” on the anterior part of the thoracic level as the secondary corrective force.



**Image 1:** Radiographs of Case Example 1 (Single Thoracic Curve)



**Figure 1:** Placement of a Primary Corrective Force and its Coupled De-rotational Force for the Thoracic Curve of Case Example 1 (Transverse View)

In Figure 2, the results are shown regarding a thoracic pad placement for Case Example 1, which inquired about the approximate locations of the pad as marked on

the PA radiograph. For this question, 39.1% of the participants selected “the superior edge of the pad should be placed on the rib attached at the apex of the thoracic curve”. However, a comparable number of participants (37%) also selected “the superior edge of the pad must extend to the apical vertebral level of the thoracic curve”. This is a similar pad placement as the middle of the pad places on the rib attached at the apex of the thoracic curve. Furthermore, 21.7% chose “the middle part of the pad should be placed on the apical vertebral level of the thoracic curve” that is a much higher pad placement than the two placements mentioned previously. As a result, this question failed to reach a clear agreement between the participants. However, regarding the left axillary area of Case Example 1, the majority (63%) considered building an axillary extension without a pad or a minor thickness pad for comfort while 34.8% chose an axillary extension with a pad (Figure 3).

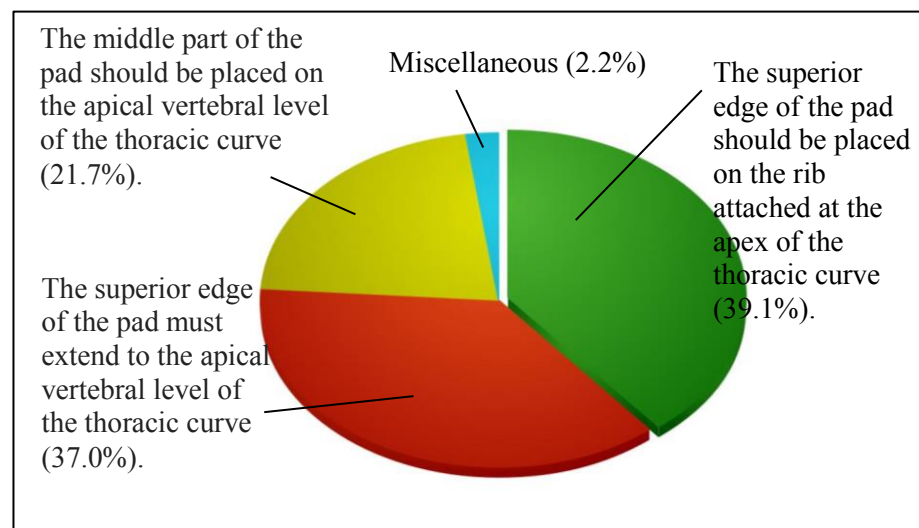


**Figure 2:** Level of a Thoracic Pad for Case Example 1 (Coronal View)

On the same case presentation, it also asked about the sagittal corrective forces for the thoracic hypokyphosis. Some participants (34.8%) said they do not apply any corrective force in the sagittal plane while 30.4% of participants indicated that they will apply corrective forces at the location of A and B like the image shown in Figure 4. In addition, we also asked opinions about the necessity of abdominal compression and lumbar lordosis reduction for Case Example 1 that had no lumbar structural curve and no lumbar hyperlordosis (Figure 5 and Figure 6). Some participants selected not

to apply abdominal compression (34.8%) and not to reduce a lumbar lordosis (45.7%) in the case example. On the other hand, some participants selected applying abdominal compression (37%) and reducing lumbar lordosis (21.7%) for all of cases not only for this case example. Others chose to apply abdominal compression (23.9%) and reduce lumbar lordosis (19.6%) only for this case example even though it does not have lumbar hyperlordosis. So, it can be concluded that most participants (37%) apply abdominal compression for all of the cases including this case example and they (45.7%) reduce lordosis for some cases not for this case example. However, these three questions were not clearly agreed amongst the participants.

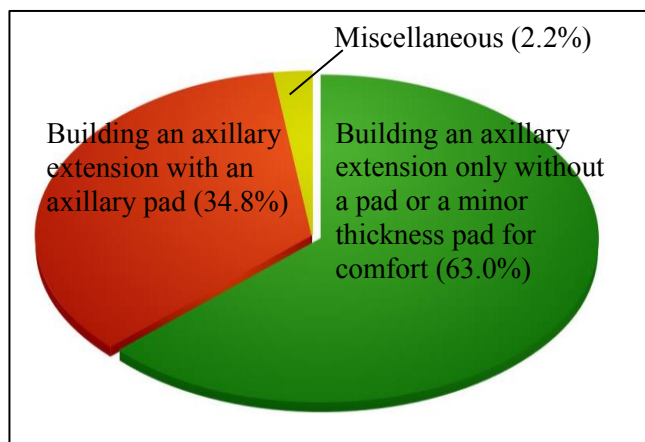


**Figure 3:** Recommend on the Left Axillary Area for Case Example 1

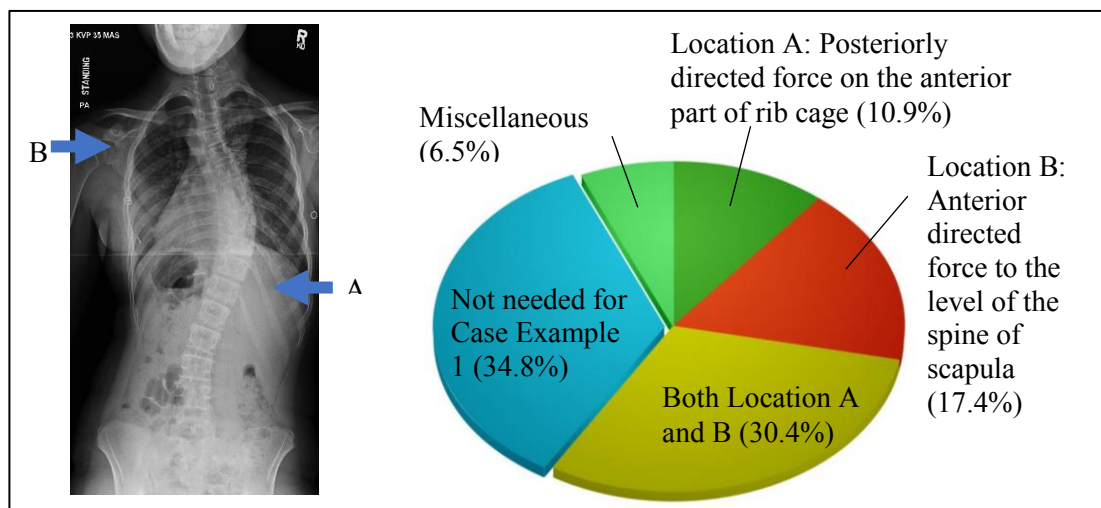


**Figure 4:** Placements of Sagittal Corrective Forces for a Thoracic Hypokyphotic Spine of Case Example 1

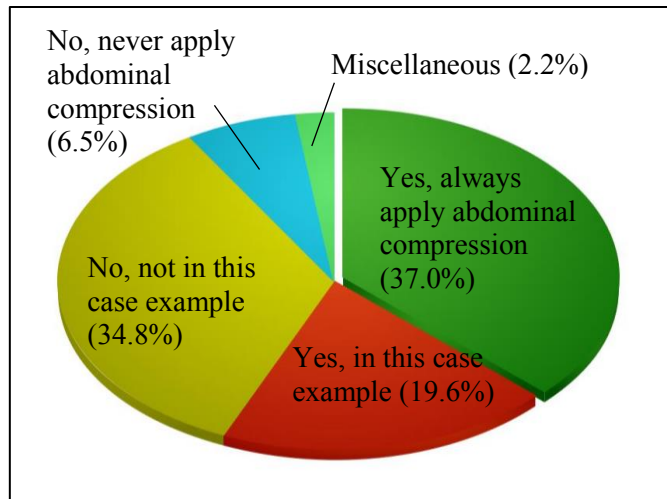


**Figure 5:** Necessity of Abdominal Compression for No Lumbar Curve Case (Case Example 1)

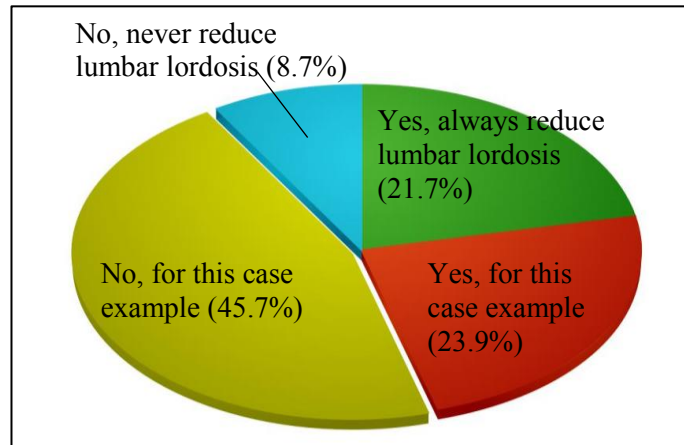


**Figure 6:** Necessity of Lumbar Lordosis Reduction for No Lumbar Hyperlordosis Case (Case Example 1)

### Questions for Case Example 2: Double Thoracic-Lumbar Curve Type (Image 2)

Regarding the placement of a primary corrective force for the lumbar curve, a majority (80.4%) selected “antero-medially directed force along the para-spinal muscles” (Figure 7). In addition, the results regarding the placements of sagittal corrective forces for Case Example 2 are shown in Figure 8. 56.5% of participants selected “apply forces on all A, B, C, and D areas”.

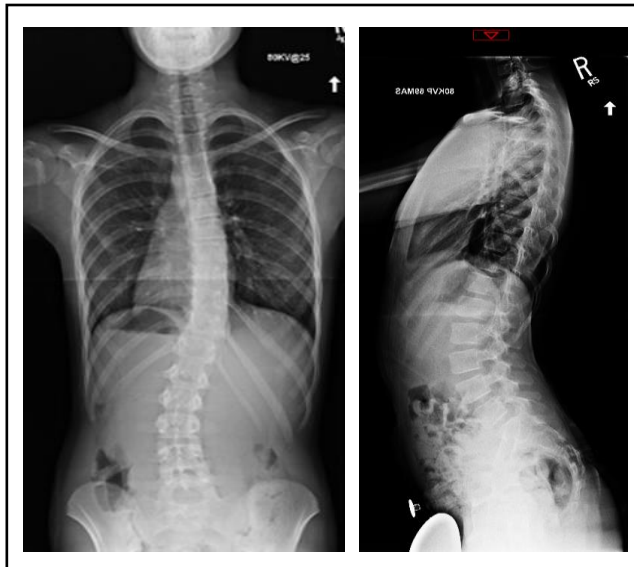


**Image 2:** Radiographs of Case Example 2 (Double Thoracic-Lumbar Curve)

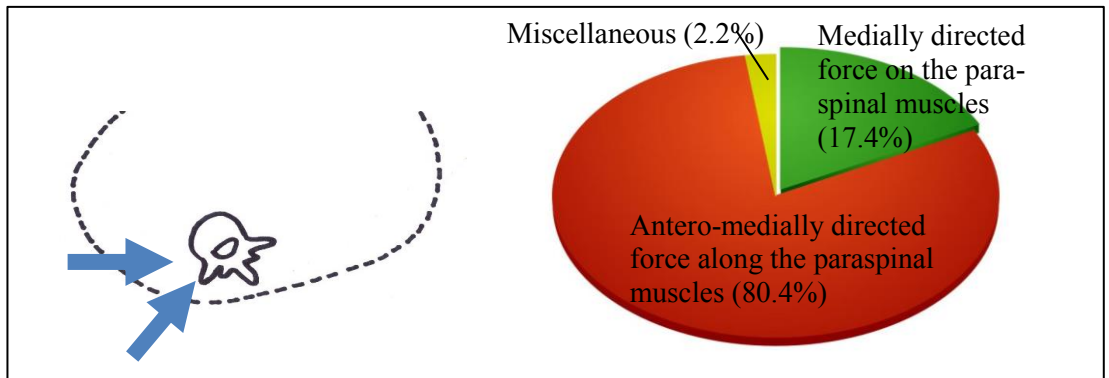


**Figure 7:** Placement of a Primary Corrective Force for the Lumbar Curve of Case Example 2

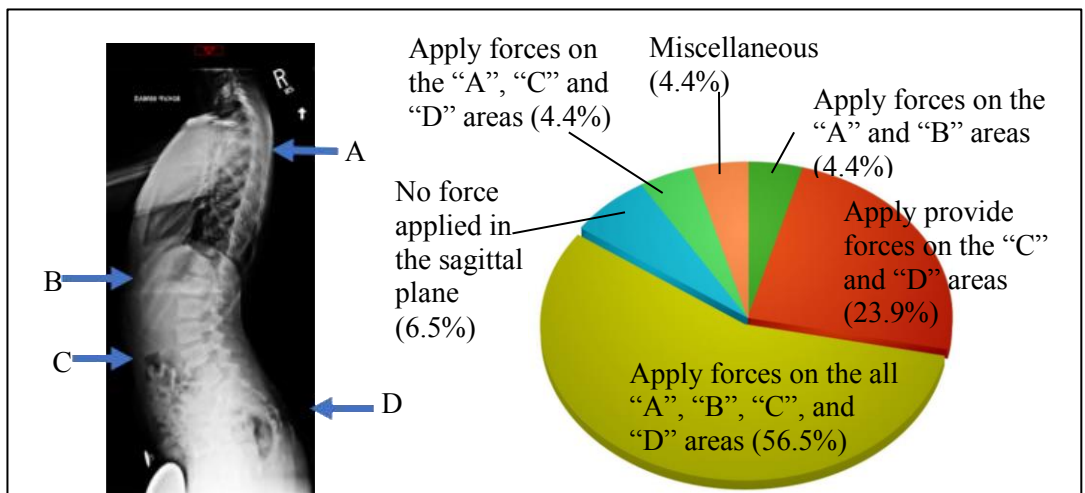


**Figure 8:** Placements of Sagittal Corrective Forces for Case Example 2

### Questions for Case Example 3: Single Lumbar Curve Type (Image 3)

The survey also inquired about the placement of the corrective force for a single lumbar curve case. The majority (65.2%) applied a corrective force along the para-spinal muscles in the lumbar region, while 34.8% of participants wanted to apply a force along the para-spinal muscles on the inferior margin of 1 or 2 ribs in addition to the lumbar region (Figure 9). For a case that has a left C7 decompensation like Case Example 3, 58% of participants chose to build a trochanteric extension and pad on the left side to improve the decompensation (Figure 10).



**Image 3:** Radiographs of Case Example 3 (Single Lumbar Curve)

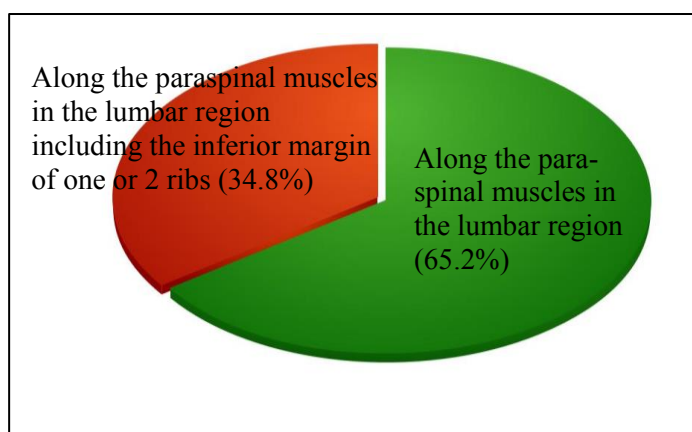


**Figure 9:** Placement of a Corrective Force for the Lumbar Curve for Case Example 3

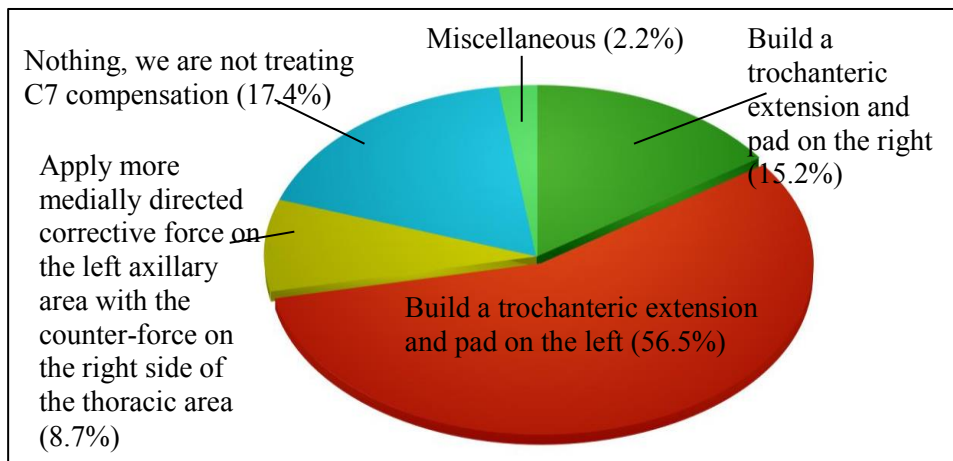


**Figure 10:** Treatment Option for a Left C7 Decompression

We also asked the participants about their opinions for treating a single lumbar curve with Cobb angles over 35 degrees. Some participants (45.7%) selected a TLSO without a sternal bar, which is classified as a low profile TLSO. However, 34.8% of participants chose a nighttime orthotic system (Figure 11).

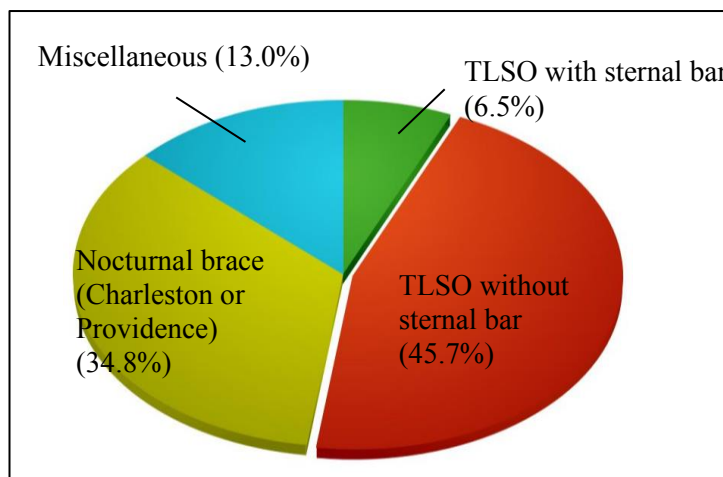


**Figure 11:** Orthotic Recommendation for Case Example 3 (a single primary curve, more than 35-degree Cobb angles, curve apex location at or below T12/L1)

### General Questions

We also asked participants about their opinions regarding their orthotic recommendation for an upper thoracic curve or cervico-thoracic curve cases. As shown in Figure 12, a clear agreement was not reached among these three options: CTLSO /

Milwaukee (37.0%), no treatment of upper thoracic curves with an orthosis (28.3%), and a TLSO with some modification or TLSO attached with a trapezius sling (26.1%).

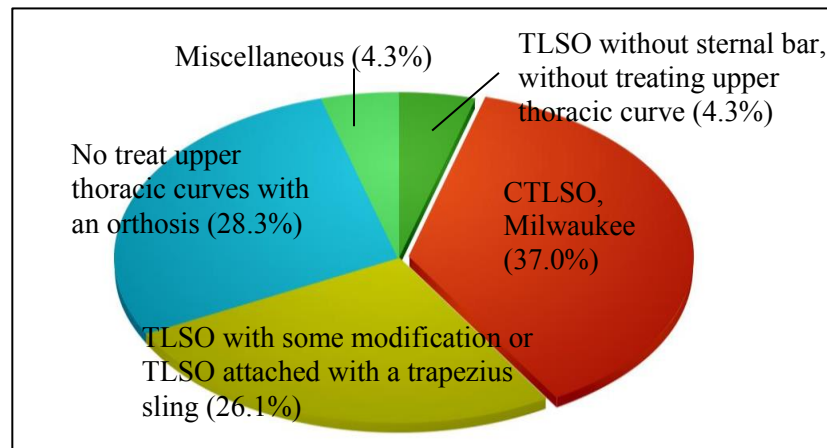


**Figure 12:** Orthotic Recommendation for Curvatures Apex at T2-T6 or C1-T1 Tilt

Regarding the opinion of “if coronal balance is made worse despite an improved Cobb angle in an orthosis”, 67.4% of the participants considered the result as an orthotic treatment failure and should adjust or re-make the orthosis (Figure 13). In Figure 14, 71.7% of participants used a trochanter extension to both address C7 decompensation and accentuate leverage forces for lumbar curves.

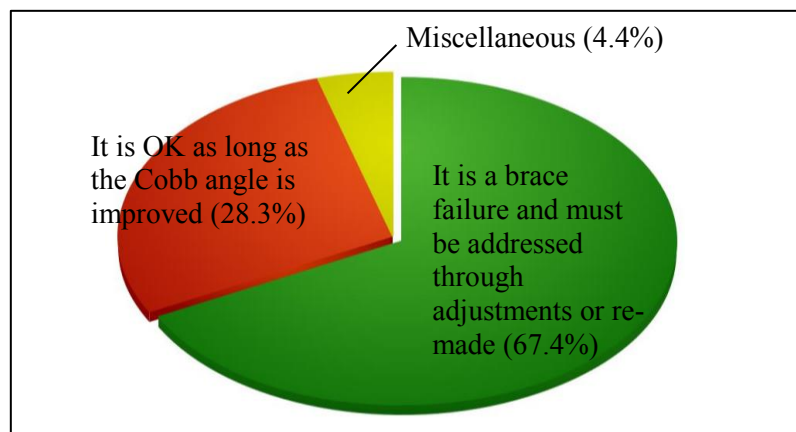


**Figure 13:** Professional Knowledge Question for Coronal Imbalance In-orthosis Despite Improved Cobb Angle

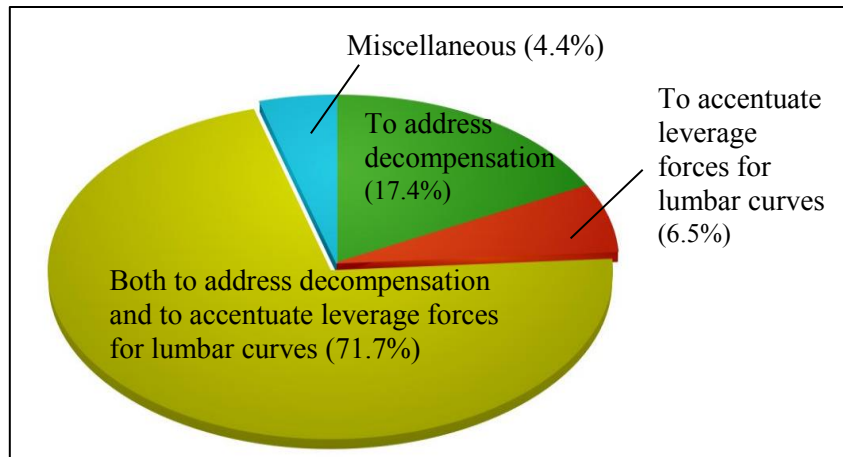


**Figure 14:** Purpose and Function of a Trochanter Extension

Regarding pelvic obliquity due to scoliosis, no clear agreement was obtained (Figure 15). 47.8% of participants chose “a good orthosis will not necessarily level the hips, even when good biomechanical correction of the deformity is achieved”. In contrast, 39.1% chose “a good orthosis will level the hips when good biomechanical correction of the deformity is achieved.

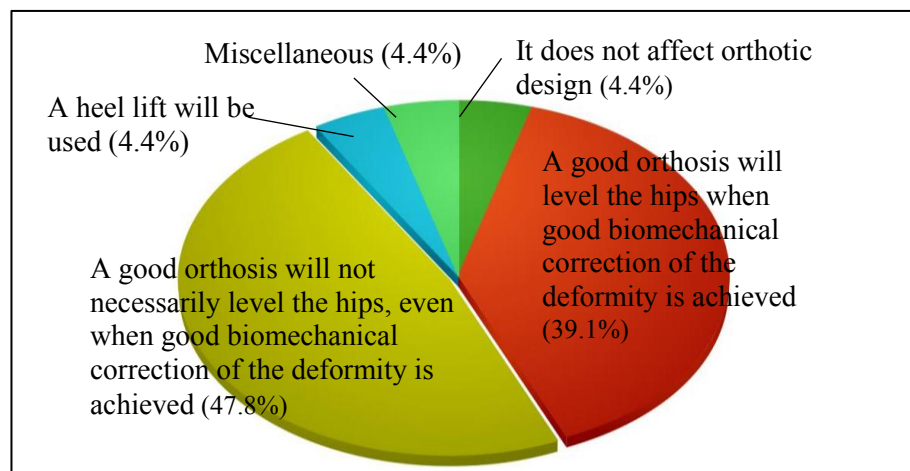


**Figure 15:** Treatment Option for Pelvic Obliquity, Secondary to Scoliosis

## DISCUSSIONS

The majority of participants considered reducing Cobb angle or coronal curvature in orthosis as well as aligning to the neutral alignment of the spine and trunk in all three planes as the most important orthotic biomechanical goal in treating AIS.

They selected coupled de-rotational forces as primary corrective forces for the thoracic curve and also selected a de-rotational force for the primary corrective force of the lumbar curve. Regarding recommendation for correction on the left axillary area, participants agreed to have an extension without any corrective force. For the placement of the lumbar corrective force, they selected applying a corrective force along the para-spinal muscles in the lumbar region only not including the inferior margin of one or two ribs. Four locations of the sagittal corrective forces for the double major curves case were agreed upon between participants. They also reached a clear agreement for the question regarding orthotic recommendations for the C7 decompensation. The majority of participants considered an orthotic treatment failure to occur if the spine (coronal view) is not balanced in-orthosis. To improve the coronal balance, they considered to build a trochanteric extension and pad on the left side. They also agreed that the purpose and function of a trochanteric extension are both to address decompensation and to accentuate leverage forces for lumbar curves.

However, there were 7 topics for which participants failed to find a clear agreement. The following are the 7 topics:

Topic 1: Thoracic pad placement

Topic 2: The placement of sagittal corrective forces for a thoracic hypokyphotic spine

Topic 3: Necessity of abdominal compression for no lumbar structural curve case

Topic 4: Necessity of lumbar lordosis reduction for no lumbar hyperlordosis case

Topic 5: Orthotic recommendations for apex at T2-T6 or C1-T1 tilt curvatures

Topic 6: Orthotic recommendations for a single primary curve, more than 35-degree Cobb angles, and curve apex location at or below T12/L1

Topic 7. Treatment options for pelvic obliquity, secondary to scoliosis

There exists a significant amount of disagreement on questions regarding the sagittal plane. Five questions focused on the sagittal plane (Q4, 10, 11, 12, and 14), yet only Q14 had a clearly agreed upon answer. Having such disagreement regarding all but one of the questions involving management of the sagittal plane also correlates with the low number of participants that felt in Q4 that a goal of orthotic treatment is “to realign the sagittal misalignment”. Q10 and Q14 presented very similar cases that would have required similar applied forces. However, the answers for Q10 and Q14

were very different. For Q10, most participants (35.6%) chose neither posteriorly directed or anteriorly directed corrective forces for a single mid-thoracic curve. For Q14, most participants (55.6%) chose all sagittal corrective forces for the case of a thoracic and lumbar combined double curve. These represent conflicting answers, suggesting that there is still a lack of understanding in the management of the sagittal plane.

Those 7 topics that had less than 50% agreement amongst participants were used to develop a literature review for a more critical look at what research may exist for each potential answer. The following inclusion criteria was used to select literature for the review:

- Studies related to idiopathic scoliosis and orthotic treatment
- Quantitative study
- Literature review article
- Descriptive paper, education materials and textbooks
- Studies published in any orthotic and prosthetic related journal

The following were excluded:

- Studies related to etiology, surgery, or physiotherapy
- Oral presentations
- Studies published prior to 1960
- Studies looking at a specific orthotic system

The results of literature review were as follows:

### **Topic 1: Placement of a Thoracic Pad for a Single Thoracic Curve**

In the “SOSORT Consensus Paper on Brace Action: TLSO Biomechanics of Correction”, the placement of the thoracic pad was also surveyed and the results were almost evenly divided. 52% of the participants chose the proper placement of a thoracic corrective pad at the apical vertebral level while 48% selected it at the level of the apical rib and below the apical vertebra.<sup>5</sup>

Table 2 showed one quantitative study and two other descriptive papers that supported that “the superior edge of a thoracic pad should be placed on the rib attached at the apex of the thoracic curve”, which 39.1% of participants had chosen to do in the survey.<sup>7-8</sup> In addition, Blount and Moe (1980) described in more detail in the book “The Milwaukee Brace” that a pad for thoracic curve correction should be placed on the ribs articulates on and distal to the apex while applying a force on the rib hump.<sup>10</sup> However, one study mentioned the best correction occurred when a pad is applied on the ribs originating from the apex as well as just above or below the apex.<sup>11</sup> The other study reported in their article that maximum stability of a thoracic curve can be achieved by placing the thoracic pad at the apex of the primary thoracic curve.<sup>10</sup> However, the article did not describe the detail of the pad placement (Table 2).

Articles and Books	Orthotic Type/System	Thoracic Corrective Pad Placement	Additional Correction Efforts
Andriacchi et al. (1976) <sup>11*</sup>	CTL SO	On the ribs originating from the apex including just above or below the apex	Additional traction method increases the correction.
Watts (1979) <sup>9</sup>	N/A	On the ribs originating from the apex and distal to the apex	A lifting force is needed on the rib cage.
Blount and Moe (1980) <sup>10</sup>	CTL SO	On the ribs originating from the apex and distal to the apex	Additional force on the rib hump increases the correction.
Laurien et al. (1983) <sup>8*</sup>	TL SO (Boston)	On the ribs originating from the apex and distal to the apex	
Patwardhan et al. (1996) <sup>12*</sup>	CTL SO and TL SO	On the rib originating from the apex	

**Table 2:** Literature review results for Topic 1: Placement of a Thoracic Pad for a Single Thoracic Curve. \* represents as quantitative studies.

Wong et al (2012) found that different locations of corrective pads can affect curve correction in the orthosis.<sup>13</sup> They put pads at 5 different locations: the prescribed location, 1cm above, 2cm above, 1cm below and 2cm below the level. The article falls short of stating an ideal level, but if 1 cm increments make enough difference to alter in-orthosis correction in a statistically significant manner, that verifies that determining the appropriate level for the corrective force is critical.

## **Topic 2: Sagittal Correction Force Placements for the Thoracic Hypokyphotic Spine**

Evidence was found to support the need for both a posteriorly directed force (a) on the anterior part of rib cage and an anterior directed force and (b) approximate to the level of the spine of the scapula for the thoracic hypokyphotic spine.

Several articles suggested that if someone has a thoracic coronal curve like Case Example 1, a force of forward flexion (anteriorly directed force) exists on the lower thoracic area in the sagittal thoracic spine, causing the sagittal thoracic spine to become relatively more vertically straight (thoracic hypokyphotic spine).<sup>12-13</sup> In order to correct the deformity, a posteriorly directed corrective force is needed on the anterior part of rib cage, as well as an anteriorly directed force on the spine of the scapula to act as a counter force of the posteriorly directed force. Lonstein (1996) also mentioned that if thoracic hypokyphosis exists, orthotic treatment should focus on preventing an increase of the hypokyphosis and also suggested having an anterior gusset on the anterior part of the rib cage.<sup>14</sup>

## **Topic 3 & Topic 4: The Necessity of Abdominal Compression and Lumbar Lordosis Reduction for Cases of No Lumbar Hyperlordosis**

Abdominal compression has the function of increasing intra-abdominal pressure for axial spinal unloading and is also related to reducing lumbar lordosis. Blount and Moe (1980) stated that abdominal compression stabilizes the lumbar spine and reduces lumbar lordosis by improving the grasp on the pelvis.<sup>10</sup> Carlson (2003), Blount and Moe (1980), and Udén and Willner (1983) agreed that abdominal compression makes a lumbar corrective pad work more effectively by loosening the tightened posterior structure of the lumbar spine if the patient has a structural lumbar curve.<sup>10,15,16</sup>

In regards to reducing lumbar lordosis in instances of no lumbar hyperlordosis, Watts (1979) recommended reducing lumbar lordosis for all cases of curve types even though there was no hyperlordosis in the lumbar spine.<sup>9</sup> The article also mentioned that reducing the lordosis can help reduce the Cobb angle of both lumbar and thoracic

curves. However, most articles do not recommend the unnecessary lumbar lordosis reduction accompanying abdominal compression for the cases of single thoracic scoliosis curves similar to Case Example 1. Kotwicki and Cheneau (2008), and Carlson (2003) mentioned that a lumbar lordosis reduction tended to reduce thoracic kyphosis and eventually reinforce the hypokyphotic thoracic spine.<sup>18, 17</sup> This was due to the fact that there was a strong positive correlation between thoracic kyphosis and lumbar lordosis.<sup>18, 19</sup> Therefore, reduction of lumbar lordosis is not necessary if someone has a thoracic curve because it makes the sagittal aspect of the entire spine straighter vertically and flatter.<sup>20, 21</sup> The reduced lumbar lordosis and its compensatory thoracic hypokyphosis can result in excessive or abnormal compressive forces and shear stresses on the vertebral structures and the discs of the spine.<sup>22</sup>

In addition, there have been many studies that considered the risks of excessive abdominal compression. Kennedy et al. (1987) reported that the spinal orthosis can cause restricted movement of the chest and abdomen.<sup>23</sup> Refsum et al. (1990) also found that in the short term, wearing a spinal orthosis can reduce vital capacity, expiratory volume, and total lung capacity while wearing an orthosis.<sup>24</sup> They concluded that a tightly fitted orthosis at the abdomen could cause several risks such as: displace the abdominal content into the chest, restrict the downward movements of the diaphragm and compress the rib cage. Ueyoshi and Shima (1985) also suggested that excessive abdominal compression for a long time may cause visceral disorders.<sup>25</sup> They recommended avoiding excessive abdominal pressure as much as possible when fabricating a spinal orthosis. Compression of the abdominal viscera is an invariable companion of a properly fitting TLSO, and increased intra-gastric pressure may result in reflux esophagitis.<sup>26</sup> However, more recently Yaszay et al. (2016) found that reduced thoracic kyphosis is correlated with decreased pulmonary status.<sup>27</sup>

#### **Topic 5: Orthotic Recommendations for Apex at T-T6 or C7-T1 Tilt Curvatures**

Evidence shows that scoliosis curvatures with an apex at T8 or above often require the CTLSO.<sup>8, 28, 29</sup> It is because a lateral head restraint and a shoulder ring are necessary to control a cervico-thoracic curve and a trapezius pad is necessary to control a high thoracic curve.<sup>32</sup> Although a CTLSO may be indicated in curves above T8,

apical vertebra up to T6 treated with a TLSO has also been reported.<sup>8,32,30</sup> In only the biomechanical aspect, treatment with a CTLSO should be the optimal option for curves having apices between T2 and T6. However, the survey results showed that 27.3% of participants provide a TLSO instead of a CTLSO after modifying and attaching a trapezius sling. The reason may be due to low patient compliance with a CTLSO design. A summary is shown in Table 3.

Articles and Books	Orthotic type	Intervention
Ogilvie (1995) <sup>32</sup>	Cervicothoracic Curve	Shoulder Ring and Head Restraint
Ogilvie (1995) <sup>32</sup>	High thoracic Curve	Trapezius pad
Laurnen et al. (1983) <sup>8</sup> and Jonasson-Rajala et al. (1984) <sup>32</sup>	Above T6	CTLSO
Laurnen et al. (1983) <sup>8</sup> , Bussel et al. (1995) <sup>31</sup> , and Ogilvie (1995) <sup>32</sup>	At T8 or above	CTLSO

**Table 3:** Literature review results for Topic 5: Orthotic Recommendations for Apex at T2-T6 or C7-T1 Tilt Curvatures.

### **Topic 6: Orthotic Recommendations for a Single Primary Curve, More Than 35 Degree Cobb Angles, Curve Apex Location at or below T12/L1**

Nocturnal orthoses (Charleston or Providence) may be ruled out for single lumbar/thoraco-lumbar curvatures that have more than 35-degree Cobb angles based on the following: Yrjönen et al. (2006) reported in their comparison study between the Boston orthotic type vs. the Providence orthotic system that the Providence night time orthosis may be good for curves less than 35 degrees in lumbar and thoracolumbar curves.<sup>31</sup> In “A Comparison Between the Boston Brace and the Charleston Bending Brace in Adolescent Idiopathic Scoliosis” by Katz et al. (1997), the Charleston orthotic system was recommended for the treatment of smaller single thoracolumbar or single lumbar curves.<sup>32</sup> It was also found that curves greater than 35 degrees increase more when treating with the Charleston orthotic system than a day-time TLSO<sup>35</sup>. D'Amato et al. (2001) also founded the effectiveness of the Providence Brace if the curve is less than 35 degrees.<sup>33</sup> However, the authors

mentioned in the article that their clinic usually add a daytime TLSO if a curve is more than 35° and curve progression is noticed. One article reported that a low-profile TLSO (a CTLSO girdle without superstructures) is a possible option because the result showed a 50-60% correction in-orthosis.<sup>34</sup>

### **Topic 7: Treatment Options for Pelvic Obliquity, Secondary to Scoliosis, but NOT from a Leg Length Difference**

Pelvic obliquity without a leg length difference is usually attributed to pelvic rotation due to scoliosis.<sup>38</sup> Based on this, it is apparent that pelvic obliquity can be reduced if the pelvic rotation is controlled by an orthosis. In addition, with respect to pelvic obliquity secondary to limb-length inequality, Lenke et al. (2001) reported that if pelvic obliquity is less than 2cm, no specific treatment intervention is needed and if it is more than 2cm, either a shoe lift or heel lift is prescribed for the short limb.<sup>39</sup> From this, it can be concluded that if the pelvic obliquity is less than 2cm, no matter if pelvic obliquity came from a true leg length difference or resulted from scoliosis, no specific treatment may be necessary.

## **CONCLUSIONS**

There was agreement found on 11 biomechanical orthotic correction topics (where more than 50% of participants chose a single answer). There were 7 topics for which participants failed to find a clear agreement (less than 50% of participants) in regards to current practice in the orthotic treatment of AIS. The most disagreement occurred on questions regarding treatment of the sagittal plane. Some areas of disagreement were clarified through the literature review. However, it was still unclear as to where the placement of a thoracic pad for a single thoracic curve should be. Most of the literature consisted of clinical observational studies or general concept descriptive papers. More quantitative investigations are still necessary in order to understand biomechanical correction concepts for treating AIS with an orthosis. Until then, orthotists should follow generally defined biomechanical correction concepts, IS deformities, and spinal biomechanics rather than relying on manufacturing systems or private regional systems.

## REFERENCES

1. Ahn UM, Ahn NU, Nallamshetty L, et al. The etiology of adolescent idiopathic scoliosis. *Am J Orthop Belle Mead NJ*. 2002;31(7):387-395.
2. Lowe TG, Edgar M, Margulies JY, et al. Etiology of idiopathic scoliosis: current trends in research. *J Bone Joint Surg Am*. 2000;82-A(8):1157-1168.
3. Richards BS, Bernstein RM, D'Amato CR, Thompson GH. Standardization of criteria for adolescent idiopathic scoliosis brace studies: SRS Committee on Bracing and Nonoperative Management. *Spine*. 2005;30(18):2068-2075; discussion 2076-2077.
4. American Academy of Othotist and Prosthetist. Point of Consensus: Orthosis Biomechanics. *J Prosthet Orthot*. 2003;15(4s):s46-s48.
5. the members of SOSORT, Rigo M, Negrini S, et al. "SOSORT consensus paper on brace action: TLSO biomechanics of correction (investigating the rationale for force vector selection)." *Scoliosis*. 2006;1(1). doi:10.1186/1748-7161-1-11.
6. de Mauroy J, Weiss H, Aulisa A, et al. 7th SOSORT consensus paper: conservative treatment of idiopathic & Scheuermann's kyphosis. *Scoliosis*. 2010;5:9. doi:10.1186/1748-7161-5-9.
7. Negrini S, Aulisa AG, Aulisa L, et al. 2011 SOSORT guidelines: Orthopaedic and Rehabilitation treatment of idiopathic scoliosis during growth. *Scoliosis*. 2012;7:3. doi:10.1186/1748-7161-7-3.
8. Laurnen EL, Tupper JW, Mullen MP. The Boston brace in thoracic scoliosis. A preliminary report. *Spine*. 1983;8(4):388-395.
9. Watts HG. Bracing in spinal deformities. *Orthop Clin North Am*. 1979;10(4):769-785.
10. Blount W, Moe J. The Technique of Nonoperative Management. In: *The Milwaukee Brace*. 2nd ed. Williams & Wilkins; 1980:59-118.
11. Andriacchi TP, Schultz AB, Belytschko TB, Dewald R. Milwaukee brace correction of idiopathic scoliosis. A biomechanical analysis and a retrospective study. *J Bone Jt Surg Am*. 1976;58(6):806-815.
12. Patwardhan AG, Gavin TM, Bunch WH, et al. Biomechanical Comparison of the Milwaukee Brace (CTLSO) and the TLSO for Treatment of Idiopathic scoliosis. *J Prosthet Orthot*. 1996;8(4):115-122.
13. Wong MS, Li M, Ng B, et al. The effect of pressure pad location of spinal orthosis on the treatment of adolescent idiopathic scoliosis (AIS). *Stud Health Technol Inform*. 2012;176:375-378.
14. Dickson RA, Lawton JO, Archer IA, Butt WP. The pathogenesis of idiopathic scoliosis. Biplanar spinal asymmetry. *Bone Jt J*. 1984;66(1):8-15.
15. Bridwell KH, Betz R, Capelli AM, Huss G, Harvey C. Sagittal plane analysis in idiopathic scoliosis patients treated with Cotrel-Dubousset instrumentation. *Spine*. 1990;15(9):921-926.
16. Burwell RG. Aetiology of idiopathic scoliosis: current concepts. *Pediatr Rehabil*. 2003;6(3-4):137-170. doi:10.1080/13638490310001642757.
17. Lonstein JE. Chapter 17 Scoliosis. In: Lovell WW, Winter RB, Morrissy RT, Weinstein SL, eds. *Lovell and Winter's Pediatric Orthopedics*. Philadelphia: Lippincott Williams & Wilkins; 1996.
18. Carlson JM. Clinical Biomechanics of Orthotic Treatment of Idiopathic Scoliosis - Journal of Prosthetics and Orthotics, 2003 | American Academy of Orthotists &

- Prosthetists. [http://www.oandp.org/jpo/library/2003\\_04S\\_017.asp](http://www.oandp.org/jpo/library/2003_04S_017.asp). Accessed August 20, 2016.
19. Udén A, Willner S. The effect of lumbar flexion and Boston Thoracic Brace on the curves in idiopathic scoliosis. *Spine*. 1983;8(8):846-850.
  20. Kotwicki T, Cheneau J. Biomechanical action of a corrective brace on thoracic idiopathic scoliosis: Cheneau 2000 orthosis. *Disabil Rehabil Assist Technol*. 2008;3(3):146-153. doi:10.1080/17483100801905744.
  21. Wong MS, Mak AF, Luk KD, Evans JH, Brown B. Effectiveness and biomechanics of spinal orthoses in the treatment of adolescent idiopathic scoliosis (AIS). *Prosthet Orthot Int*. 2000;24(2):148-162.
  22. Clément J-L, Geoffray A, Yagoubi F, et al. Relationship between thoracic hypokyphosis, lumbar lordosis and sagittal pelvic parameters in adolescent idiopathic scoliosis. *Eur Spine J Off Publ Eur Spine Soc Eur Spinal Deform Soc Eur Sect Cerv Spine Res Soc*. 2013;22(11):2414-2420. doi:10.1007/s00586-013-2852-z.
  23. Scholten PJ., Veldhuizen AG, Grootenboer HJ. Stability of the human spine: a biomechanical study. *Clin Biomech*. 1988;3(1):27-33. doi:10.1016/0268-0033(88)90121-0.
  24. Carlson BB, Burton DC, Asher MA. Comparison of trunk and spine deformity in adolescent idiopathic scoliosis. *Scoliosis*. 2013;8(1):1.
  25. Jean L. Analysis of the Dynamic Sagittal Balance of the Lumbo-Pelvi-Femoral Complex. In: Klika V, ed. *Biomechanics in Application*. INTECH Open Access Publisher; 2011:221-246. <https://www.intechopen.com/books/biomechanics-in-applications/analysis-of-the-dynamic-sagittal-balance-of-the-lumbo-pelvi-femoral-complex>. Accessed December 29, 2017.
  26. Kennedy JD, Robertson CF, Olinsky A, Dickens DR, Phelan PD. Pulmonary restrictive effect of bracing in mild idiopathic scoliosis. *Thorax*. 1987;42(12):959-961.
  27. Refsum HE, Naess-Andresen CF, Lange JE. Pulmonary function and gas exchange at rest and exercise in adolescent girls with mild idiopathic scoliosis during treatment with Boston thoracic brace. *Spine*. 1990;15(5):420-423.
  28. Ueyoshi A, Shima Y. Studies on spinal braces. With special reference to the effects of increased abdominal pressure. *Int Orthop*. 1985;9(4):255-258.
  29. Kling TF, Drennan JC, Gryboski JD. Esophagitis complicating scoliosis management with the Boston thoracolumbosacral orthosis. *Clin Orthop*. 1981;(159):208-210.
  30. Yaszay B, Bastrom TP, Bartley CE, Parent S, Newton PO. The effects of the three-dimensional deformity of adolescent idiopathic scoliosis on pulmonary function. *Eur Spine J Off Publ Eur Spine Soc Eur Spinal Deform Soc Eur Sect Cerv Spine Res Soc*. 2017;26(6):1658-1664. doi:10.1007/s00586-016-4694-y.
  31. Bussel M, Merritt J, Fenwick L. Spinal Orthoses. In: Redford JB, Basmajian JV, Trautman P, eds. *Orthotics: Clinical Practice and Rehabilitation Technology*. New York: Churchill Livingstone; 1995:71-101.
  32. Ogilvie JW. Orthotics. In: Lonstein JE, Winter RB, Bradford DS, Ogilvie JW, eds. *Moe's Textbook of Scoliosis and Other Spinal Deformities*. W.B. Saunders; 1995.
  33. Jonasson-Rajala E, Josefsson E, Lundberg B, Nilsson H. Boston thoracic brace in the treatment of idiopathic scoliosis. Initial correction. *Clin Orthop*. 1984;(183):37-41.

34. Yrjönen T, Ylikoski M, Schlenzka D, Kinnunen R, Poussa M. Effectiveness of the Providence nighttime bracing in adolescent idiopathic scoliosis: a comparative study of 36 female patients. *Eur Spine J Off Publ Eur Spine Soc Eur Spinal Deform Soc Eur Sect Cerv Spine Res Soc*. 2006;15(7):1139-1143. doi:10.1007/s00586-005-0049-9.
35. Katz DE, Richards BS, Browne RH, Herring JA. A comparison between the Boston brace and the Charleston bending brace in adolescent idiopathic scoliosis. *Spine*. 1997;22(12):1302-1312.
36. D'Amato CR, Griggs S, McCoy B. Nighttime bracing with the Providence brace in adolescent girls with idiopathic scoliosis. *Spine*. 2001;26(18):2006-2012.
37. Watts HG, Hall JE, Stanish W. The Boston brace system for the treatment of low thoracic and lumbar scoliosis by the use of a girdle without superstructure. *Clin Orthop*. 1977;(126):87-92.
38. Gum JL, Asher MA, Burton DC, Lai S-M, Lambart LM. Transverse plane pelvic rotation in adolescent idiopathic scoliosis: primary or compensatory? *Eur Spine J*. 2007;16(10):1579-1586. doi:10.1007/s00586-007-0400-4.
39. Lenke LG, Betz RR, Harms J, Bridwell KH, et al. Adolescent idiopathic scoliosis: A new classification to determine extent of spinal arthrodesis. *J Bone Joint Surg Am*. 2001;83(8):1169-1181.

#### 4.4 Discussion and Conclusion

##### *Strengths and Weaknesses of the Study:*

One of strengths in this study is that the survey represented an population adequate enough to validate the collected data. To determine the “expert” qualification, the selection guideline for the sample size was utilized from the recommendation of the international Society on Scoliosis Orthopaedic and Rehabilitation Treatment (SOSORT), “*Guidelines on "Standards of management of idiopathic scoliosis with corrective braces in everyday clinics and in clinical research": SOSORT Consensus 2008*” (Negrini et al., 2009). Thus, only data collected from the forty-six qualified participants were analysed even though fifty people completed the survey. Three participants out of the 50 did not have either a credentialed orthotist or orthotist/prosthetist designation, and one participant had been treating AIS for less than 2 years. Thus, forty-six participants were considered as the “experts” for this survey in the orthotic treatment for AIS. Additionally, the majority (67.4%) of the participants each had over 15 years of experience. All qualified participants had at least 5 years of experience. Most participants answered that they fit at least one corrective orthosis weekly or bi-weekly. 39% of participants said they fit more than one orthosis per week. This inclusion criterion also met the SOSORT definition of the “experts”.

In addition, when conducting the survey, there were approximately sixty active SOS members. The facts that the data were collected from the forty-six people among this specific population and the qualified participants were also working at various scoliosis clinics located across all places in the USA showed the strong representativeness of the sample. The data reflects the consensus of current agreed practices in America.

After the data was collected through the survey, a focus group meeting was organized during the 42<sup>nd</sup> Academy Annual Meeting and Scientific Symposium held in March, 2016 (Orlando, FL, USA) to obtain detailed qualitative data from scoliosis experts and clinicians regarding the areas of disagreement identified through the survey project. Thus, the data could be considered as representing the expert opinions of experienced spinal orthotists regarding the current practice of orthotic treatment and

the key biomechanical elements in treating AIS.

The weakest point of this survey was the demographic limit. The survey link was sent out to spinal orthotists who have been working in the USA. So, the collected data represented the current practice of orthotic treatment only within the USA.

***Key Findings from the Survey and Literature Review:***

There were 7 topics for which participants failed to find a clear agreement due to less than 50% of agreement. However, there was agreement on 11 biomechanical orthotic correction topics where more than 50% of participants chose a single answer. The following topics were where participants failed to find clear agreement between experts:

Topic 1: Thoracic pad placement

Topic 2: The placement of sagittal corrective forces for a thoracic hypokyphotic spine

Topic 3: Necessity of abdominal compression in a case where there was no lumbar structural curve

Topic 4: Necessity of lumbar lordosis reduction in a case where there was no lumbar hyperlordosis

Topic 5: Orthotic recommendations for apex at T2-T6 or C1-T1 tilt curvatures

Topic 6: Orthotic recommendations for a single primary curve, more than 35-degree Cobb angles, and curve apex location at or below T12/L1

Topic 7. Treatment options for pelvic obliquity, secondary to scoliosis

Among these topics, Topic 1, Topic 2, Topic 3 and Topic 4 were specifically related to biomechanical corrective forces which should be applied by a scoliosis orthosis, while Topic 5, Topic 6 and Topic 7 were about orthotic device options or recommendations. Three topics (Topic 2, Topic 3, and Topic 4) among the four related to biomechanical corrective forces in the sagittal plane.

For each of these topics, a literature review was also conducted to find out whether there was any scientific evidence in these as secondary sources. For Topic 1, most

studies supported the statement that “the superior edge of a thoracic pad should be placed on the rib attached at the apex of the thoracic curve or placed on one or two levels caudal to the apex”. Evidence for Topic 2 showed that force (a) is necessary in orthotic treatment for the thoracic hypokyphotic spine with the counter force (b). These articles did not mention a posterior directed force applied on the anterior part of the thoracic region. However, they motioned one of the coupled de-rotational forces, which is a posterior-laterally directed force applied on the anterior part of the thoracic area. Topic 3 and 4 should be combined together. Abdominal compression has the function of superimposing a longitudinal stretch on the lumbar and thoracic spines by increasing intra-abdominal pressure, and is also related to reducing lumbar lordosis. Most articles regarding this combined topic proposed that if someone has a thoracic scoliosis curve similar to this case, unnecessary reduction of lumbar lordosis including abdominal compression is contraindicated.

However, none of the conclusions above, from the literature evidence were obtained from scientifically valid, quantitative investigations. Thus, it could be concluded that more quantitative investigations are necessary to understand biomechanical correction concepts for treating AIS with an orthosis. Three biomechanical topics that were necessary to be defined through future studies were:

- (a) Where should the superior level of a thoracic corrective force be applied, on the apical vertebra level or at the apical rib of a thoracic curve?
- (b) Does a de-rotational force need to be applied for a single thoracic curve in addition to an anterior-medially directed force, which is the primary thoracic corrective force?
- (c) Is reducing a lumbar lordosis necessary as a primary corrective force for a lumbar or a thoracolumbar curve?

These questions, identified through the survey and literature review, provided the fundamental motives and direction in developing a new 3D non-invasive spinal alignment assessment tool, and also the purpose for developing the corresponding 3D spinal alignment parameters used to quantify AIS deformities through this thesis. The

results also contributed the research questions and rationale of the future study, “Optimal Corrective Force Placements of Spinal Orthoses in Treating AIS,” which would be conducted using the assessment tool and parameters developed throughout this thesis.

**Chapter 5. Radiographic Spinal Alignment Parameters  
System and Radiographic Spinal Misalignment  
Analyses for Adolescent Idiopathic Scoliosis**

## **5.1 Introduction**

For this thesis, two spinal alignment parameter systems were developed to quantify the spinal misalignment and deformities of AIS. These systems were based on the AIS spine's misalignment characteristics of the spinal segments and the neutral spine's specific biomechanical properties. One set are a radiographic spinal alignment parameters (RSAPs) system, which can quantify the coronal and sagittal 2D spinal misalignment of AIS through radiographic analysis, which is the focus of this chapter. The second set are parallel parameters based on motion capture.

In this chapter, the design and developmental rationale of the radiographic spinal alignment parameters (RSAPs) are described and details of the measurement methods for these RSAPs are also explained. This chapter also introduces a study aimed to determine whether RSAPs are useful in quantifying 2D AIS misalignment and examine whether these 2D measures adequately reflect 3D AIS misalignment.

To achieve these goals, the relationship between sagittal and coronal misalignment patterns was tested using RSAPs. It was also investigated whether RSAPs can define the sagittal misalignment patterns of the AIS spinal column. Finally, the defined sagittal misalignment patterns were compared with a classification of typical coronal curve types based on the apex of the curves. This is the most commonly used gold standard coronal misalignment classification method, achieved through the radiographic analyses of the posterior-anterior (PA). The experiment used coronal and sagittal spinal radiographs, taken from the 100 AIS patients.

## **5.2 Design Rationale of The Spinal Alignment Parameters for AIS**

### **5.2.1 Functions and Neural Alignment of Spine**

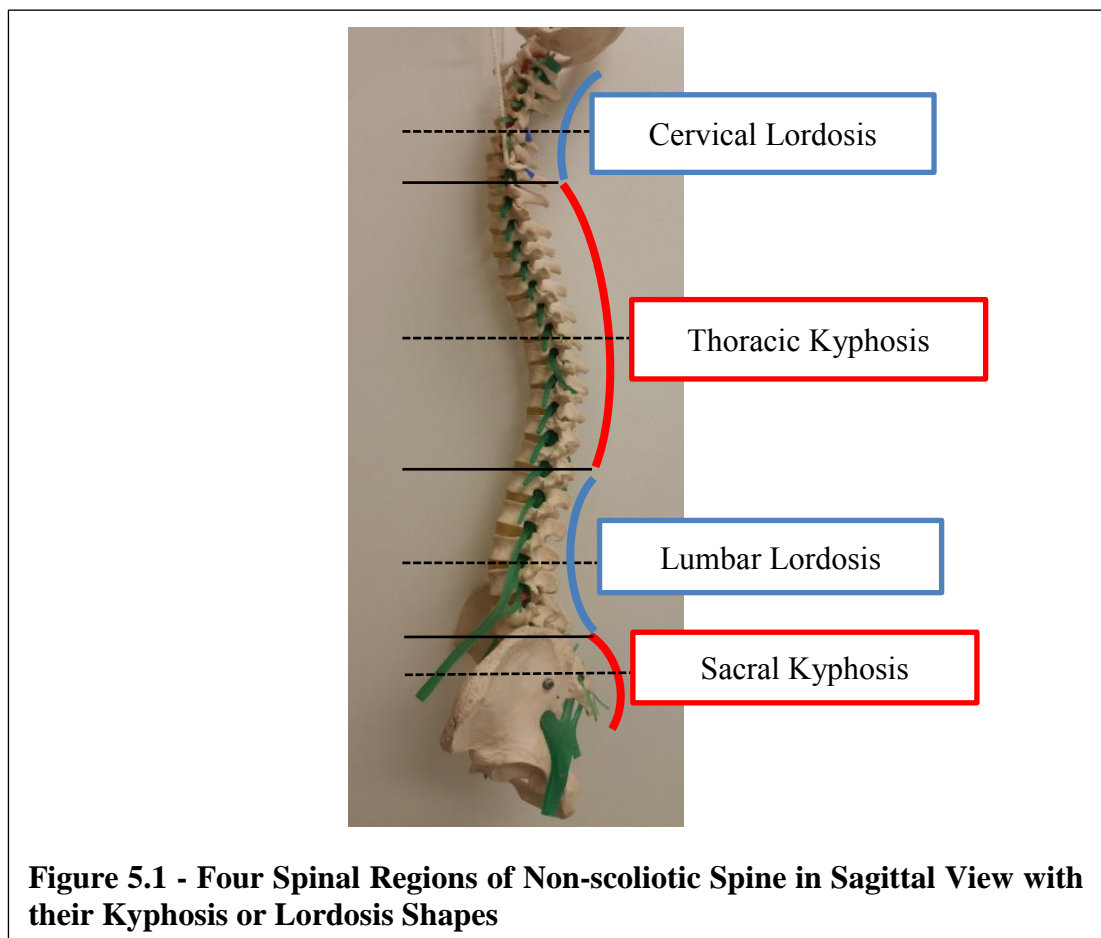
A human spine is a complex and flexible structure. However, it is also a strong and stable mechanical structure. The spine supports the upright body including the head through the spinal column while balancing over the pelvis and lower limbs during for example standing (Kapandji, 1970). It also controls the torso and neck movements and protects the spinal cord, nerve roots, and internal organs.

The functional part of the spinal column consists of 33 vertebrae (7 cervical vertebrae, 12 thoracic vertebrae, 5 lumbar vertebrae, 5 sacral vertebrae, and 4 coccygeal vertebrae) and 23 intervertebral discs in the spine (Dalton, 2011). The spine is divided into five regions. The cervical region consists of 7 vertebrae located in the neck area, labelled C1-C7. The thoracic region consists of 12 vertebrae (labelled T1-T12), while the lumbar region has 5 vertebrae (labelled L1-L5). The superior vertebra of the thoracic region (T1) connects with the last cervical vertebra (C7), and the last thoracic vertebra (T12) connects with the superior vertebra of the lumbar region (L1). The sacrum which is a large and solid bone formed by the fusion of the sacral vertebra S1–S5, is located inferior to the lumbar region and attached to the coccyx and the pelvis. The coccyx (tailbone) formed by fusing four coccygeal vertebrae, is a small bone attached to the inferior part of the vertebral column (Dalton, 2011).

The cervical spine produces a wide multi-directional range of flexion, extension, lateral bending, and rotary cervical motions. The thoracic vertebrae contribute little to thoracic flexion, extension, or lateral bending motion because of rib cage restrictions. The greatest spinal movement in the thoracic region is rotary motion due to the oblique orientation of the thoracic facet joints. In the lumbar spine, there is very little rotary motion, but the spine exhibits a greater range in flexion, extension, and lateral bending motion than the thoracic spine due to the vertical orientation of the lumbar facet joints (White & Panjabi, 1990).

From the coronal view, the spine appears as a straight vertical column when standing, and the line of gravity (LoG), which passes through the middle of the nose, the midlines of the sternum, umbilicus, and symphysis pubis, is in line with the spine. From the sagittal view, the upright bipedalism of humans contributes to unique sagittal structural features and alignment of each spinal region that produce two different C-shaped spinal curvatures (Kuntz, 2013; Bernhardt and Bridwell, 1989; Kapandji, 1970) (Figure 2.1). The posteriorly convex C-shape curves are called “Kyphosis”, which is found in the thoracic and sacral regions. The anteriorly convex C-shape curves are called “Lordosis” and are found in the cervical and lumbar regions. Each kyphosis

or lordosis curvature also consists of two types of segments based on the sagittal vertebral inclination slope (tilt) orientation: anteriorly tilted and posteriorly tilted segments (Figure 5.1). Therefore, the three spinal regions can be divided into six different segments. The vertebrae of the lower cervical, upper thoracic, and lower lumbar segments, are anteriorly tilted respectively and produce anteriorly directed shear forces. However, the vertebrae of the upper cervical, lower thoracic, and upper lumbar segments, are posteriorly tilted respectively and can produce posteriorly directed shear forces on those segments (Castelein and Veraart, 1992; Castelein et al., 2005; Kouwenhoven et al., 2007; Schlösser et al., 2015).



During standing, the LoG passes just posterior to C4 and C5, anterior to the thoracic region, just posterior to L3, and through S1 in the sagittal view. So, in the non-scoliotic spine, the cervical and lumbar regions are located anterior to the LoG producing external extension moments whereas the thoracic and sacral regions are placed posterior to the LoG, yielding external flexion moments.

It has been shown that there are significant differences in the degree of vertebral tilt and the anterior-posterior direction of the spinal curvature in the sagittal plane between the non-scoliotic and scoliotic spines (Castelein and Veraart, 1992). Clinically, the loss of natural kyphosis and lordosis in the sagittal plane, and the changes of the relationship between the LoG and the spinal segments, are often observed in the full spine lateral (sagittal) radiograph.

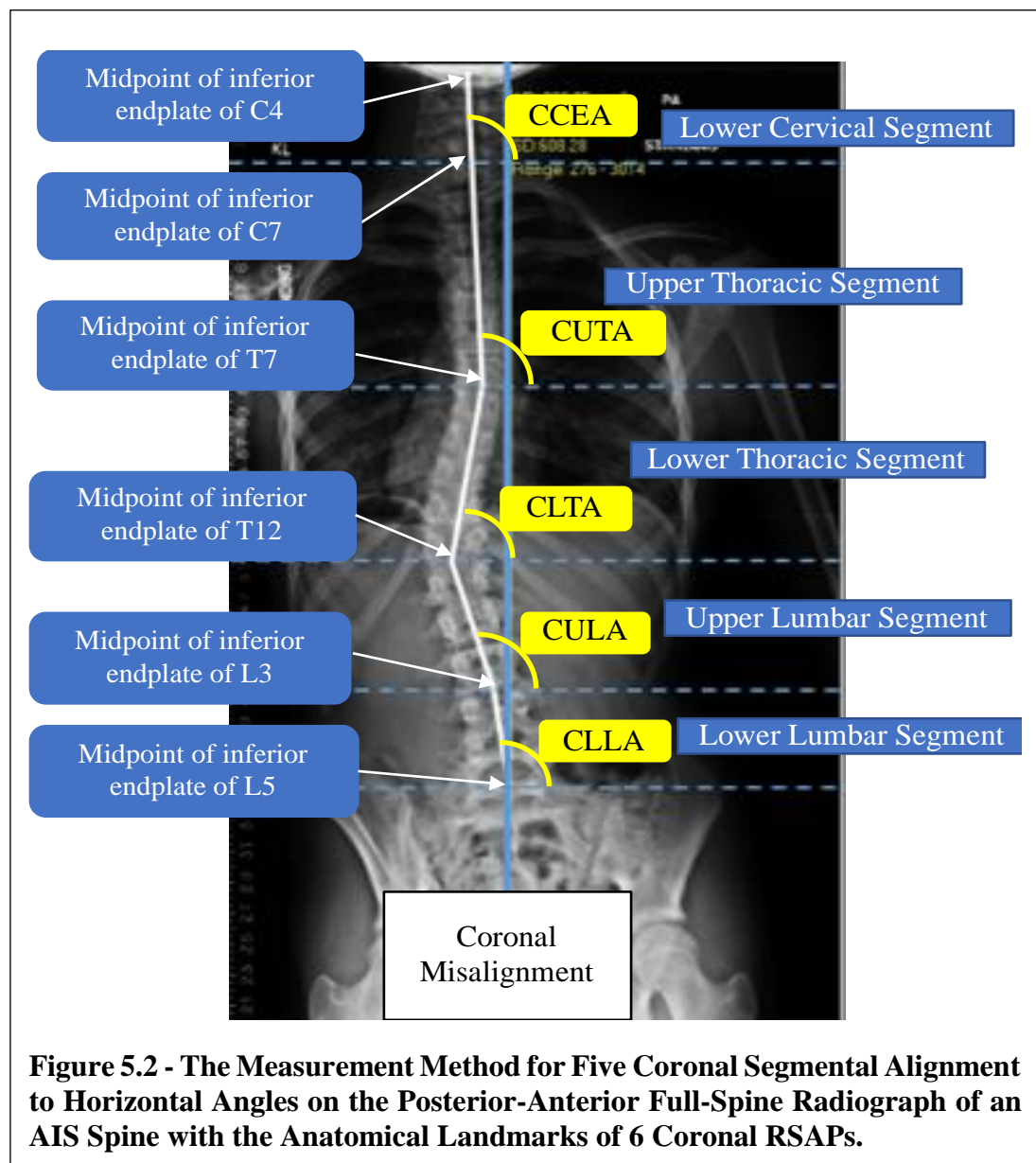
### 5.2.2 Radiographic Spinal Alignment Parameters

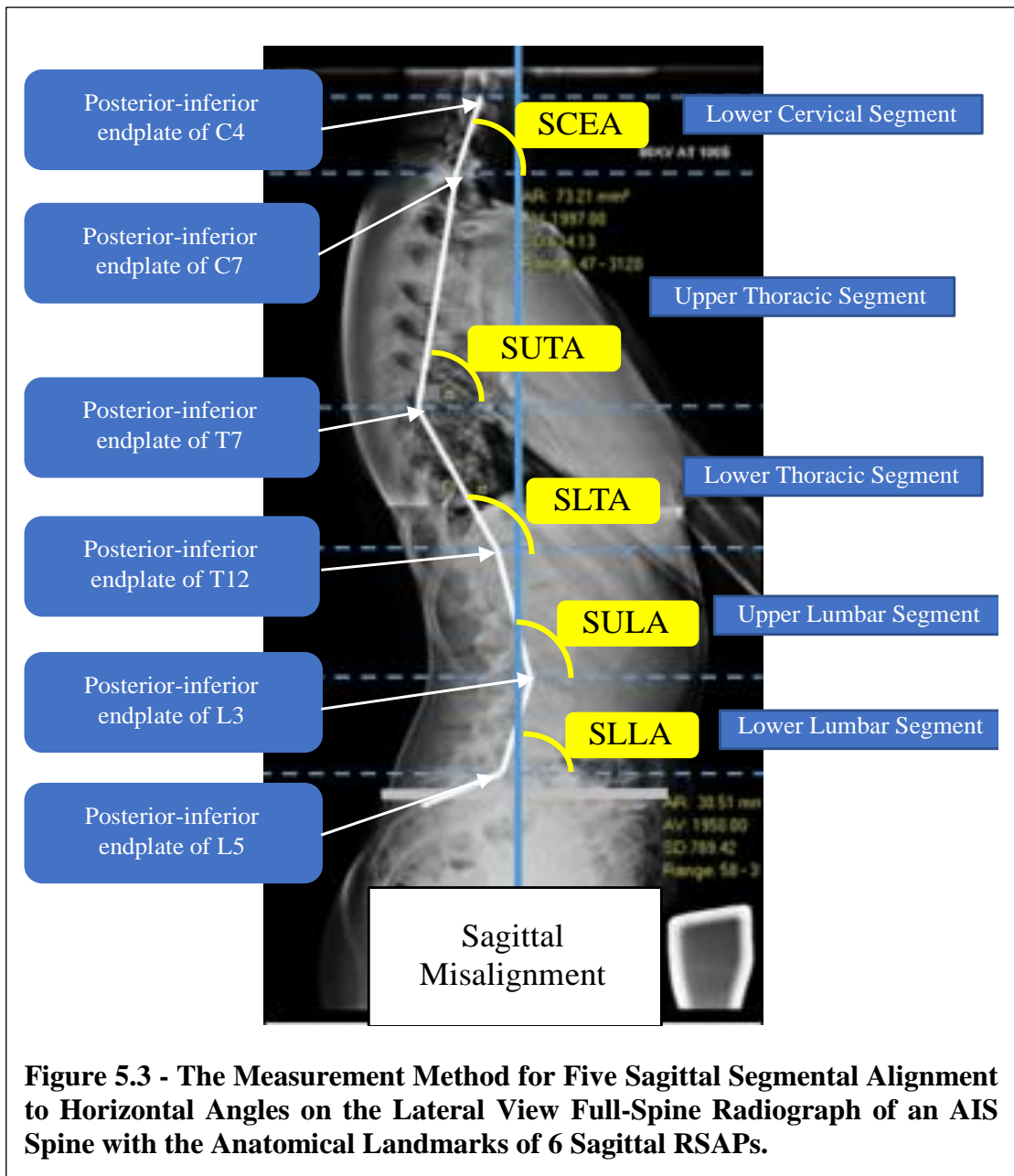
Typically, only a PA radiograph is taken in the clinic and this coronal plane view is assessed using the Cobb angle method in which coronal curve types are classified based on the apex of the curves. This is inadequate for a 3D study of the spine; hence a new method was proposed in this study. The radiographic spinal alignment parameters system (RSAPs) was developed. The system reflects the 3D osseous structural characteristics of a human's erect spine as well as the unique features in each spinal bony structural segment and uses the landmarks of vertebral bodies seen on both the coronal and sagittal plane radiographs. Thus, RSAPs consist of five sagittal and five coronal spinal alignment parameters, which can be used for radiographic evaluation of spinal alignment. The values of these parameters are determined by measuring each segmental alignment's angles related to a global horizontal line in two planes using both a PA full spine radiograph (coronal) and a lateral full spine radiograph (sagittal). Only five of the six spinal segments (the lower cervical, upper thoracic, lower thoracic, upper lumbar, and lower lumbar segments), were of interest in use for developing the parameters for quantifying AIS misalignment because a scoliotic curve does not occur in the upper cervical segment and sacrum. The other reason is that an upper cervical segment and sacrum are not usually detected through a full spine PA radiograph taken in the scoliosis clinic for the purposes of diagnosis, outcome measurement for orthotic treatment and surgical intervention of AIS.

The following are the ten radiographic spinal alignment parameters (RSAPs) developed: *Coronal Lower Cervical Alignment to Horizontal Angle (CCEA)*, *Coronal*

*Upper Thoracic Alignment to Horizontal Angle (CUTA), Coronal Lower Thoracic Alignment to Horizontal Angle (CLTA), Coronal Upper Lumbar Alignment to Horizontal Angle (CULA), Coronal Lower Lumbar Alignment to Horizontal Angle (CLLA), Sagittal Lower Cervical Alignment to Horizontal Angle (SCEA), Sagittal Upper Thoracic Alignment to Horizontal Angle (SUTA), Sagittal Lower Thoracic Alignment to Horizontal Angle (SLTA), Sagittal Upper Lumbar Alignment to Horizontal Angle (SULA), and Sagittal Lower Lumbar Alignment to Horizontal Angle (SLLA)*

Figure 5.2 and Figure 5.3 show coronal and sagittal misalignments of the spinal column connected with all 10 RSAPs including the measuring method and anatomical landmarks of RSAPs on the PA and lateral radiographs.





### 5.3 Materials and Methods

#### 5.3.1 Subjects

This was a retrospective study that used a series of paired PA, standing, full-spine radiographs and lateral view, standing, full-spine radiographs taken at the same time point for 100 patients. The subjects were randomly selected from the pool of patients with confirmed adolescent idiopathic scoliosis seen at the scoliosis clinic in Gillette

Children's Specialty Healthcare located in St. Paul, Minnesota, USA between 2005 and 2012. The 100 randomly selected pairs of spinal radiographs (one PA and one lateral view from each patient) satisfied the following conditions: patient must be 10 years or older when the radiograph was taken, have a Risser value of 0–2, have a primary curve angle of 20°–50°, and have had no prior orthotic treatments for scoliosis. Any radiographs, even if they met medical conditions, were excluded when: patients had leg-length discrepancies of more than 2cm, any deformities of the lower extremities, and any surgical procedures on the lower extremities or spine to rule out other possible misdiagnosis for postural scoliosis.

This study obtained ethics approval through the Institutional Review Board of the University of Minnesota, located in Minneapolis, Minnesota, USA, which is affiliated with the ethics committee at Gillette Children's Specialty Healthcare for the data collection portion of the study. The approval for the data analysis was done through an agreement with Eastern Michigan University, located in Ypsilanti, Michigan, USA.

### 5.3.2 Outcome Measures

#### **Radiographic Spinal Alignment Parameters:**

The five sagittal and five coronal RSAPs were measured on the PA and lateral view, standing, full-spine radiographs of 100 AIS patients through the *Carestream Picture Archiving and Communication System* (PACS) digital-imaging program as previously shown in Figure 5.2 by one operator.

#### **Three Sagittal Deviation Angles:**

In addition to the sagittal RASPs, three sagittal deviation angles were also recorded. These angles denoted the deviation of three key anatomical landmarks (C4/5, T7/8, L3/4) of the cervical lordosis, thoracic kyphosis, and lumbar lordosis curvatures from the Sagittal Central Sacral Line (SCSL). The SCSL is a vertical line drawn from the midpoint of S1. The midpoint of the S1 is the most reliable point of reference and has the additional benefit that the LoG in the sagittal plane passes through it when standing.

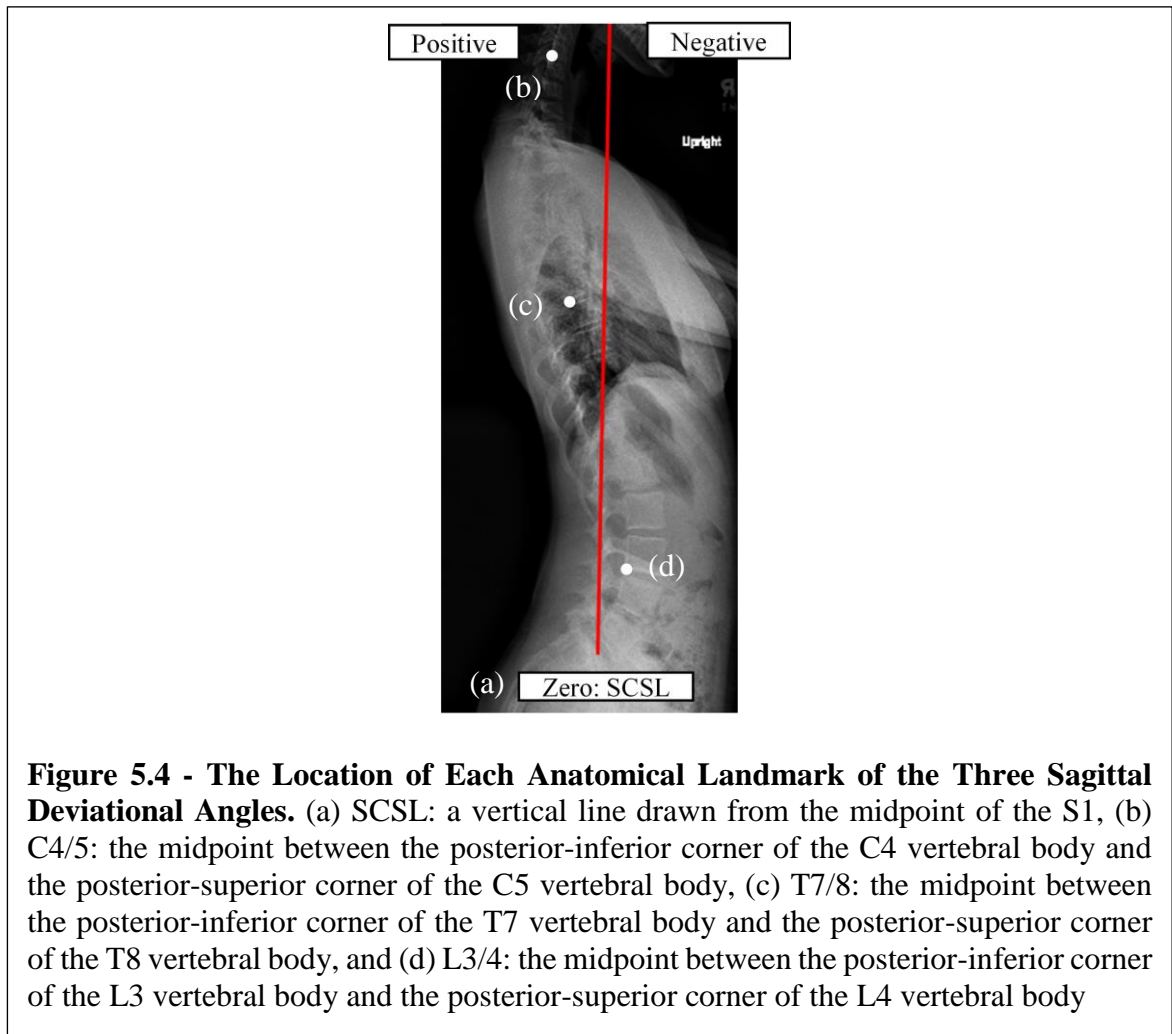


**Figure 5.4 - The Location of Each Anatomical Landmark of the Three Sagittal Deviational Angles.** (a) SCSL: a vertical line drawn from the midpoint of the S1, (b) C4/5: the midpoint between the posterior-inferior corner of the C4 vertebral body and the posterior-superior corner of the C5 vertebral body, (c) T7/8: the midpoint between the posterior-inferior corner of the T7 vertebral body and the posterior-superior corner of the T8 vertebral body, and (d) L3/4: the midpoint between the posterior-inferior corner of the L3 vertebral body and the posterior-superior corner of the L4 vertebral body

Figure 5.4 shows the exact location of each anatomical landmark for the three sagittal deviational angles and the SCSL. The descriptions of the three sagittal deviational angles are:

- *SAC4 (Sagittal Angle of C4): Sagittal deviational angle between the SCSL and the C4/5. This is a sagittal C4 decompensation angle which is represented as a spinal balance.*
- *SAT7 (Sagittal Angle of T7): Sagittal deviational angle measured between the SCSL and the T7/8*
- *SAL3 (Sagittal Angle of L3): Sagittal deviational angle measured between the SCSL and the L3/4*

If there is no misalignment in the spine and the spine has ideal alignment, the SAC4 and SAL3 should be close to “0” and the SAT7 should have a positive value. If any key anatomical landmark is located anterior to the SCSL, the measurement was marked as a negative value; if it was located on the SCSL, the measurement was marked as a zero (neutral) value; and if it was located posterior to the SCSL, it was marked as a positive value.

### 5.3.3 Deformity Classification

The 100 lateral view radiographs were also sorted into distinct sagittal misalignment patterns by grouping the combinations of the positive, negative, or zero values of the SAC4, SAT7, and SAL3.

Next, the 100 coronal view radiographs were classified into the eight accepted coronal curve patterns depending on the location of the apical vertebra of the coronal curve (Kotwicki, 2008; Lonstein, 1996). For example, a lower cervical/upper thoracic curve was determined if the apex was between the C7 and T5 levels, a middle thoracic curve if the apex was between T6 and T9, a lower thoracic curve if the apex was between T9/10 and T11/12, a thoracolumbar curve if it was at T12, L1 or T12/L1, and a lumbar curve if it was between L2 and L4. The curves were further classified by single major curve, double curve, or triple curve type.

### 5.3.4 Data Analysis

Correlation matrices were constructed using Pearson correlation coefficients to measure the strength of a linear association between the sagittal and coronal spinal parameters and discover any general relationships between the segments and were tested for significance with an  $\alpha$  of 0.05 using the *IBM SPSS Statistics* analysis software (Appendix 5.1).

The measurements of the five sagittal alignment parameters for each sagittal misalignment pattern sorted by the combinations of the positive, negative, or zero values of the SAC4, SAT7, and SAL3 were analyzed statistically and the descriptive

statistics, tests of normality, and two-sample tests were performed using IBM SPSS Statistics Version 25 software (IBM Corporation, Armonk, NY, United States) (Appendix 5.2). Most of the comparisons yielded normal distributions, but 4 out of 35 did not have normal distributions due to their limited sample size. Thus, both parametric tests (two-tailed t-test) and non-parametric tests (two-tailed Mann-Whitney U test) were performed to identify distinct sagittal alignment patterns by comparing each sorted pattern with the “the least misaligned or the closest to neutrally aligned type” among the patterns. The designation of this type was done by “close to zero” values for SAC4 and SAL3 and positive values for SAT7. Statistical significance for all testing was set with an  $\alpha$  of 0.05. Other forms of descriptive statistics are also presented in appendix 5.3 and 5.4. In addition, Microsoft Excel was used to illustrate the coronal and sagittal misalignment patterns.

#### **5.4 Results**

The average age of the 100 randomly selected AIS patients (97 females and 3 males) was 12.6 years old. Table 5.1 presents the correlation matrix between each sagittal and coronal segmental alignment to horizontal angles, which was performed in order to discover any general relationships between the segments in a plane and between the two anatomical planes. In the sagittal plane, there was a strong positive correlation between SUTA and SCEA. SULA also had positive correlations with SLTA and SLLA. In the coronal plane, CUTA had negative correlations with CLTA, CULA, and CLLA. CLLA also had negative correlations with CUTA and CLTA, but had a positive correlation with CULA. For the relationships between sagittal misalignment and coronal misalignment patterns, CLTA had a negative correlation with SCEA. SUTA had a positive correlation with CUTA and negative correlations with CULA and CLLA. While CLLA had a negative correlation with SUTA, it had positive corrections with SLTA and SULA.

Seven major sagittal misalignment patterns were identified. Table 5.2 shows the mean and standard deviation for the measurements of the five sagittal spinal alignment parameters by each sagittal misalignment pattern type. It also displays the results of the non-parametric two-sample tests performed in order to verify whether each sagittal

misalignment type is distinct by comparing the mean values of the sagittal spinal alignment parameters for Type 1 (the least misaligned or the closest to neutrally aligned type) with the means for Type 2, Type 3, Type 4, Type 5, Type 6, and Type 7.

Coronal/ Sagittal SAPs	<b>Correlation Between Sagittal and Coronal Spinal Alignment Parameters</b>									
	Pearson Correlation Coefficient (r)									
	* Correlation is significant at the 0.05 level (2-tailed), n=100									
	SCEA	SUTA	SLTA	SULA	SLLA	CCEA	CUTA	CLTA	CULA	CLLA
SCEA	1									
SUTA	*0.58	1								
SLTA	0.08	0.11	1							
SULA	0.09	-0.08	*0.38	1						
SLLA	0.13	-0.07	-0.10	*0.48	1					
CCEA	-0.18	-0.09	0.03	-0.04	-0.12	1				
CUTA	0.17	*0.29	-0.10	-0.14	0.17	-0.02	1			
CLTA	*-0.24	-0.11	-0.04	-0.07	-0.08	-0.09	*-0.53	1		
CULA	-0.05	*-0.27	0.05	0.13	-0.01	0.13	*-0.60	-0.09	1	
CLLA	0.01	*-0.28	*0.24	*0.28	-0.06	0.01	*-0.32	*-0.28	*0.64	1

**Table 5.1 - The Results of the Correlation Matrices between Sagittal and Coronal Spinal Alignment Parameters**

Sagittal SAPs	<b>Seven Sagittal Misalignment Patterns</b>						
	Mean ±Std. Deviation (p = significance value, <0.05)						
	<b>Type 1</b> (n= 16)	<b>Type 2</b> (n= 34)	<b>Type 3</b> (n= 23)	<b>Type 4</b> (n= 7)	<b>Type 5</b> (n= 7)	<b>Type 6</b> (n= 9)	<b>Type 7</b> (n= 4)
<b>SCEA</b>	70.1±4.5	79.0±7.3 (p = .000)	79.9±6.9 (p = .000)	76.9±5.3 (p = .012)	70.9±5.4 (p = .579)	72.1±8.2 (p = .522)	84.8±7.1 (p = .002)
<b>SUTA</b>	72.9±3.3	85.5±7.2 (p = .000)	88.1±5.0 (p = .000)	80.9±2.9 (p = .000)	79.6±3.2 (p = .000)	82.7±3.8 (p = .000)	95.0±6.4 (p = .000)
<b>SLTA</b>	103.0±4.2	111.8±4.2 (p = .000)	100.4±5.4 (p = .128)	93.6±5.6 (p = .001)	107.6±4.7 (p = .033)	104.6±4.6 (p = .487)	105.5±2.4 (p = .437)
<b>SULA</b>	107.1±3.6	109.3±4.7 (p = .180)	102.7±3.1 (p = .000)	97.7±6.7 (p = .001)	96.9±4.9 (p = .000)	96.3±4.6 (p = .000)	95.3±1.0 (p = .000)
<b>SLLA</b>	80.1±5.3	77.0±6.6 (p = .100)	77.2±4.8 (p = .107)	76.1±3.8 (p = .154)	68.4±4.0 (p = .000)	55.7±5.6 (p = .000)	63.5±8.5 (p = .005)

**Table 5.2 - Seven Sagittal Misalignment Patterns.** The means and standard deviations of five sagittal spinal alignment parameters for the 7 newly identified sagittal misalignment pattern types and results of non-parametric two-sample tests comparing Type 1 (the least misaligned type) with other 6 sagittal misalignment patterns. Cells colored grey denote significant values with p-value < 0.05.

In addition, these seven sagittal misalignment patterns were classified with the eight widely accepted coronal curve types. Table 5.3 displays the mean and the standard deviation for each sagittal spinal alignment parameters separated by each coronal curve type.

<b>Seven Sagittal Misalignment Patterns and Sagittal SAPs by the Apex Location of Coronal Curves</b>								
<b>Sagittal Misalignment Patterns</b>	<b>Coronal Curve Types</b>							
	<b>Single MT (n = 19)</b>	<b>Single LT (n = 4)</b>	<b>Single TL (n = 19)</b>	<b>Single L (n = 3)</b>	<b>Double T-T (n = 2)</b>	<b>Double TL-T (n = 21)</b>	<b>Double T-L (n = 26)</b>	<b>Triple T-T-L (n = 6)</b>
<b>Type 1 (n = 16)</b>			n = 3			n = 8	n = 4	n = 1
<b>Type 2 (n = 34)</b>	n = 6	n = 2	n = 11		n = 1	n = 3	n = 8	n = 3
<b>Type 3 (n = 23)</b>	n = 8		n = 2		n = 1	n = 5	n = 6	n = 1
<b>Type 4 (n = 7)</b>	n = 2					n = 4	n = 1	
<b>Type 5 (n = 7)</b>			n = 2			n = 1	n = 3	n = 1
<b>Type 6 (n = 9)</b>		n = 2	n = 1	n = 3			n = 3	
<b>Type 7 (n = 4)</b>	n = 3						n = 1	
<b>Sagittal RSAPs (Mean ± Standard Deviation)</b>								
<b>SCEA</b>	79.3±6.5	68.5±7.0	75.1±6.5	74.7±9.1	77.0±2.8	76.6±8.5	76.4±8.3	81.2±8.4
<b>SUTA</b>	89.2±5.0	79.5±2.1	80.4±6.7	80.0±3.6	84.5±0.7	81.0±9.0	83.1±7.0	89.5±9.8
<b>SLTA</b>	102.4±8.2	105.8±4.4	107.8±7.5	107.7±3.1	105.5±7.8	102.9±7.1	106.7±6.0	107.2±8.0
<b>SULA</b>	101.8±6.1	103.5±6.6	105.8±7.6	95.7±0.5	104.5±0.7	105.2±6.0	104.4±6.4	104.0±8.7
<b>SLLA</b>	77.6±7.5	68.0±11.0	73.0±7.9	50.7±6.0	71.0±1.4	77.6±4.9	74.7±9.7	74.2±3.2

**Table 5.3 - (Upper) The 7 major sagittal misalignment patterns and their classification by the apex location of coronal curves. (Lower) The mean and the standard deviation of each sagittal segment to horizontal angle classified by each coronal curve type. (MT: middle thoracic, LT: lower thoracic, TL: thoracolumbar, L: lumbar major, T-T: thoracic-thoracic, TL-T: thoracolumbar-thoracic, T-L: thoracic-lumbar, T-T-L: thoracic-thoracic-lumbar)**

## 5.5 Discussion and Conclusion

### 5.5.1 Scopes of RSAPs in Quantifying 2D AIS Spinal Misalignment

The biggest outcome of this study was to be able to identify seven major sagittal misalignment patterns and to understand the relationship between the coronal and sagittal misalignment patterns in the AIS spine. These issues had not been clearly defined or examined in the literature before this study.

Table 5.1 shows the correlation matrix between each coronal and sagittal segmental alignment. These tests were performed to define the relationship between each sagittal

and coronal segmental alignment to horizontal angles. One of the notable results from Table 5.1 was that SUTA (greater values, more inclined posteriorly) had a negative correlation with CULA and CLLA (lower values, more inclined to the right), while having a positive correlation with CUTA (greater values, more inclined to the left). This indicated that there is a high probability that the sagittal upper thoracic segment will extend more posteriorly compared to the naturally anteriorly inclined, segmental alignment to horizontal angle if there is a right long thoracic curve on the PA radiograph. There was a negative correlation between SCEA (greater values, more inclined posteriorly) and CLTA (less values, more inclined to the right). This is reasonable because if the lower thoracic segment is inclined to the right on the PA radiograph, the lower cervical segment would be extended more posteriorly from the naturally anteriorly inclined segmental alignment to horizontal angle. This means that if an extension occurs in the lower segment of cervical spine, there exists at least one thoracic curve in the coronal plane. CLLA (less values, more inclined to the right) had a positive correlation with both SLTA and SULA (less values, more inclined anteriorly). If the lower lumbar segment is inclined to the right on the PA radiograph, there will be a high possibility of a right long thoracic curve, with either or both of the lower thoracic segment and the upper lumbar spine more anteriorly inclined, which will increase the extension moment in both segments. This data illustrates the 3D nature of AIS where a curve in one plane is associated to a large degree with a curve in the other plane. In only 16 of the 100 cases in this study was a coronal curve present with the absence of a sagittal deformity. In other words, 84% of curves occurred in both planes and were three dimensional.

In Figure 5.5(a), all seven sagittal misalignment patterns have been simply illustrated based on the means of the measurements of the five sagittal spinal alignment parameters by each sagittal misalignment pattern type (Table 5.2). Figure 5.5(b) - (h) shows the simple illustrations and typical radiographic examples of each sagittal misalignment pattern type compared to the least misaligned type (Type 1). Each misalignment type was named depending on which segments had changes in the inclination direction of the sagittal segmental alignment to horizontal angles in the visual comparison with Type 1.

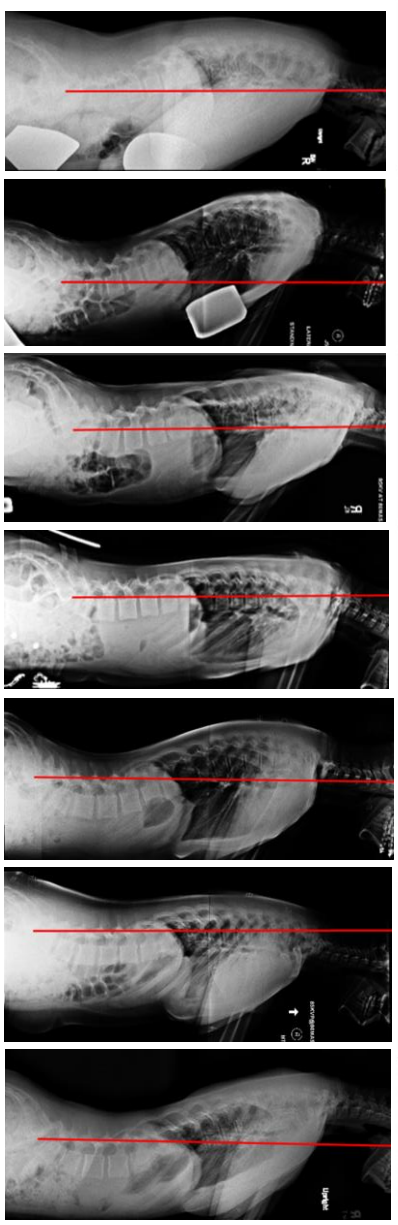
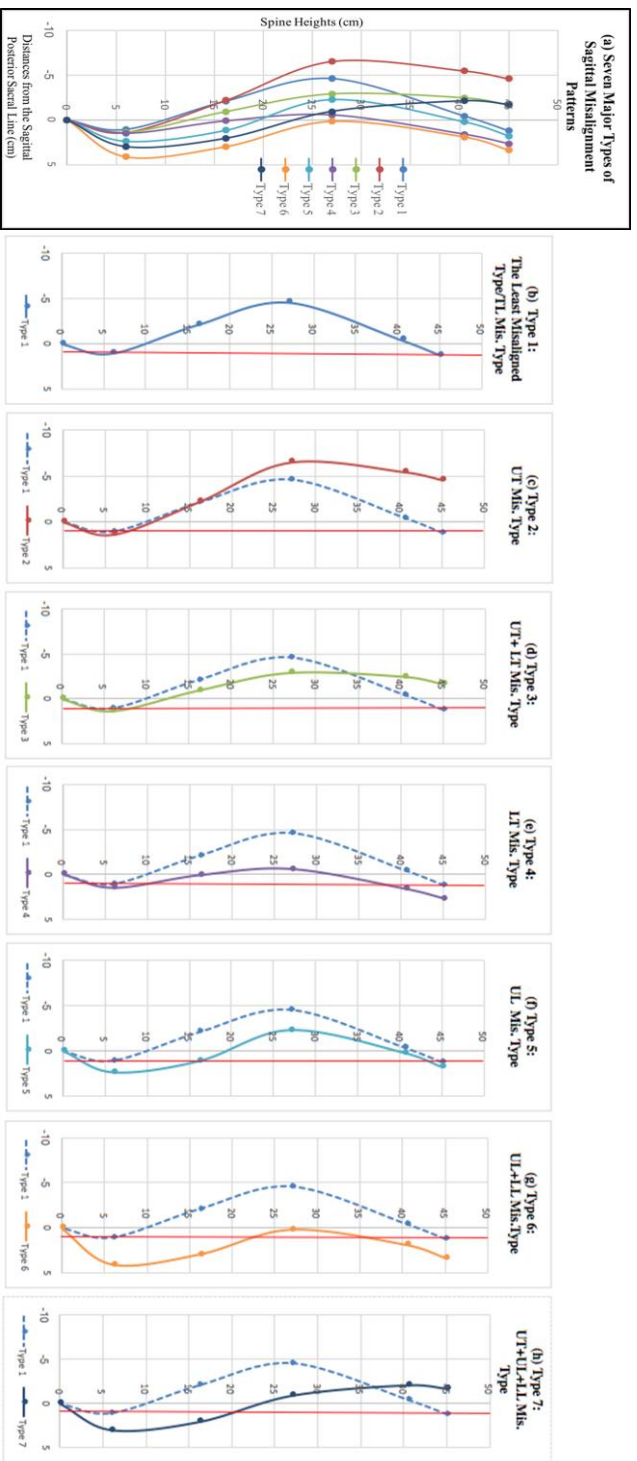


**Figure 5.5 - Illustrations and Radiographic Examples of the Seven Proposed Sagittal Misalignment Patterns with Sagittal Central Sacral Lines (red colored vertical lines).** Each type is named for the segments that display a straighter curve compared to Type 1, the least misaligned type. (a) All seven shown on the same plot. (b) Type 1. (c)-(h) Types 2-7 in solid lines, with Type 1 in dotted lines for comparison. (UT: upper thoracic segment, LT: lower thoracic segment, TL: thoracolumbar area, UL: upper lumbar segment, and LL: lower lumbar segment).

These sagittal misalignment illustrations also supported the results found from the correlation matrix (table 5.1) in most cases (except Type 1) by indicating that there is a loss of natural thoracic kyphosis (vertical flattening) coupled with the compensatory extension on the upper thoracic segment. In some cases (Type 2, 3, and 7), lower cervical extension was observed. In most cases (except Type 1), either or both the lower thoracic and upper lumbar segments, which are naturally posteriorly inclined, became less posteriorly inclined and the segment became relatively vertical. This also indicated that there is an extension moment in the upper lumbar or lower thoracic segments when standing.

Thus, it can be concluded that the AIS sagittal deformity is caused by creating extension in the spine (extension moment). Flattening (more vertically straight) with upper torso compensatory extension (sometimes including the lower cervical segment), was the major sagittal deformity of the thoracic region. This extension mechanism supports the anteriorly directed force hypothesis presented in Dickson et al.'s biplanar spinal theory (1984) and Burwell's pathogenesis theory (2003) especially for the deformity of the thoracic region. Therefore, orthotic treatment can be improved by applying a counteracting posteriorly directed corrective force simply on the location where an anteriorly directed force exists, which will reduce the extension moment of the spine where AIS sagittal misalignment occurs (Burwell, 2003; Dickson et al., 1984).

### 5.5.2 Limitations of Using RSAPs for Defining 3D AIS Misalignment

There were still some limitations however, in defining the 3D AIS misalignment with the 2D concept of RSAPs. Although it has been shown that RSAPs could define the sagittal misalignment patterns and the relationship between coronal and sagittal spinal misalignment patterns of the AIS spines. It is still taking a 2D planar approach to what is a 3D situation.

In addition, radiographic technology is the current gold standard tool used for the diagnosis of AIS and assessment of deformity progression and outcome measures of

surgical AIS treatment. However, critical concerns have been raised relating to the use of radiographic technology for the assessment of AIS orthotic treatment because there is a high risk of radiation over-exposure for adolescents and an increasing awareness of the potential oncogenic effects of radiation exposure (Lin, 2010; Ronckers et al., 2010). Thus, it is essential to find ways to avoid or reduce radiation exposure during AIS orthotic treatment.

In conclusion, this study found that RSAPs are useful in quantifying the 2D AIS misalignment. It was found that RSAPs have some limitations when used for defining 3D AIS deformities and misalignment. The use of radiographic technology works against efforts to reduce radiation exposure. Hence, a 3D method of assessing spinal alignment parameters that can quantify 3D AIS deformities and misalignment without using radiographic exposure is needed. Skin level spinal alignment parameters (SSAPs) could be developed by modifying the concept used in RSAPs for use with surface land markers. The key skeletal anatomical landmarks of RSAPs could be transferred to skin surface anatomical landmarks. This approach and the resulting developed SSAPs system are introduced in the next chapter.

**Chapter 6. Skin Level Spinal Alignment Parameters  
System and Concurrent Validity Test**

## **6.1 Introduction**

In Chapter 5, a 2-dimensional (2D) concept of radiographic spinal alignment parameters (RSAPs) was developed and identified seven major sagittal misalignment patterns. The relationship between the coronal and sagittal misalignment patterns of adolescent idiopathic scoliosis (AIS), which had not been previously clarified, showed that AIS curves are 3 dimensional (3D) in nature in over 84% of cases. Thus, a method to quantify the 3D spinal misalignment of AIS and eliminate the need to take serial radiographs was developed. RSAPs were converted to the 3D concept of skin level spinal alignment parameters (SSAPs) that can be used for non-invasive assessment. The key osseous anatomical landmarks of RSAPs were also transferred to the closest anatomical locations on the skin surface. However, it was not clear whether the transferred skin surface level anatomical landmarks of SSAPs represent the similar characteristic to the underlying bone structure assessed by RSAPs.

Before using SSAPs to quantify 3D AIS spinal misalignment non-invasively, a validation of the measurements of SSAPs was required. Thus, a concurrent validity experiment was performed to find out whether SSAPs correspond to the previously established radiographic parameters (RSAPs) for the same construct (subject). This study statistically and visually examined the relationships between the parameter values measured from the skin level anatomical landmarks of SSAPs and the corresponding parameter values measured from the original osseous landmarks of RSAPs on bi-planar spine radiographs, taken at the same time with AIS subjects. This chapter describes how the concurrent validity of SSAPs was established and introduces the location of the surface level anatomical landmarks of SSAPs.

## **6.2 Materials and Methods**

### **6.2.1 Subjects**

This was a prospective study. Patients, who were between 10 and 16 years old with a confirmed AIS diagnosis, were recruited from the orthopedic clinic at Keimyung University's Dongsan Medical Center located in Daegu, Republic of Korea. Like before, patients were excluded if they had leg-length discrepancies of more than 2 cm,

any deformities of the lower limbs, or any surgical procedures on the lower limbs or spine. After explaining the procedure of the study to each patient and their parent or legal guardian, two written consent forms (one from the patient and the other from the parent or legal guardian) were obtained in-person during their regular clinic visit before taking their two full-spine radiographs.

## 6.2.2 Outcome Measures

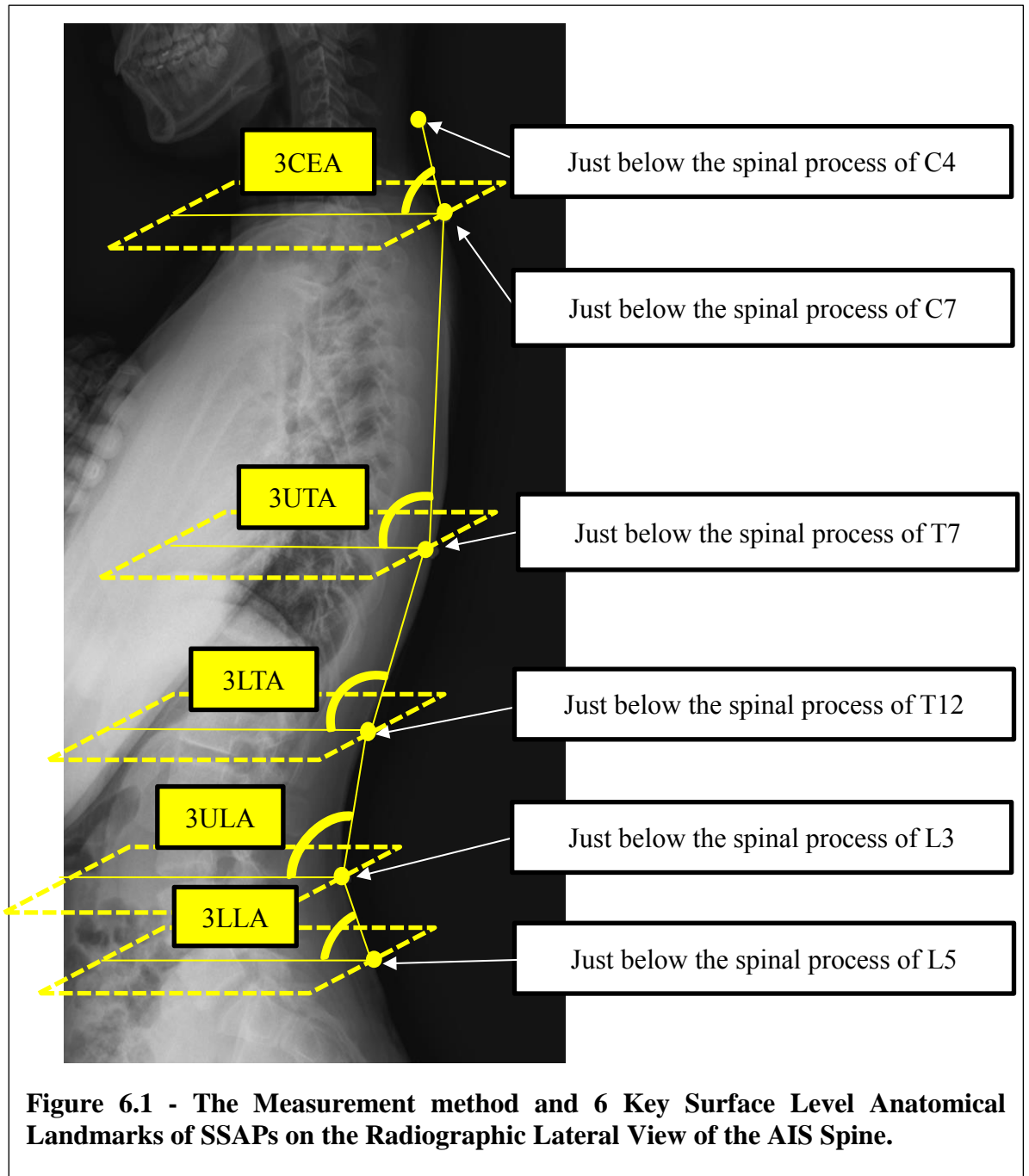
### **Skin level Spinal Alignment Parameters:**

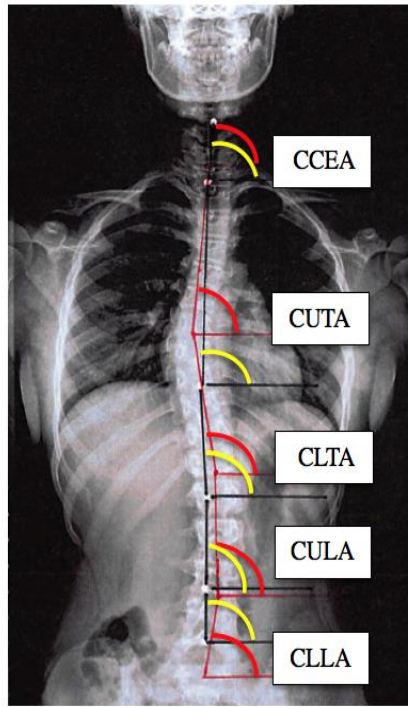
SSAPs consist of a total of five skin level parameters: **3CEA** (3D Lower Cervical Alignment to Horizontal Angle), **3UTA** (3D Upper Thoracic Alignment to Horizontal Angle), **3LTA** (3D Lower Thoracic Alignment to Horizontal Angle), **3ULA** (3D Upper Lumbar Alignment to Horizontal Angle), **3LLA** (3D Lower Lumbar Alignment to Horizontal Angle). Figure 6.1 shows the measurement method and location of the 6 key surface level anatomical landmarks as identified by radio-opaque balls on the skin surface and which were used to create the SSAPs. All SSAPs angles were measured as deviation from the global horizontal line during standing. In this study, these five parameters were measured from both posterior-anterior (PA) (coronal) and lateral (sagittal) view radiographs to compare with the five coronal and five sagittal parameters of RSAPs.

### **Radiographic Spinal Alignment Parameters:**

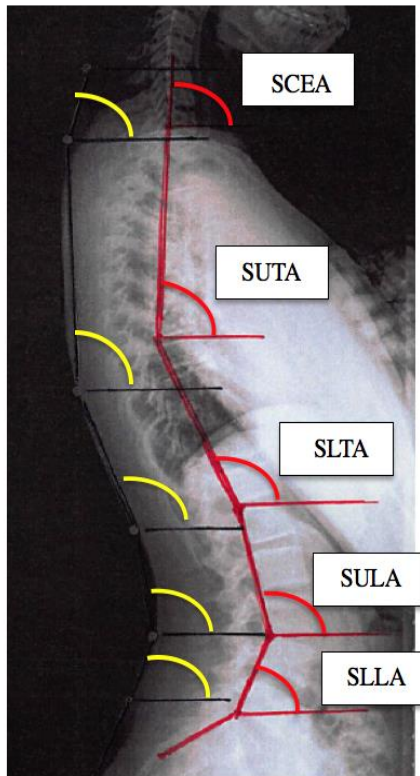
The five coronal and five sagittal alignment angles of RSAPs were also measured from the osseous anatomical landmarks of the posterior-anterior (PA) (coronal) and lateral (sagittal) view radiographs. These osseous anatomical landmarks were introduced in Chapter 5. Five coronal alignment parameters were the followings: **CCEA** (Coronal Cervical Alignment to Horizontal Angle), **CUTA** (Coronal Upper Thoracic Alignment to Horizontal Angle), **CLTA** (Coronal Lower Thoracic Alignment to Horizontal Angle), **CULA** (Coronal Upper Lumbar Alignment to Horizontal Angle), and **CLLA** (Coronal Lower Lumbar Alignment to Horizontal Angle). Five sagittal alignment parameters were the followings: **SCEA** (Sagittal Lower Cervical Alignment to Horizontal Angle), **SUTA** (Sagittal Upper Thoracic

Alignment to Horizontal Angle), **SLTA** (Sagittal Lower Thoracic Alignment to Horizontal Angle), **SULA** (Sagittal Upper Lumbar Alignment to Horizontal Angle), and **SLLA** (Sagittal Lower Lumbar Alignment to Horizontal Angle). Figure 6.2 shows how to measure the 10 segmental alignment angles for both systems on the radiographs.





(a)



(b)

**Figure 6.2 - Measurement Methods and 10 Anatomical Landmarks (5 Coronal and 5 Sagittal Segmental Alignment to Horizontal Angles) of Each System on the (a) posterior-anterior full-spine radiograph and the (b) lateral view full-spine radiograph of an AIS patient. Red: RSAPs and Yellow: SSAPs**

### 6.2.3 Procedures

This study involved two full spine radiographs of AIS subjects, one from the coronal PA view and the other from the sagittal lateral view (Figure 6.2). The PA and lateral view radiographs of each AIS patient's spine were taken with 5mm radiographically visible metal balls attached on the surface level of 7 spinous processes of the vertebral bodies (C4, C7, T7, T12, L3, and L5), that corresponded to key anatomical landmarks of RSAPs (Figure 6.1). The values for each angle were measured from the surface level anatomical landmarks (from the metal balls) and from the actual location of skeletal anatomical landmarks of RSAPs through the two different radiographic views (Figure 6.2) and then these two sets of measured values were compared.

### 6.3 Data Analysis

First, the data was examined to determine if they followed a normal distribution for each parameter (IBM SPSS software, version 25). The normal distribution was confirmed by calculating the skewness and kurtosis  $z$ -values, the  $p$ -value of the Shapiro-Wilk test, and visually inspecting the normal probability Q-Q plots for each category of the independent variable (Cramer, 1998; Cramer and Howitt, 2004; Shapiro and Wilk, 1965) (Appendix 6.1). All test statistics for skewness and kurtosis were within one standard deviation of normal and all  $p$ -values for the Shapiro-Wilk test were nonsignificant (above 0.05). The visual inspection of the Q-Q plots also showed that the distribution was close enough to a normal distribution. Therefore, it can be concluded that the data were normally distributed.

Second, the data was analyzed using *Pearson's Correlation Coefficient* ( $r$ ) (IBM SPSS software, version 25) to determine the relationship between the values measured from the 5mm metal balls attached on surface level spinal anatomical landmarks and from the original radiographic spinal anatomical landmarks on the radiographs of each patient (Appendix 6.2). The results of the *Test of Significance* defined the relationship between the two variables is linear. The criterion for statistical significance ( $\alpha$ ) was set at  $p < 0.05$ . *Pearson's Correlation Coefficient* ( $r$ ) was used to calculate the strength and

direction of linear relationships between the corresponding parameter values. The relationship between two variables is generally considered strong when their  $r$  value is larger than 0.7.

#### 6.4 Results

Thirteen (12 Female and 1 Male) AIS patients were recruited for the study. The average age of the patients was 14.8 years old. Table 6.1 displays the means and standard deviations of all parameters measured from the osseous landmarks of RSAPs and skin level landmarks of SSAPs on the PA and lateral view radiographs.

Parameters		Mean (Standard Deviation) of Values	
		measured from osseous landmarks (RSAPs)	measured from the skin level landmarks (SSAPs)
PA (coronal) radiograph	CCEA/3CEA-C	90.85 (2.85)	91.08 (3.01)
	CUTA/3UTA-C	97.85 (7.55)	93.62 (4.13)
	CLTA/3LTA-C	80.54 (6.96)	84.69 (4.73)
	CULA/3ULA-C	85.00 (8.86)	87.46 (6.68)
	CLLA/3LLA-C	99.69 (8.14)	94.15 (6.20)
Lateral (sagittal) radiograph	SCEA/3CEA-S	86.77 (5.28)	75.46 (5.03)
	SUTA/3UTA-S	89.00 (6.40)	90.54 (5.35)
	SLTA/3LTA-S	103.31 (5.06)	102.54 (4.37)
	SUTA/3ULA-S	100.54 (6.64)	96.77 (7.73)
	SLLA/3LLA-S	77.23 (11.61)	78.85(10.33)

**Table 6.1 - Means and Standard Deviations of Parameter Values** (-C: any SSAP parameter measured from the PA radiograph, -S: any SSAP parameter measured from the sagittal radiograph)

The *Pearson's Correlation Coefficient* ( $r$ ) and the  $p$ -value of the *Test of Significance* between parameter values are shown in Table 6.2. There was a statistically significant linear relationship between each RSAP parameter that was measured from the osseous anatomical landmarks and from each corresponding SSAP parameter, which was measured from the surface level anatomical landmarks (metal balls) with the  $p$ -values of less than 0.05.

In addition, all parameters of SSAPs were measured from the PA (SSAP - C) and lateral (SSAP - S) radiographs had a strong and significant positive linear relationship ( $r > 0.7$ ) with 9 coronal and sagittal spinal alignment parameters (CCEA, CUTA, CLTA, CULA, CLLA, SUTA, SLTA, SULA, and SLLA) of RSAPs except SCEA.

Further, the *Pearson's Correlation Coefficient* of SCEA and 3CEA-S was almost 0.7 (0.69) and so it could be considered that this also shows a strong relationship (Bland and Altman, 1986).

Parameters		Pearson's Correlation (correlation coefficient, <i>r</i> )	Test of Significance (Sig. <i>p</i> <0.05)
PA (coronal) X-rays	CCEA/3CEA-C	0.95	.000
	CUTA/3UTA-C	0.87	.000
	CLTA/3LTA-C	0.79	.001
	CULA/3ULA-C	0.81	.001
	CLLA/3LLA-C	0.70	.008
Lateral (sagittal) X-rays	SCEA/3CEA-S	0.69	.009
	SUTA/3UTA-S	0.92	.000
	SLTA/3LTA-S	0.96	.000
	SULA/3ULA-S	0.89	.000
	SLLA/3LLA-S	0.83	.000

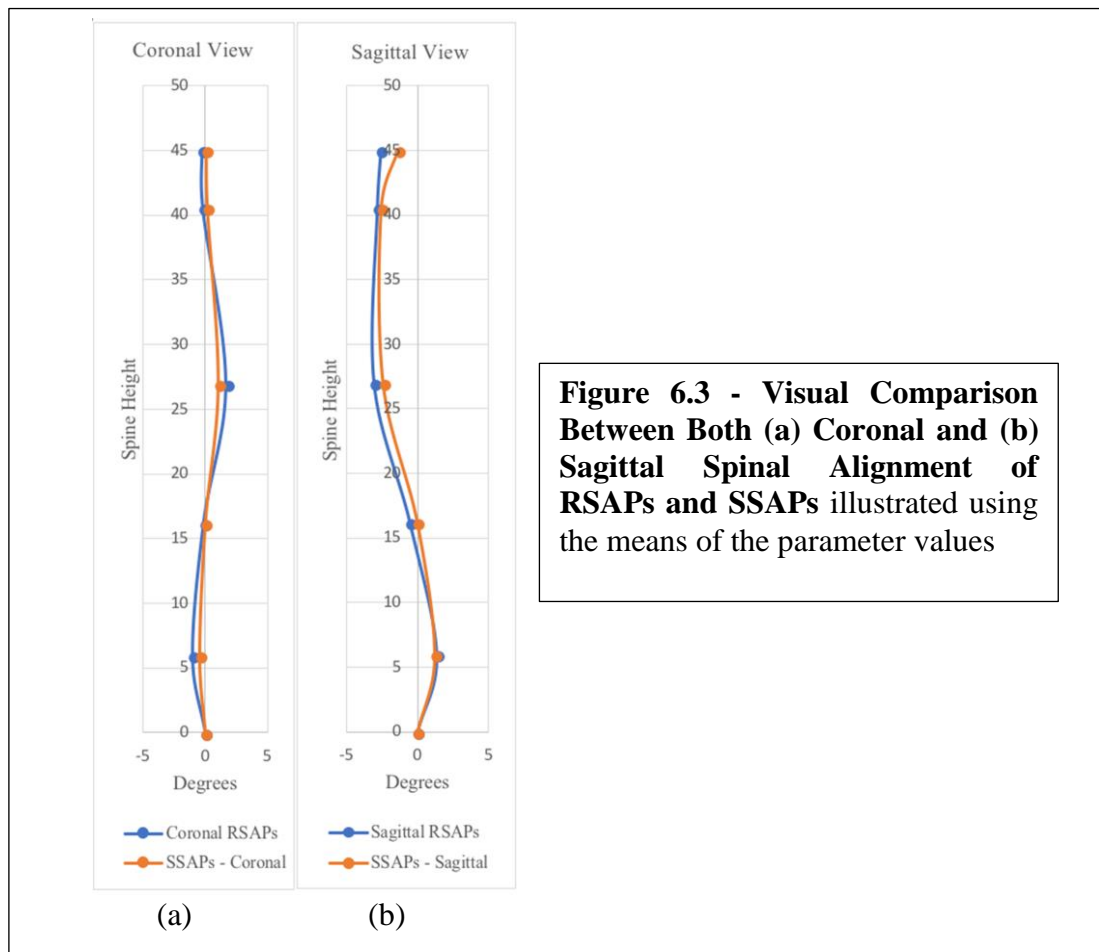
**Table 6.2 - The Pearson's Correlation Coefficient (r) with Each p-values of the Test of Significance** between parameters measured from the radiographic osseous anatomical landmarks and the surface level metal balls.

## 6.5 Discussion and Conclusion

### *Skin profile Vs Osseous profile*

As shown in Figure 6.2 and Figure 6.3, the skin profile of the spinal alignment differed from its osseous profile as one would expect. The difference between the skin profile and osseous profile for the spinal alignment was considered as a natural and obvious outcome according to the results of many other studies (Bryant et al., 1989; Gracovetsky, 2010; Marks et al., 2003).

Nevertheless, the results of the *Test of Significance* showed that there was a statistically significant linear relationship between each RSAP parameter that was measured from the osseous anatomical landmarks and from each corresponding SSAP parameter, which was measured from the surface level anatomical landmarks. In addition, the Pearson's correlation test also indicated there was a strong relationship between all parameters of RSAPs and SSAPs-C or SSAPs-S. Hence, these were considered as meaningful relationships and it could be concluded that SSAPs correspond to the previously established radiographic parameters (RSAPs) for the same construct (subject).



***Relationship between sagittal RSAPs and SSAPs measured from the sagittal view (SSAPs-S).***

It was also observed that the stronger linear relationship between the two values from the two methods, the less the difference between the means of two values was, as shown in Table 6.1 and Figure 6.3. For example, SLTA and 3LTA-S had the strongest positive linear relationship ( $r=0.96$ ). Visual inspection of each subject also supported this (Figure 6.4).

Even though SCEA and 3CEA-S had the weakest positive linear relationship ( $r=0.69$ ), visual inspection of each subject also showed their unique pattern and linear relationship (Figure 6.3 (b)) (Figure 6.5). The SCEA-S of all subjects had lower values than SCEA, and the mean difference of the parameters was 11.31 degrees (Table 6.1). It is likely that the distance between the skin surface and vertebral bodies was not

uniform along the length of the spine because on the lower segment of the cervical spine, there are posterior para-muscle groups which form a thinner cover on the spinous processes of the cervical spine than on the other segments (Netter, 1987).

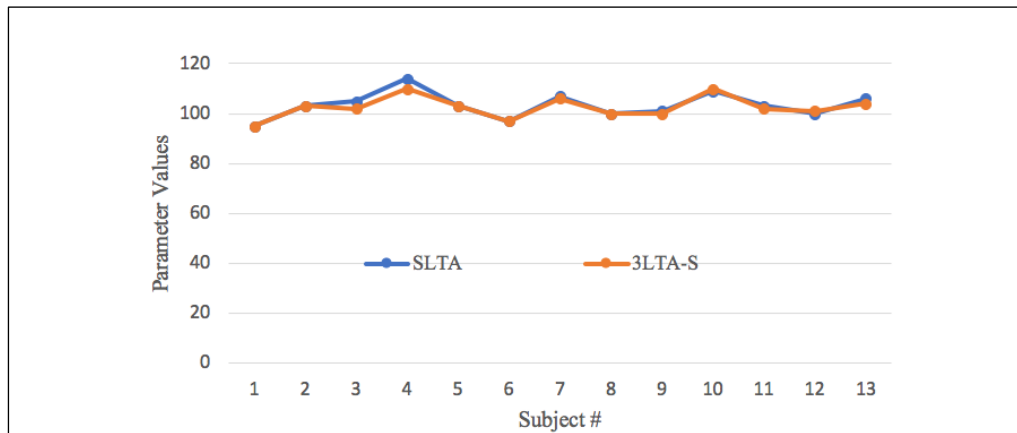


**Figure 6.4 - Comparison between SLTA and 3LTA-S by Each Subject**

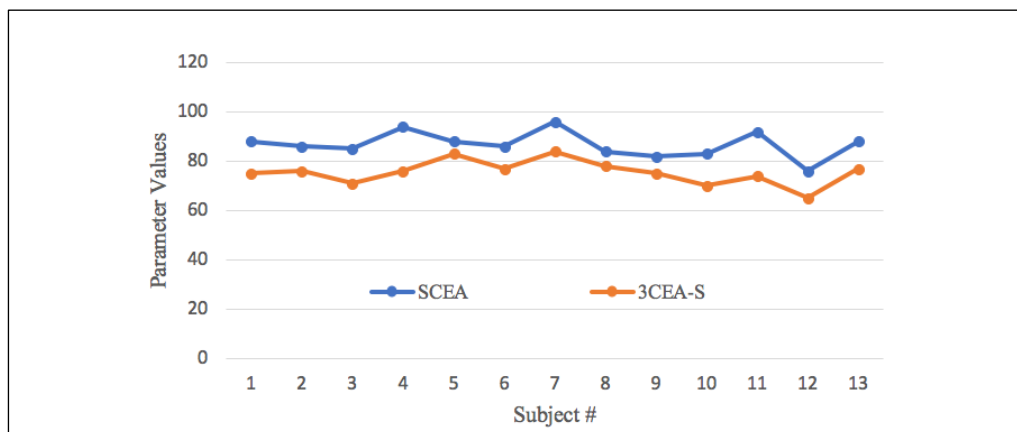
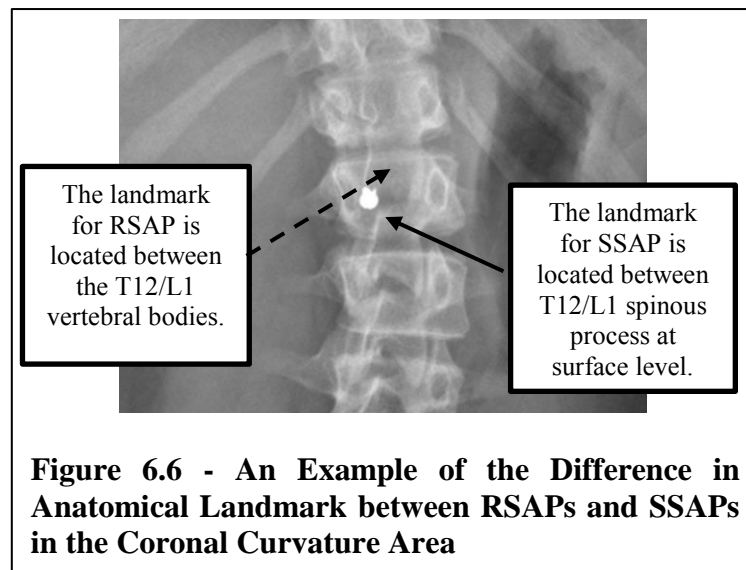


**Figure 6.5 - Comparison between SCEA and 3CEA-S by Each Subject**

***Relationship between coronal RSAPs and SSAPs measured from the coronal view (SSAPs-C)***

Both tests also indicated there was a strong linear relationship between each parameter of coronal RSAPs and 3SAPs-C measured on the PA radiograph. However, all SSAPs measured from the PA radiograph had a lower value than each corresponding RSAP except CCEA/3CEA-C (Table 6.1). The anatomical landmarks of SSAPs are located on the surface level of the spinous processes because the spinous

processes are the most easily palpated anatomical landmarks in the spinal column observed from the skin surface. If there is a structural coronal curvature, as shown in Figure 6.6, the spinous process usually rotates to the concave side of the coronal curvature for patients with AIS deformities (as shown in the previous chapter), resulting in a lower estimation of coronal curve severity than expected (Figure 6.3 (a)). In addition, all of subjects had no cervical structural curve, the mean values of both CCEA and 3CEA-C were similar and close to 90 degrees.



In conclusion, the previously established RSAPs were converted to the 3D concept of skin level spinal alignment parameters (SSAPs) to quantify 3D AIS spinal misalignment for non-invasive assessment method. This concurrent validity experiment found that SSAPs correspond strongly to the previously established radiographic parameters (RSAPs) for the same construct. There was a statistically and visually significant linear relationship between each RSAP parameter that measured from the osseous anatomical landmarks and each corresponding SSAP parameter measured from the surface level anatomical landmarks on bi-planar spine radiographs, taken at the same time using 13 AIS subjects. These results indicated that SSAPs can be used for skin surface level analysis in order to quantify 3D misalignment patterns and deformities of patients with AIS. However, the absolute values were different

between the two methods indicating that the surface method would required its own normal values to be established. These are presented in chapter 8.

**Chapter 7. Development of a Non-Invasive Digital  
Calculating and Visualisation Assessment  
Application**

## 7.1 Introduction

A non-invasive digital calculating and visualisation assessment tool that could be used with the 3-dimensional skin level parameters (3DSPs) as an interactive clinical tool was developed using motion capture technology. This non-invasive assessment application was built using Nexus motion capture software (Vicon Motion Systems Ltd., United Kingdom) and Motek D-Flow visualisation software (Motek Medical, The Netherlands). As mentioned in previous chapters, on beginning this project the biomechanical principles employed during orthotic treatment of AIS were not clearly defined in the literature or in the community of practice in orthotics. There was no strong evidence in the literature to support decision-making for some key biomechanical principles. Thus, the ultimate goal in developing this application was to produce a tool to help clinicians to identify the optimal placements of corrective forces in the orthotic treatment for AIS. This platform would allow a small feasibility study to be conducted utilizing the application to determine the optimal placements of the corrective forces applied by an orthosis in 5 case studies and once adopted more generally post this PhD to contribute toward establishing the biomechanical principles of orthotic treatment for AIS.

In the development of the non-invasive digital calculating and visualisation assessment tool, there were two main activities (1) the development and establishment of 3DSPs previously reported in this thesis and (2) the development of the assessment application itself which is the focus of this chapter. First, the final version of 3DSPs including the spinal alignment parameters (SSAPs) that were implemented in the application and the key anatomical landmarks needed to record them are summarised. The final version of 3DSPs was established by adding other important 3D measurements to SSAPs developed from the previous chapter. The reasons why these measurements were added to the SSAPs are also explained. In addition, calculation equation examples for some of parameters built within the application are introduced.

Next, the development process for the application is described with some examples for modules, configurations, and a series of equations built within the application. These are explained based on the following sections: “overview of the application

concept”, “the application settings for data collection”, “the application for the calculation of parameter values”, “the application for the visualisation of parameter values, their colour indicators, and the spinal alignment”, and “the application for force (or load) measurements”.

## 7.2 Development of 3D Skin Level Parameters

### 7.2.1 Measurements of 3D Skin Level Parameters

The application had the capability for calculating a total of 11 3D skin level parameters (3DSPs) that can be measured from the skin surface. The 3DSPs included the five SSAPs and six additional 3D non-spinal alignment parameters. The SSAPs developed to quantify the spinal alignment of AIS were validated through the concurrent validity test introduced in Chapter 6. Non-spinal alignment parameters, which cannot be measured with traditional radiographs but are considered clinically important, were added to the SSAPs to assess other features of AIS deformities.

Five 3D spinal alignment parameters (3D SSAPs) are: **3CEA** (3D Lower Cervical Alignment to Horizontal Angle), **3UTA** (3D Upper Thoracic Alignment to Horizontal Angle), **3LTA** (3D Lower Thoracic Alignment to Horizontal Angle), **3ULA** (3D Upper Lumbar Alignment to Horizontal Angle), and **3LLA** (3D Lower Lumbar Alignment to Horizontal Angle). All SSAPs angles were measured as deviation from the global horizontal line and Chapter 6 (Figure 6.1) and Figure 7.1 shows how to measure one of the SSAPs (3UTA) as an example.

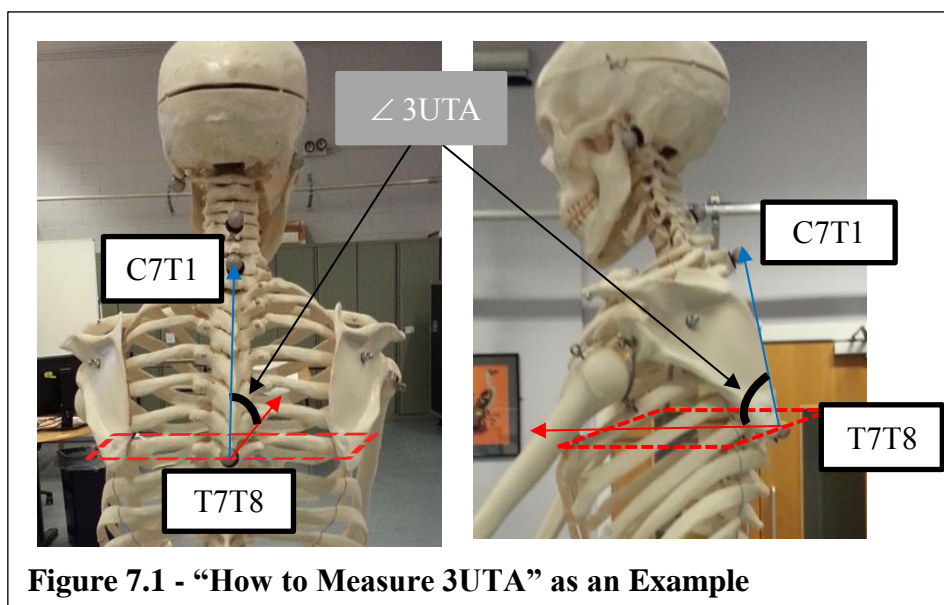
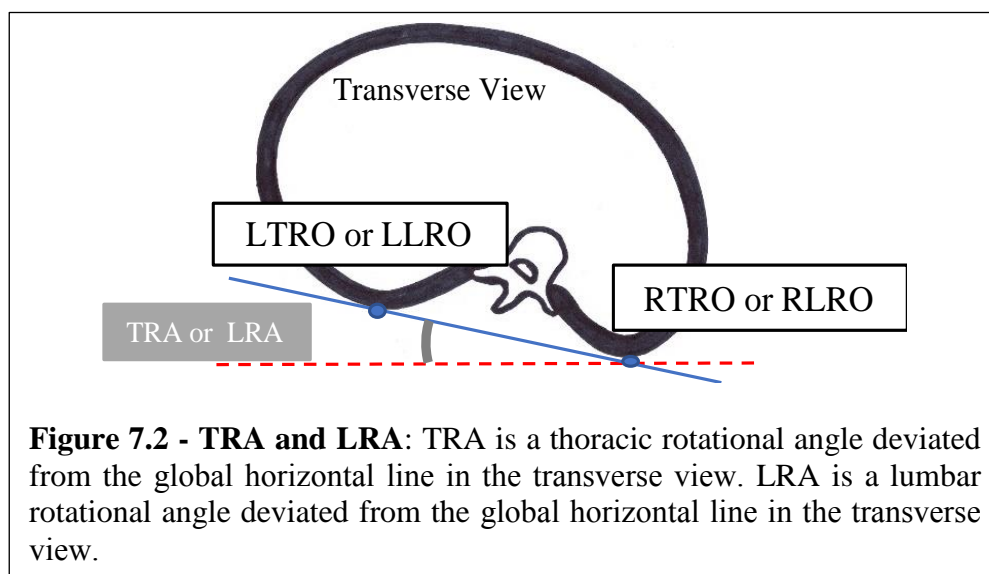


Figure 7.1 - “How to Measure 3UTA” as an Example

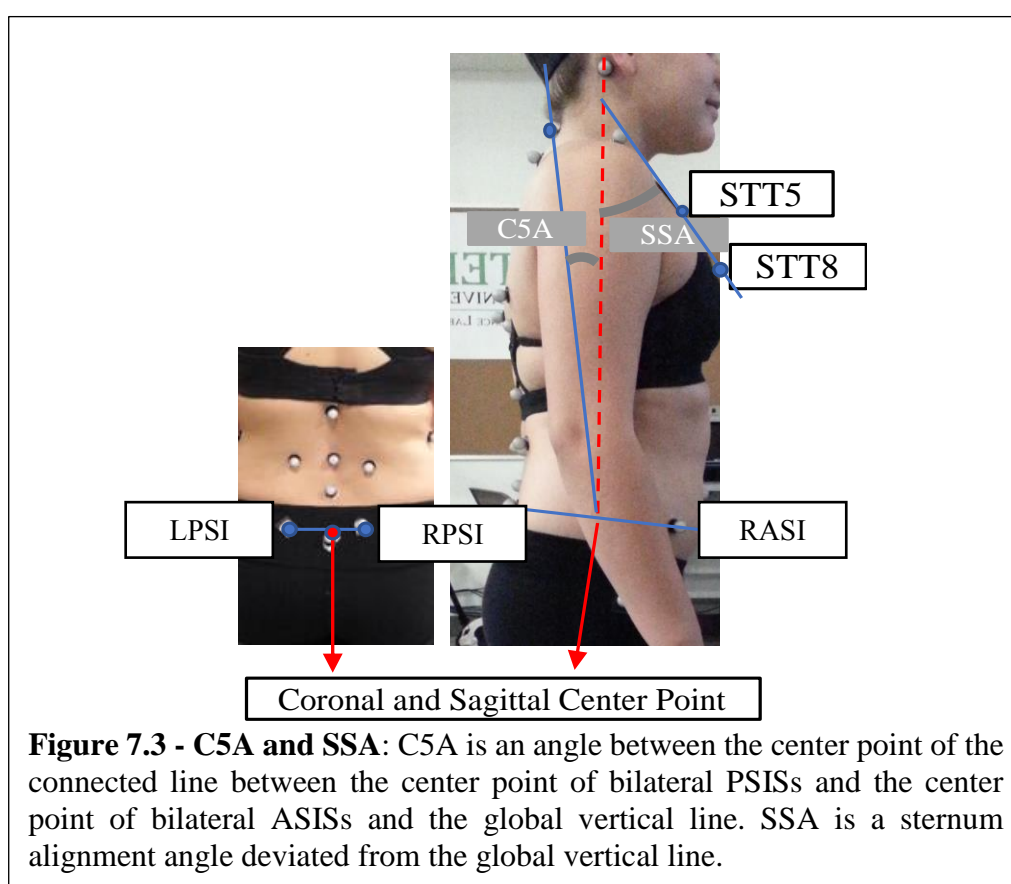
Six 3D non-spinal alignment parameters are: **TRA** (Thoracic Rotation Angle), **LRA** (Lumbar Rotation Angle), **C5A** (C5 Balance Angle), **SSA** (Sternal Angle), **PTA** (Pelvic Tilt Angle), and **SCA** (Sacral Alignment to Horizontal Angle). The clinical definitions of the 3D non-spinal alignment parameters are described in the following paragraphs.

**TRA and LRA:** The axial rotation of the spinal column and of an individual vertebra is one of major pathological and biomechanical characteristics of AIS. This creates the asymmetric shape of the rib cage and paraspinal muscles on the convex side of a spinal curvature. In scoliosis clinics, the displayed prominence is measured using a scoliometer to measure the severity of the axial rotation from the AIS spine. The term **TRA** refers to the asymmetric shape of the rib cage in the transverse plane of the thoracic spine and term **LRA** refers to the asymmetric shape of the paraspinal muscles in the transverse plane of the lumbar spine. Both are similar to the scoliometer measurement or “Angle of Trunk Rotation (ATR)” of the radiographic measurement (Patias et al, 2010). Figure 7.2 shows how to measure six 3D non-spinal parameters from the surface level.



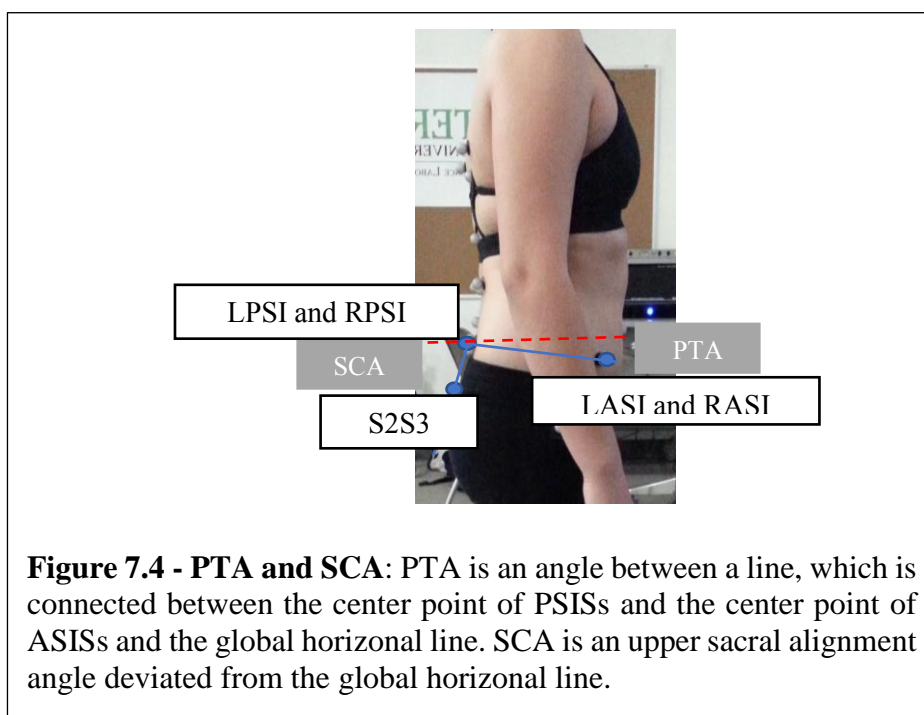
**C5A and SSA:** The term **C5A** refers to a 3D spinal balance angle between the C4/5 and the vertical line drawn from the Centre Point. Achieving spinal balance is one of important parameters for successful orthotic treatment. In the survey project (Chapter

4), 67.4% of the participants considered that not to achieve spinal balance would be understood as an orthotic treatment failure. Consequently, to correct this, they should adjust or re-make the orthosis “if coronal balance is made worse despite an improved Cobb angle in an orthosis”. **SSA** is used is to examine the 3D sternum misalignment of AIS. The sternum angle may be changed if AIS deformity occurs due to the extension pathomechanism, which was found through the radiographic study in Chapter 5. To measure both defines the mid-points of the bilateral ASIS and PSIS and both parameters measures the deviational angle from the global vertical line drawn from the bisect line between the defined the midpoints as shown in Fig 7.3.



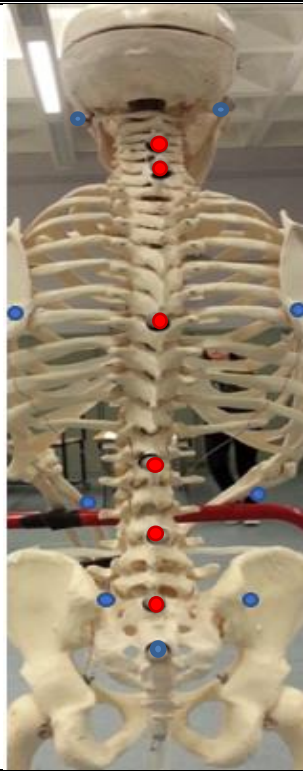
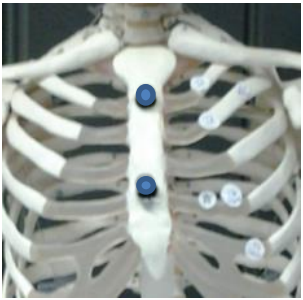
**PTA and SCA:** The terms PTA and SCA come from the pelvic parameter (incidence) mentioned by Boulay et al. (2006) and Klineberg et al. (2011). In these articles, the pelvic incidence refers to the combination of pelvic tilt and sacral slope degrees measured from the radiograph and correlates with lumbar lordosis and compensatory mechanisms of lumbar deformity (Klineberg et al., 2011). Smaller

radiographic pelvic incidence values corresponded to a more reduced and flattened sagittal lumbar lordosis (Boulay et al., 2006). Thus, PTA and SCA are similar to pelvic tilt and sacral slope degrees (Figure 7.4).



Capability of calculating the 2D concept of five coronal and sagittal SSAPs were also built in the application because it could compare the differences between the 3D concept of SSAPs while conducting a study to identify the optimal placements of corrective forces in the orthotic treatment for AIS. Measuring methods for these parameters was also explained in the previous chapter (Chapter 6).

- Five coronal SSAPs: **CCEA** (Coronal Lower Cervical Alignment to Horizontal Angle), **CUTA** (Coronal Upper Thoracic Alignment to Horizontal Angle), **CLTA** (Coronal Lower Thoracic Alignment to Horizontal Angle), **CULA** (Coronal Upper Lumbar Alignment to Horizontal Angle), and **CLLA** (Coronal Lower Lumbar Alignment to Horizontal Angle)
- Five sagittal SSAPs: **SCEA** (Sagittal Lower Cervical Alignment to Horizontal Angle), **SUTA** (Sagittal Upper Thoracic Alignment to Horizontal Angle), **SLTA** (Sagittal Lower Thoracic Alignment to Horizontal Angle), **SULA** (Sagittal Upper Lumbar Alignment to Horizontal Angle), and **SLLA** (Sagittal Lower Lumbar Alignment to Horizontal Angle)

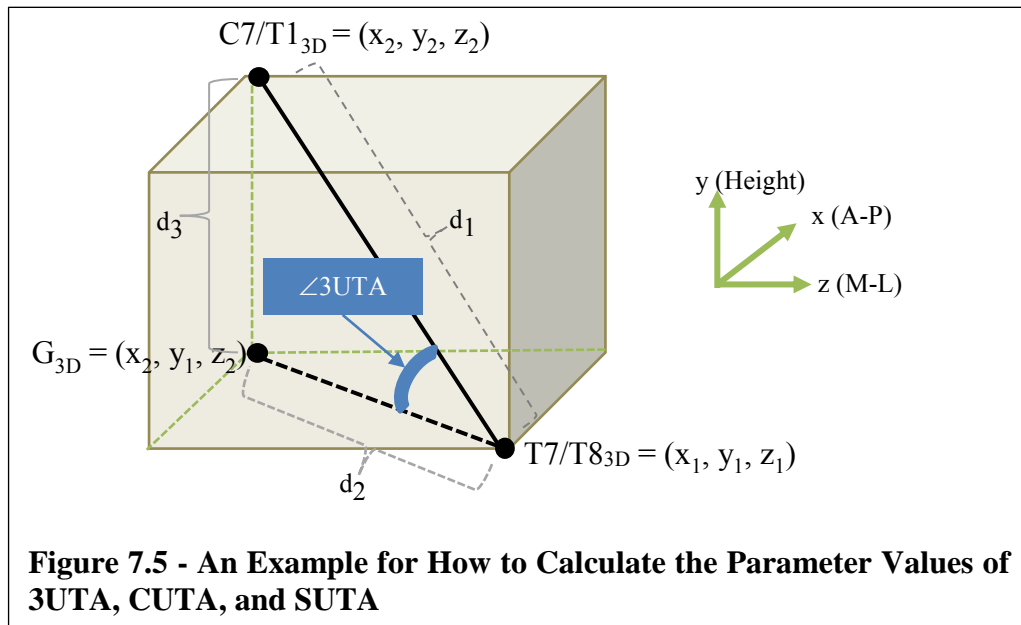
Name of Landmarks	19 Key Anatomical Landmarks of 11 3D Skin Level Parameters (3DSPs)	
LTC1		Left Mastoid Process at C1 Level
RTC1		Right Mastoid Process at C1 Level
C4C5		Just below the spinal process of C4
C7T1		Just below the spinal process of C7
T7T8		Just below the spinal process of T7
T12L1		Just below the spinal process of T12
L3L4		Just below the spinal process of L3
L5S1		Just below the spinal process of L5
S2S3		Just below the spinal process of S2
LTRO		Left inferior angle of scapular at T7/T8 level
RTRO		Right inferior angle of scapular at T7/T8 level
LLRO		Left paraspinal muscles at L3/L4 level
RLRO		Right paraspinal muscles at L3/L4 level
LPSI		Left posterior superior iliac spine
RPSI		Right posterior superior iliac spine
STT5		Superior part of the sternum at T5 rib level
STT8		Highest point of the sternum
LASI		Left anterior superior iliac spine
RASI		Right anterior superior iliac spine

**Table 7.1 - The List of 19 Key Surface Level Anatomical Landmarks of 3DSPs** (Red dots and written descriptions indicate the landmarks of five spinal alignment parameters SSAPs while blue dots indicate the landmarks of the six 3D non-spinal alignment parameters)

Table 7.1 shows the list of 19 key surface level anatomical landmarks required to calculate the 11 parameters. The location of the 6 key surface level anatomical landmarks which were used to create the SSAPs are introduced in Figure 6.1 and also shown with red dots in Table 7.1. Thirteen blue dots are represented as the key surface level anatomical landmarks of 3D non-spinal alignment parameters.

### 7.2.2 Examples of Calculation Methods for Parameters

The method of how to make equations for the calculation of the parameters in the scripts of the 3D assessment application is shown using the trigonometric equations of Upper Thoracic Angles (**3UTA**, **CUTA**, and **SUTA**) of SSAPs as an example.



*Examples of Equations for 3UTA, CUTA, and SUTA (Figure 7.5):*

(a) Calculation for 3UTA values

$$d_1 (\text{distance between } T7/T8 \text{ and } C7/T1) = \sqrt{(x_2 - x_1)^2 + (y_2 - y_1)^2 + (z_2 - z_1)^2}$$

$$d_2 (\text{distance between } T7/T8 \text{ and } G_{3D}) = \sqrt{(x_2 - x_1)^2 + (z_2 - z_1)^2}$$

$$\angle 3UTA = \text{Cos}^{-1}(d_1/d_2)$$

(b) Calculation for CUTA values

$$d_1 (\text{distance between } T7/T8 \text{ and } C7/T1) = \sqrt{(z_2 - z_1)^2 + (y_2 - y_1)^2}$$

$$d_2 (\text{distance between } T7/T8 \text{ and } G_{Cor}) = |z_2 - z_1|$$

$$\angle CUTA = \text{Cos}^{-1}(d_1/d_2)$$

But,  $\angle CUTA = 180 - \theta$  if  $z_2 < z_1$

(c) Calculation for SUTA values

$$d_1 (\text{distance between T7/T8 and C7/T1}) = \sqrt{(x_2 - x_1)^2 + (y_2 - y_1)^2}$$

$$d_2 (\text{distance between T7/T8 and } G_{Sag}) = |x_2 - x_1|$$

$$\angle SUTA = \text{Cos}^{-1}(d_1/d_2)$$

But,  $\angle SUTA = 180 - \theta$  if  $x_2 < x_1$

### 7.3 Development of Non-Invasive Digital Calculating and Visualisation Assessment Application

#### 7.3.1 Overview of Application Concept

The digital calculating and visualisation assessment application was programmed with the coding language “Lua” through written scripts in the Motek (D-flow) software. The entire D-Flow application made for this project appears in Figure 7.6. A developer can easily combine together different kinds of modules each with its own specific tasks and capabilities to create a desired application in D-Flow software.

The developed D-flow application was linked to Vicon Nexus software. VICON infrared motion capture cameras (Vicon Motion Systems Ltd., United Kingdom) were used for this project and can capture reflective markers and run in conjunction with VICON NEXUS software 2.2.3 (Vicon Motion Systems Ltd., United Kingdom) (Figure 7.7). The 3D Cartesian coordinated geometric data obtained from VICON cameras and Nexus software are generated into the programmed equations of the D-Flow application to calculate the values of each parameter digitally and visualise the parameter values and spinal alignment.

In addition, this application has capabilities to indicate the colours of the values and the alignment segments of a spine in real time on the DRS window by showing in one of two colours depending on whether each value is within the reference range for that parameter. The colour indicator concept can provide immediate feedback in assessing

whether the corrective force applied on the scoliotic spine is optimal by comparing the colour changes before and after corrective forces are applied on the AIS spine.

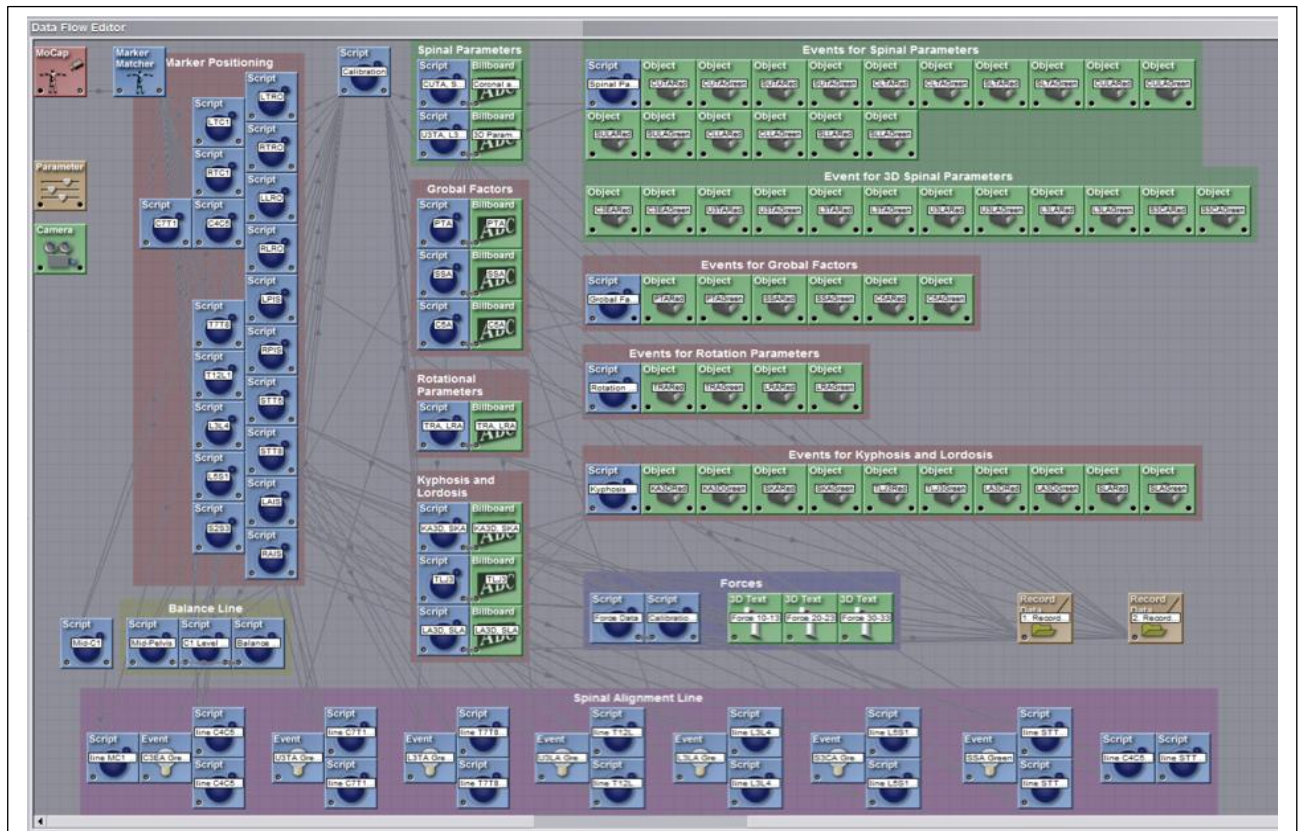


**Figure 7.6 - The D-flow Application:** A screen shot of the entire D-flow application developed for the digital calculating and visualisation system. It was programmed with the coding language *Lua* through “Motek (D-flow)” Technology.

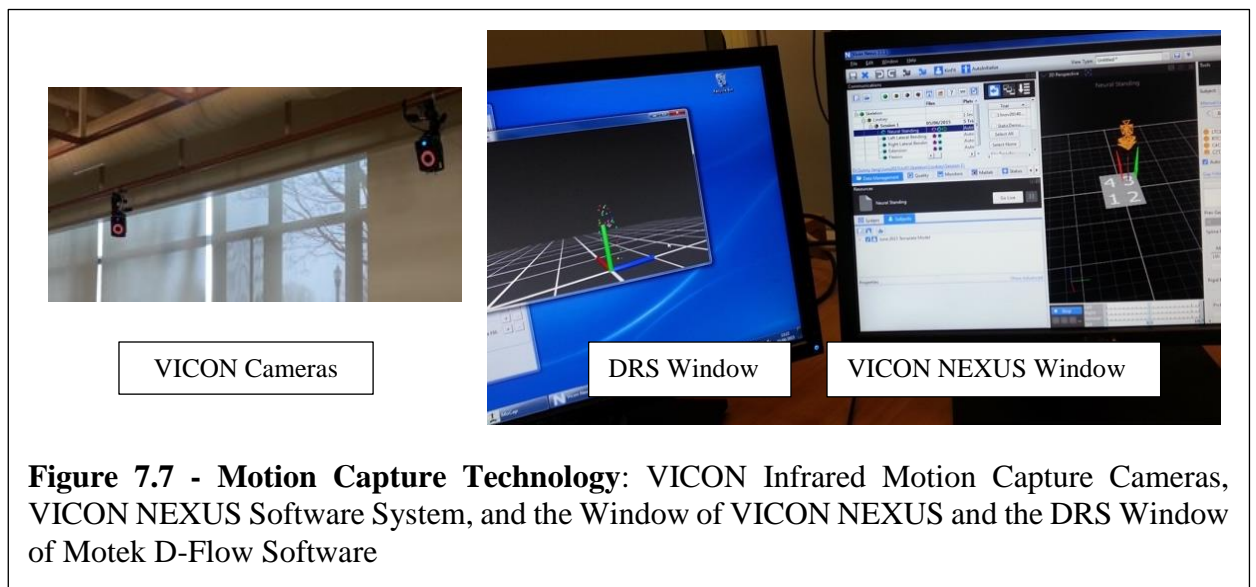
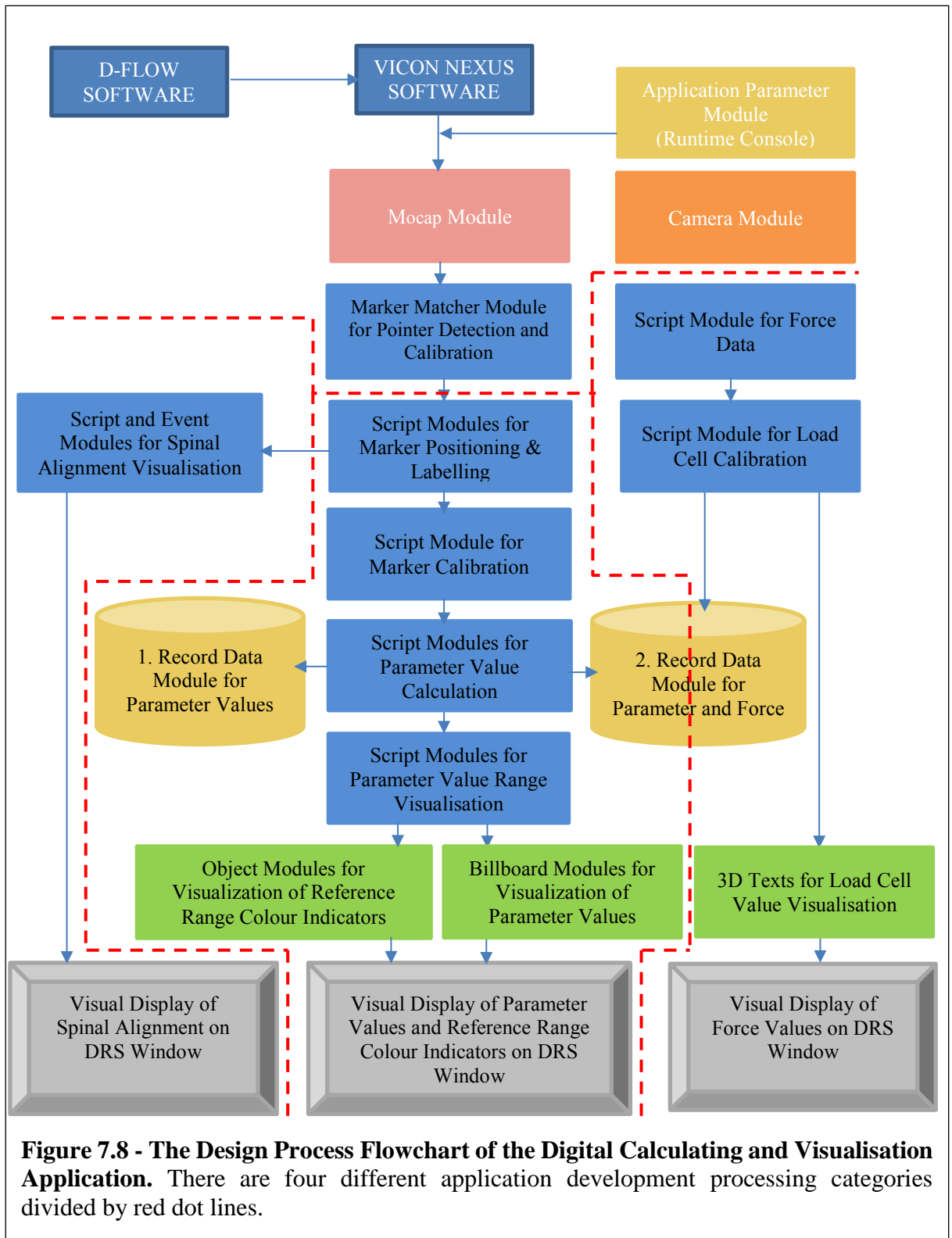


**Figure 7.7 - Motion Capture Technology:** VICON Infrared Motion Capture Cameras, VICON NEXUS Software System, and the Window of VICON NEXUS and the DRS Window of Motek D-Flow Software



This application mainly consists of four different application development processing categories: (1) application setting for data collection, (2) application for the

calculation and visualisation of parameter values, (3) application for the visualisation of spinal alignment, and (4) application for measuring corrective forces (or loads) after corrective forces applied. Figure 7.8 shows these categories by dividing them with red dot lines. The design process flowchart of the digital calculating and visualisation application developed using Nexus and Motek D-Flow software is introduced in Figure 7.8.

### 7.3.2 Application Setting for Data Collection

Once the motion capture system is calibrated with aiming and masking the cameras, and setting the volume of origin, the application can be opened in the D-Flow software. The *Mocap module*, after setting up a “Live” mode receives all data coming from the Nexus and the cameras (Figure 7.9).

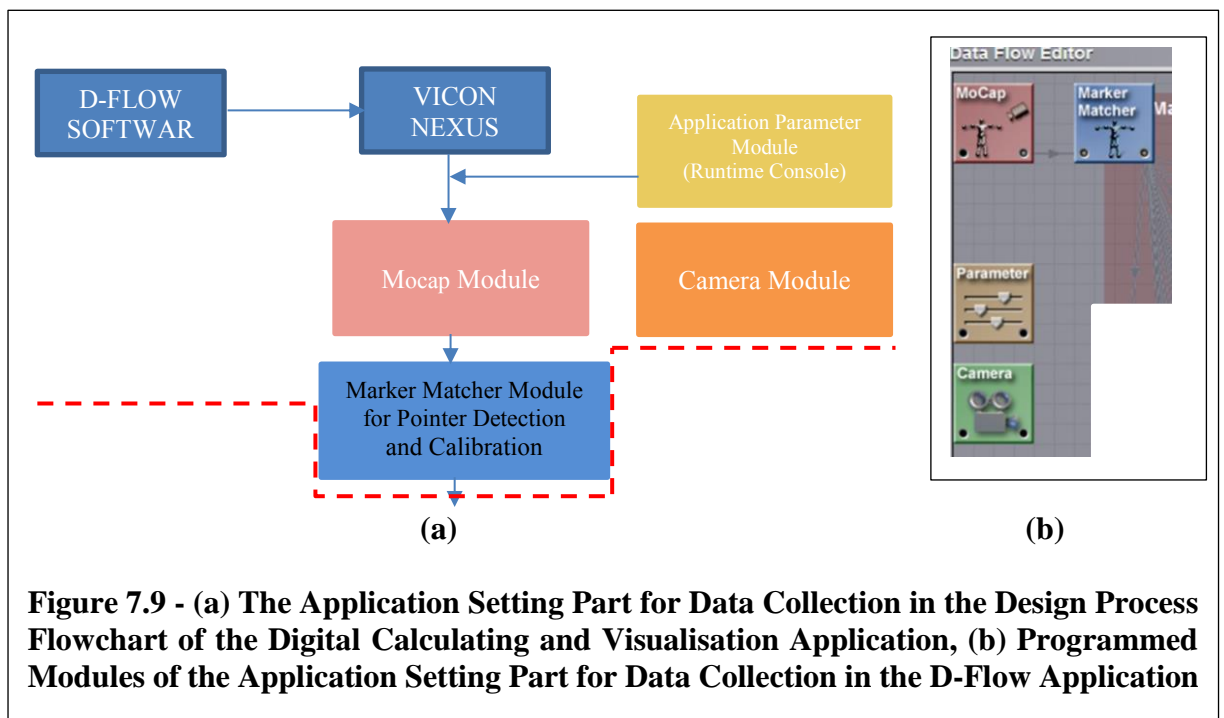
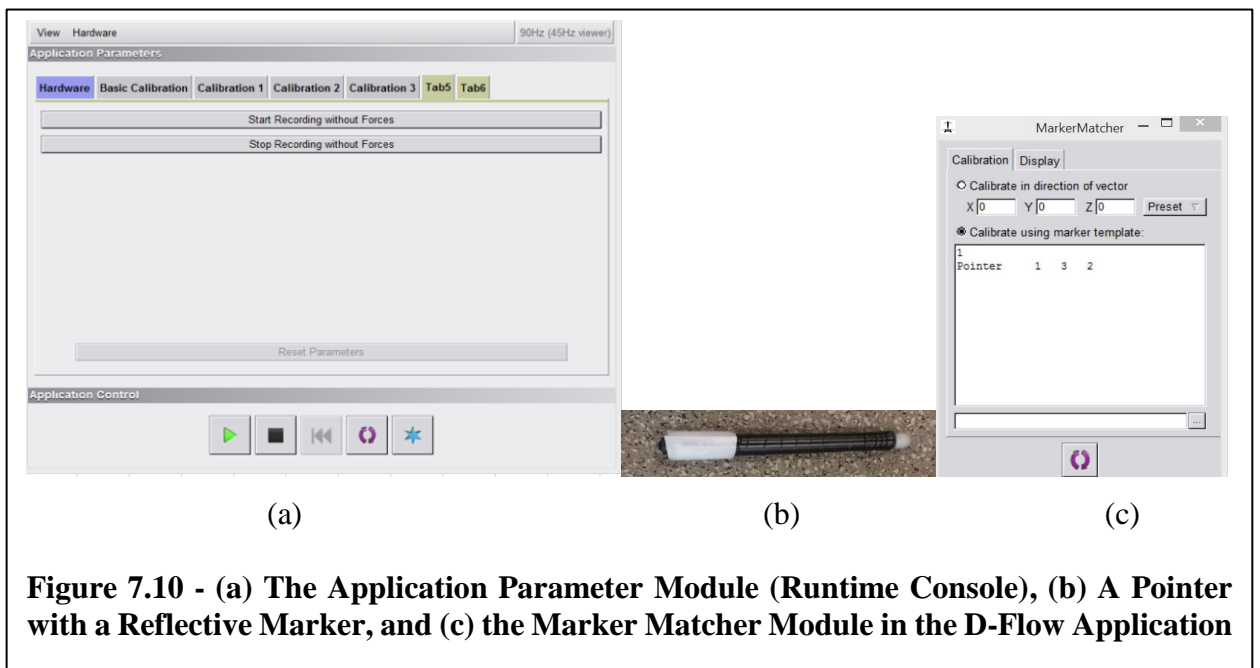


**Figure 7.9 - (a) The Application Setting Part for Data Collection in the Design Process Flowchart of the Digital Calculating and Visualisation Application, (b) Programmed Modules of the Application Setting Part for Data Collection in the D-Flow Application**

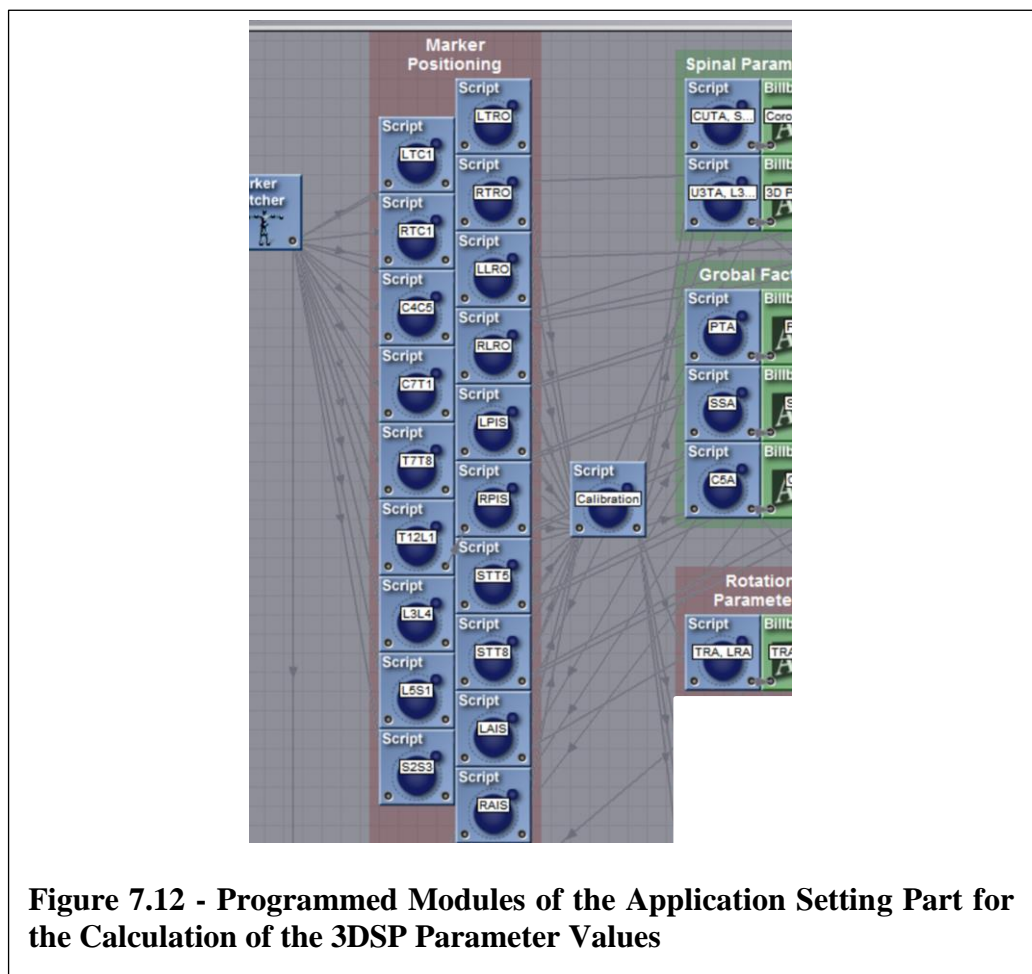
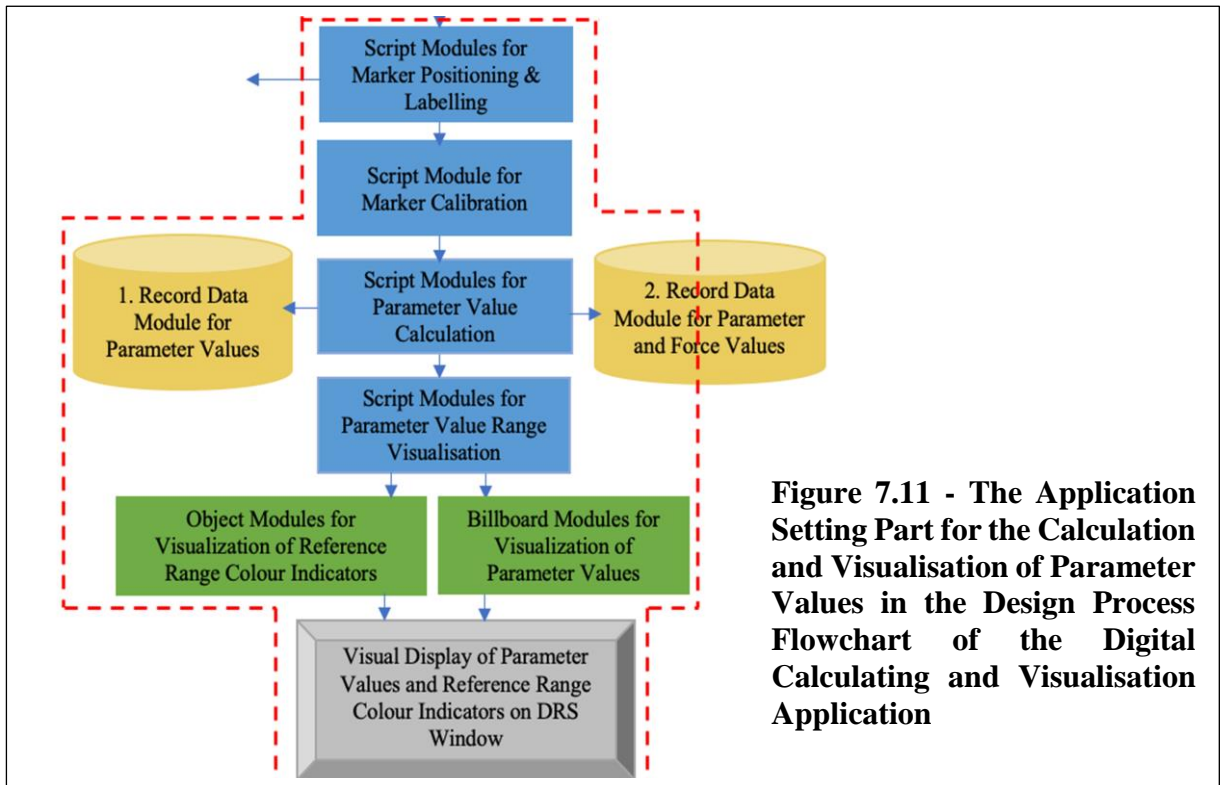
Various types of equipment were made during the development of the application. *An adapted pointer* was made and interfaced to this software combination by attaching a reflective marker on the end tip of the pointer (Figure 7.10 (b)). The end tip of the adapted pointer was used to move around and touch the 19 key surface level

anatomical landmarks of 3DSPs on the surface level of the torso instead of collecting from reflective markers attached on all anatomical landmarks of the body's surface. Whenever this pointer touches these landmarks on the torso, the application could generate the 3D Cartesian coordinated geometric data of the landmarks from the tip of pointer. Thus, a user is required to click the calibration button of the **Application Parameter Module (Runtime Console)** while the pointer is touching each landmark on the subject's torso (Figure 7.9 (a) and 7.10 (a)). The **Marker Matcher Module** was added in the software to identify the tip of the pointer (Figure 7.9 and 7.10 (c)).



### 7.3.3 Application for the Calculation of Parameter Values

This section describes how to set the application for the calculation and visualisation of the 3DSPs. Figure 7.11 summarizes the overview of the calculation and visualisation of the 3DSPs using a flow chart. In order to label or name each landmark properly and capture their coordinates, the script modules in the **“Marker Positioning”** and **“Calibration”** are created (Figure 7.12).



The followings are the details of coding programmed in the script module for the landmark of C7T1 in the “**Marker Positioning**” group to show how to label the landmark as an example:

```

----Calibration Anatomical Landmark Global Frame-----
--Initilisation of variables
ini = ini or 0
allinputs = allinputs or {}
input = input or {}
outputs.setchannels("C7T1x", "C7T1y", "C7T1z")
--Initilisation Code
if ini == 0 then
for i = 1, 3 do
allinputs[i] = "Channel"..i
end
inputs.setchannels(unpack(allinputs))
ini = 1
end
for i = 1, 3 do
input[i] = inputs.get("Channel"..i)
end
-----C7T1-----
ALx=input[1]
ALy=input[2]
ALz=input[3]
outputs.set("C7T1x", ALx)
outputs.set("C7T1y", ALy)
outputs.set("C7T1z", ALz)
print(ALx, ALy, ALz)

```

The data obtained from the tip of the pointer and the named landmarks of 3DPS processes the channels of the “**Calibration**” script module. Here are the details of coding programmed in the “**Calibration**” module:

```

--[[In this script data will be received from a static
calibration file for the position of all markers
for one frame. It will be stored as variables and output
to the calibration script. Event handling will ensure this
script is only run once and will not update when a dynamic
file is played]]--
--Initilisation of variables
ini = ini or 0
allinputs = allinputs or {}
input = input or {}
outputs.setchannels("LTC1x", "LTC1y", "LTC1z",
"RTC1x", "RTC1y", "RTC1z",
"C4C5x", "C4C5y", "C4C5z",
"C7T1x", "C7T1y", "C7T1z",
"T7T8x", "T7T8y", "T7T8z",
"T12L1x", "T12L1y", "T12L1z",

```

```

        "L3L4x", "L3L4y", "L3L4z",
        "L5S1x", "L5S1y", "L5S1z",
        "S2S3x", "S2S3y", "S2S3z",
        "LTROx", "LTROy", "LTROz",
        "RTROx", "RTROy", "RTROz",
        "LLROx", "LLROy", "LLROz",
        "RLROx", "RLROy", "RLROz",
        "LPISx", "LPISy", "LPISz",
        "RPISx", "RPISy", "RPISz",
        "STT5x", "STT5y", "STT5z",
        "STT8x", "STT8y", "STT8z",
        "LAISx", "LAISy", "LAISz",
        "RAISx", "RAISy", "RAISz")
--Initialisation code
if ini == 0 then
for i = 1, 57 do
allinputs[i] = "Channel"..i
end
inputs.setchannels(unpack(allinputs))
ini = 1
end
for i = 1, 57 do
input[i] = inputs.get("Channel"..i)
end
--Assign inputs to marker positions-----
-----Anatomy Landmark-----
LTC1x = input[1]
LTC1y = input[2]
LTC1z = input[3]
RTC1x = input[4]
RTC1y = input[5]
RTC1z = input[6]
C4C5x = input[7]
C4C5y = input[8]
C4C5z = input[9]
C7T1x = input[10]
C7T1y = input[11]
C7T1z = input[12]
T7T8x = input[13]
T7T8y = input[13]
T7T8z = input[15]
T12L1x = input[16]
T12L1y = input[17]
T12L1z = input[18]
L3L4x = input[19]
L3L4y = input[20]
L3L4z = input[21]
L5S1x = input[22]
L5S1y = input[23]
L5S1z = input[24]
S2S3x = input[25]
S2S3y = input[26]

```

```

S2S3z = input[27]
LTROx = input[28]
LTROy = input[29]
LTROz = input[30]
RTROx = input[31]
RTROy = input[32]
RTROz = input[33]
LLROx = input[34]
LLROy = input[35]
LLROz = input[36]
RLROx = input[37]
RLROy = input[38]
RLROz = input[39]
LPISx = input[40]
LPISy = input[41]
LPISz = input[42]
RPISx = input[43]
RPISy = input[44]
RPISz = input[45]
STT5x = input[46]
STT5y = input[47]
STT5z = input[48]
STT8x = input[49]
STT8y = input[50]
STT8z = input[51]
LAISx = input[52]
LAISy = input[53]
LAISz = input[54]
RAISx = input[55]
RAISy = input[56]
RAISz = input[57]
--Set outputs
outputs.set("LTC1x", LTC1x)
outputs.set("LTC1y", LTC1y)
outputs.set("LTC1z", LTC1z)
outputs.set("RTC1x", RTC1x)
outputs.set("RTC1y", RTC1y)
outputs.set("RTC1z", RTC1z)
outputs.set("C4C5x", C4C5x)
outputs.set("C4C5y", C4C5y)
outputs.set("C4C5z", C4C5z)
outputs.set("C7T1x", C7T1x)
outputs.set("C7T1y", C7T1y)
outputs.set("C7T1z", C7T1z)
outputs.set("T7T8x", T7T8x)
outputs.set("T7T8y", T7T8y)
outputs.set("T7T8z", T7T8z)
outputs.set("T12L1x", T12L1x)
outputs.set("T12L1y", T12L1y)
outputs.set("T12L1z", T12L1z)
outputs.set("L3L4x", L3L4x)
outputs.set("L3L4y", L3L4y)

```

```

outputs.set("L3L4z", L3L4z)
outputs.set("L5S1x", L5S1x)
outputs.set("L5S1y", L5S1y)
outputs.set("L5S1z", L5S1z)
outputs.set("S2S3x", S2S3x)
outputs.set("S2S3y", S2S3y)
outputs.set("S2S3z", S2S3z)
outputs.set("LTROx", LTROx)
outputs.set("LTROy", LTROy)
outputs.set("LTROz", LTROz)
outputs.set("RTROx", RTROx)
outputs.set("RTROy", RTROy)
outputs.set("RTROz", RTROz)
outputs.set("LLROx", LLROx)
outputs.set("LLROy", LLROy)
outputs.set("LLROz", LLROz)
outputs.set("RLROx", RLROx)
outputs.set("RLROy", RLROy)
outputs.set("RLROz", RLROz)
outputs.set("LPISx", LPISx)
outputs.set("LPISy", LPISy)
outputs.set("LPISz", LPISz)
outputs.set("RPISx", RPISx)
outputs.set("RPISy", RPISy)
outputs.set("RPISz", RPISz)
outputs.set("STT5x", STT5x)
outputs.set("STT5y", STT5y)
outputs.set("STT5z", STT5z)
outputs.set("STT8x", STT8x)
outputs.set("STT8y", STT8y)
outputs.set("STT8z", STT8z)
outputs.set("LAISx", LAISx)
outputs.set("LAISy", LAISy)
outputs.set("LAISz", LAISz)
outputs.set("RAISx", RTC1x)
outputs.set("RAISy", RTC1y)
outputs.set("RAISz", RTC1z)

```

The script modules in the “*Spinal Parameter*” group can calculate the values of all 3DSP parameters (Figure 7.12). The equations for measuring the angles based on the Trigonometry and Pythagoras’ theorem were programmed in the calculating scripts using a Lua programming language (The equation diagram of 3UTA were already shown in Figure 7.5 as an example of how to develop the equations). The calculated parameter values can be stored as text and then exported to the Excel file.

The following are the details of coding programmed in the script module for the parameter values of 3UTA to show how to calculate the parameter values as an

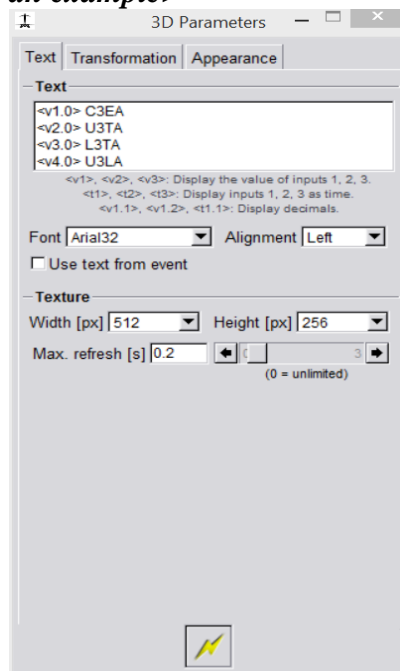
example and the screen shot of the billboard module for visualisation of the values of 3UTA:

```
-- Initialization of all (not local) variables
ini = ini or 0
-----
if ini == 0 then
x=x or {}
y=y or {}
z=z or {}
ini = 1
end

for n=1, 5 do
x[n]=inputs.get("x"..n)
y[n]=inputs.get("y"..n)
z[n]=inputs.get("z"..n)
end

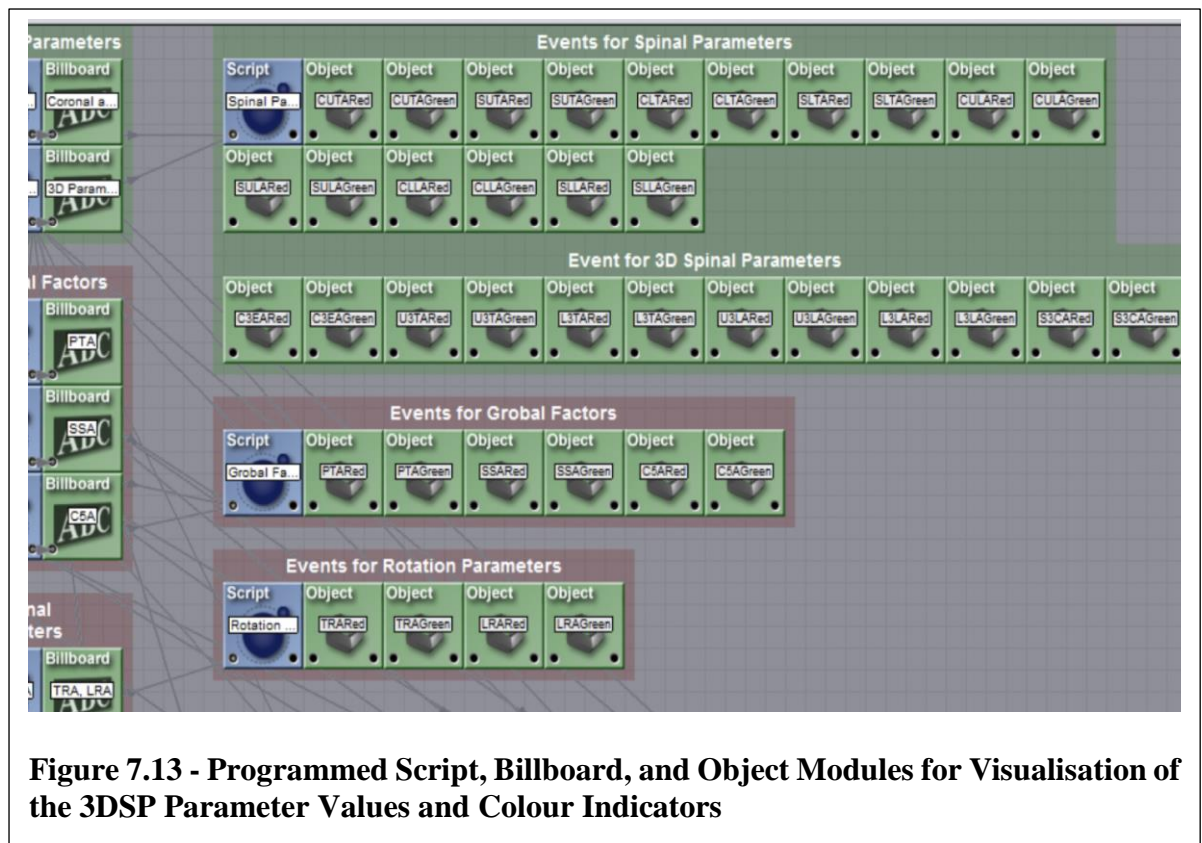
-----U3TA-----
-----
a1 = math.pow(x[4] - x[5], 2)
a2 = math.pow(y[4] - y[5], 2)
a3 = math.pow(z[4] - z[5], 2)
A = math.sqrt(a1+a2+a3)
B = math.sqrt(a1+a3)
U3TA = math.acos(B/A)
U3TAangle = math.deg(U3TA)
outputs.set("U3TAangle", U3TAangle)
```

< The screen shot of the billboard module for visualisation of the values of 3UTA as an example >



### 7.3.4 Application for Visualisation of Parameter Values and Colour Indicators

The calculated values of the 3DSP parameters are streamed to another set of script statements and the texts of the parameter values are able to be shown on the DRS window by the programmed billboard modules (Figure 7.13 and 7.14(a)). The reference range colour indicators of the parameters are built by programming the script and object modules in the each “*Event*” group, visualised in one of two colours depending on whether the value is within the reference range for that parameter (red: outside range, green: within range) on the DRS window, and located next to the calculated values of each parameter (Figure 7.13 and 7.14 (a)). The reference ranges for each 3DSP parameters were used from the results of the test, “Normal Values and Reference Ranges of the Surface Level Spinal Alignment Parameters System”, which would be explained in Chapter 8.



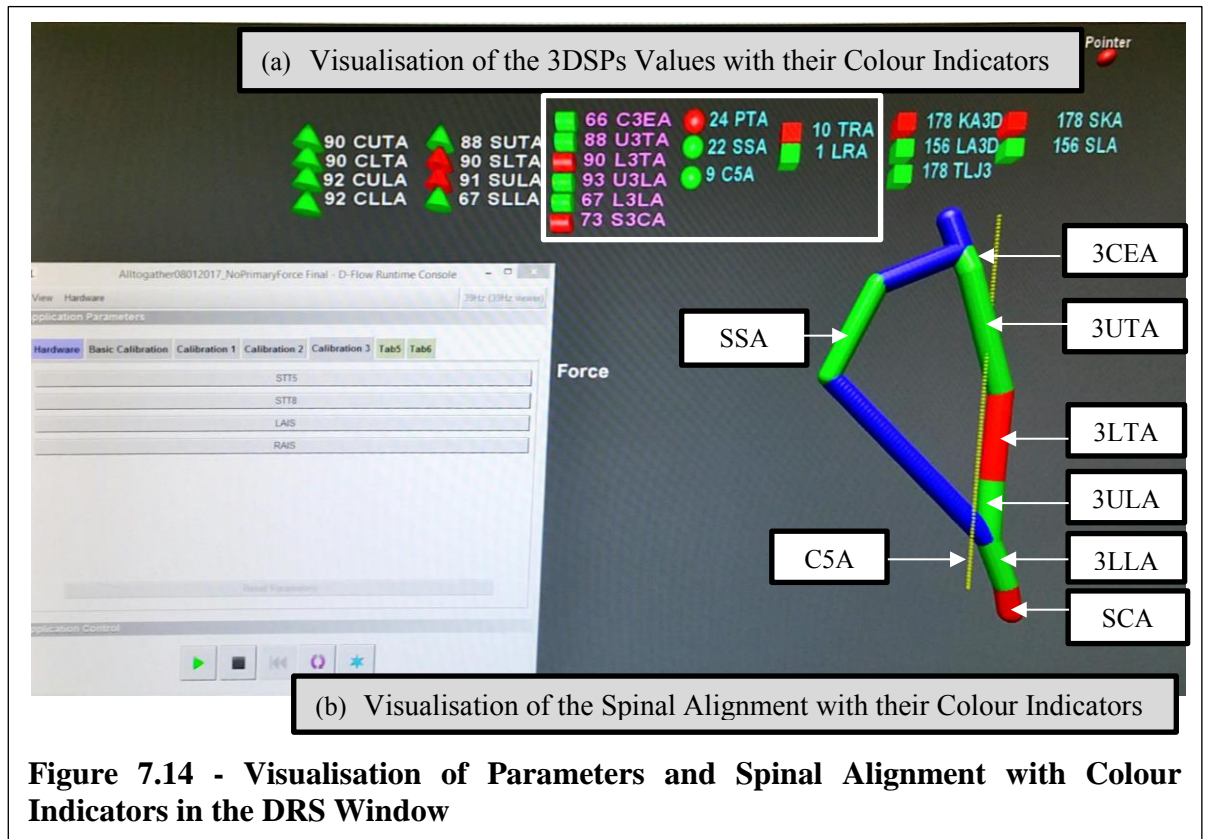


**Figure 7.14 - Visualisation of Parameters and Spinal Alignment with Colour Indicators in the DRS Window**

The followings are the details of coding programmed in the script modules:

```

--All events handled in this script

--Initilisation of variables
ini = ini or 0
allinputs = allinputs or {}
input = input or {}

--Initilisation code
if ini == 0 then
for i = 1, 20 do
allinputs[i] = "Channel"..i
end

inputs.setchannels(unpack(allinputs))
ini = 1
end

for i = 1, 20 do
input[i] = inputs.get("Channel"..i)
end

--Show U3TA-----

```

```
if input[9] > 80.10 then
  broadcast("U3TARed")
elseif input[9] < 75.12 then
  broadcast("U3TARed")
else broadcast("U3TAGreen")
end
```

```
--Show L3TA-----
if input[10] > 103.03 then
  broadcast("L3TARed")
elseif input[10] < 96.96 then
  broadcast("L3TARed")
else broadcast("L3TAGreen")
end
```

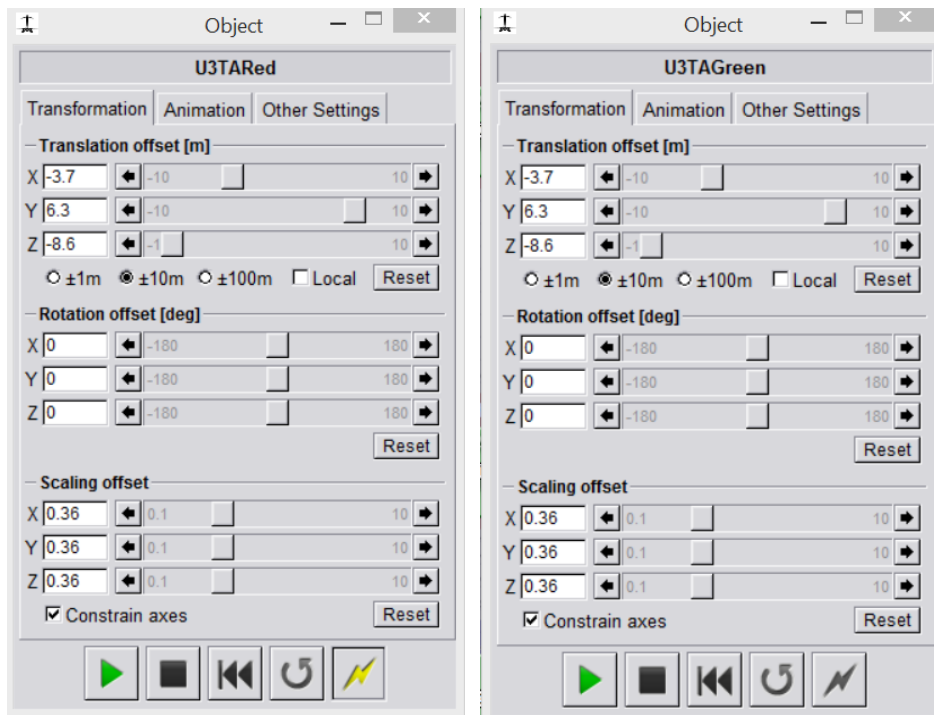
```
--Show U3LA-----
if input[11] > 100.23 then
  broadcast("U3LARed")
elseif input[11] < 95.98 then
  broadcast("U3LARed")
else broadcast("U3LAGreen")
end
```

```
--Show L3LA-----
if input[12] > 79.88 then
  broadcast("L3LARed")
elseif input[12] < 72.33 then
  broadcast("L3LARed")
else broadcast("L3LAGreen")
end
```

```
--Show C3EA-----
if input[13] > 65.19 then
  broadcast("C3EARed")
elseif input[13] < 56.36 then
  broadcast("C3EARed")
else broadcast("C3EAGreen")
end
```

```
--Show S3CA-----
if input[14] > 62.72 then
  broadcast("S3CARed")
elseif input[14] < 58.32 then
  broadcast("S3CARed")
else broadcast("S3CAGreen")
end
```

**<The screen shot of the red and green object Modules of 3UTA as an example>**



### 7.3.5 Application for Visualisation of Spinal Alignment and Colour Indicators

This application can also display the visualisation of the spinal alignment with the colour indicator for each segment by programming script and event modules (Figure 7.14 (b) and 7.16). Figure 7.15 summarizes the overview of the visualisation of the spinal alignment and the colour indicators of each segment using a flow chart. The script modules are designed to connect the landmarks of each parameter for the spinal alignment visualisation and the event modules are able to determine the colour of the connected line depending on the parameter values being within the reference range or not (Figure 7.14 (b) and 7.16).

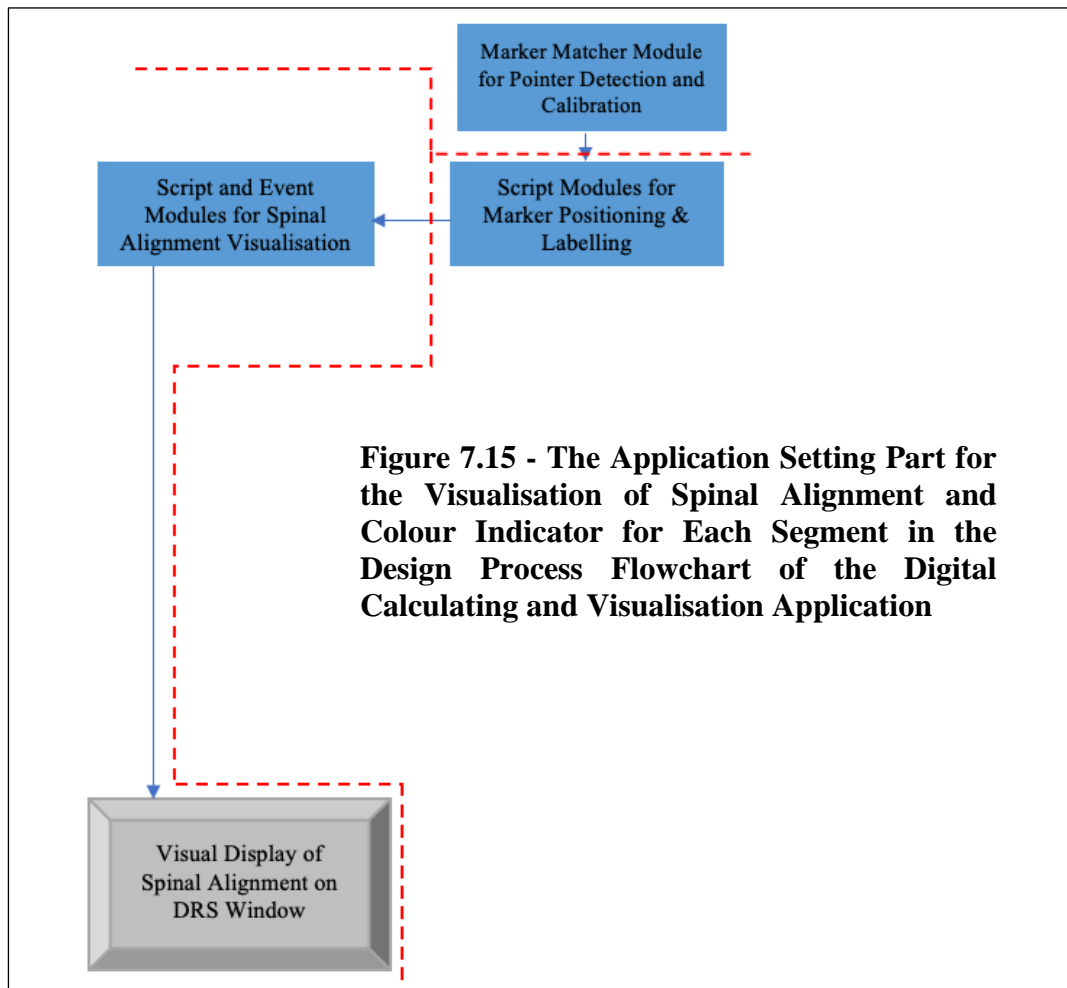


**Figure 7.15 - The Application Setting Part for the Visualisation of Spinal Alignment and Colour Indicator for Each Segment in the Design Process Flowchart of the Digital Calculating and Visualisation Application**

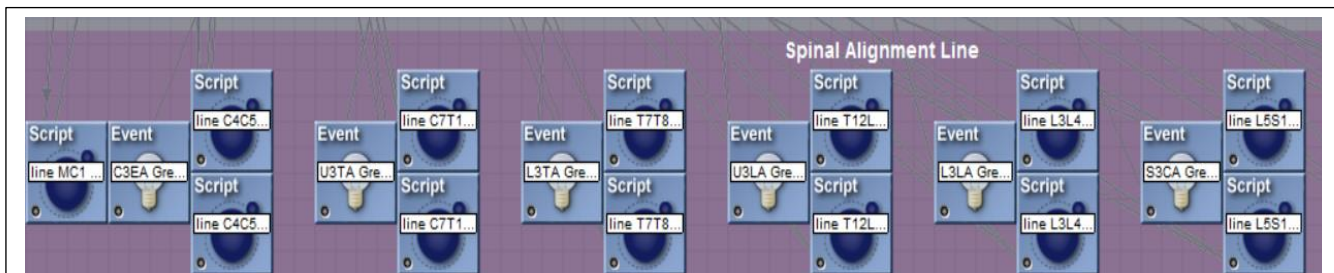
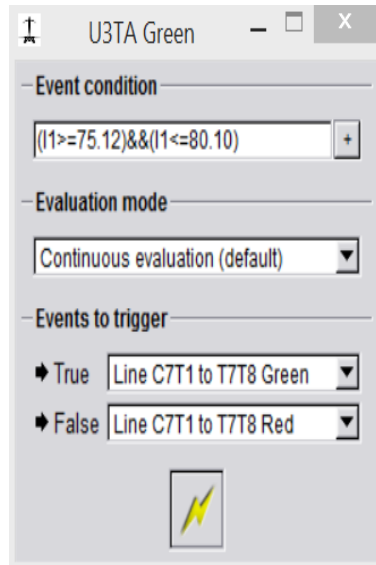


**Figure 7.16 - Programmed Script and Event Modules for Visualisation of Spinal Alignment**

Here are the screen shot of the 3UTA event module and details of coding programmed in the script of the segment of 3UTA in the “*Spinal Alignment Line*” group to show how to visualise the spinal alignment as an example:

<The screen shot of the 3UTA event module>



**1. Line C7T1 to T7T8 for Green Colour**

*ini = ini or 0*

*line=line or {}*

*if ini==0 then*

*mysize=0.03*

*mycolour="Green"*

*for n = 1, 50 do*

*line[n]=object.create("Sphere", mycolour)*

*node.setscaling(line[n],mysize,mysize,mysize)*

*end*

*ini=1*

*end*

*x1=inputs.get("x1")*

*y1=inputs.get("y1")*

*z1=inputs.get("z1")*

*x2=inputs.get("x2")*

*y2=inputs.get("y2")*

*z2=inputs.get("z2")*

*dx=(x2-x1)/49*

*dy=(y2-y1)/49*

*dz=(z2-z1)/49*

*mylength=(((x2-x1)^2)+((y2-y1)^2)+((z2-z1)^2))^0.05*

*for n=1, 50 do*

*node.setposition(line[n],x1+((n-1)\*dx),y1+((n-1)\*dy),z1+((n-1)\*dz))*

*end*

**2. Line C7T1 to T7T8 for Red Colour**

```

ini = ini or 0
line=line or {}

if ini==0 then

mysize=0.03
mycolour="Red"

for n = 1, 50 do
line[n]=object.create("Sphere", mycolour)
node.setscaling(line[n],mysize,mysize,mysize)
end

ini=1
end

x1=inputs.get("x1")
y1=inputs.get("y1")
z1=inputs.get("z1")
x2=inputs.get("x2")
y2=inputs.get("y2")
z2=inputs.get("z2")
dx=(x2-x1)/49
dy=(y2-y1)/49
dz=(z2-z1)/49
mylength=(((x2-x1)^2)+((y2-y1)^2)+((z2-z1)^2))^0.05

for n =1, 50 do
node.setposition(line[n],x1+((n-1)*dx),y1+((n-1)*dy),z1+((n-1)*dz))
end

```

### 7.3.6 Application for Applied Force Measurements and Visualisation

The application also has the capacity to measure corrective force through the connections of load cells while applying the corrective forces (Figure 7.17 (a)). The measurements also can be shown on the DRS window (Figure 7.17 (b) and 7.18). Figure 7.19 summarizes the overview of the applied force measurements and visualisation using a flow chart.

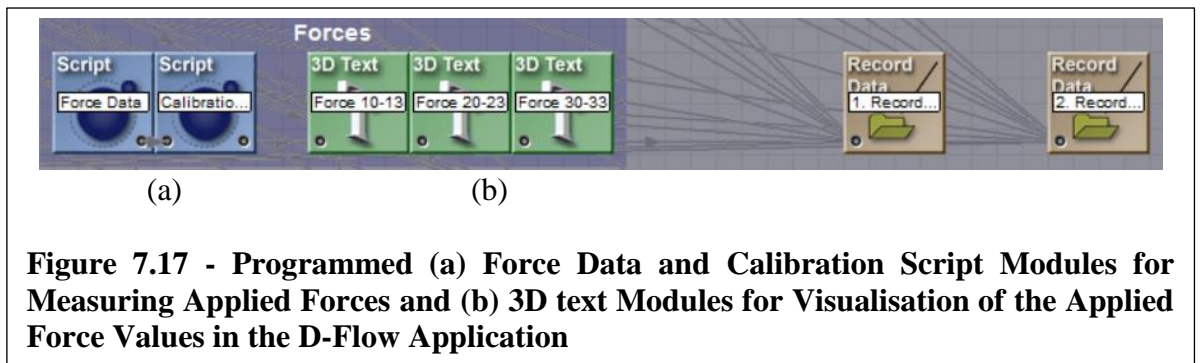


**Figure 7.17 - Programmed (a) Force Data and Calibration Script Modules for Measuring Applied Forces and (b) 3D text Modules for Visualisation of the Applied Force Values in the D-Flow Application**

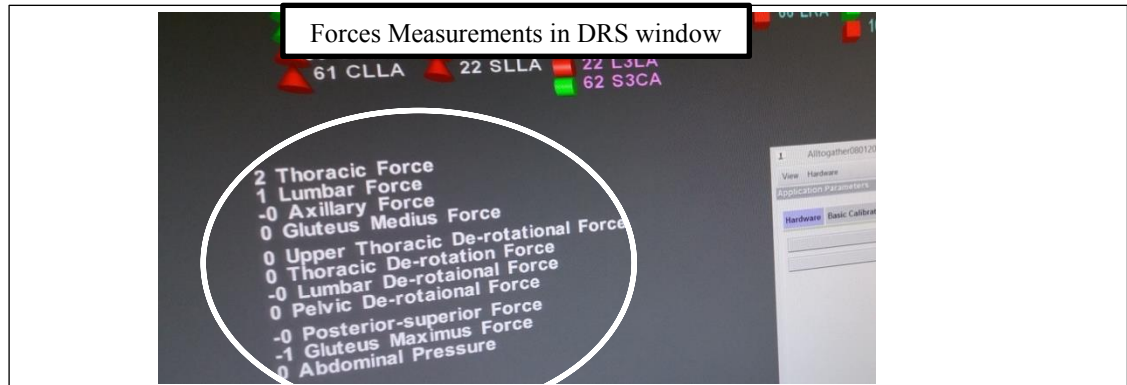


**Figure 7.18 - Visualisation of Applied Force Values in the DRS Window**

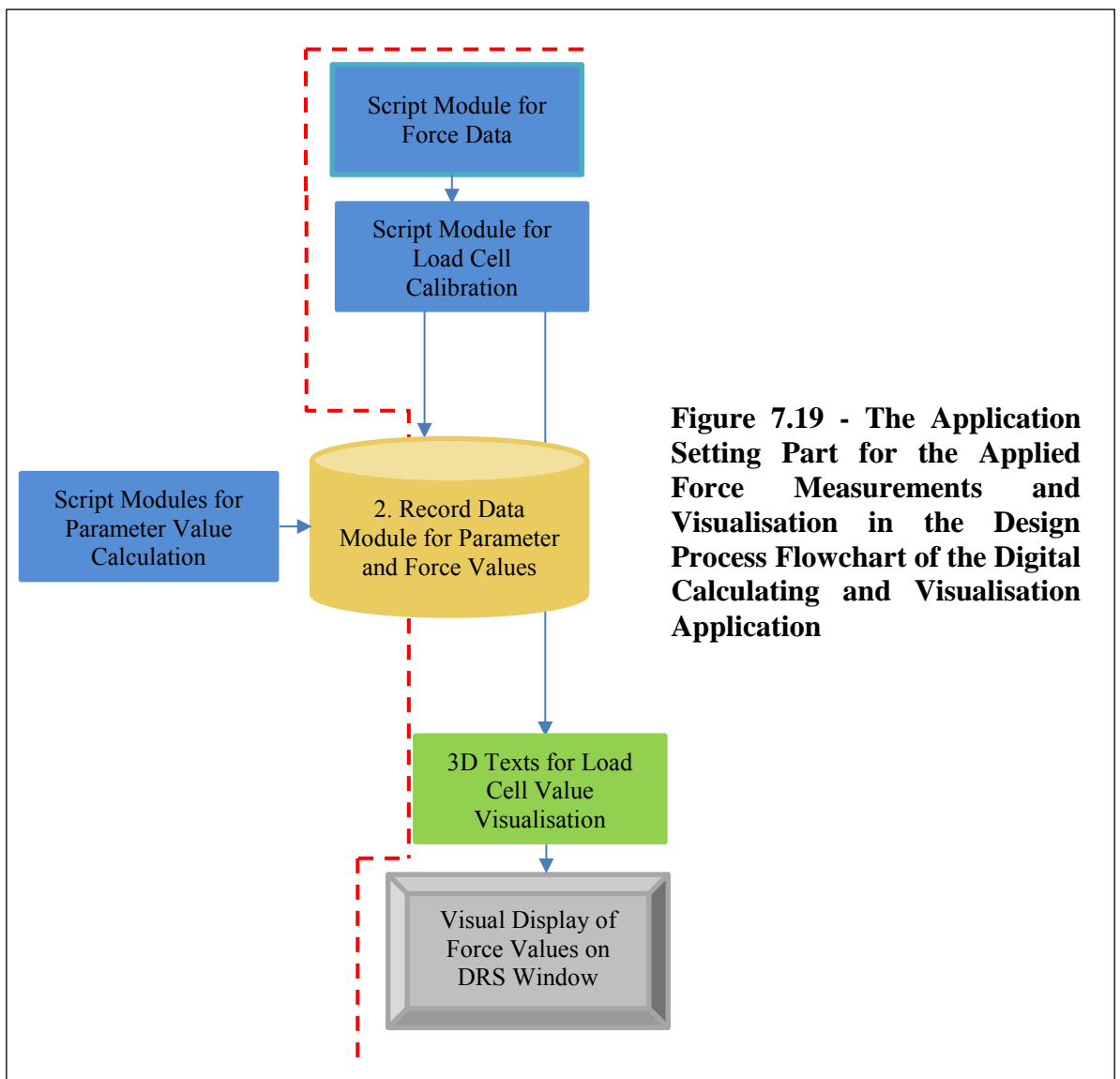
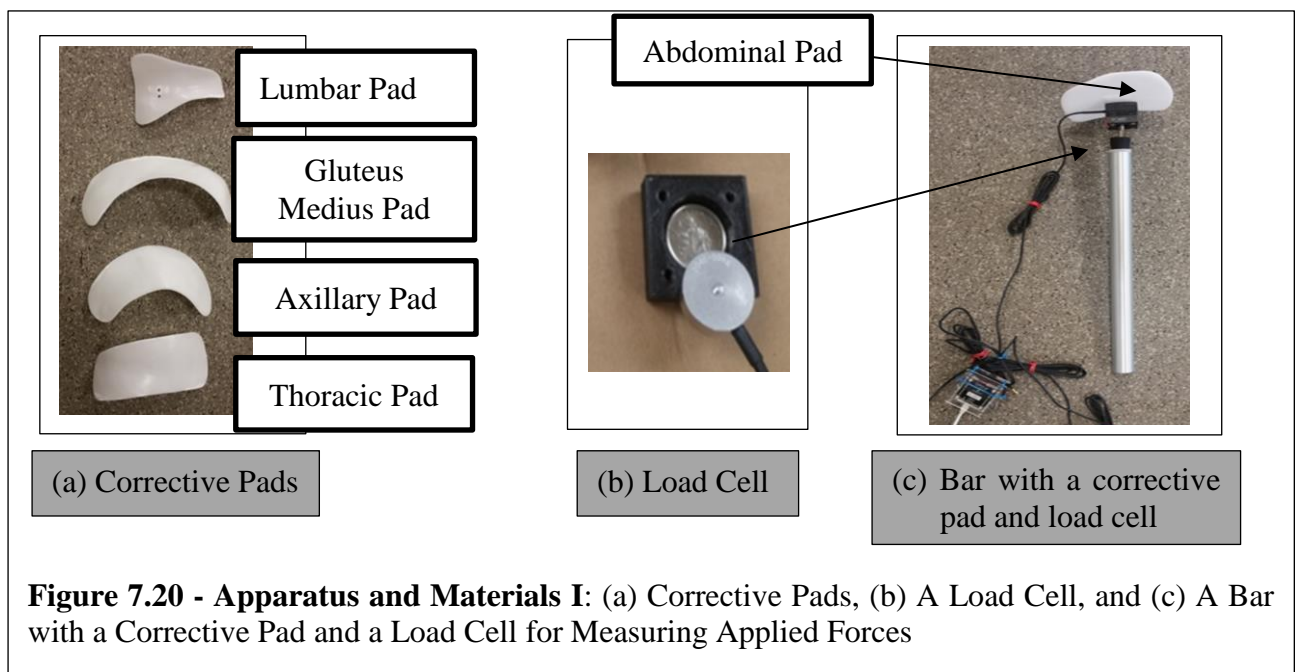


**Figure 7.19 - The Application Setting Part for the Applied Force Measurements and Visualisation in the Design Process Flowchart of the Digital Calculating and Visualisation Application**

Prior to developing the application for the applied force measurements and visualisation, it was necessary to create a *Scoli-Standing Frame*, fabricate corrective pads, and connect load cells to the corrective pads in order to measure the optimal corrective forces while corrective pads are applied on a scoliotic spine.

Thus, various corrective pads were made of well-padded co-polymer to apply corrective force on the AIS spine similar to the pads of an orthotic device (Figure 7.20 (a)). Button type load cells were connected by wires to the application to measure the applied corrective force, and placed between the corrective pads and bars to identify the optimal placements of 3D biomechanical corrective forces (Figure 7.20 (b) and (c)).



A *Scoli-Standing Frame* was developed to maintain the posture of an AIS patient and apply corrective pads properly during testing (Figure 7.21 (b)). As shown in Figure 7.21, these bars are clamped into the uprights of the *Scoli-Standing Frame*. The heights and angles of the corrective pads can be adjusted using the adjustable cramps of the frame, and the horizontal placements of the pads can be moved by adjusting the placements of the uprights on the upper and lower rings of the frames.

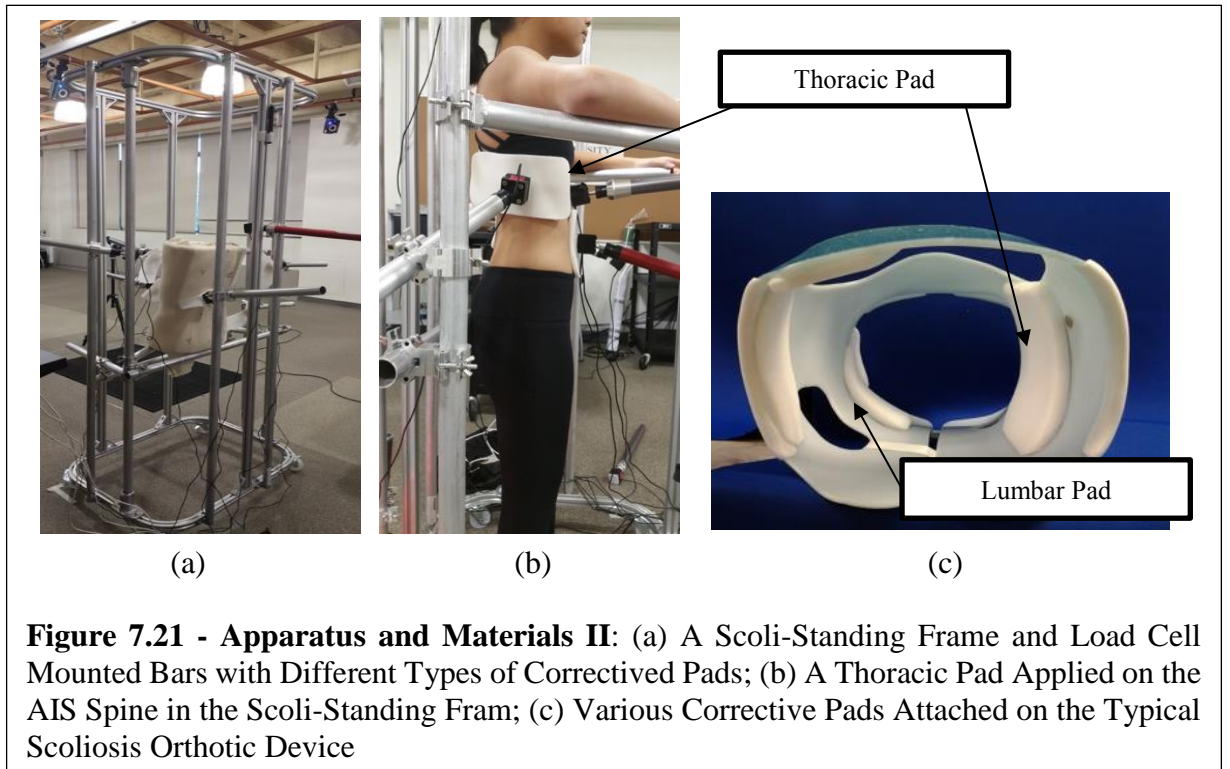


**Figure 7.21 - Apparatus and Materials II:** (a) A Scoliosis Standing Frame and Load Cell Mounted Bars with Different Types of Corrective Pads; (b) A Thoracic Pad Applied on the AIS Spine in the Scoliosis Standing Frame; (c) Various Corrective Pads Attached on the Typical Scoliosis Orthotic Device

To measure corrective force values, 12 button type load cells were connected to the three PhidgetBridges each with 4-Wheatstone bridge circuits giving 12 outputs (Figure 7.22). Each load cell has excitation lines and an output line that gives a very small voltage, which is amplified by the bridge. The power lines from the load transducers were wired into the 5V power terminal and the ground terminal. The other two signal wires were connected to the + and - terminals on the Bridge. Through a USB cable, the PhidgetBridge was connected to the computer, and configured using the Phidget Control Panel.

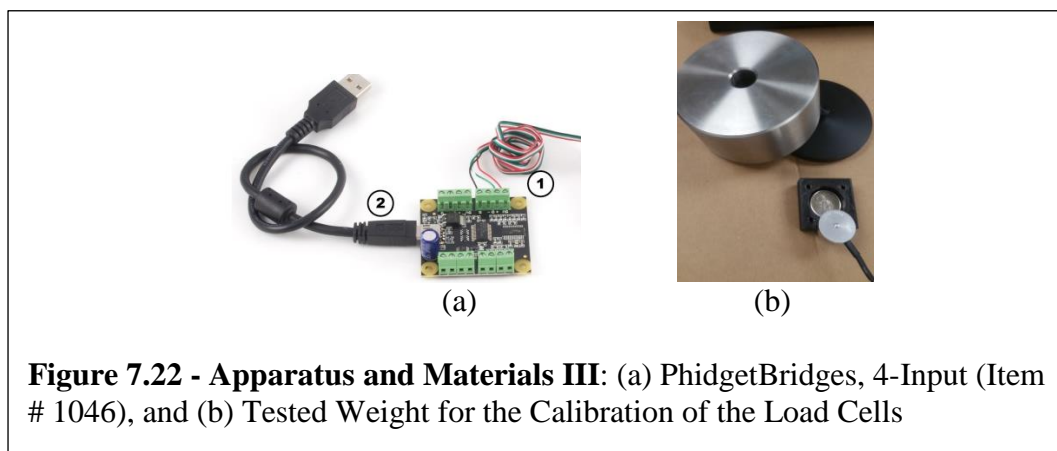


**Figure 7.22 - Apparatus and Materials III:** (a) PhidgetBridges, 4-Input (Item # 1046), and (b) Tested Weight for the Calibration of the Load Cells

To read applied forces on the load cells, a script module “Force Data” was added in the D-Flow (Figure 7.17 (a)).

Each load cell was calibrated using a simple regression equation by applying a possible maximum load and zero load.

$$\text{Computer output } (y) = A * \text{Force applied } (x) + B$$

In here, x is an applied loading force in Newtons and y is a reading voltage value.

Figure 7.22 (b) shows the loading of the weight for the calibration of a load cell. First no weight ( $x_0$ ) was applied to the sensor and the output was recorded ( $y_0$ ). The *possible maximum* weight ( $x_m$ ) was then placed on the sensor. After waiting the approximate same amount of time for the output to settle, the output was recorded ( $y_m$ ). The maximum mass which was tested for this calibration was 4.095kg giving a loading weight of 4.095 x 9.81 or 40.2N ( $y_m$ ). A and B were defined with the following equations.

$$\text{Possible maximum applied (or loading) force} = x_m$$

$$\text{No applied (or loading) force} = x_0$$

$$\text{Reading Voltage value when the maximum force was applied} = y_m$$

$$\text{Reading Voltage value with no loading} = y_0$$

$$y_0 = Ax_0 + B \text{ but } x_0 = 0 \text{ hence}$$

$$B = y_0$$

$$y_m = Ax_m + B = Ax_m + y_0$$

$$A = (y_m - y_0) / x_m$$

Appendix 7.1 indicates A and B for each load cells.

Here are the details of coding programmed for the “**Force Data and Calibration**” scripts and the screen shot of the 3D text module for visualisation of the force values:

## **1. Force Data**

*require 'winapi'*

*ini = ini or 0*

*if ini==0 then*

*mycount=0*

*function getforce()*

*p,f=winapi.spawn\_process('c:\python27\python.exe C:\pyprogs\sunnymultiplebridges.py')*

*end*

*infilename='C:\pyprogs\forcefile.txt'*

*ini=1*

*end*

*myperiodrun=50*

*myperiodread=10*

*mycount=mycount+1*

*if mycount==1 then*

*getforce()*

*end*

*if mycount==myperiodread+1 then*

*f=assert(io.open(infilename,"r"))*

*--t=f:read("\*all")*

*outputs.set("force10",f:read("\*number"))*

*outputs.set("force11",f:read("\*number"))*

*outputs.set("force12",f:read("\*number"))*

*outputs.set("force13",f:read("\*number"))*

*outputs.set("force20",f:read("\*number"))*

*outputs.set("force21",f:read("\*number"))*

*outputs.set("force22",f:read("\*number"))*

*outputs.set("force23",f:read("\*number"))*

*outputs.set("force30",f:read("\*number"))*

*outputs.set("force31",f:read("\*number"))*

*outputs.set("force32",f:read("\*number"))*

*outputs.set("force33",f:read("\*number"))*

*f:close()*

*end*

*if mycount==myperiodrun+myperiodread then*

*mycount=0*

*end*

## **2. Calibration of Load Cells**

*ini = ini or 0*

*if ini == 0 then*

*val=val or {}*

*ini = 1*

```

end

for n=1, 12 do
val[n]=inputs.get("val"..n)
end

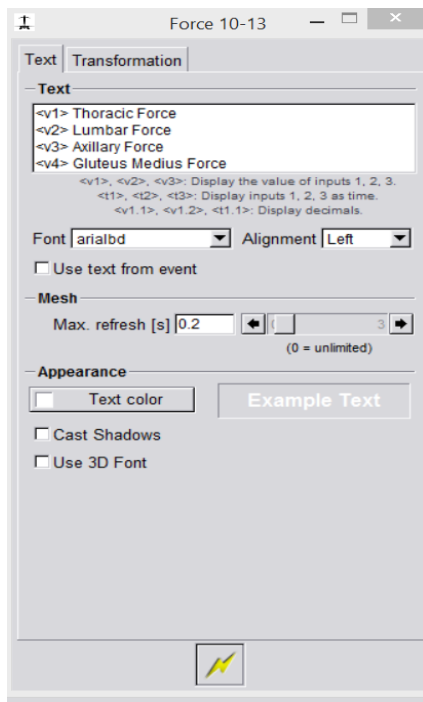
load10=(val[1]-282)/2.3394642
load11=(val[2]-149)/2.3145763
load12=(val[3]-271)/2.3145763
load13=(val[4]-206)/2.3643521
load20=(val[5]-134)/2.0905851
load21=(val[6]-108)/2.0905851
load22=(val[7]-278)/2.3145763
load23=(val[8]-261)/2.3892401
load30=(val[9]-201)/-1.9412575
load31=(val[10]-172)/2.2150246
load32=(val[11]-204)/2.3643521
load33=(val[12]-140)/2.2896884

outputs.set("load10", load10)
outputs.set("load11", load11)
outputs.set("load12", load12)
outputs.set("load13", load13)
outputs.set("load20", load20)
outputs.set("load21", load21)
outputs.set("load22", load22)
outputs.set("load23", load23)
outputs.set("load30", load30)
outputs.set("load31", load31)
outputs.set("load32", load32)
outputs.set("load33", load33)

print(load10)
print(load11)
print(load12)
print(load13)
print(load20)
print(load21)
print(load22)
print(load23)
print(load30)
print(load31)
print(load32)
print(load33)

```

**<The screen shot of the 3D text module for visualisation of the force values>**



#### 7.4 Discussion and Conclusion

The purpose of developing this digital calculating and visualisation system as an AIS assessment tool was for use in visualizing the 3D misalignments and deformities of AIS by providing immediate colour feedback in real time. Furthermore, this application could be used to identify the optimal placement of 3D biomechanical corrective forces by comparing the changes of the parameters and colour indicators before and after corrective force application. In this way the solution can be optimised so that the measured spinal alignment parameter values are closest to the reference range values of the non-scoliosis subjects. Thus, this application was used for exploring the existing disagreements among the professional community involved in the orthotic treatment of AIS (Chapter 4). The implementation test results of this developed digital calculating and visualisation system are presented in Chapter 10.

**Chapter 8. Normal Values and Reference Ranges of the  
Surface Level Spinal Alignment Parameters  
System**

## **8.1 Introduction**

There is a lack of understanding of the 3D misalignment patterns and deformities of Adolescent Idiopathic Scoliosis (AIS), and therefore no universally agreed-upon biomechanical principles in the orthotic treatment of AIS have been achieved to date. To address these concerns, 3D skin level parameters (3DSPs) including SSAPs were developed. Testing established their concurrent validity with radiographic alignment parameters in adolescents with AIS and the ability to quantify the 3D misalignment and deformities of AIS. A non-invasive digital calculating and visualisation assessment application was also developed. This application has the capacity to measure the 3D parameters and visualize the values and shape of spinal misalignment by utilizing motion capture technology as mentioned in the previous chapter. On the screen of the application, the values of each parameter are shown in one of two colours depending on whether the value is within the reference range for that parameter. Thus, defining the reference ranges of SSAPs was necessary before using this application for a future study to define the optimal orthotic corrective force placements for AIS.

The purpose of this study was to use motion capture technology to investigate the reference ranges of 11 3D skin level parameters (3DSPs) including SSAPs, by measuring each parameter from the anatomically neutral spine and trunk of non-scoliotic adolescents in the same age range as those with AIS. This study also examined if the measured spinal alignment parameters accurately portray the structural characteristics and unique features of a non-scoliotic and neutral spine and trunk.

## **8.2 Materials and Methods**

### **8.2.1 Subjects**

Twenty non-scoliotic adolescent girls in the same age range as those with AIS were recruited, and each parameter's measurements were taken from the anatomically neutral and non-scoliotic spines and trunks. AIS is more than 10 times more common and more likely to have curve progression to 30 degrees in girls than in boys, with an overall ratio of 11:1 (Miler, 1999). To match the gender dominance of the scoliosis group and for orthotic treatment, only girls were recruited.

- Subject inclusion criteria:  
Subjects were included if they were females between the ages 10 and 15, who lacked any scoliosis deformities.
- Subject exclusion criteria:  
Any subject was excluded if they had leg-length discrepancies of more than 2 cm, had any deformities of the lower extremities or other spine deformities, or had any surgical procedures on the lower extremities or spine.

### 8.2.2 Outcome Measures and Procedures

The 11 3DSPs including five 3D SSAPs and six 3D non-spinal alignment parameters, were measured. Five coronal and six sagittal SSAPs were also measured to examine if the measured SSAPs accurately portray the structural characteristics and unique features of a non-scoliotic and neutral spine and trunk. The measured parameters were:

- Five 3D spinal alignment parameters: **3CEA** (3D Lower Cervical Alignment to Horizontal Angle), **3UTA** (3D Upper Thoracic Alignment to Horizontal Angle), **3LTA** (3D Lower Thoracic Alignment to Horizontal Angle), **3ULA** (3D Upper Lumbar Alignment to Horizontal Angle), **3LLA** (3D Lower Lumbar Alignment to Horizontal Angle)
- Six 3D non-spinal alignment parameters: **TRA** (Thoracic Rotation Angle), **LRA** (Lumbar Rotation Angle), **PTA** (Pelvic Tilt Angle), **SCA** (Sacral Alignment to Horizontal Angle, equivalent to 3SCA), **C5A** (C5 Balance Angle), and **SSA** (Sternal Angle)
- Five coronal alignment parameters: **CCEA** (Coronal Lower Cervical Alignment to Horizontal Angle), **CUTA** (Coronal Upper Thoracic Alignment to Horizontal Angle), **CLTA** (Coronal Lower Thoracic Alignment to Horizontal Angle), **CULA** (Coronal Upper Lumbar Alignment to Horizontal Angle), and **CLLA** (Coronal Lower Lumbar Alignment to Horizontal Angle)
- Five sagittal alignment parameters: **SCEA** (Sagittal Lower Cervical Alignment to Horizontal Angle), **SUTA** (Sagittal Upper Thoracic Alignment to Horizontal

Angle), **SLTA** (Sagittal Lower Thoracic Alignment to Horizontal Angle), **SULA** (Sagittal Upper Lumbar Alignment to Horizontal Angle), and **SLLA** (Sagittal Lower Lumbar Alignment to Horizontal Angle)

Forty reflective markers (14mm plastic balls) were attached on the key surface level anatomical landmarks of the parameters using a special tape that is non-irritating to the skin (Figure 8.1). During data collection, each subject stood still in a comfortable position with their arms flexed at a consistent angle (60 degrees) on the armrest of a standing support frame. Instructions for positioning in the frame were developed on the basis of the radiographic positioning guidelines of the Scoliosis Research Society (SRS):

- a. Centre the participant in the frame
- b. The pelvis and feet must be neutral position
- c. The patient's forearms rest on the armrest bars of the frame. Shoulders are relaxed and the elbows flexed to 60 degrees.
- d. The patient's knees rest on the knee pads, and the head is in neutral facing forward.



The Vicon Nexus software system (Oxford, U.K) and its cameras collected three-dimensional (3D) Cartesian coordinate geometric data from the markers (Figure 8.2 (a)). Each capture time lasted about 10 seconds. The values for each 3DSP were calculated from the geometric data obtained from the reflective markers using equations programmed in bespoke Lua script modules in Motek (D-flow) software (Amsterdam, Netherlands) (Figure 8.2 (b)).

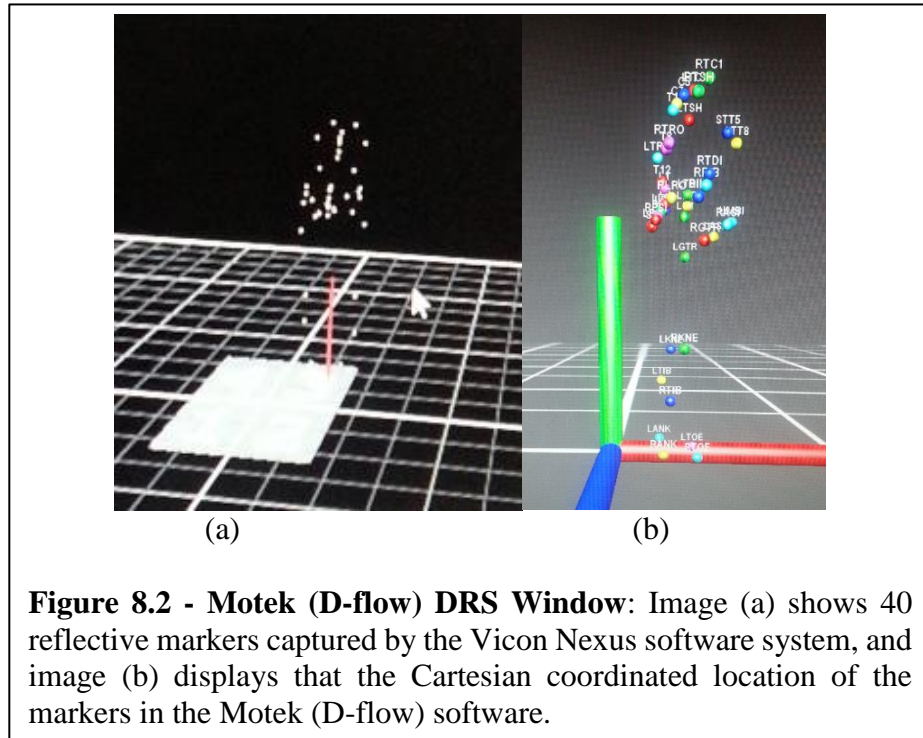


**Figure 8.2 - Motek (D-flow) DRS Window:** Image (a) shows 40 reflective markers captured by the Vicon Nexus software system, and image (b) displays that the Cartesian coordinated location of the markers in the Motek (D-flow) software.

### 8.3 Data Analysis

First, a normality test was performed for each parameter using IBM SPSS Statistics Version 25 software (New York, USA) to determine whether the data was normally distributed. The normal distribution can be confirmed by calculating the skewness and kurtosis z-values (Equation 8.1) (Appendix 8.1), the p-value of the Shapiro-Wilk test (Appendix 8.2), and visual inspection of the normal probability Q-Q plots (Appendix 8.3) for each category of the independent variable (Shapiro & Wilk, 1965; Cramer, 1998; Cramer & Howitt, 2004).

$$\text{Skewness (or Kurtosis) z-value} = \frac{\text{Skewness Measure (or Kurtosis Measure)}}{\text{Standard Error}} \quad (8.1)$$

All z-values for the parameters were within +/- 1.96 and all p-values of the Shapiro-Wilk test were nonsignificant ( $\alpha = 0.05$ ). This indicates that the data were a little skewed and kurtotic for each parameter, but, they did not deviate significantly from normality. Each parameter was normally distributed.

Second, the mean, standard deviation (SD), and 95% confidence interval (CI) for each parameter were calculated. The lower bound and upper bound of the 95% CI were used for defining the ranges of the normal values for SSAPs. The reference ranges were defined using the mean and SD of each parameter and classified into three categories (Redmond et al., 2008; Moseley et al., 2001):

- a. Neutral Alignment Category: Values in the range between mean +/- 1 SD
- b. Potentially Abnormal Alignment Category: Values in the range from mean +/- 1 SD to mean +/- 2 SD
- c. Malalignment Category: Values in the range more than mean +/- 2 SD

Finally, the spinal alignment of non-scoliotic spines were illustrated through Microsoft Excel using the means of the coronal and sagittal SSAPs and visually examined to find out whether the parameters accurately reflect the structural characteristics of a non-scoliotic spine and the unique coronal and sagittal features in each spinal bony structural segment in normal populations.

## **8.4 Results**

The average age of the twenty non-scoliotic adolescent girls that participated in the study was 12.5 years old. Table 8.1 shows the mean and standard deviation of each SSAP. The ranges of the normal values of each parameter (lower and upper bound of the 95% CI) is shown in Table 8.1. Each reference ranges for neutral alignment, potentially abnormal alignment, and malalignment categories are displayed in Table 8.2.

In Figure 8.3, the blue dotted line presents the coronal spinal alignment of the non-scoliotic spines, which was plotted based on the means of the coronal SSAPs (CCEA,

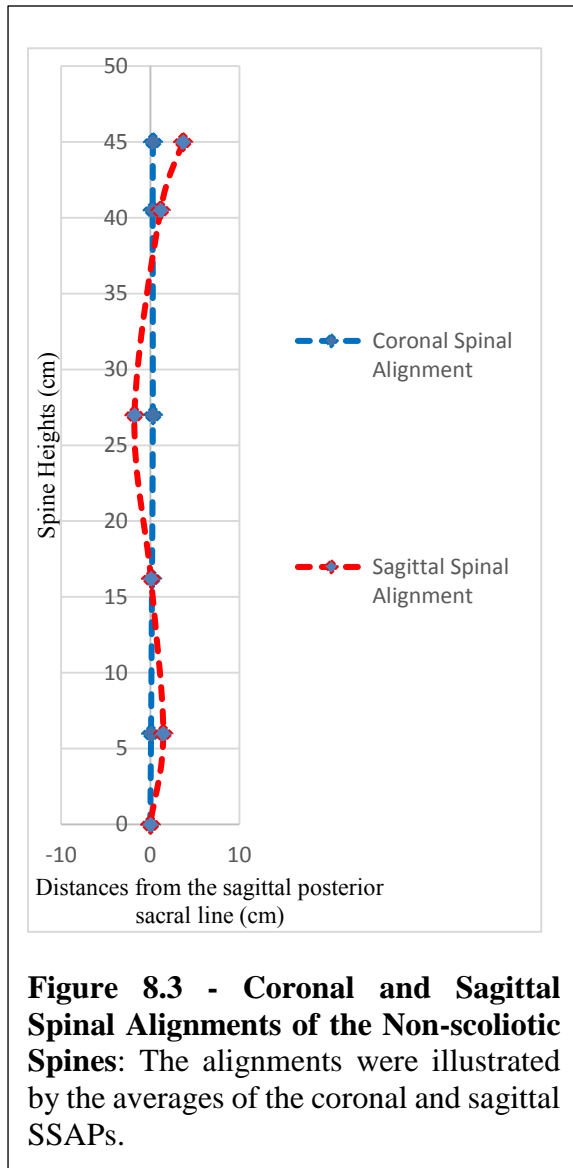
CUTA, CLTA, CULA, and CLLA). The red dotted line is the sagittal spinal alignment of the non-scoliotic spines plotted using the means of the sagittal SSAPs (SCEA, SUTA, SLTA, SULA, and SLLA).

3DSPs		Mean $\pm$ SD	95% Confidence Interval	
			Lower Bound	Upper Bound
Skin Level Spinal Alignment Parameters	3CEA	60.78 $\pm$ 9.43	56.36	65.19
	3UTA	77.61 $\pm$ 5.32	75.12	80.10
	3LTA	100.00 $\pm$ 6.49	96.96	103.03
	3ULA	98.10 $\pm$ 4.55	95.98	100.23
	3LLA	76.10 $\pm$ 8.07	72.33	79.88
Skin Level Non- Spinal Alignment Parameters	TRA	-1.54 $\pm$ 3.52	-3.19	0.11
	LRA	-0.46 $\pm$ 3.53	-2.11	1.19
	PTA	11.41 $\pm$ 5.48	8.84	13.97
	C5A	5.45 $\pm$ 3.37	3.87	7.03
	SSA	21.74 $\pm$ 7.63	18.17	25.31
	SCA	60.52 $\pm$ 4.71	58.32	62.72

**Table 8.1 - The Mean, Standard Deviation (SD), and 95% Confidence Interval (CI) for Each 3DSPs**

3DSPs/ Coronal and Sagittal SSAPs	Mal- alignment	Potentially Abnormal Alignment	Neutral Alignment			Potentially Abnormal Alignment	Mal- alignment
	< - 2 SD	- 2 SD	-1 SD	Mean	+ 1 SD	+ 2 SD	> + 2 SD
CCEA	< 88.84	88.84	89.21	89.58	89.95	90.32	> 90.32
CUTA	< 86.15	86.15	88.12	90.08	92.05	94.02	> 94.02
CLTA	< 85.21	85.21	87.36	89.51	91.66	93.81	> 93.81
CULA	< 85.07	85.07	87.23	89.39	91.54	93.70	> 93.70
CLLA	< 85.35	85.35	87.25	89.16	91.06	92.96	> 92.96
SCEA	< 41.91	41.91	51.34	60.78	70.21	79.64	> 79.64
SUTA	< 66.96	66.96	72.37	77.79	83.20	88.61	> 88.61
SLTA	< 86.48	86.48	93.09	99.70	106.31	112.92	>112.92
SULA	< 88.37	88.37	93.05	97.74	102.42	107.10	>107.10
SLLA	< 59.90	59.90	68.11	76.32	84.53	92.73	> 92.73
3CEA	< 41.91	41.91	51.34	60.78	70.21	79.64	> 79.64
3UTA	< 66.96	66.96	72.29	77.61	82.93	88.26	> 88.26
3LTA	< 87.01	87.01	93.50	100.00	106.49	112.98	>112.98
3ULA	< 89.01	89.01	93.56	98.10	102.65	107.20	>107.20
3LLA	< 59.97	59.97	68.03	76.10	84.17	92.24	> 92.24
TRA	< -8.59	-8.59	-5.07	-1.54	1.98	5.50	> 5.50
LRA	< -7.52	-7.52	-3.99	-0.46	3.07	6.60	> 6.60
PTA	< 0.45	0.45	5.93	11.41	16.88	22.36	> 22.36
C5A	< -1.29	-1.29	2.08	5.45	8.82	12.20	> 12.20
SSA	< 6.48	6.48	14.11	21.74	29.36	36.99	> 36.99
SCA	< 51.10	51.10	55.81	60.52	65.23	69.94	> 69.94

**Table 8.2 - The Reference Ranges of Each Parameter Classified by Three Different Categories**



## 8.5 Discussion and Conclusion

In the coronal plane, the non-scoliotic spine should be vertical and straight without any curvature, and ideally the values all five coronal SSAPs should be 90 degrees. As shown in Table 8.2, the means of CCEA, CUTA, CLTA, CULA, and CLLA were close to 90 degrees, and the coronal spinal alignment was visually a vertical and straight line in Figure 8.3. Secondly, the values of all five 3D SSAPs corresponded to the inclined slope and reclined slope degrees of neutral sagittal alignment in each spinal segment. The means of the sagittal SSAPs also had similar values as the ones of the 3D SSAPs in the same segment because each coronal SSAP's mean had approximately 90

degrees. In addition, the non-scoliotic spine and trunk should not have any thoracic posterior rib humps or lumbar paraspinal muscle asymmetry shapes. These rotational deformities are usually due to the axial rotation of the thoracic or lumbar areas in the scoliotic spine. The means of the measurements of TRA (mean: -1.54 degrees) and LRA (mean: -0.46 degrees) indicated that there are no rotational deformities in both the thoracic and lumbar spines since their values were close to zero degrees (Table 8.1). This evidence suggested that the 3D skin level parameters are representative of the structural characteristics of normal spines and capture the unique features in each spinal bony structural segment.

The reference ranges of all 3D skin level parameters (3DSPs) were identified in non AIS subjects. The reference ranges for the eleven parameters were used in the non-invasive digital calculating and visualization assessment application and can also be used as target values for orthotic correction.

**Chapter 9. Discriminative Validity Study for the 3D  
Surface Level Parameters System Between Non-  
Scoliosis Group and Scoliosis Group**

## 9.1 Introduction

This chapter introduces a test performed to investigate the discriminative validity (or contrast validity) of the 3D surface level parameters system (3DSPs) by comparing the collected data from the non-scoliosis group and a scoliosis group. The 3DSPs consist of the skin level spinal alignment parameters (SSAPs) and non-spinal alignment parameters (SNSPs). The purpose of this validity test was to examine the degree to which the test measures can discriminate between the non-scoliosis group and scoliosis group, since these groups are known to differ (Polit & Yang, 2016).

## 9.2 Methods and Data Analysis

For the non-scoliosis group, the measurements of the 3DSPs collected from 20 non-scoliotic adolescent girls (average age: 12.5 years old) in Chapter 8 were used. For the scoliosis group, data was collected from 5 AIS adolescent girls (average age: 13.2 years old). A secondary data analysis was performed to utilize the collected data of those two groups to investigate the validity of 3DSPs. Table 9.1 introduces the details of the subject characteristics of each group.

Factors	Scoliosis Group (n=5)	Non-Scoliosis Group (n=20)
Gender	Adolescent girls	Adolescent girls
Average Age	12.5 years old	13.2 years old
Inclusion Criteria	Included girls between the ages of 10 and 15, who had a confirmed diagnosis of AIS, with a Risser value of 0–3, and with primary curve angles of 20°–50°.	Included girls between the ages of 10 and 15, who lacked any scoliosis deformities.
Exclusion Criteria	Excluded if they had leg-length discrepancies of more than 2 cm, had any deformities of the lower extremities or other spine deformities, or had any surgical procedures on the lower extremities or spine.	

**Table 9.1- Subject Characteristics of the Scoliosis Group and Non-Scoliosis Group**

Nonparametric independent two tailed t-tests (IBM SPSS Statistics, Version 25. Armonk, NY, USA) were performed, based on the means of each 3DSP of both groups to discover any significant differences between the non-scoliosis group (n=20) and the scoliosis group (n=5). The criterion for statistical significance was set at  $p < 0.05$ .

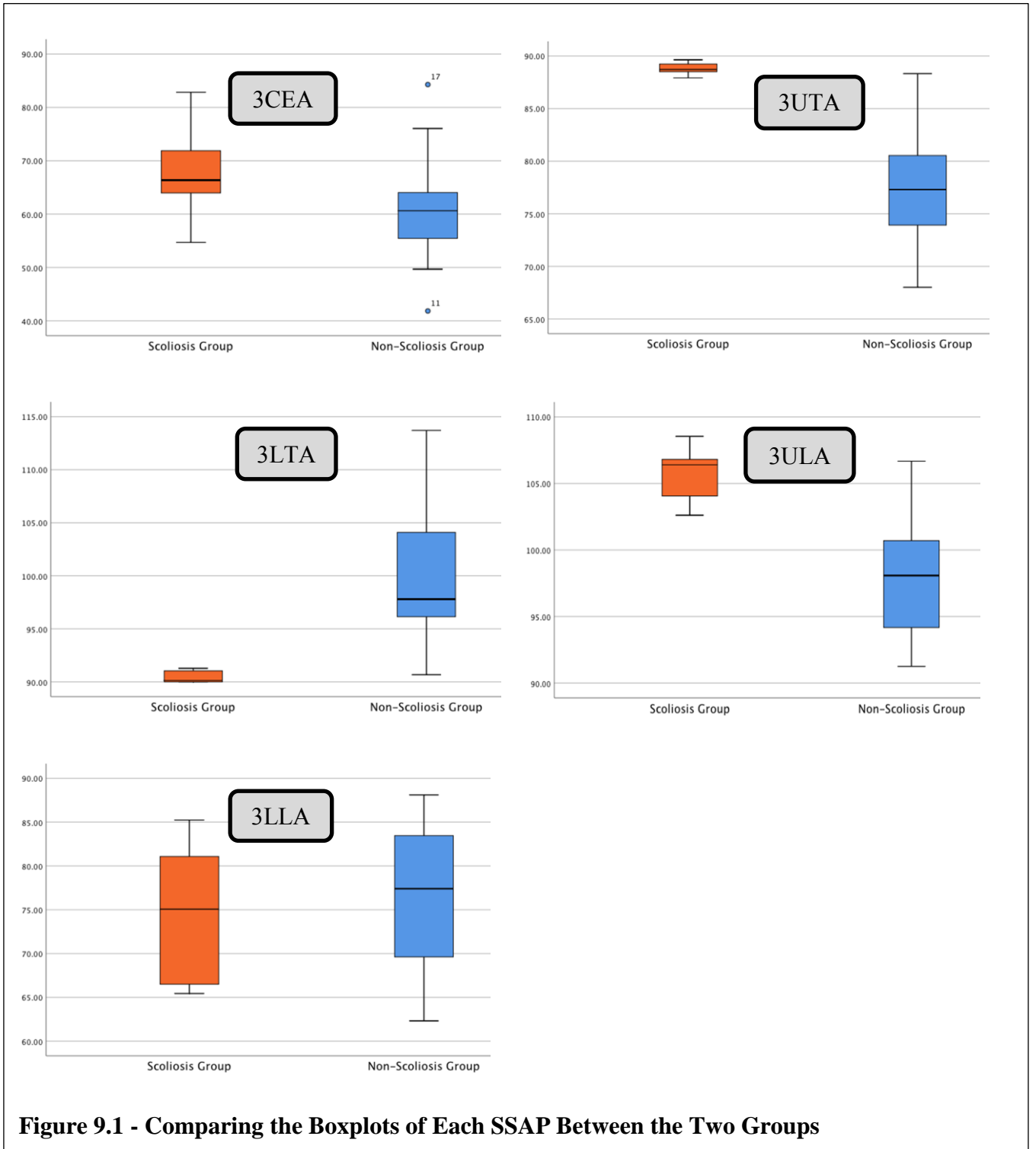
### 9.3 Results

Table 9.2 displays the descriptive statistics and the p-values of the performed test statistics (nonparametric Mann Whitney U tests) for each 3DSP between the scoliosis group and non-scoliosis group. There was a statistically significant difference between both groups for 7 out of 11 3DSPs (3UTA, 3LTA, 3ULA, TRA, LRA, C5A, and SCA).

3DSPs		Mean $\pm$ SD		Sig. ( $\alpha=0.05$ )
		Scoliosis Group (n=5)	Non-Scoliosis Group (n=20)	
Skin Level Spinal Alignment Parameters (SSAPs)	<b>3CEA</b> (3D Lower Cervical Alignment to Horizontal Angle)	67.95 $\pm$ 10.38	60.78 $\pm$ 9.43	.148
	<b>3UTA</b> (3D Upper Thoracic Alignment to Horizontal Angle)	88.80 $\pm$ 0.66	77.61 $\pm$ 5.32	.000
	<b>3LTA</b> (3D Lower Thoracic Alignment to Horizontal Angle)	90.49 $\pm$ 0.62	100.00 $\pm$ 6.49	.000
	<b>3ULA</b> (3D Upper Lumbar Alignment to Horizontal Angle)	105.68 $\pm$ 2.35	98.10 $\pm$ 4.55	.003
	<b>3LLA</b> (3D Lower Lumbar Alignment to Horizontal Angle)	74.66 $\pm$ 8.73	76.10 $\pm$ 8.07	.767
Skin Level Non- Spinal Parameters (SNSPs)	<b>TRA</b> (Thoracic Rotation Angle)	21.77 $\pm$ 27.30	-1.54 $\pm$ 3.52	.019
	<b>LRA</b> (Lumbar Rotation Angle)	20.37 $\pm$ 17.40	-0.46 $\pm$ 3.53	.000
	<b>PTA</b> (Pelvic Tilt Angle)	15.08 $\pm$ 7.10	11.41 $\pm$ 5.48	.371
	<b>C5A</b> (C5 Balance Angle)	19.73 $\pm$ 17.71	5.45 $\pm$ 3.37	.035
	<b>SSA</b> (Sternal Angle)	21.86 $\pm$ 18.36	21.74 $\pm$ 7.63	.767
	<b>SCA</b> (Sacral Alignment to Horizontal Angle)	68.40 $\pm$ 9.05	60.52 $\pm$ 4.71	.019

**Table 9.2 - The Mean, Standard Deviation (SD), and Result of the Nonparametric Independent Two Tailed T-test for Each Parameter Between the Non-scoliosis Group and Scoliosis Group**

Figure 9.1 and 9.2 shows the box plots of each parameter to visually compare between the scoliosis group and non-scoliosis group. Appendix 9.1 gives the descriptive statistics and the results of the performed test statistics.



**Figure 9.1 - Comparing the Boxplots of Each SSAP Between the Two Groups**

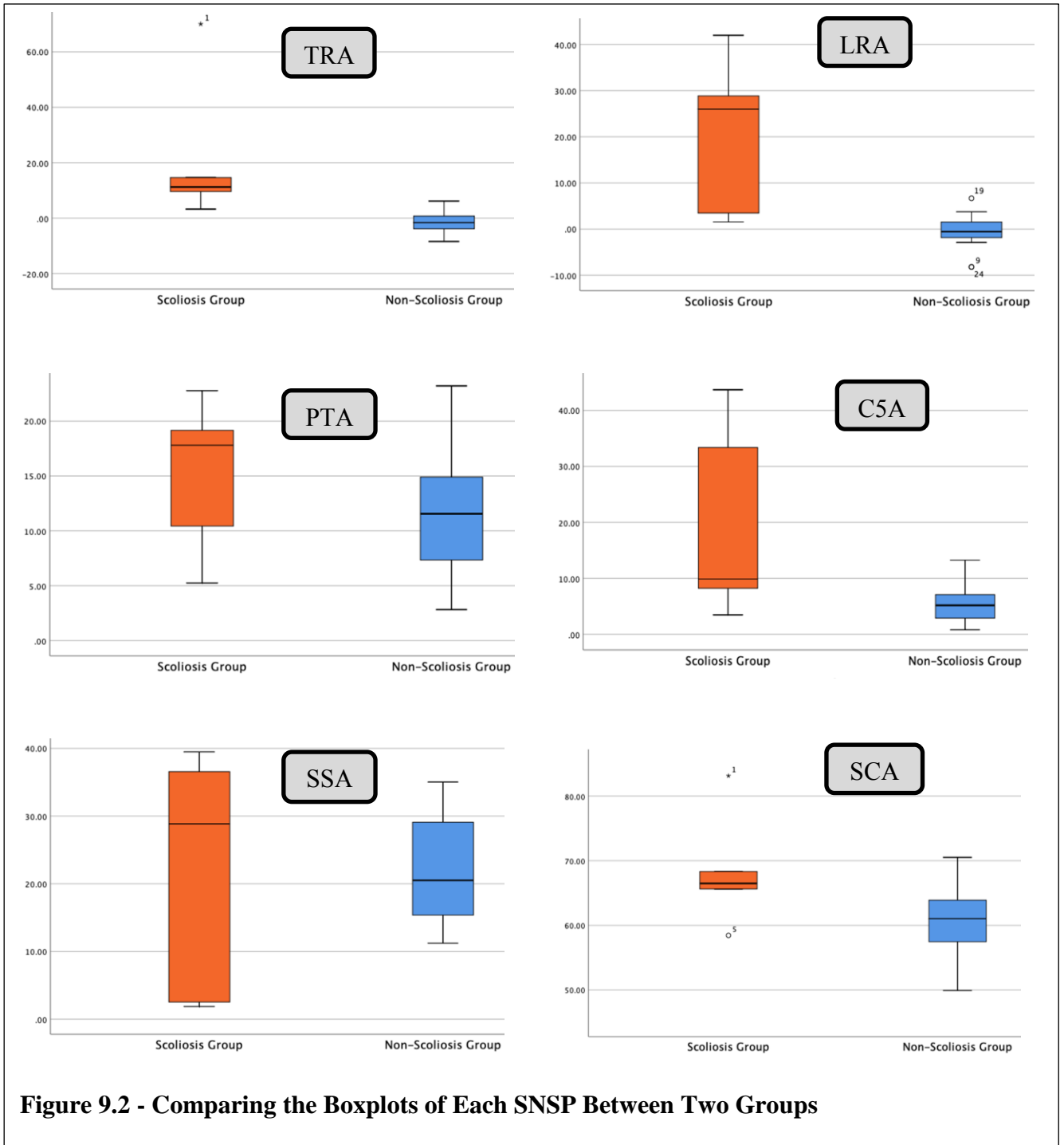


**Figure 9.2 - Comparing the Boxplots of Each SNSP Between Two Groups**

## 9.4 Discussion and Conclusion

For the SSAPs, the 3SCEA (lower cervical segment) and the 3LLA (lower lumbar segment) showed no significant difference between the two groups. However, the results in these two parameters fit the skeletal structure of the spinal column itself, because these two segments are located at the end points of the spinal column. The lower lumbar segment is close to the lowest end point of the spinal column and thus, scoliotic misalignment is usually not present, or it is mild, not severe if it presents. Similarly, there are few cases which have misalignment in the lower cervical segment, and in this study, there was no misalignment found in the lower cervical segment of any of the 5 scoliosis spines. For these reasons, it makes sense that these two segments of the two groups show no significant difference between the two groups.

The values of 3UTA ( $88.80 \pm 0.66$ ) and 3LTA ( $90.49 \pm 0.62$ ) measured from the scoliosis group were found to be closer to 90 degrees than those of the non-scoliosis group (3UTA:  $77.61 \pm 5.32$  and 3LTA:  $100.00 \pm 6.49$ ). The upper thoracic and lower thoracic segments appeared relatively straighter (i.e. vertical and flat) and had lost their natural thoracic kyphosis. This result is consistent with Dickson et al (1984)'s findings. Dickson et al. stated in their article that if an individual has a thoracic coronal curve, a force of forward flexion (anteriorly directed force) exists on the sagittal thoracic spine, causing the sagittal thoracic spine, especially for the lower part of the thoracic region, to become relatively vertical (Dickson et al, 1984). The upper lumbar segment in the scoliosis spines (3ULA:  $105.68 \pm 2.35$ ) was tilted much more posteriorly compared to the non-scoliosis spines (3ULA:  $98.10 \pm 4.55$ ).

In addition, the C5 spinal balance values in the scoliosis spines (C5A:  $19.73 \pm 17.71$ ) was more decompensated (imbalanced) than the non-scoliosis spines (C5A:  $5.45 \pm 3.37$ ). This result also corresponds to the finding of the extension pathomechanism which was identified in the study "Sagittal Misalignment Pattern of AIS" introduced in Chapter 5. The values of the thoracic and lumbar rotational deformities of the scoliosis spines (TRA:  $21.77 \pm 27.30$  and LRA:  $20.37 \pm 17.40$ ) were much greater than those of the non-scoliosis spines (TRA:  $-1.54 \pm 3.52$  and LRA:  $-0.46 \pm 3.53$ ), which show almost no rotational deformities. This study found that the

PTA and SSA had no statistically significant difference between two groups, while the SCA showed a statistically significant difference. SCA is similar to a sagittal sacral slope angle. This result seems sensible because the sacrum is a part of the spinal column that is directly affected by the scoliotic deformity; but the pelvis and sternum are not the parts of the spinal column. The PTA and SCA both follow a similar pattern by having higher values in the scoliosis group compared to the non-scoliosis group. This may correspond to the results of Klineberg et al.'s (2011) radiographic study. They reported that the pelvic incidence (pelvic tilt and sacral slope angles), which is measured from the osseous landmarks on the radiograph and is similar to these two combined measurements (PTA and SCA), correlates with lumbar lordotic posture that may be seen in lumbar scoliotic spines.

In conclusion, the study examined the discriminative validity of the 11 parameters of 3DSP between the two groups and 7 parameters (three SSAPs and SCA, TRA, LRA, and C5A) of them showed statistically significant differences between the scoliosis and non-scoliosis groups. Given the small size of the scoliosis group, this was encouraging. Thus, all 11 parameters were taken forward to the final experimental chapter of this thesis which uses the new system and data to examine the feasibility of its use during orthotic fitting.

**Chapter 10. Evaluation of The Digital Calculating and  
Visualisation Assessment Application; Pilot  
Study Results: Optimal Corrective Force  
Placements of Spinal Orthoses in Treating AIS**

## 10.1 Introduction

In this thesis, the non-invasive digital calculating and visualisation assessment application and the 3D skin level measurable parameters were developed to facilitate future research studies which aim to examine the still unclear 3D orthotic biomechanical corrective concepts used when treating AIS with orthotic devices.

These unclear biomechanical questions were identified from the survey project “Current Practice in Orthotic Treatment of AIS” (Chapter 4) which concluded that more quantitative investigations were still needed related to the three biomechanical topics:

- (a) Where should the superior level of a thoracic corrective force be applied on the apical vertebra level or at the apical rib of a thoracic curve?
- (b) Does a de-rotational force need to be applied for a single thoracic curve in addition to an anterior-medially directed force, which is the primary thoracic corrective force?
- (c) Is reducing a lumbar lordosis necessary as a primary corrective force for a lumbar or a thoracolumbar curve?

A question regarding the placement of a thoracic corrective force has long been an unsolved controversial topic among clinicians and researchers. The survey (Jang et al. 2019; chapter 4) reported that 39.1% of participants had chosen the ideal corrective location as “the superior edge of a thoracic pad should be placed on the rib at the apex of the thoracic curve” while 37.0% of participants selected “the superior edge of the pad must extend to the apical vertebral level of the thoracic curve” (Jang et al., 2019). In 2009, the “SOSORT Consensus Paper showed that 52% of the participants also chose the proper placement of a thoracic corrective pad at the apical vertebral level, while 48% selected it at the level of the apical rib and below the apical vertebra (Rigo et al., 2006).

If such controversies are to be resolved, the effect of different orthotic solutions on the spinal shape must be measurable in 3D. This chapter presents the practicality of using the new developed system in clinical practice. To prepare for this pilot feasibility

study, four clinical research studies were completed and have been reported in this thesis. First, to quantify AIS deformities, measurable spinal alignment parameters were developed through the results of a research study, titled: “*Radiographic Analysis of Sagittal Spinal Misalignment Patterns in Adolescent Idiopathic Scoliosis*” (Chapter 5). Second, the validity of the parameters was tested through another study, titled: “*Concurrent Validity of 3-Dimensional Skin Level Spinal Alignment Parameters*” (Chapter 6). Third, the reference ranges of values for each spinal alignment parameter were defined in the study, “*Reference Values of 3-Dimensional Surface Level Spinal Alignment Parameters*” (Chapter 8). Fourth, a discriminative validity study for the 3D surface level parameters system were performed between non-scoliotic and scoliosis groups (Chapter 9).

The purposes of the pilot feasibility study presented here were to: (1) test if the application can be used to examine unclear and long-term unsolved biomechanical questions such as the optimal placements of 3D biomechanical corrective forces and 3D misalignment patterns of AIS, and to (2) demonstrate the feasibility of implementing the developed digital calculating and visualisation assessment application as an AIS assessment tool in clinical practice.

## **10.2 Methods**

### 10.2.1 Subjects

Adolescents who have been diagnosed with AIS were recruited from clinicians through local scoliosis or orthotic and prosthetic (O & P) clinics by posting the recruiting flyer in the clinics.

**Inclusion Criteria:** Subjects must have AIS deformities with a confirmed diagnosis and must satisfy these conditions: age between 10 and 15 years, with a Risser value of 0 to 3, and with primary curve angles of 20° to 50°.

**Exclusion Criteria:** Any subject was excluded if the patient has a leg-length discrepancy of more than 2 cm, has any deformities of the lower limbs, or has had surgical procedures on the lower limbs or spine.

Hence, prior to the study, the following conditions were screened for eligibility to this study:

- a. Current age and DOB (Date of Birth): Minimum Age: 10 yrs. Maximum Age: 15 yrs.
- b. AIS diagnosis confirmed age: Adolescent type or not?
- c. Surgical records on lower limbs or spine: Yes or No
- d. Prior orthotic treatment of this condition: Yes or No
- e. Leg length discrepancy:  $> 2\text{cm}$  or  $\leq 2\text{ cm}$
- f. Radiograph studies available

Each participant provided a PA full spine radiograph associated with their scoliosis and taken without an orthosis prior to or on the test day. After recruiting subjects, two written consent forms (an assent form from the participant and a parental consent form from the parent/legal guardian) were sent to the parents via email prior to their visits or given to them in person during their visit. The signed parental consent and participant assent forms were obtained in-person before data collection during a visit after verbally explaining the procedure of the study using words easily understood by adolescent children. Prior to signing, enough time was given to the potential subject to consider participation without pressure. In addition, if a participant felt uncomfortable at any time during the study, it was made clear that they could refuse to participate or withdraw from the study.

Ethical approval was obtained from Eastern Michigan University for this study. The two ethics committee approval letters are attached in Appendix 10.1.

### 10.2.2 Apparatus

To conduct this study, the following apparatus were utilized: (1) Vicon Nexus software with motion capture cameras, (2) the digital calculating and visualisation application with D-flow software, (3) a pointer, (4) a Scoli-Standing Frame, and (5) eleven corrective force application bars (Figure 10.1). The corrective pads were fabricated of copolymer and formed just like the corrective pads of an orthotic device and attached on each bar (Figure 7.2). A load cell was already mounted between the

bar and the corrective pad to measure the applied force. The corrective pad located on the end of the bar was used to apply corrective forces to the subject's spine. These bars could be attached to the frame at various heights and positions around the frame and at adjustable angles (Figure 10.2).



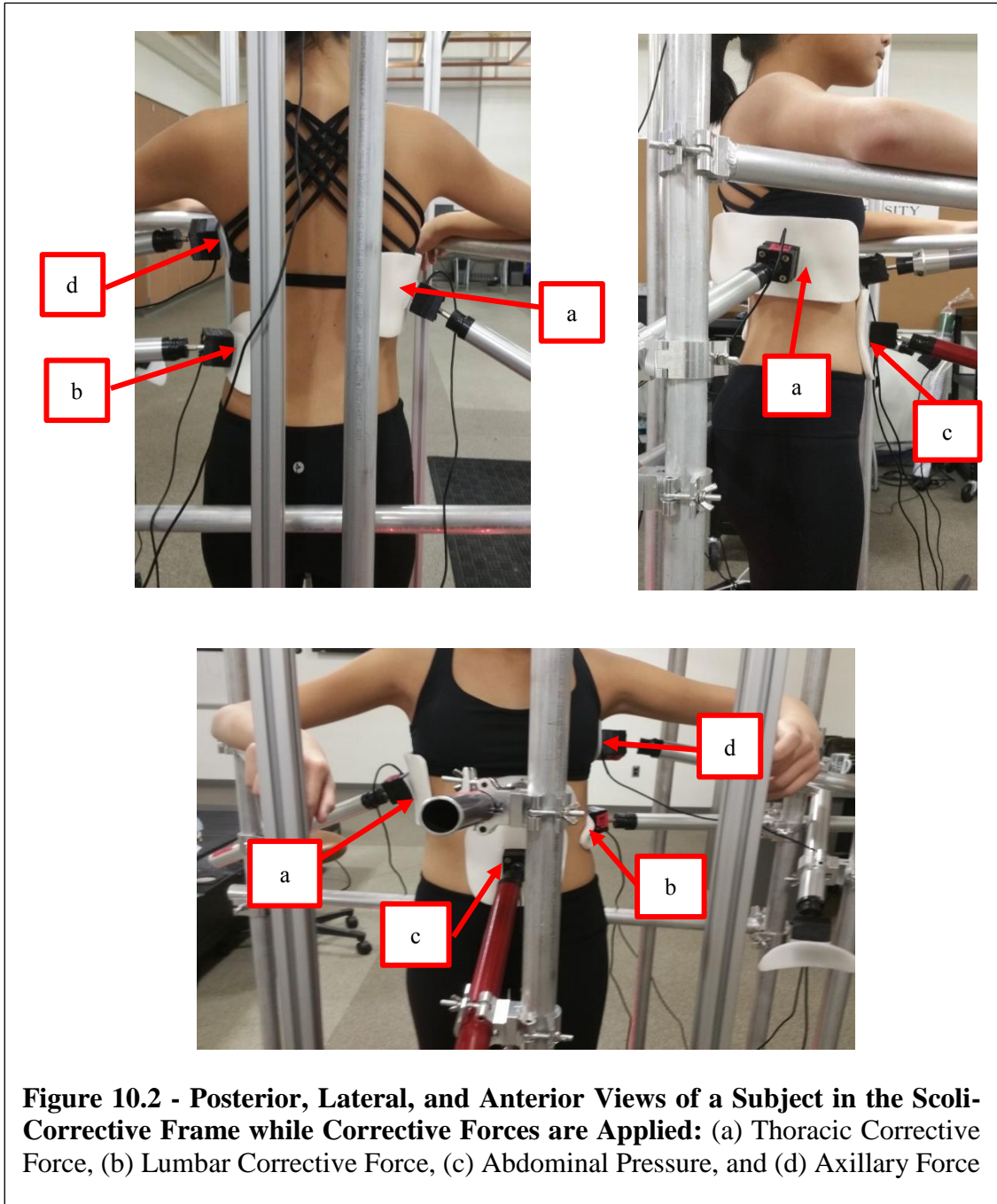
**Figure 10.1 - Setup and Connection with All Equipment and Apparatus**

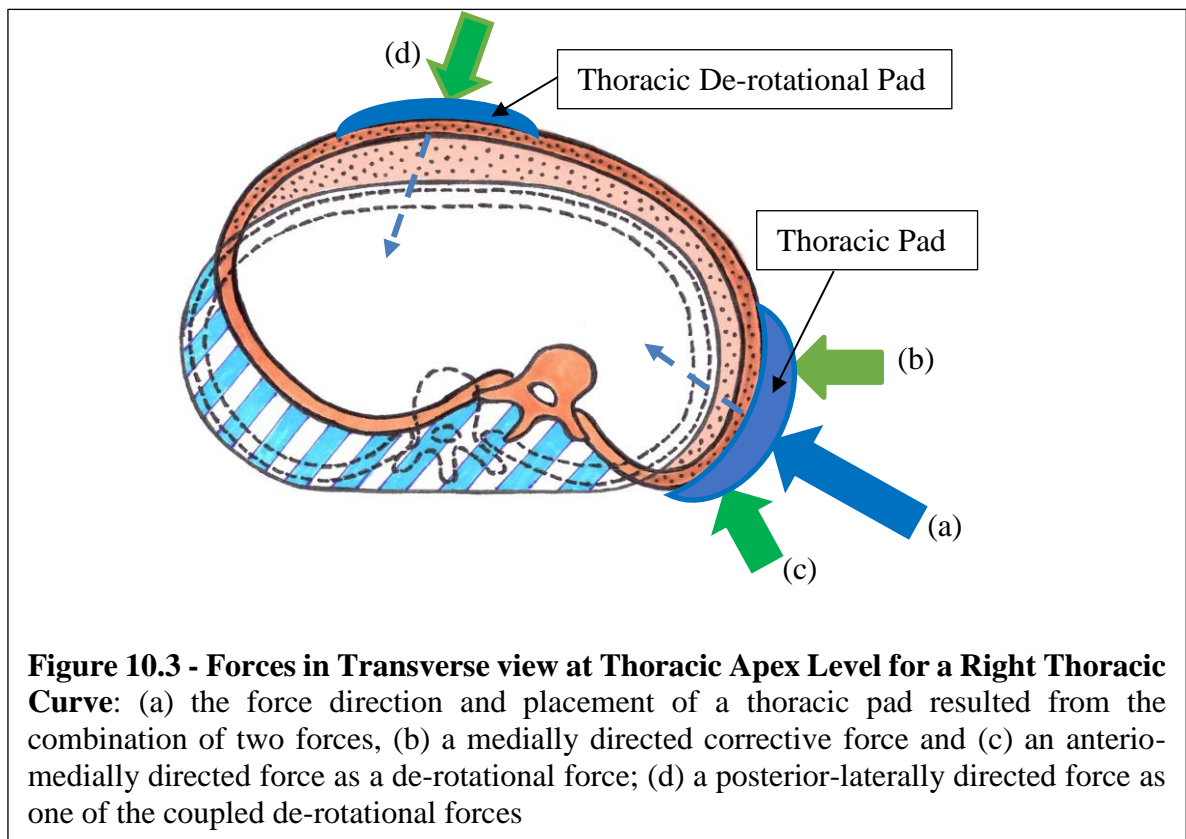
The following lists the seven pads (among the eleven pads) used for this study:

- (1) **Thoracic pad:** The thoracic pad was fabricated with two force components combined of a medially directed corrective force placed on the lateral thoracic region on the convex side of the curve, and an anterior-medially directed force applied at the posterior-lateral side of the apical rib of the thoracic curve, as a de-rotational force for a thoracic curve. The thoracic pad was applied based on the resultant force of these two forces in the transverse plane when conducting this study as shown in Figure 10.3 and simultaneously placed on the ribs by providing a superior-medially directed force in the coronal plane.

- (2) **Thoracic de-rotational pad:** The thoracic de-rotational pad was applied on the anterior part of the rib cage at the apex level of the thoracic curve to provide a posterior-laterally directed force as a counter force for a thoracic corrective force (Figure 10.3).
- (3) **Lumbar pad:** The lumbar pad was also fabricated to provide two force components such as a medially directed corrective force and an anterior-medially directed force as a de-rotational force on the paraspinal muscle of the lumbar curve.
- (4) **Axillary pad** and (5) **Gluteus medius pad:** Each pad was applied on the contralateral side of any major corrective force applied in the coronal plane to provide a coronal counter force.
- (6) **Abdominal pad:** The abdominal pad was applied on the abdomen to provide a posteriorly directed force. (7) **Gluteus maximus pad:** This force was applied as a sagittal counter force for an abdominal pressure.

The following lists the four pads, which were mounted in the application but not used for this study: Upper thoracic de-rotational pad to provide a posterior-laterally directed force on the deltopectoral region as a counter force for an upper thoracic curve; Lumbar de-rotational pad to provide a posterior-laterally directed force, as a counter force for a lumbar corrective curve; Pelvic de-rotational pad to provide a medially directed corrective force on the pelvis; and Posterior-superior pad to provide anteriorly directed force on the upper back as a sagittal counter force.





### 10.2.3 Procedure

During the visit, each participant changed into special clothing (black sports bra and black bike pants) in a private room. The 19 key anatomical landmarks on the skin of the patient's torso were palpated and these areas were marked using a non-permanent pen. During the entire procedure, the parent or accompanying adult and only research-related, qualified personnel were present.

During data collection, each participant was asked to stand still with their arms relaxed on the arm rests of the *Scolio-Corrective Frame* (Figure 10.2). Instructions for positioning in the frame were the same as the one used for the project, "Normal Values and Reference Ranges of the Surface Level Spinal Alignment Parameters System", which was introduced in the chapter 8:

- a. Centre the participant in the frame
- b. The pelvis and feet must be neutral position
- c. The patient's forearms rest on the armrest bars of the frame. Shoulders are relaxed and the elbows flexed to 60 degrees.

- d. The patient's knees rest on the knee pads, and the head is in neutral facing forward.

The motion capture cameras captured the 3D Cartesian-coordinates from a reflective marker built into a pointer. When the pointer gently touches each key anatomical landmark on the skin of the patient's scoliotic spine and torso, the buttons of the *Runtime Console* in the application could be pressed to record the position of the point. In this way, all the anatomical landmarks could be recorded and then used to calculate the eleven 3D spinal parameters previously described.

Each individual needed a different combination of corrective forces and corrective pads depending on the curve types that the person had and which unique research question was being answered, among the following choices:

- (a) Where should the superior level of a thoracic corrective force be applied on the apical vertebra level or at the apical rib of a thoracic curve?
- (b) Does a de-rotational force need to be applied for a single thoracic curve in addition to an anterior-medially directed force, which is the primary thoracic corrective force?
- (c) Is reducing a lumbar lordosis necessary as a primary corrective force for a lumbar or a thoracolumbar curve?

Two sets of data were collected. One measured baseline data when no force was applied; and the other collected data while corrective forces were applied through the corrective pads. Thus, the effect of the 3D biomechanical corrective forces applied was identified by comparing the parameter values before and after applying corrective forces on the AIS spine and torso (Figure 10.2). On the computer visualisation screen, the values of each parameter were shown in one of two colours depending on whether or not the value was within the reference range for that parameter (red: outside range, green: within range). On the screen, the colour of each parameter was changed to green if that segment of the torso and spine have been corrected to within normal/reference ranges. The visual feedback was used by the operator to define the placements of the optimal corrective forces for that individual.

#### 10.2.4 Primary and Secondary Outcome Measures

3D skin level parameters (3DSPs) and coronal and sagittal SSAPs were measured before and after corrective forces were applied with the pads (Table 10.1).

For evaluation for lumbar lordosis reduction, a skin level pelvic incidence (SPI) was calculated by combining the measurements of PTA and SCA together. SPI is similar to a radiographic pelvic incidence, which is the combination of the pelvic tilt and sacral slope degrees measured from radiograph. This radiographic concept was introduced in Chapter 7 based on these articles produced by Boulay et al. (2006) and Klineberg et al. (2011). Boulay et al. (2006) reported in the article that smaller radiographic pelvic incidence values corresponded to a more reduced and flattened sagittal lumbar lordosis curve.

<b>3DSPs</b>	<b>Parameters</b>
Skin Level Spinal Alignment Parameters (SSAPs)	3CEA (3D Lower Cervical Alignment to Horizontal Angle)
	3UTA (3D Upper Thoracic Alignment to Horizontal Angle)
	3LTA (3D Lower Thoracic Alignment to Horizontal Angle)
	3ULA (3D Upper Lumbar Alignment to Horizontal Angle)
	3LLA (3D Lower Lumbar Alignment to Horizontal Angle)
Skin Level Non-Spinal Parameters (SNSPs)	TRA (Thoracic Rotation Angle)
	LRA (Lumbar Rotation Angle)
	PTA (Pelvic Tilt Angle)
	C5A (C5 Balance Angle)
	SSA (Sternal Angle)
	SCA (Upper Sacral Angle)

**Table 10.1 - 3D Skin Level Parameters for Outcome Measures**

Corrective forces were applied via corrective pads and the magnitude of each applied force was recorded while maintaining corrective pressures. For this study, the applied forces were as follows: Thoracic Force; Lumbar Force; Thoracic-Lumbar Force (combined with thoracic and lumbar forces), Axillary Force; Gluteus Medius Force; Thoracic De-Rotational Force; Gluteus Maximus Force; Abdominal Pressure. The optimal correction was defined as those spinal alignment parameters reached within the reference ranges as defined by the previous study (Chapter 8).

### 10.2.5 Data Analysis

Subsequently it was decided to create a more detailed analysis for the optimal corrections of each case. The collected values were analyzed to determine if the value fell within three-reference range categories, (based on the data presented in Chapter 8, Table 8.2). Thus, the values in Figure 10.4 – Figure 10.8, were displayed with one of three different colours to better explain the results of the analysis. In the figures, the values are displayed with “green” when the values are within the mean  $\pm$  1SD of the non-scoliosis spines and are thus considered as “neutral alignment”. The “blue” coloured values are represented as “potential abnormal alignment,” because their values are greater than the mean  $\pm$  1SD and less than the mean  $\pm$  2SD of non-scoliosis spines, while the “red” coloured values are considered as “malalignment” when the values are greater than the mean  $\pm$  2SD.

### 10.3 Results for Demographic Characteristics

Five AIS adolescent girls (average age: 13.2 years old) were recruited (Figure 10.3). Their demographic characteristics, coronal curve types, Cobb angle degrees, and the values of the coronal and sagittal SSAPs are displayed in table 10.2. Figure 10.3 shows the PA, full spine radiograph of each subject. The measurements of the coronal and sagittal SSAPs are shown with one of two colours depending on whether the value is within the reference range for each parameter (red: outside range, green: within range), based on the 95% confidence interval of each SSAP measured from the non-scoliosis group (Table 8.1). Table 10.3 also shows the values measured for 3D SSAPs with one of two colours depending on whether the value is within the reference range for each parameter.

Sub-ject	Age (yrs.)	Coronal Curve Type	Apex	Cobb Angle (°)	Coronal SSAPs						Sagittal SSAPs			
					CUTA	CLTA	CULA	CLLA	SUTA	SLTA	SULA	SLLA		
1	14.4	Single MT Curve	T8/9	25°	91.15	88.86	67.88	59.51	89.41	90.58	114.31	54.07		
2	12.4	Double T-L Curve	T8/9	21°	90.08	90.00	89.53	106.25	89.24	90.00	102.60	81.07		
			L2/3	22°										
3	12.8	Double TL-T Curve	T7	20°	90.74	89.39	84.98	90.38	88.71	90.85	103.20	85.25		
			T12/L1	19°										
4	14.4	Double T-L Curve	T8	23°	90.32	89.87	88.57	91.91	89.86	90.04	106.25	72.43		
			L1/2	20°										
5	12.1	Single TL Curve	T12	15°	89.50	90.00	106.06	115.45	87.98	90.00	101.06	66.50		

(MT: middle thoracic, LT: lower thoracic, TL-T: thoracolumbar-thoracic, T-L: thoracic-lumbar)

**Table 10.2 - Demographic Characteristics of the Study Subjects with Coronal and Sagittal Spinal Alignment Parameters Measured from the Skin Surface.** The values of the coronal and sagittal SSAPs are displayed based on the two-reference categories (red: outside range, green: within range).

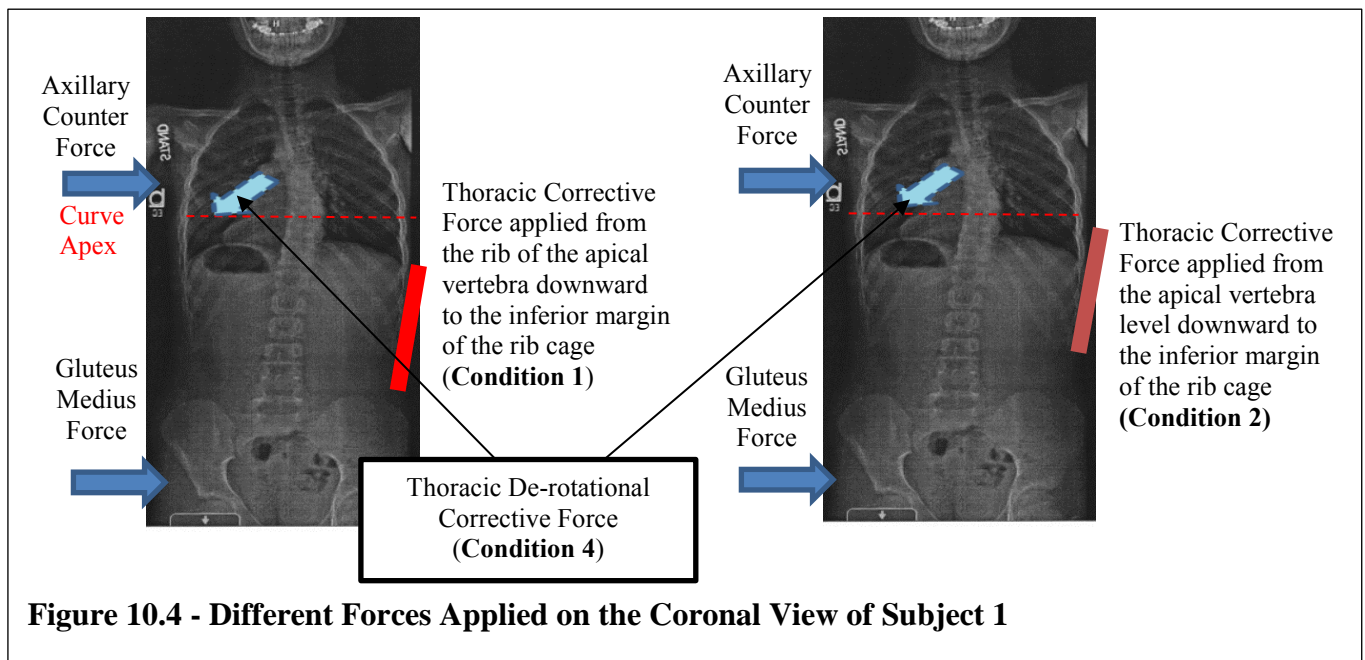
Subject	SSPPs						SNSPs					
	3CEA	3UTA	3LTA	3ULA	3LLA	TRA	LRA	PTA	C5A	SSA	SCA	
1	88.63	87.54	93.00	113.06	66.97	63.71	26.89	1.00	1.87	1.86	65.48	
2	66.37	89.24	90.00	102.61	81.08	3.28	3.48	5.25	8.23	39.49	65.62	
3	54.70	88.51	91.04	104.06	85.23	9.61	1.55	10.43	9.89	28.85	66.48	
4	71.88	89.64	90.14	106.40	75.06	11.27	28.86	17.80	3.47	2.54	68.33	
5	82.84	87.92	90.00	108.54	66.50	14.66	25.98	22.77	33.38	36.56	58.45	

**Table 10.3 - The Values of 3DPPs of Each Subject** are displayed based on the two-reference categories (red: outside range, green: within range).

## 10.4 Case Study for Subject 1

### 10.4.1 Methods

Subject 1 had a single, right thoracic curve at T8/9 (a long C curve type). For this single thoracic curve case, four different force combinations were applied to test two of the three research questions: “(a) Where should the superior level of a thoracic corrective force be applied: on the apical vertebral level or at the apical rib of a thoracic curve? and (b) Does a de-rotational force need to be applied with an anterior-medially directed force for a single thoracic curve?”. Thus, the optimal correction compared the values between when the superior edge of a thoracic force was applied on either the apical rib of a thoracic curve (Condition 1), or on the rib of the apical vertebra (Condition 2) by a thoracic pad (Figure 10.4). When the thoracic pad was applied, two coronal counter forces were also applied on the contralateral axillary and gluteus medius areas as shown in Figure 10.4. Two sagittal lumbar corrective forces were applied by an abdominal pad and a gluteus maximus pad (Condition 3). Comparisons were also noted between “with (Condition 4)” or “without” a posterior-laterally directed, thoracic de-rotational corrective force (Figure 10.4). The values applied by each force were compared to the values from when no force was applied.



#### 10.4.2 Findings

Table 10.4 shows all values of 3DSPs measured without any force applied and all values during the application of one of the four different force combinations (Condition 1+3, 2+3, 1+3+4, and 2+3+4). The result showed that the 3D spinal alignment (SSAPs) was improved when the superior level of the thoracic corrective force (17N) was applied on the apical rib of a thoracic curve with two coronal counter forces (axially force: 14N and gluteus medius force :3N) and without any de-rotational force applied. Condition 1+3 had two green, two blue, and one red colours, while no force was applied on the spine had three blue and two red colours. At that time 17N was exerted by the thoracic pad. However, the 3D non-spinal parameters were mostly improved when the thoracic de-rotational force was applied simultaneously, when the superior level of the thoracic corrective force was applied on the rib of the apical vertebra of a thoracic curve (Condition 2+3+4). Condition 2+3+4 resulted in three green, one blue, and two red colours, while no force applied on the spine resulted in three blue and three red colours. Especially the thoracic rotation angle (TRA) in Condition 2+3+4 had improved the most by changing from 63.71 degrees to 14.66 degrees, even though TRA did not move into the green category. The improvement of Condition 2+3+4 was better than Condition 1+3+4. The thoracic de-rotational force applied in 2+3+4 was 4N while 8N was applied in Condition 1+3+4.

For the skin level pelvic instance (SPI), the SPI values in all conditions should have lower values than the case of no force applied, because two sagittal lumbar corrective forces (an abdominal pad and a gluteus maximus pad) were applied in all 4 conditions. However, it was showed that Condition 1+3+4 (62.26) as well as Condition 2+3+4 (63.33) had less values than the case of no force applied (66.48) while the values of SPI in Condition 1+3 and 2+3 were increased.

Subject 1		SSAPs						SNSPs					
3DSPs / Applied Forces		3CEA	3UTA	3LTA	3ULA	3LLA	TRA	LRA	PTA	C5A	SSA	SCA	
No Force		88.63	87.54	93.00	113.06	66.97	63.71	26.89	1.00	1.87	1.86	65.48	
Cond. 1+3	Th(17N)@AR, Cax(14N), GMe(3N), Abd (2N), and GMa (10N)	73.14	89.99	90.00	102.57	78.73	61.57	26.10	1.05	1.51	3.15	68.35	
Cond. 2+3	Th(17N)@AV, Cax(14N), GMe(3N), Abd (2N), and GMa (10N)	65.06	89.96	90.05	108.75	72.26	74.21	34.32	1.27	1.53	5.95	68.02	
Cond. 1+3+4	Th(16N)@AR, ThD(8N), Cax(13N), GMe(3N), Abd (2N), and GMa (10N)	57.00	89.99	90.00	122.93	50.55	25.63	40.36	0.76	6.60	39.15	61.50	
Cond. 2+3+4	Th(26N)@AV, ThD(4N), Cax(16N), GMe(6N), Abd (2N), and GMa (10N)	80.59	89.98	90.55	121.80	62.91	14.66	33.44	0.88	5.03	25.71	62.45	

(Cond.: Condition; @: at; AR: Apical Rib; AV: Apical Vertebral Level; Th: Thoracic Corrective Force; ThD: Thoracic De-rotational Corrective Force; Cax: Axillary Counter Force; GMe: Gluteus Medius Force; Abd: Abdominal Pressure; GMa: Gluteus Maximus Force)

**Table 10.4 - Subject 1: The Values of 3DSPs Measured by the Application with and without Applied Specific Forces.** The values were classified into one of the three-reference range categories (green: neutral alignment, blue: potential abnormal alignment, and red: malalignment).

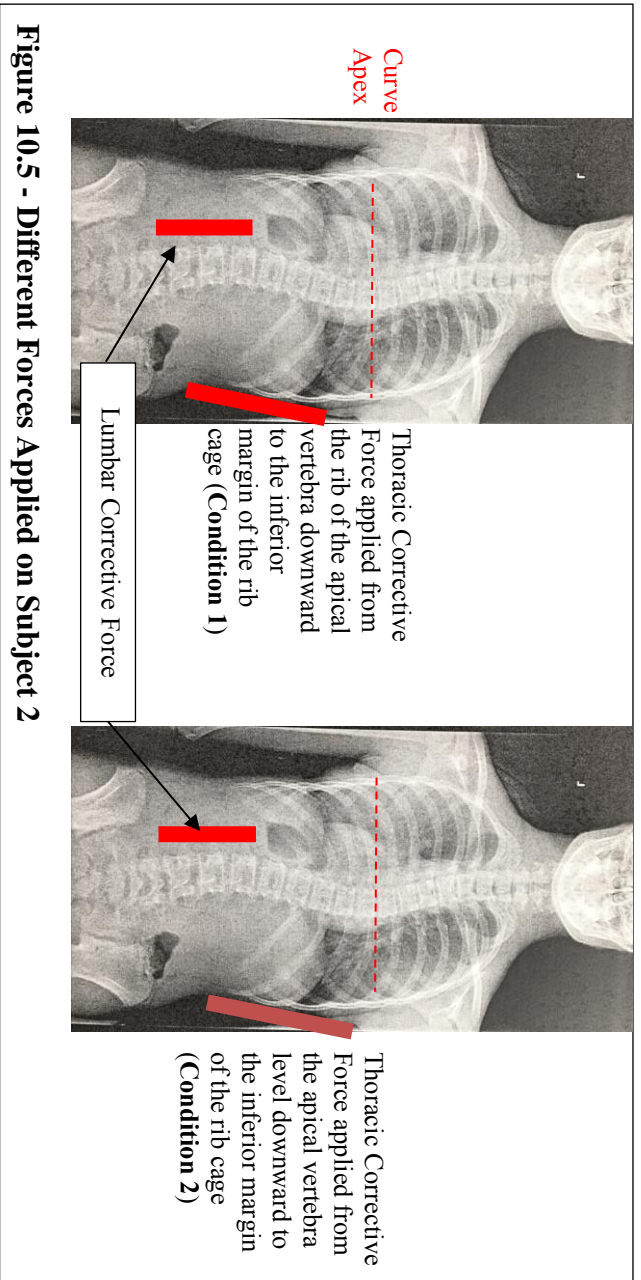
## 10.5 Case Study for Subject 2

### 10.5.1 Methods

Subject 2 had a double thoracic and lumbar curve. The Cobb angle measurement of the right thoracic curve was  $21^\circ$  (apex at T8/9), and  $22^\circ$  for the left lumbar curve (apex at L2/3). Two different thoracic corrective force combinations with an axillary counter force were applied to test the questions of “(a) Where should the superior level of a thoracic corrective force be applied: on the apical vertebral level, or at the apical rib of a thoracic curve?”, like Subject 1. However, in this case, a lumbar corrective force was also applied for a lumbar curve (Condition 5). The values of the 3DSPs were measured when no force applied and compared when the superior level of the thoracic corrective force applied at the apical rib (Condition 1+5) or on the apical vertebral level (Condition 2+5) (Table 10.5 and Figure 10.5).

### 10.5.2 Findings

The results are shown in Table 10.5 and indicated that the both 3D spinal alignment and non-spinal parameters were improved when the superior level of the thoracic corrective force (19N) was applied at the apical rib of the thoracic curve just as it did in the case of Subject 1. Condition 1+5 had seven green, three blue, and one red colours among 11 of 3DSPs, while the spine when no force was applied had four green, two blue, and five red colours. However, there were a major differentiation between Subject 1 and 2 in the results. Even though Subject 2 was without any applied sagittal force and without a posterior-laterally directed thoracic de-rotational corrective force, the non-spinal parameters were improved. Especially the spinal positions for TRA ( $1.68^\circ$ ) and LRA ( $-0.88^\circ$ ) were moved into the neutral alignment range.



Subject 2		SSAPs						SNSPs					
3DSPs / Applied Forces		3CEA	3UTA	3LTA	3ULA	3LLA	TRA	LRA	PTA	C5A	SSA	SCA	
No Force		66.37	89.24	90.00	102.61	81.08	3.28	-3.48	5.25	8.23	39.49	65.62	
Cond. 1+5	Th(19N) @ AR, Lu(17N), CAX(4N),	71.55	79.47	90.48	91.65	72.12	1.68	-0.88	6.39	7.10	20.09	48.71	
Cond. 2+5	Th(12N) @ AV, Lu(13N), CAX(4N),	70.39	88.79	90.49	94.64	65.18	-2.56	7.72	10.15	6.32	25.16	53.06	

(Cond.: Condition; @: at; AR: Apical Rib; AV: Apical Vertebral Level; Th: Thoracic Corrective Force; Lu: Lumbar Corrective Force; CAX: Axillary Counter Force)

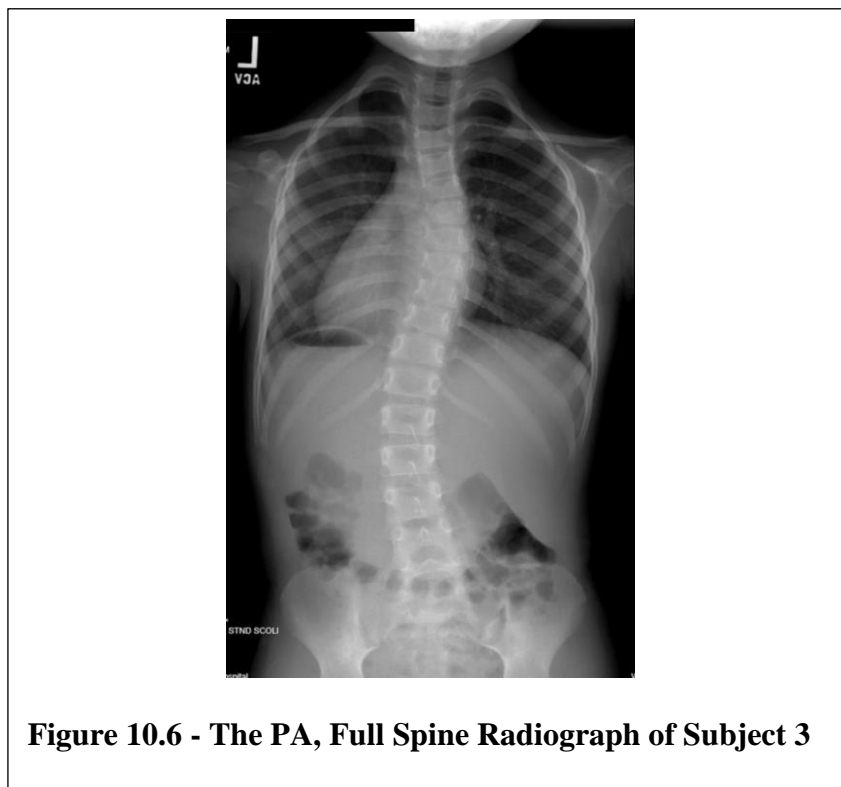
**Table 10.5 - Subject 2: The Values of 3DSPs Measured by the Application with and without Applied Specific Forces.**

The values were classified into one of the three-reference range categories (green: neutral alignment, blue: potential abnormal alignment, and red: malalignment).

## 10.6 Case Study for Subject 3

### 10.6.1 Methods and Findings

Subject 3 had a double thoraco-lumbar and thoracic curve (Figure 10.6). The Cobb angle measurement for the left thoraco-lumbar curve was  $19^\circ$  with the apex at T12/L1 and the right thoracic curve was  $20^\circ$  with a T7 apex. To confirm the result defined from the cases of Subjects 1 and 2 for the placement of a thoracic corrective force, the superior level of the force was applied on the apical vertebral level, not at the rib attached to the apical vertebrae, without any sagittal corrective forces (Condition 2). In this case, a thoraco-lumbar corrective force was applied for a thoraco-lumbar curve (Condition 6). It was shown that 3ULA, LRA, PTA of 3DSPs values became worse and only SLTA was improved. Condition 2 had two green, three blue, and six red colours among 11 of 3DSPs, while the spine with no force applied had four green, four blue, and three red colours. The result is displayed in Table 10.6.



<b>Subject 3</b>		SSAPs						SNSPs					
3DSPs / Applied Forces		3CEA	3UTA	3LTA	3ULA	3LLA	TRA	LRA	PTA	C5A	SSA	SCA	
No Force		54.70	88.51	91.04	104.06	85.23	-9.61	1.55	10.43	9.89	28.85	66.48	
Cond. 2+6	Th(16N) @ AV, TL(6N), CAX(4N)	44.57	89.99	103.81	108.30	64.25	-35.51	12.37	25.85	48.81	31.23	69.57	

(Cond.: Condition; @: at; AV: Apical Vertebral Level; Th: Thoracic Corrective Force; TL: Thoraco-Lumbar Corrective Force; CAX: Axillary Counter Force)

**Table 10.6 - Subject 3: The Values of 3DSPs Measured by the Application with and without Applied Specific Forces.**

The values were classified into one of the three-reference range categories (green: neutral alignment, blue: potential abnormal alignment, and red: malalignment).

## 10.7 Case Study for Subject 4

### 10.7.1 Methods

Subject 4 had a double thoracic and lumbar curve. The Cobb angle measurement for the right thoracic curve was  $23^\circ$  (apex at T8), while  $20^\circ$  was measured for the left lumbar curve (apex at L1/2) (Figure 10.7). The coronal curve pattern of Subject 4 was similar to the one of Subject 2. However, the lumbar curve of Subject 4 was more severe and dominant than the thoracic curve. Four different corrective force combinations were applied to test these two questions: “(a) Where should the superior level of a thoracic corrective force be applied: on the apical vertebral level, or at the apical rib of a thoracic curve? and (c) Is reducing a lumbar lordosis necessary as a primary corrective force for a lumbar or a thoracolumbar curve?” Thus, the correction data compared the values between when the superior edge of a thoracic force was applied on either the apical rib of a thoracic curve (Condition 1) or on the rib of the apical vertebra (Condition 2) while applying a lumbar corrective force on the lumbar curve (Condition 5). For the question (c), the optimal correction data also compared values between “with (Condition 3)” and “without” the combined forces applied on the abdomen and gluteus maximus in addition to one of the thoracic force placements. Then the values collected from the four difference force combinations were compared to the values from when no force was applied (Condition 1+5, 2+5, 1+3+5, and 2+3+5).



**Figure 10.7 - The PA, Full Spine Radiograph of Subject 4**

Subject 4		SSAPs						SNSPs						
		3CEA	3UTA	3LTA	3ULA	3LLA	TRA	LRA	PTA	C5A	SSA	SCA		
3DSPs / Applied Forces														
No Force		71.88	89.64	90.14	106.40	75.06	11.27	28.86	17.80	3.47	2.54	68.33		
Cond. 1+5	Th (15N) @ AR, Lu(16N), Cax(5N)	85.33	89.98	90.07	100.69	68.28	17.76	24.32	17.87	24.32	21.69	61.65		
Cond. 2+5	Th(17N) @ AV, Lu(16N), Cax(5N)	68.65	89.98	90.01	105.37	65.84	29.38	46.35	9.15	10.75	10.22	61.99		
Cond. 1+3+5	Th(6N) @ AR, Lu(17N), Cax(10N), Abd (15N), GMx (10N)	59.16	76.40	90.09	91.56	75.12	5.50	27.01	8.35	12.64	8.42	60.02		
Cond. 2+3+5	Th (11N) @ AV, Lu(13N), Cax(13N), Abd (13N), GMx (10N)	45.78	89.95	90.03	97.58	86.70	32.26	32.26	8.40	38.43	12.69	77.16		

(Cond.: Condition; @: at; AR: Apical Rib; AV: Apical Vertebral Level; Th: Thoracic Corrective Force; Cax: Axillary Counter Force; Abd: Abdominal Pressure; GMx: Gluteus Maximus Force)

**Table 10.7 - Subject 4: The Values of 3DSPs Measured by the Application with and without Applied Specific Forces.** The values were classified into one of the three-reference range categories (green: neutral alignment, blue: potential abnormal alignment, and red: malalignment).

### 10.7.2 Findings

The findings were displayed in Table 10.7. The 3D spinal alignment parameters were improved mostly when the superior level of the thoracic corrective force (6N) was applied on the apical rib of the thoracic curve, as shown in the other cases, and when concurrent sagittal corrective forces to reduce the lumbar lordosis were applied on the abdominal (15N) and gluteus maximus areas (10N), which is the case of Condition 1+3+5. In this case, a lumbar corrective force (17N) was applied for the lumbar curve. Condition 1+3+5 had five green, four blue, and two red colours among 11 of 3DSPs, while the spine with no force applied had two green, five blue, and four red colours. In the comparison between Condition 1+5 (four green) and Condition 2+5 (three green), Condition 1+5 had slightly better correction in the number of the green colour, as like the case of Subject 2.

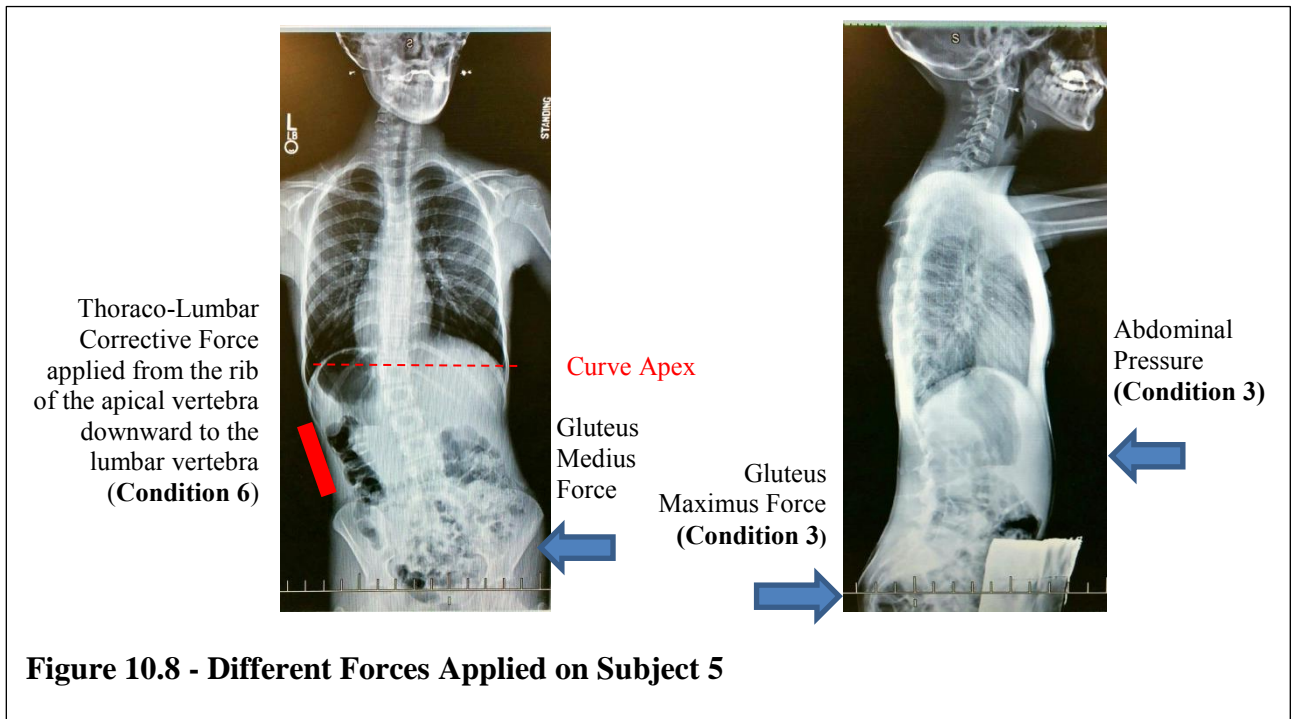
It showed that SPI in Condition 1+3+5 (68.37), which had two sagittal lumbar corrective forces were applied on the abdominal and gluteus maximus areas, had lower values than when no force was applied (86.13) while having more SPI values in Condition 1+5 (79.52), and Condition 2+5 (70.84), which had no two sagittal lumbar corrective forces. However, Condition 2+3+5 (85.56) had higher SPI values than Condition 1+5 and 2+5, while having still lower values than the case with no force applied.

## 10.8 Case Study for Subject 5

### 10.8.1 Methods and Findings

Subject 5 had a left single thoraco-lumbar curve (Cobb angle: 15°) at apex T12. Testing was performed to evaluate the question for (c) Is reducing a lumbar lordosis necessary as a primary corrective force for a lumbar or a thoracolumbar curve?”. Thus, all parameter values were compared between “with (Condition 3)” and “without” the combined forces applied on the abdomen and gluteus maximus when the superior level of the thoracic corrective force was applied on the rib of the apical vertebra downward to the lumbar area for the thoraco-lumbar curve (Condition 6) (Figure 10.8).

The results displayed in Table 10.8 also indicated a similar result to the case of Subject 4, which the 3D spinal alignment parameters were improved the most when the abdominal pressure and gluteus maximus force were applied (Condition 6+3). Condition 6+3 had seven green, one blue, and three red colours among 11 of 3DSPs, while the spine with no force applied had one green, three blue, and seven red colours. At that time the force applied on the thoraco-lumbar curve was 14N, and the forces applied on the abdomen and gluteus maximus were 36N and 22N in Condition 6+3. It showed that SPI in Condition 6+3 (78.97), which had two sagittal lumbar corrective forces applied on the abdominal and gluteus maximus areas, had lower values than the case when no force was applied (81.22) or Condition 6, which had no sagittal lumbar corrective forces applied (93.29).



Subject 5		SSAPs						SNSPs					
3DSFs / Applied Forces		3CEA	3UTA	3LTA	3ULA	3LLA	TRA	LRA	PTA	C5A	SSA	SCA	
No Force		82.84	87.92	90.00	108.54	66.50	14.66	25.98	22.77	33.38	36.56	58.45	
Cond. 6	TL(12N) @ AR, CAx(4N), GMe(9N)	65.50	88.77	105.02	96.67	62.58	5.14	47.68	26.17	16.11	49.94	67.12	
Cond. 6+3	TL(14N) @ AR, CAx(4N), GMe(22N), Abd(36N), GMx(22N)	68.11	82.97	99.07	102.43	52.69	1.68	7.85	20.97	14.44	29.30	58.00	

(Cond.: Condition; @: at; AR: Apical Rib; AV: Thoraco-Lumbar Corrective Force; CAx: Axillary Counter Force; GMe: Gluteus Medius Force; GMx: Abdominal Pressure; TL: Thoraco-Lumbar Corrective Force; TR: Axillary Counter Force; GMe: Gluteus Medius Force)

**Table 10.8 - Subject 5: The Values of 3DSFs Measured by the Application with and without Applied Specific Forces.**

The values were classified into one of the three-reference range categories (green: neutral alignment, blue: potential abnormal alignment, and red: malalignment).

## 10.9 Discussion and Conclusion

The results from the five cases showed the two systems which could help orthotists provide the optimal placements of biomechanical corrective forces that should be achieved by an orthosis. This is because this pilot study can answer these specific questions:

- (a) **Where should the superior level of a thoracic corrective force be applied on the apical vertebra level or at the apical rib of a thoracic curve?** All 5 case studies provided data related to this question. Based on the results found from all five cases, it could be concluded that the superior edge of a thoracic pad of a scoliosis corrective orthosis must be placed on the rib attached at the apex of the coronal thoracic curve in order to achieve the desired correction.
- (b) **Does a de-rotational force need to be applied with an anterior-medially directed force for a single thoracic curve?** One of the 5 studies provided data on this question. Based on the case of Subject 1, a posterior-laterally directed thoracic de-rotational force could not improve 3D spinal alignment (SSAPs) of AIS. However, the thoracic rotational angle (TRA) was improved the most while the thoracic de-rotational force was applied on the anterior part of the rib cage at the apex level of thoracic curve. Hence, clinicians need to be careful when applying the thoracic de-rotational force.
- (c) **Is reducing a lumbar lordosis necessary as a primary corrective force for a lumbar or a thoracolumbar curve?** Three (Subject 1, 4, and 5) of 5 case studies provided data on this question. The SPI of all three cases had smaller values when applying forces on the abdomen and gluteus maximus areas. However, in the cases of Subject 4 and 5, which had either a major lumbar curve or thoraco-lumbar curve, the parameters were improved. However, in the case of Subject 1, which had neither a lumbar curve nor a thoraco-lumbar curve, the parameters were improved the most when applying these two lumbar sagittal corrections. Reducing a lumbar lordosis, which applies forces to the abdominal and gluteus maximus

areas, might be needed to facilitate correction for a lumbar or a thoracolumbar curve.

In addition, it showed that the application can detect the coronal and sagittal misalignment. Subject 2 and 4 had a similar coronal curve pattern. Their coronal SSAPs also had the same pattern (Table 10.2). Both Subject 3 and 5 had a major thoraco-lumbar curve. It also showed their coronal SSAPs had the same pattern as each other (Table 10.2).

The mean of the optimal corrective forces recorded through the application when the parameters were improved the most by each case, were calculated in Table 10.9 to compare with one study performed to measure the optimal corrective forces achieved by an orthosis with flexible matrix composed of pressure sensors (Périeré et al., 2003). It was found that the recorded forces in this study had similar values to the mean of the forces calculated from 12 AIS patients in that study.

Subject/ Parameters improved at the most	Thoracic Corrective Force	Thoracic De- rotational Force	Lumbar Corrective Force	Thoraco- Lumbar Corrective Force	Axially Counter Force	Gluteus Medius Counter Force	Abdominal Pressure	Gluteus Maximus Force
1 SSAPs	17	n/a	n/a	n/a	14	3	2	n/a
1 SNSPs	26	4	n/a	n/a	16	6	2	10
2 3DSPs	19	n/a	17	n/a	4	n/a	n/a	n/a
4 3DSPs	6	n/a	17	n/a	10	n/a	15	10
5 3DSPs	n/a	14	n/a	14	4	22	36	22
Mean	17	9	17	14	9.6	10.33	13.75	14

**Table 10.9 - Recorded Forces (N) When the Parameters were Most Improved in Each Case.**

However, in utilizing the application to discover the misalignment of AIS, it was observed that the misalignment in the coronal plane tended to be reduced in magnitude. Most coronal spinal alignment parameters reported in the five cases, displayed near neutral alignment, even though curvature could be seen in the PA radiographs. However, the application could detect the direction of the coronal curves (Table 10.2). The possible explanation of this observation was also mentioned in Chapter 5. It is suggested that this finding occurred because the spinous process

usually rotates to the concave side of the coronal curvature for patients with AIS deformities, resulting in a lower estimation of coronal curve severity than expected.

In conclusion, the non-invasive digital calculating and visualisation assessment application and 3D skin level measurable parameters could be used to provide an answer to unclear and long-term unsolved biomechanical questions such as the optimal placements of 3D biomechanical corrective forces and 3D misalignment patterns of AIS. It also showed that this developed calculating and visualisation assessment application could be a useful and feasible AIS assessment tool for use in future clinical studies and clinical practice.

## **Chapter 11. Summary, General Discussion, and Recommendations**

## 11.1 Introduction

The main purpose of this thesis was to develop new effective 3D surface level measurable parameters to quantify the 3D AIS deformities and spinal misalignment, and to build a suitable 3D non-invasive digital assessment tool that can be used with the 3D surface level alignment parameters to identify, describe and evaluate the parameters. After these tools were developed, they were tested and the tools were used to investigate the ultimate goals of this thesis to shed light on orthotic controversies in the treatment of AIS such as: to quantify the 3D misalignment and deformities of AIS for better understanding of the 3D characteristics of AIS deformity; to clarify some key biomechanical elements of AIS that have not been solved before; and to contribute to the knowledge of 3D spinal biomechanical corrective concepts for the orthotic treatment of AIS.

## 11.2 Answers to the Research Questions Posed

To achieve the main purpose and ultimate goals of this thesis, (a) the clinical rationale for the thesis and the development of both tools were developed in Chapter 1 and 2; (b) to find literature evidence, literature reviews were also completed in Chapter 3; (c) six research studies were performed and presented in Chapter 4, 5, 6, 8, 9, and 10; (d) the development process and procedures of the two systems were presented in Chapter 7. The pilot study was performed for verifying the feasibility and implementation of the systems, as described in Chapter 10.

Thus, the results and findings accomplished through this thesis are discussed by addressing the eight objectives of this thesis, as framed in Chapter 2:

- 1. To determine whether there are (a) any *commonly used* measurable parameters that can quantify the 3D misalignment and deformity of AIS and biomechanically influence success in orthotic treatment; (b) any non-invasive assessment tools that can assess the deformity of AIS; and (c) any studies which have already defined the 3D biomechanical orthotic correction of AIS.**

AIS is a three-dimensional (3D) deformity of the spinal column, vertebrae, rib cage, and trunk. However, there was a lack of knowledge about the deformities of AIS acting in 3D space, especially for sagittal deformities. This may lead clinicians to make assumptions in treating AIS and thus induce significant quality deviations within each of the scoliosis orthotic device systems (Rigo et al., 2006; Bagnall et al., 2009). This knowledge gap also may have contributed to orthotic treatment failure rates that have been described as considerably inconsistent and varied (Dolan and Weinstein, 2007; Lonstein and Winter, 1994).

In **Chapter 3**, three literature reviews were performed. The purpose of the first review was to find studies which could identify any *commonly used* measurable parameters that are capable of quantifying the 3D misalignment and deformity of AIS and can biomechanically influence the success of the orthotic treatment. The Cobb angle method has been used as gold standard in measuring the curvature on the radiograph for the diagnosis, progression assessment, and treatment outcome of AIS. Several reviews found that there was a correlation between the initial Cobb angle reduction in the orthosis and a successful orthotic outcome (Korovessis et al., 2000; Bassett et al., 1986; Castro, 2003; Simith, 2003; Katz and Durrani, 2001; Clin et al., 2010; Zhang et al., 2015). However, it was discovered that the Cobb angle was not always proportional to the severity of the AIS deformities and unable to adequately quantify the global misalignments and 3D deformities of AIS because it measures the angle of localized curvatures on the 2D radiograph (Shufflebarger and King, 1987; Dickson and Weinstein, 1999; Kotwicki, 2008). The other three measurements found through the same search were reviewed and the review concluded that none of them could quantify the 3D misalignment of AIS.

Among the pathological features in the all three planes, the coronal misalignment pattern is the most studied area because the two-dimensional (2D) coronal PA radiographic image is the most utilized as the primary clinical assessment tool. However, the awareness of the potential oncogenic effects of radiation exposure has increased, and several studies found that there is a higher risk of breast cancer in patients who had been exposed to radiation frequently (Ardran et al., 1980; Doody et

al., 2000; Ronckers et al., 2010). Another literature review was performed to find whether there are any non-invasive assessment tools that can assess the 3D deformity of AIS spine in the literature. The review concluded that various assessment tools utilizing surface topographic technology cannot detect a full torso. The EOS imaging device was too expensive to use in most scoliosis clinics and could not completely eliminate the radiation exposure. Thus, this literature review indicated that motion capture technology may be one of the options currently available to measure the 3D alignment of the spine because it can accurately generate 3D Cartesian coordinated geometric data gained from reflective markers attached to the skin surface over anatomical landmarks of the AIS spine. However, no study was found that verified that the motion capture technology can assess and quantify spinal deformities in real time. Thus, the second review concluded that no assessment tool was found to provide the immediate or real-time feedback of orthotic correction by visualizing both measurement values and spine alignment while defining optimal orthotic correction performed on an actual patient's scoliotic spine.

The results of the third review, performed to find if there are any studies which already defined the 3D biomechanical orthotic correction of AIS, indicated that most studies used the 3D finite element or reconstruction model of a scoliotic spine instead of a real scoliotic spine in identifying the optimal biomechanical correction for orthotic treatment.

Thus, **Chapter 3** concluded that there was a need to develop a new measurable parameter system to comprehensively quantify the AIS 3D deformities and global misalignment, and consequently yield a better understanding of 3D AIS misalignment and deformity. Secondly, a new suitable 3D non-invasive and radiation-free digital assessment tool was also needed that can be used with the new measurable parameters and provide the immediate feedback of the optimal corrective forces applied on the AIS spine.

**2. To identify major biomechanical corrective elements that had raised disagreement among clinicians who treat AIS.**

The biomechanical principles employed during the orthotic treatment of AIS are not fully defined through scientific analyses, even though major scoliosis academic and professional groups such as Scoliosis Research Society (SRS), the International Society on Scoliosis Orthopaedic and Rehabilitation Treatment (SOSORT), and American Academy of Orthotics and Prosthetics (AAOP), have made ongoing efforts to define best practice guidelines for orthotic biomechanics of AIS. Thus, the survey and literature review project, “*Current Practice Standards in Orthotic Treatment of Adolescent Idiopathic Scoliosis*,” which the author conducted as the chair of the Spinal Orthotic Scientific Society of the American Academy of Orthotists and Prosthetists, was introduced in **Chapter 4** (Jang et al., 2019). This project assessed the current practice and status of orthotic treatment for AIS by surveying 46 qualified scoliosis orthotic experts and reviewed literature to find out whether there was any scientific evidence in these resources as secondary sources.

This survey study concluded that more scientifically valid and quantitative investigations are necessary to understand the following three biomechanical concepts: (a) Where should the superior level of a thoracic corrective force be applied, on the apical vertebra level or at the apical rib of a thoracic curve? (b) Does a de-rotational force need to be applied for a single thoracic curve in addition to an anterior-laterally directed force, and which is the primary thoracic corrective force? (c) Is reducing a lumbar lordosis necessary as a primary corrective force for a lumbar or a thoracolumbar curve? These questions contributed to the research questions and rationale of the later pilot study in this thesis. Thus, in **Chapter 10**, the feasibility of the assessment tool and measurable parameters developed through this thesis was evaluated by defining these research questions.

**3. To determine whether the newly developed RSAPs are useful in quantifying coronal and sagittal AIS misalignment, especially for sagittal misalignment patterns which had not been clearly defined prior to this study.**

For this thesis, two spinal alignment measurable parameter systems were developed to quantify the spinal misalignment and deformities of AIS. First, a radiographic spinal alignment parameters (RSAPs) system was developed based on the 3D osseous

structural characteristics of a human's erect spine and the unique features in each spinal bony structural segment. RSAPs consist of five sagittal and five coronal spinal alignment parameters. The values of these parameters are determined by measuring each segmental alignment's angles related to the global horizontal line in two planes using both a PA full spine radiograph (coronal) and a lateral full spine radiograph (sagittal).

The retrospective study was conducted in **Chapter 5** by analyzing a series of paired PA, standing, full-spine radiographs and lateral view, standing, full-spine radiographs taken at the same time point for 100 patients who were randomly selected. This study found that RSAPs was verified as a useful measurement in quantifying 2D AIS misalignment. The significant results of this study were to be able to identify seven major sagittal misalignment patterns, and to understand the relationship between the coronal and sagittal misalignment patterns in the AIS spine by using the developed RSAPs. This finding was useful because the sagittal misalignment patterns and relationship between the coronal and sagittal misalignment patterns had not been clearly defined prior to this study and had existed as a long-term unsolved task in the field.

**4. To verify whether the validated RSAPs can be used on skin surface level landmarks to measure 3D spinal alignment by performing a concurrent validity test between the values measured from the skin level anatomical landmarks of SSAPs and corresponding values measured from the original osseous landmarks of RSAPs.**

To quantify the 3-dimensional (3D) spinal misalignment of AIS and eliminate the need to take serial radiographs, the 3D concept of skin level spinal alignment parameters (SSAPs) was developed by converting the key osseous anatomical landmarks of the previously established RSAPs in **Chapter 5** to the closest anatomical locations on the skin surface. In **Chapter 6**, a concurrent validity test was conducted to find out whether SSAPs correspond to the previously established radiographic parameters (RSAPs) for the same subject. The PA and lateral view radiographs of 13

AIS patient's spine were taken with 5mm radiographically visible metal balls attached on the surface level that corresponded to key anatomical landmarks of RSAPs.

The results of this study showed that there was a statistically significant, strong, and positive linear relationship between each RSAP segmental parameter that was measured from the osseous anatomical landmarks and from each corresponding SSAP parameter, which was measured from the surface level anatomical landmarks (metal balls).

**5. To examine if SSAPs reflect the structural characteristics of a human's erect spine and to ascertain the unique features in each spinal osseous structural segment.**

In **Chapter 6**, both coronal and sagittal spinal alignment profiles of RSAPs and SSAPs were illustrated by using the means of the parameter values, which were visually compared using the data collected for the concurrent validity experiment. Even though the absolute values were different between the two methods, these visual comparisons also verified that the skin profile of SSAPs could reflect the structural characteristics of a human's erect spine and the unique features of each spinal osseous structural segment. Thus, **Chapter 6** concluded that SSAPs can be used for skin surface level analysis in order to quantify 3D misalignment patterns and deformities of patients with AIS.

**6. To identify reference (normal) ranges for all 3DSPs including SSAPs to use in developing a digital assessment tool.**

**Chapter 7** introduced the development procedure of a non-invasive digital calculating and visualisation assessment application by utilizing motion capture technology. It also explained the development of the 3D surface level parameters system (3DSPs) that can be used with the application. The 3DSPs system was developed based on five SSAPs validated in **Chapter 6** by adding six key non-spinal alignment parameters. 3DSPs could be used not only to comprehensively quantify 3D global spinal misalignments of AIS but also to detect other major deformities from the skin surface level. This application can measure the 3D parameters and visualize the

values and shape of spinal misalignment. By connecting with load cells mounted to the position adjustable bars with different types of corrected pads on the scoliotic standing frame, this application also allows the operator to measure optimal placements of corrective forces in the orthotic treatment, and also measure the force values applied by corrective pads with the load cells. The application has a capability to indicate in colour, the values and the alignment segments of a spine in real time on the computer screen by showing them in one of two colours, depending on whether each value is within the reference range for that parameter. The colour indicator concept can provide immediate feedback in assessing whether the corrective force applied on the scoliotic spine is optimal, simply by comparing the colour changes on the screen before and after corrective forces are applied on the AIS spine.

For identifying the reference ranges of 11 3DSPs, the study was performed in **Chapter 8**. Twenty non-scoliotic adolescent girls in the same age range as those with AIS were recruited. The values of each 3DSP parameter were measured using motion capture technology. By employing two different reference range classification methods, the reference range of 3DSPs were defined.

**7. To investigate the discriminative validity (or contrast validity) of 3DSPs by comparing existing data collected from non-scoliosis and scoliosis groups.**

**Chapter 9** examined the discriminative validity of the 11 parameters of 3DSP by comparing the values between the non-scoliosis group and scoliosis group. For the non-scoliosis group, the measurements of the 3DSPs collected from 20 non-scoliotic adolescent girls in **Chapter 8** were used. Their average age was 12.5 years. For the scoliosis group, data was collected from 5 AIS adolescent girls whose average age was 13.2 years. Seven parameters (3UTA, 3LTA, 3ULA, SCA, TRA, LRA, and C5A) of 11 3DSPs showed statistically significant differences between the scoliosis and non-scoliosis groups. Considering that the subject size of the scoliosis group was small, the results of this test were reasonable. Thus, all 11 parameters were taken forward to the final experimental chapter of this thesis.

## **8. To test if the developed digital assessment tool can identify the key elements of the 3D orthotic biomechanical corrective concepts with 3DSPs.**

**Chapter 10** examined the feasibility of using the newly developed non-invasive digital calculating and visualisation assessment application and the 3D measurable parameters (3DSPs) with 5 AIS cases. This was achieved by identifying unclear and long-term unsolved biomechanical questions between the scoliosis experts, which were previously introduced in **Chapter 4**. The results from the five cases showed that the two systems could help orthotists provide the optimal placements of biomechanical corrective forces that should be achieved by an orthosis. The feasibility of the application and parameters was accomplished by demonstrating how to quantify the 3D misalignment and deformities of AIS, to assess the optimal locations of corrective forces applied on the AIS torso, and then to present the measurements and spinal alignment shapes in a visual digital real-time feedback format.

### **11.3 General Discussion: General Overview of the Important Contributions**

Through the studies of this thesis, a new non-invasive and radiation-free digital calculation and visualisation assessment application was successfully developed, as well as a new 3D measurable spinal parameter system (3DSPs), including both radiographic spinal alignment parameters (RSAPs), and skin surface spinal alignment parameters (SSAPs).

This section discusses the results and findings, which were achieved while undertaking this thesis by addressing the purposes and ultimate goals of this thesis mentioned above.

#### **11.3.1 Quantification of the Misalignment and Deformities of AIS and Better Knowledge of 3D Characteristics of AIS Deformity**

One of the remarkable outcomes of this thesis, as mentioned previously, was to identify the relationship between each coronal and sagittal segmental alignment and to define seven sagittal misalignment patterns of AIS. This had been a long-term, unsolved task in the field, which had not been clearly defined prior to this study. This

was accomplished using the radiographic spinal alignment parameters (RSAPs) by quantifying the spinal misalignment of AIS in the radiographic analysis study (**Chapter 5**). The other most valuable outcome and originality of this thesis was establishing that 3DSPs can quantify the 3D misalignment and deformities of AIS spines and eventually help to understand the 3D AIS deformity characteristics by comparing the values of 3DSPs measured from the non-scoliotic spines (**Chapter 9**).

The findings for understanding the 3D misalignment and deformities were also consistent between what we learned from the radiographic analysis study performed with the RSAPs and from the 3D skin level analysis study performed with 3DSPs. The 3D deformity is more severe than the coronal deformity due to the 3D nature of AIS, in which a curve in one plane is associated to a large degree with a curve in the other plane (**Chapter 5** and Table 10.2, and Table 10.3 in **Chapter 10**). The following are the summaries of the findings:

#### ***Loss of Natural Thoracic Kyphosis in the Thoracic Structural Curve***

In the sagittal plane, the upper thoracic and lower thoracic segments in the scoliosis spines appeared relatively straighter (i.e. vertical and flat) and had lost their natural thoracic kyphosis if there is a thoracic curve in the coronal plane. The 3D global skin level analysis also found there was a tendency to have a loss of natural thoracic kyphosis (vertically flattening) coupled with the compensatory extension of the upper thoracic spine if any structural curve exists in the thoracic region. These results corresponded to Dickson et al's biplanar spinal theory (1984) and Burwell's pathogenesis theory (2003).

#### ***Cervical Compensatory Mechanism***

In addition to the loss of natural thoracic kyphosis in the thoracic structural curve, both the radiographic analysis (**Chapter 5**) and 3D skin level analysis studies (**Chapter 9**) found that in most cases, if there was any thoracic structural curve in the coronal plane, a compensatory extension was observed in the lower cervical segment by having greater values of the both SCEA, 3CEA and C5A in the scoliosis spines than in the non-scoliosis spines. Dickson et al's biplanar spinal theory (1984) only

explained the relationship between the upper and lower thoracic segments when a thoracic curve exists. Thus, this thesis found that the lower cervical segment also became extended, just like the extension of the upper thoracic segment, as a compensatory mechanism against the anteriorly directed force which occurred at the lower level of the thoracic region.

### ***Length of Curve VS. Apex of Curve***

The results of the radiographic analysis study also indicated that there was a tendency of either (or both) of the lower thoracic and the upper lumbar segments to be more anteriorly inclined (more vertical) in the sagittal plane, in the presence of any long C thoracic curve. This phenomenon increases the extension moment in both segments. When the curve is classified as a thoracic curve, the curve is named based on the apical location of the curve. However, in many cases with single thoracic curves, the deformity (or coronal curve) goes beyond the thoracic spine and extends inferiorly to the lumbar spine like a long C-shape curve. As mentioned above, when this kind of curve exists, the lower thoracic segment and the upper lumbar spine are more anteriorly inclined than in the neutral alignment. Sometimes in the radiographs, the lower lumbar segment also became more anteriorly inclined. This thesis suggests that the length of the deformity should be noted when assessing AIS deformities, rather than considering only the apical location of the curve.

### ***Multiple Structural Curves***

In 16 of the 100 cases in the radiographic analysis study, a coronal curve was present but there was the absence of a sagittal deformity, or close to neutral sagittal alignment. It was further noted that the cases had either double or triple coronal curves, or even some of single thoraco-lumbar curves. This may be due to multiple curves compensating or offsetting each other as the curve changed to the opposite direction as it met another curve. For single thoraco-lumbar curve cases, the apex is located at the thoraco-lumbar junction, and the 3D deformities may therefore be less visible than usual in the sagittal plane. One reason this occurs may be that the osseous structure is changed completely at the junction. However, further research is needed to define the reason why some of single thoraco-lumbar curves are less severe in another plane.

### *Similarity of Rotational Deformity between Thoracic and Lumbar Spine*

Dickson et al. (1984)'s biplanar spinal theory and Burwell (2003)'s pathogenesis theory mentioned in their articles that there is an anteriorly directed force on the thoracic spine if there is a thoracic curve. Furthermore, Burwell (2003) and Gum et al. (2007) claimed that the anteriorly directed force became a rotational force as the deformity becomes worse. They also observed that the segment which contains the coronal-structural curve rotates to the concave side of the curve, as viewed from the transverse plane. Thus, clinicians usually measure the rotational degree of the thoracic and lumbar spines with a scoliometer while performing Adam's forward bend test to examine and define where a structural curve is located. The results of 3D skin level analysis study (**Chapter 8 and 10**) supported the studies and the clinical observations mentioned above (Burwell, 2003; Gum et al., 2007). Table 10.3, 8.1, and 8.2 showed that the values of the thoracic and lumbar rotational deformities (TRA and LRA) of the scoliosis spines were much greater than those of the non-scoliosis spines which show almost no rotational deformities.

In addition, several authors also stated that a compensatory rotation may occur immediately next to the segment where a structural curve exists by rotating to the opposite direction of the deformity segment (Gum et al., 2007; Watters, 2012). As seen in Subject 1 and 5 (Table 10.3), the adjacent segment also showed some degree of rotation but the rotation degree was less than the values measured from the segment that has the deformity. Thus, it can be concluded that the collected data from the application in the study performed in **Chapter 10**, supports the existence of the compensatory rotation in the segments connected with the deformity segment, as revealed by the Gum et al.'s study and Watters et al.'s theory. Since this application is able to detect the rotational deformities, taking a set of side bending radiographs used to identify whether the curve is structural or not might be eliminated at the clinic.

### *Differentiation of AIS Deformity between Thoracic and Lumbar Spines*

In addition, the lumbar region was displaced more anteriorly as viewed from the sagittal plane when there was any structural lumbar curve in the coronal plane. The

deformity and misalignment of the lumbar region has not been a well-known area of study prior to this thesis. The 3D skin level analysis test showed the same result as the radiographic analysis study, namely that the lumbar region displaced more anteriorly as the lower lumbar segment in the scoliosis spines was tilted more anteriorly than the non-scoliosis spines. This was because the upper lumbar segment in the scoliosis spines was tilted much more posteriorly and the lower lumbar segment was tilted much more anteriorly, compared to the non-scoliosis spines. Even though the same pathomechanism occurs in the thoracic and lumbar spines, the resulting deformity in the lumbar spine differs from the thoracic spine. While the lumbar spine is displaced anteriorly if there is an AIS deformity, the thoracic spine does not displace more anteriorly. However, the entire thoracic spine became more vertically flat (straighter) with the existence of compensatory extension on the upper segments. This deformity difference between the lumbar and thoracic spines can be explained easily by the difference in the osseous structure and function of the thoracic and lumbar spines. While the thoracic spine contributes little to flexion and extension due to oblique orientation of its vertebral facets, the lumbar spine allows the greatest movement for flexion and extension due to the vertical orientation of the facets.

#### ***Anteriorly Directed Force and Increase of Extension of Spine***

Dickson et al. (1984)'s biplanar spinal theory and Burwell (2003)'s pathogenesis theory only explained thoracic AIS deformity. However, this thesis found that the AIS deformity occurred where an anteriorly directed force exists, not only at the thoracic region but also at any part of the spine. It may also be concluded that the 3D deformities of AIS are caused by creating extension in the spine (an extension moment). The 3D Characteristics of AIS Deformity between the thoracic and lumbar spine were differently represented due to their unique anatomical structure. These findings explain why we should assess the AIS deformities in multi planes or 3 dimensions and provide clinicians with a better understanding of the AIS deformity itself. Orthotic treatment can be improved by applying more exact placements for the corrective forces on the spine in the 3D views.

### 11.3.2 Clarification of the Existing Disagreement: Biomechanical Elements in the Orthotic Treatment of AIS

In **Chapter 3**, the third literature review could not find any studies which already defined the 3D biomechanical orthotic correction of AIS. The review also indicated that most studies found through the search used the 3D finite element or reconstruction model of a scoliotic spine instead of a real scoliotic spine in identifying the optimal biomechanical correction of orthotic treatment. Later, one study was found and it measured the corrective forces under each orthosis of 12 AIS patients with a flexible matrix composed of pressure sensors (Périé et al., 2003). However, in the study, there was a lack of explanation about the relationship between corrective forces measured under the pad and how an optimal alignment should be achieved by the orthosis.

Since the non-invasive assessment tool and 3D measurable parameters of this thesis showed how to solve the current existing disagreement about biomechanical elements in the orthotic treatment of AIS, this thesis may be the first study which could measure the optimal placement of 3D biomechanical corrective forces that possibly can be achieved by an orthotic device by using the method of simulating forces with corrective pads applied toward the AIS spine. The following summarizes the findings from the study conducted in **Chapter 10** relevant to the current existing disagreement about biomechanical elements of AIS introduced in **Chapter 4**:

#### *The Superior Level of a Thoracic Corrective Force*

The results found from all five cases indicated that the superior edge of a thoracic pad of a scoliosis corrective orthosis should be placed on the rib attached at the apex of the coronal thoracic curve in order to achieve the desired correction instead of at the vertebral level of the apex. Prior to this thesis, ambiguity and uncertainty of the placement of a thoracic corrective force had been a long-term task to be solved in the scoliosis community as shown in **Chapter 4**. In the survey results of “SOSORT Consensus Paper on Brace Action: TLSO Biomechanics of Correction”, the European scoliosis expert opinions regarding the placement of the thoracic pad were almost evenly divided (Rigo et al., 2006) just as it was in the survey results performed with American scoliosis experts in **Chapter 4**. Another study reported in their article that

maximum stability of a thoracic curve can be achieved by placing the thoracic pad at the apex of the primary thoracic curve (Blount and Moe, 1980). Other articles recommended that a thoracic pad would be placed on the ribs originating from the apex and distal to the apex which is the same concept confirmed in the results of this thesis (Andriacchi et al., 1976; Watts, 1979; Larnen et al., 1983; Patwardhan et al., 1996). However, all articles mentioned above were described in theory-based descriptive papers and their suggestions for a thoracic pad placement were not based on any quantitative study. Thus, the recommendation of this thesis was that the superior edge of a thoracic pad of a scoliosis corrective orthosis should be placed on the rib attached at the apex of the coronal thoracic curve. This clear result may help resolve one of the most important biomechanical questions and current existing disagreements in orthotic treatment of AIS.

#### ***Necessity of Posterior-Laterally Directed De-Rotational Force for a Thoracic Curve***

In the literature about how to effectively correct the rotated elements of the scoliosis, Jang (the author) and Hudson (2013) described that biomechanical de-rotation may be accomplished as follows: one of the thoracic de-rotational forces (a posterior-laterally directed thoracic de-rotational force) is generally applied on the anterior part of the rib cage at the apex level of the thoracic curve as viewed from the transverse plane while the other de-rotational force (an anterior-medially directed thoracic de-rotational force) applies as the part of the corrective thoracic pad components (Jang and Hutson, 2013).

In **Chapter 10** of this thesis, one (Subject 1) of the 5 cases investigated the necessity of a posterior-laterally directed thoracic de-rotational force because Subject 1 had a single thoracic curve. The results indicated that the values of TRA improved the most, while the rotational force could not improve 3D spinal alignment (SSAPs) of AIS. The reason why the SSAPs were not improved may be due to the lack of sagittal corrective forces on the thoracic region, which is a posteriorly directed force on the lower part of the sternum. Thus, a future follow-up biomechanical study is needed to test how much improvement can be achieved in the values of SSAPs by applying a resultant force combination of the posterior-laterally directed thoracic de-rotational force and

posteriorly directed force on the lower part of the sternum. Hence, clinicians need to be careful when applying the thoracic de-rotational force until further study results are known.

### ***Necessity of Sagittal Corrective Forces for Reducing the Lumbar Lordosis of the Lumbar or Thoraco-lumbar curve***

In general, spinal biomechanical theory, to reduce the lumbar lordosis, the posteriorly directed force of an abdominal pressure and an anteriorly directed force of a gluteus maximus pad should be applied. Three (Subject 1, 4, and 5) of 5 cases in **Chapter 10** were tested for this question. In the cases of Subject 4 and 5, which had either a major lumbar curve or thoraco-lumbar curve, the parameters were improved the most when applying these two lumbar sagittal corrections. It can be concluded that two lumbar sagittal correction forces, applied on the abdominal and gluteus maximus areas, are needed to facilitate correction for a lumbar or a thoracolumbar curve or when any hyper-lumbar lordosis exists. In the case of Subject 1, the parameters also were improved. Even though this case had neither a lumbar curve nor a thoraco-lumbar curve and had a single thoracic curve, the values measured of SULA and SLLA (Table 10.2) indicated that Subject 1 had a hyper-lumbar lordosis and may be a Type 7 sagittal misalignment pattern. This result supports several articles which mentioned that abdominal compression can stabilize the lumbar spine, reduce lumbar lordosis by improving the grasp on the pelvis, and eventually contribute to improving lumbar curve correction (Blount and Moe, 1980; Udén and Willner, 1983; Carlson, 2003).

In addition, the SPI values (combination of PTA and SCA) of all three cases (Subject 1, 4, and 5) when the lumbar sagittal corrective forces were applied, had smaller values prior to applying the two sagittal lumbar corrective forces. This corresponded to the results of Klineberg et al.'s (2011) radiographic study. They reported that pelvic incidence, which was calculated by the combination of the values of pelvic tilt and sacral slope angle measured from the osseous landmarks on the radiograph, correlates with lumbar lordotic posture. Thus, it may be concluded that the value of SPI, which is similar to the pelvic incidence, also correlates with lumbar lordotic posture.

### 11.3.3 Uses of 3D Non-Invasive Digital Assessment Tool and Measurable Parameters for Scoliosis Clinics and Future Studies

As shown above, quantitative data measured from the newly developed digital assessment application with 3DSPs, provided the opportunity to identify possible solutions to unclear and long-term unsolved biomechanical questions between scoliosis experts. The pilot study showed some evidence that could resolve the existing disagreement among the professional community involved in the orthotic treatment of AIS by comparing the 3D misalignment parameters before and after corrective force application, and by analyzing the effect of various corrective forces on spine and trunk alignment through the digital assessment application.

The following are the positive attributes of this application in more detail:

- the utilization of non-invasive motion capture technology
- the capability to use this tool without markers attached on the torso of the patient
- elimination or reduction of the number of times patients would need to have radiographs, decreasing radiation exposure risks to AIS patients, by providing clinicians and researchers with a validated alternative way to measure orthotic treatment outcomes immediately at the clinic site.
- the immediate or real-time values and visual feedback information of the patient's orthotic corrections, simulated for defining optimal orthotic correction based on research using an actual patient's scoliotic spine.
- the capacity to measure the 3D parameters, visualize the parameter values and the shape of the 3D misalignment patterns of the AIS spine, and then conveniently present it on the computer screen in one of two colours, depending on where the value falls within the ideal correction reference range for that parameter.
- the capacity to measure corrective force and load measurements through the connection of a force transducer. It also can display the

values of applied corrective forces immediately on the computer screen.

Thus, this thesis not only offered this investigator a tool to use 3DSPs for developing the new assessment application, but also may offer opportunities for other researchers to use the 3DSPs system to further define 3D AIS misalignment and deformity in future studies. In addition, these two combined systems could allow a validated 3D outcome assessment opportunity in scoliosis clinics by offering a visual 3D optimal biomechanical orthotic corrective approach to spinal orthotists, providing immediate colour feedback in real time and recording the corrective forces applied on the AIS spine through the application. It also showed that the application can detect the coronal and sagittal misalignment. In addition, the scoli-standing frame built for this application may be very useful clinically. It can be used for holding the AIS patient in the correct position while scanning in order to fabricate an optimal orthosis. This may eliminate or reduce casting procedures and reduce fabrication time.

#### **11.4 Limitations and Recommendations for Further Study**

The scope of the thesis also revealed some limitations and challenges in providing the functionality of the application and its measurable parameters: (a) the spinal alignment detected using these systems, is not the alignment of the actual osseous structure of the spinal column; and (b) palpating the exact locations of spinous processes from the skin surface levels is challenging in some AIS spines, especially for those patients who have more soft tissue around the torso.

In addition, there are some limitations in the studies performed in Chapter 9 and Chapter 10. Due to the small AIS sample size ( $n=5$ ) of these studies, further research should focus on obtaining a larger sample size to determine whether the developed parameters can distinguish the spinal deformities between the non-scoliosis group and scoliosis group and thus contribute to establishing data toward a more widely and universally accepted biomechanical correction theory.

Significant additional improvement may be needed in the application to make it easy to use by clinicians in scoliosis clinics. For example, the application has no capability to display dynamically and continuously real-time feedback information for the parameter values and spinal alignment shapes, it can only currently show the situation ‘before’ and ‘after’ the force is applied in the assessment application. If this function could be improved to provide continuous feedback, the step of touching the anatomical landmarks with a pointer to obtain the coordinate data from them after the force is applied, can be excluded and continuous feedback could be given as the force is applied. This improvement could also reduce the assessment time.

In addition, a future prospective study into the topic of the relationship between optimal immediate corrections in 3DSPs and successful treatment outcomes is needed. The treatment goal of AIS is not to correct the misaligned spine completely in order to make it like a non-scoliotic spine. As mentioned in **Chapter 1**, the goal is to prevent the deformity progression or to delay surgery during the growth period. Thus, a future research study must focus on determining how much correction of 3DSPs is required to achieve the treatment goal. Additionally, there are several other questions to be addressed by future research such as:

- What is inter- and intra- reliability in measuring 3DSPs?
- Which measurements among 3DSPs are clinically significant indicators of progression of the deformity?
- Is there a correlation between 3DSPs and the Cobb angles of the curve, including coronal curve types?

For the pilot feasibility study, only five AIS subjects were recruited even though the recruitment occurred through two major scoliosis clinics near by the study conducting site. The results from the thesis study, which investigated the optimal placements of 3D corrective forces, were able to indicate the biomechanical basis for resolving the existing disagreement among the professional community involved in the orthotic treatment of AIS. However, to contribute in establishing a unified and comprehensive 3D biomechanical corrective theory in orthotic treatment, which could lead to the improvement of treatment outcomes in AIS clearly and completely, a future study

would require a larger sample size and thus provide a greater variety of different curve types. It is therefore necessary for this type of assessment equipment to find its way into clinical sites themselves and to be used in regular practice so that a database of treatment can be established.

In conclusion, this thesis has established the performance and clinical application of the combination of the two newly developed measurable parameters and assessment applications. These incorporated potentially clinically useful and novel assessment tools that may allow a fundamentally safe and validated 3D orthotic outcome assessment opportunity for AIS patients. The two systems also offered a visual 3D optimal biomechanical orthotic corrective approach to interdisciplinary scoliosis specialists and orthotic practitioners by providing immediate visual feedback information in real time for parameter values, spinal alignment shapes, and applied force values. Furthermore, it is hoped that the availability of these systems can stimulate the opportunity to undertake further useful research and continue to improve the quality of life of AIS patients.

## **References**

Adam CJ, Askin GN, Pearcy MJ (2008) Gravity-Induced Torque and Intravertebral Rotation in Idiopathic Scoliosis: *Spine* 33:E30–E37.

Andriacchi TP, Schultz AB, Belytschko TB, Dewald R (1976) Milwaukee brace correction of idiopathic scoliosis. A biomechanical analysis and a retrospective study. *J Bone Joint Surg Am* 58:806–815.

Ardran GM, Coates R, Dickson RA, Dixon-Brown A, Harding FM (1980) Assessment of scoliosis in children: low dose radiographic technique. *Br J Radiol* 53:146–147.

Asher MA, Manna BJ (1999) Optimizing surgical improvement of trunk asymmetry from idiopathic scoliosis: a preliminary report. In: *Research into Spinal Deformities 2* (Stokes IAF, ed), pp 250–253. IOS Press.

Aubin C-E, Dansereau J, Parent F, Labelle H, De Guise JA (1997) Morphometric evaluations of personalised 3D reconstructions and geometric models of the human spine. *Medical and Biological Engineering and Computing* 35:611–618.

Bagnall KM, Grivas TB, Alos N, Asher M, Aubin C-E, Burwell GR, Dangerfield PH, Edouard T, Hill D, Lou E, Moreau A, O'Brien J, Stokes I, Weiss H-R, Raso J (2009) The International Research Society of Spinal Deformities (IRSSD) and its contribution to science. *Scoliosis* 4.

Bernhardt M, Bridwell KH (1989) Segmental analysis of the sagittal plane alignment of the normal thoracic and lumbar spines and thoracolumbar junction. *Spine* 14:717–721.

Bland JM, Altman D (1986) Statistical methods for assessing agreement between two methods of clinical measurement. *The Lancet* 327:307–310.

Blount W, Moe J (1980) The Technique of Nonoperative Management. In: *The Milwaukee Brace*, 2nd ed., pp 59–118. Williams & Wilkins.

Boulay C, Tardieu C, Hecquet J, Benaim C, Mouilleseaux B, Marty C, Prat-Pradal D, Legaye J, Duval-Beaupère G, Pélissier J (2006) Sagittal alignment of spine and pelvis regulated by pelvic incidence: standard values and prediction of lordosis. *Eur Spine J* 15:415–422.

Bradford DS, Moe JH, Montalvo FJ, Winter RB (1974) Scheuermann's Kyphosis and Roundback Deformity: Results of Milwaukee Brace Treatment. *JOURNAL OF BONE AND JOINT SURGERY-BRITISH VOLUME-* 56:740–758.

Bryant JT, Reid JG, Smith BL, Stevenson JM (1989) Method for determining vertebral body positions in the sagittal plane using skin markers. *Spine* 14:258–265.

Burwell RG (2003) Aetiology of idiopathic scoliosis: current concepts. *Pediatric Rehabilitation* 6:137–170.

Carlson JM (2003) Clinical Biomechanics of Orthotic Treatment of Idiopathic Scoliosis - Journal of Prosthetics and Orthotics, 2003 | American Academy of Orthotists & Prosthetists. Journal of Prosthetics and Orthotics 15.

Castelein RM, Dieën JH van, Smit TH (2005) The role of dorsal shear forces in the pathogenesis of adolescent idiopathic scoliosis – A hypothesis. Med Hypotheses 65:501–508.

Castro FP (2003) Adolescent idiopathic scoliosis, bracing, and the Hueter-Volkman principle. The Spine Journal 3:180–185.

Chan A, Lou E, Hill D, Faulkner G (2012) Design and validation of transducers to measure interface force distribution in a spinal orthosis. Medical Engineering & Physics 34:1310–1316.

Clin J, Aubin C-É, Sangole A, Labelle H, Parent S (2010) Correlation Between Immediate In-Brace Correction and Biomechanical Effectiveness of Brace Treatment in Adolescent Idiopathic Scoliosis: Spine 35:1706–1713.

Cramer D (1998) Fundamental Statistics for Social Research: Step-by-step Calculations and Computer Techniques Using SPSS for Windows. Psychology Press.

Cramer D, Howitt DL (2004) The SAGE Dictionary of Statistics: A Practical Resource for Students in the Social Sciences. SAGE.

Dalton D (2011) The Vertebral Column. In: Joint Structure and Function: A Comprehensive Analysis, 5th ed. (Levangie PK, Norkin CC, eds), pp pp.139-191. Philadelphia, PA: F.A. Davis Company.

Danielsson AJ, Hasserius R, Ohlin A, Nachemson AL (2007) A Prospective Study of Brace Treatment Versus Observation Alone in Adolescent Idiopathic Scoliosis: A Follow-up Mean of 16 Years After Maturity. Spine 32:2198–2207.

Desbiens-Blais F, Clin J, Parent S, Labelle H, Aubin C-E (2012) New brace design combining CAD/CAM and biomechanical simulation for the treatment of adolescent idiopathic scoliosis. Clinical Biomechanics 27:999–1005.

Dickson RA (2010) Spinal Deformities. In: Children's Orthopaedics and Fractures (Benson M, Fixsen J, Macnicol M, Parsch K, eds), pp 599–637. London: Springer London.

Dickson RA, Lawton JO, Archer IA, Butt WP (1984) The pathogenesis of idiopathic scoliosis. Biplanar spinal asymmetry. Bone & Joint Journal 66-B:8–15.

Dickson RA, Weinstein SL (1999) Bracing (and screening)-yes or no? JOURNAL OF BONE AND JOINT SURGERY-BRITISH VOLUME- 81:193–198.

Długosz M, Chwała W, Maciejasz P, Alda W (2012) Realistic model of spine geometry in the human skeleton in the Vicon system. Bio-Algorithms and Med-Systems 8.

Dolan LA, Weinstein SL (2007) Surgical rates after observation and bracing for adolescent idiopathic scoliosis: an evidence-based review. *Spine* 32:S91–S100.

Doody MM, Lonstein JE, Stovall M, Hacker DG, Luckyanov N, Land CE (2000) Breast cancer mortality after diagnostic radiography: findings from the U.S. Scoliosis Cohort Study. *Spine* 25:2052–2063.

Ghandhari H, Hesarikia H, Ameri E, Noori A (2013) Assessment of Normal Sagittal Alignment of the Spine and Pelvis in Children and Adolescents. *BioMed Research International* 2013:1–7.

Gignac D, Aubin C-É, Dansereau J, Labelle H (2000) Optimization method for 3D bracing correction of scoliosis using a finite element model. *Eur Spine J* 9:185–190.

Gracovetsky S (2010) Chapter4: The Skin Motion Problem. In: *Non-invasive Assessment of Spinal Function*, pp pp 39-52. Montreal, Quebec, Canada: Serge Gracovetsky.

Gum JL, Asher MA, Burton DC, Lai S-M, Lambart LM (2007) Transverse plane pelvic rotation in adolescent idiopathic scoliosis: primary or compensatory? *European Spine Journal* 16:1579–1586.

Gur G, Turgut E, Ayhan C, Baltaci G, Yakut Y (2017) Acute effects of spinal bracing on scapular kinematics in adolescent idiopathic scoliosis. *Clin Biomech (Bristol, Avon)* 47:14–19.

Hayashi K, Upasani VV, Pawelek JB, Aubin C-É, Labelle H, Lenke LG, Jackson R, Newton PO (2009) Three-dimensional analysis of thoracic apical sagittal alignment in adolescent idiopathic scoliosis. *Spine* 34:792–797.

Hui SCN, Pialasse J-P, Wong JYH, Lam T, Ng BKW, Cheng JCY, Chu WCW (2016) Radiation dose of digital radiography (DR) versus micro-dose x-ray (EOS) on patients with adolescent idiopathic scoliosis: 2016 SOSORT- IRSSD “John Sevastic Award” Winner in Imaging Research. *Scoliosis and Spinal Disorders* 11:46.

Humbert L, De Guise JA, Godbout B, Cresson T, Aubert B, Branchaud D, Chav R, Gravel P, Parent S, Dubousset J, Skalli W (2009) Fast 3D reconstruction of the spine from biplanar radiography: a diagnosis tool for routine scoliosis diagnosis and research in biomechanics. *Computer Methods in Biomechanics and Biomedical Engineering* 12:151–152.

Jang S, Hutson J (2013) Latero-posterior directed migration of trunk to the concave side of the curve: a biomechanical principle in treating the three dimensional deformity of idiopathic scoliosis with a custom molded high profile TLSO. *Scoliosis* 8:P13.

Jang SH, Davis KL, Thach SD (2019) Current Practice in Orthotic Treatment of AIS. *JPO: Journal of Prosthetics and Orthotics* 31:23.

- Jaremko JL, Poncet P, Ronsky J, Harder J, Dansereau J, Labelle H (2002) Indices of torso asymmetry related to spinal deformity in scoliosis. *Clinical Biomechanics* 3:559–568.
- Kane W (1977) Scoliosis prevalence: a call for a statement of terms. *Clinical Orthopaedics and Related Research* 126:43–46.
- Kapandji IA (1970) The vertebral column as a whole. In: *The Physiology of the Joints: The trunk and the vertebral column*, 2nd ed., pp 8–51. E. & S. Livingstone.
- Karimi MT, Ebrahimi MH, Mohammadi A, McGarry A (2016) Evaluation of the influences of various force magnitudes and configurations on scoliotic curve correction using finite element analysis. *Australas Phys Eng Sci Med*.
- Katz DE (2010) Brace Wear Control of Curve Progression in Adolescent Idiopathic Scoliosis. *The Journal of Bone and Joint Surgery (American)* 92:1343.
- Katz DE, Durrani A (2001) Factors that influence outcome in bracing large curves in patients with adolescent idiopathic scoliosis. *Spine* 26:2354–2361.
- Klineberg E, Schwab F, Ames C, Hostin R, Bess S, Smith JS, Gupta MC, Boachie O, Hart RA, Akbarnia BA, Burton DC, Lafage V (2011) Acute Reciprocal Changes Distant from the Site of Spinal Osteotomies Affect Global Postoperative Alignment. *Advances in Orthopedics* 2011:1–7.
- Komeili A, Westover L, Parent EC, El-Rich M, Adeeb S (2015a) Correlation Between a Novel Surface Topography Asymmetry Analysis and Radiographic Data in Scoliosis. *Spine Deform* 3:303–311.
- Komeili A, Westover L, Parent EC, El-Rich M, Adeeb S (2015b) Monitoring for idiopathic scoliosis curve progression using surface topography asymmetry analysis of the torso in adolescents. *Spine J* 15:743–751.
- Kotwicki T (2008) Evaluation of scoliosis today: Examination, X-rays and beyond. *Disability and Rehabilitation* 30:742–751.
- Kotwicki T, Cheneau J (2008) Biomechanical action of a corrective brace on thoracic idiopathic scoliosis: Cheneau 2000 orthosis. *Disabil Rehabil Assist Technol* 3:146–153.
- Kouwenhoven J-WM, Smit TH, van der Veen AJ, Kingma I, van Dieën JH, Castelein RM (2007) Effects of dorsal versus ventral shear loads on the rotational stability of the thoracic spine: a biomechanical porcine and human cadaveric study. *Spine* 32:2545–2550.
- Krištof M, Hudák R, Taká A, Živ J, Fialka L, Taká R, others (2010) Contact pressure measurement in trunk orthoses. In: *Computational Cybernetics and Technical Informatics (ICCC-CONTI)*, 2010 International Joint Conference on, pp 175–179. IEEE.

- Kuntz CI (2013) Evaluation of Spinal Alignment: Part I—Coronal Alignment. *Contemp Neurosurg* 35:1.
- La Maida GA, Zottarelli L, Mineo GV, Misaggi B (2013) Sagittal balance in adolescent idiopathic scoliosis: radiographic study of spino-pelvic compensation after surgery. *European Spine Journal* 22:859–867.
- Labelle H, Bellefleur C, Joncas J, Aubin C-É, Chretien F (2007) Preliminary evaluation of a computer-assisted tool for the design and adjustment of braces in idiopathic scoliosis: a prospective and randomized study. *Spine* 32:835–843.
- Laurnen EL, Tupper JW, Mullen MP (1983) The Boston brace in thoracic scoliosis. A preliminary report. *Spine* 8:388–395.
- Lin EC (2010) Radiation Risk From Medical Imaging. *Mayo Clin Proc* 85:1142–1146.
- Liu X, Thometz J, Tassone J, Paulsen L, Lyon R (2013) Historical review and experience with the use of surface topographic systems in children with idiopathic scoliosis. *OA Musculoskeletal Medicine* 01;1(1):9.
- Liu XC, Thometz JG, Lyon RM, Klein J (2001) Functional classification of patients with idiopathic scoliosis assessed by the Quantec system: a discriminant functional analysis to determine patient curve magnitude. *Spine* 26:1274–1278; discussion 1279.
- Lonstein JE (1996) Chapter 17 Scoliosis. In: Lovell and Winter's *Pediatric Orthopedics* (Lovell WW, Winter RB, Morrissy RT, Weinstein SL, eds). Philadelphia: Lippincott Williams & Wilkins.
- Lonstein JE, Winter RB (1994) The Milwaukee brace for the treatment of adolescent idiopathic scoliosis. A review of one thousand and twenty patients. *J Bone Joint Surg Am* 76:1207–1221.
- Lou E, Hill D, Raso J (2008) Brace Treatment for adolescent idiopathic scoliosis. *Studies in Health Technology and Informatics* 135:265–273.
- Lowe TG, Edgar M, Margulies JY, Miller NH, Raso VJ, Reinker KA, Rivard CH (2000) Etiology of idiopathic scoliosis: current trends in research. *J Bone Joint Surg Am* 82-A:1157–1168.
- Lu Z (2011) PubMed and beyond: a survey of web tools for searching biomedical literature. *Database (Oxford)* 2011 Available at: <https://academic.oup.com/database/article/doi/10.1093/database/baq036/460587> [Accessed March 10, 2019]
- Lyon R, Liu XC, Thometz JG, Nelson ER, Logan B (2004) Reproducibility of spinal back-contour measurements taken with raster stereography in adolescent idiopathic scoliosis. *Am J Orthop* 33:67–70.
- Marks MC, Stanford CF, Mahar AT, Newton PO (2003) Standing lateral radiographic positioning does not represent customary standing balance. *Spine* 28:1176–1182.

- Modi HN, Suh SW, Song H-R, Yang J-H, Ting C, Hazra S (2009) Drooping of Apical Convex Rib-vertebral Angle in Adolescent Idiopathic Scoliosis of More Than 40 Degrees: A Prognostic Factor for Progression. *Journal of Spinal Disorders & Techniques* 22:367–371.
- Moseley AM, Crosbie J, Adams R (2001) Normative data for passive ankle plantarflexion--dorsiflexion flexibility. *Clin Biomech (Bristol, Avon)* 16:514–521.
- National Center for Biotechnology Information (US) (2019). PubMed Help. Available at: <https://www.ncbi.nlm.nih.gov/books/NBK3827/> [Accessed June 21, 2019].
- Negrini S, Grivas TB, Kotwicki T, Rigo M, Zaina F, the international Society on Scoliosis Orthopaedic and Rehabilitation Treatment (SOSORT) (2009) Guidelines on “Standards of management of idiopathic scoliosis with corrective braces in everyday clinics and in clinical research”: SOSORT Consensus 2008. *Scoliosis* 4:2.
- Netter FH (1987) Musculoskeletal System. Part I. Anatomy. Physiology and Metabolic Disorders. In: *The Ciba Collection of Medical Illustrations*, pp 2–7. CIBA-GEIGY Corporation.
- Parent S, Newton PO, Wenger D (2005) Adolescent idiopathic scoliosis: etiology, anatomy, natural history, and bracing. *Instr Course Lect* 54:529–536.
- Patias P, Grivas TB, Kaspiris A, Aggouris C, Drakoutos E (2010) A review of the trunk surface metrics used as Scoliosis and other deformities evaluation indices. *Scoliosis* 5:12.
- Patwardhan AG, Gavin TM, Bunch WH, Dvonch VM, Vanderby R, Meade KP, Sartori M (1996) Biomechanical Comparison of the Milwaukee Brace (CTLSO) and the TLSO for Treatment of Idiopathic scoliosis. *Journal of Prosthetics and Orthotics* 8:115–122.
- Patwardhan AG, Rimkus A, Gavin TM, Bueche M, Meade KP, Bielski R (1996) Geometric analysis of coronal decompensation in idiopathic scoliosis. *Spine* 21:1192–1200.
- Périé D, Aubin C-E, Petit Y, Beauséjour M, Dansereau J, Labelle H (2003) Boston brace correction in idiopathic scoliosis: a biomechanical study. *Spine* 28:1672–1677.
- Polit DF, Yang F (2016) *Measurement and the Measurement of Change: A Primer for the Health Professions*. Wolters Kluwer.
- Propst-Proctor SL, Bleck EE (1983) Radiographic determination of lordosis and kyphosis in normal and scoliotic children. *J Pediatr Orthop* 3:344–346.
- Reamy B, Slakey J (2001) Adolescent idiopathic scoliosis: review and current concepts. *American Family Physician* 64:111–116.
- Redmond AC, Crane YZ, Menz HB (2008) Normative values for the Foot Posture Index. *Journal of Foot and Ankle Research* 1:6.

- Richards BS, Bernstein RM, D'Amato CR, Thompson GH (2005) Standardization of criteria for adolescent idiopathic scoliosis brace studies: SRS Committee on Bracing and Nonoperative Management. *Spine* 30:2068–2075; discussion 2076-2077.
- Rigo M, Negrini S, Weiss HR, Grivas T, Maruyama T, Kotwicki T (2006) SOSORT consensus paper on brace action: TLSO biomechanics of correction (investigating the rationale for force vector selection). *Scoliosis* 1:11.
- Ronckers CM, Land CE, Miller JS, Stovall M, Lonstein JE, Doody MM (2010) Cancer mortality among women frequently exposed to radiographic examinations for spinal disorders. *Radiat Res* 174:83–90.
- Rowe D (2003) The scoliosis research society brace manual. Available at: <https://www.srs.org/UserFiles/file/bracing-manual/section1.pdf> [Accessed January 20, 2017].
- Schiller JR, Thakur NA, Ebersson CP (2010) Brace Management in Adolescent Idiopathic Scoliosis. *Clinical Orthopaedics and Related Research*® 468:670–678.
- Schlösser TPC, Colo D, Castelein RM (2015) Etiology and pathogenesis of adolescent idiopathic scoliosis. *Semin Spine Surg* 27:2–8.
- Schmid S, Studer D, Hasler C-C, Romkes J, Taylor WR, Brunner R, Lorenzetti S (2015) Using Skin Markers for Spinal Curvature Quantification in Main Thoracic Adolescent Idiopathic Scoliosis: An Explorative Radiographic Study. *PLoS One* 10.
- Schüleïn S, Mendoza S, Malzkorn R, Harms J, Skwara A (2013) Rasterstereographic evaluation of interobserver and intraobserver reliability in postsurgical adolescent idiopathic scoliosis patients. *J Spinal Disord Tech* 26:E143-149.
- Schumann K, Püschel I, Maier-Hennes A, Weiss H-R (2008) Postural changes in patients with scoliosis in different postural positions revealed by surface topography. *Stud Health Technol Inform* 140:140–143.
- Shapiro SS, Wilk MB (1965) An Analysis of Variance Test for Normality (Complete Samples). *Biometrika* 52:591–611.
- Shufflebarger HL, King WF (1987) Composite measurement of scoliosis: a new method of analysis of the deformity. *Spine* 12:228–232.
- Simith M (2003) Spinal balance and in-orthosis correction. *Journal of Prosthetics and Orthotics* 15:s40–s45.
- Solomito M (2011) The Use of Motion Analysis Technology as an Alternative Means of Assessing Spinal Deformity in Patients with Adolescent Idiopathic Scoliosis.
- Somoskeöy S, Tunyogi-Csapó M, Bogyó C, Illés T (2012) Clinical validation of coronal and sagittal spinal curve measurements based on three-dimensional vertebra vector parameters. *Spine J* 12:960–968.

- Soucacos PN, Zacharis K, Gelalis J, Soultanis K, Kalos N, Beris A, Xenakis T, Johnson EO (1998) Assessment of curve progression in idiopathic scoliosis. *Eur Spine J* 7:270–277.
- Soucacos PN, Zacharis K, Soultanis K, Gelalis J, Xenakis T, Beris AE (2000) Risk factors for idiopathic scoliosis: review of a 6-year prospective study. *Orthopedics* 23:833–838.
- Stagnara P, De Mauroy JC, Dran G, Gonon GP, Costanzo G, Dimnet J, Pasquet A (1982) Reciprocal angulation of vertebral bodies in a sagittal plane: approach to references for the evaluation of kyphosis and lordosis. *Spine* 7:335–342.
- Stokes IA, Burwell RG, Dangerfield PH (2006) Biomechanical spinal growth modulation and progressive adolescent scoliosis – a test of the “vicious cycle” pathogenetic hypothesis: Summary of an electronic focus group debate of the IBSE. *Scoliosis* 1:16.
- Stokes IAF (1989) Axial rotation component of thoracic scoliosis. *Journal of Orthopaedic Research* 7:702–708.
- Stokes IAF (2007) Analysis and simulation of progressive adolescent scoliosis by biomechanical growth modulation. *European Spine Journal* 16:1621–1628.
- Sun X, Ding Q, Sha S, Mao S, Zhu F, Zhu Z, Qian B, Wang B, Cheng JCY, Qiu Y (2016) Rib-vertebral angle measurements predict brace treatment outcome in Risser grade 0 and premenarchal girls with adolescent idiopathic scoliosis. *Eur Spine J* 25:3088–3094.
- Sun X, Wang B, Qiu Y, Zhu Z, Zhu F, Yu Y, Qian B, Ma W, Liu Z, Mao S (2010) Outcomes and predictors of brace treatment for girls with adolescent idiopathic scoliosis. *Orthopaedic Surgery* 2:285–290.
- Takasaki H (1971) Moiré topography. *Journal of the Japan society of photogrammetry* 10:1–12.
- Theologis TN, Fairbank JC, Turner-Smith AR, Pantazopoulos T (1997) Early detection of progression in adolescent idiopathic scoliosis by measurement of changes in back shape with the Integrated Shape Imaging System scanner. *Spine* 22:1223–1227; discussion 1228.
- Udén A, Willner S (1983) The effect of lumbar flexion and Boston Thoracic Brace on the curves in idiopathic scoliosis. *Spine* 8:846–850.
- Vialle R, Levassor N, Rillardon L, Templier A (2005) Radiographic Analysis of the Sagittal Alignment and Balance of the Spine in Asymptomatic Subjects. *Journal of Bone and Joint Surgery, American volume* 87:260–267.
- Watters H, Volansky K, Wilmarth M (2012) The Schroth Method of Treatment for a Patient Diagnosed with Scoliosis: A Case Report. *Journal of Novel Physiotherapies* 2

Available at: <http://dx.doi.org/10.4172/2165-7025.1000113> [Accessed February 27, 2019].

Watts HG (1979) Bracing in spinal deformities. *Orthop Clin North Am* 10:769–785.

Weinstein SL, Dolan LA, Wright JG, Dobbs MB (2013) Effects of Bracing in Adolescents with Idiopathic Scoliosis. *New England Journal of Medicine* 369:1512–1521.

Weinstein SL, Ponseti IV (1983) Curve progression in idiopathic scoliosis. *J Bone Joint Surg Am* 65:447–455.

Weiss HR, Hawes MC (2004) Adolescent idiopathic scoliosis, bracing and the Hueter-Volkman principle. *Spine* 4:484–485.

White AA, Panjabi MM (1990) Kinematics of The Spine. In: *Clinical Biomechanics of the Spine*, 2nd ed., pp 85–125. Lippincott.

Wynarsky GT, Schultz AB (1991) Optimization of skeletal configuration: studies of scoliosis correction biomechanics. *J Biomech* 24:721–732.

Yrjönen T, Ylikoski M, Schlenzka D, Poussa M (2007) Results of brace treatment of adolescent idiopathic scoliosis in boys compared with girls: a retrospective study of 102 patients treated with the Boston brace. *European Spine Journal* 16:393–397.

Zabjek KF, Leroux MA, Coillard C, Prince F, Rivard CH (2008) Postural characteristics of adolescents with idiopathic scoliosis. *Journal of Pediatric Orthopaedics* 28:218–224.

## **Appendices**

**Appendix 5.1** The Correlation Matrices between Sagittal and Coronal Spinal Alignment Parameters

**Correlations (All Curves with Deviations)**

		SCEA	SUTA	SLTA	SULA	SLLA	CCEA	CUTA	CLTA	CULA	CLLA
SCEA	Pearson Correlation	1	.575**	.080	.085	.128	-.179	.171	-.241*	-.049	.013
	Sig. (2-tailed)		.000	.430	.399	.204	.074	.089	.016	.630	.898
	N	100	100	100	100	100	100	100	100	100	100
SUTA	Pearson Correlation	.575**	1	.107	-.082	-.072	-.094	.287**	-.108	-.266**	-.276**
	Sig. (2-tailed)	.000		.290	.417	.477	.352	.004	.283	.008	.005
	N	100	100	100	100	100	100	100	100	100	100
SLTA	Pearson Correlation	.080	.107	1	.380**	-.096	.034	-.098	-.039	.050	.244*
	Sig. (2-tailed)	.430	.290		.000	.344	.739	.330	.703	.623	.014
	N	100	100	100	100	100	100	100	100	100	100
SULA	Pearson Correlation	.085	-.082	.380**	1	.475**	-.038	-.139	-.074	.126	.281**
	Sig. (2-tailed)	.399	.417	.000		.000	.707	.169	.461	.212	.005
	N	100	100	100	100	100	100	100	100	100	100
SLLA	Pearson Correlation	.128	-.072	-.096	.475**	1	-.120	.167	-.081	-.010	-.056
	Sig. (2-tailed)	.204	.477	.344	.000		.235	.097	.421	.923	.581
	N	100	100	100	100	100	100	100	100	100	100
CCEA	Pearson Correlation	-.179	-.094	.034	-.038	-.120	1	-.021	-.086	.135	.015
	Sig. (2-tailed)	.074	.352	.739	.707	.235		.837	.395	.182	.884
	N	100	100	100	100	100	100	100	100	100	100
CUTA	Pearson Correlation	.171	.287**	-.098	-.139	.167	-.021	1	-.529**	-.601**	-.316**
	Sig. (2-tailed)	.089	.004	.330	.169	.097	.837		.000	.000	.001
	N	100	100	100	100	100	100	100	100	100	100
CLTA	Pearson Correlation	-.241*	-.108	-.039	-.074	-.081	-.086	-.529**	1	-.091	-.281**
	Sig. (2-tailed)	.016	.283	.703	.461	.421	.395	.000		.369	.005
	N	100	100	100	100	100	100	100	100	100	100
CULA	Pearson Correlation	-.049	-.266**	.050	.126	-.010	.135	-.601**	-.091	1	.642**
	Sig. (2-tailed)	.630	.008	.623	.212	.923	.182	.000	.369		.000
	N	100	100	100	100	100	100	100	100	100	100
CLLA	Pearson Correlation	.013	-.276**	.244*	.281**	-.056	.015	-.316**	-.281**	.642**	1
	Sig. (2-tailed)	.898	.005	.014	.005	.581	.884	.001	.005	.000	
	N	100	100	100	100	100	100	100	100	100	100

\*\* . Correlation is significant at the 0.01 level (2-tailed).

\* . Correlation is significant at the 0.05 level (2-tailed).

**Appendix 5.2** Descriptive statistics and all statistics test performed for 7 sagittal misalignment patterns

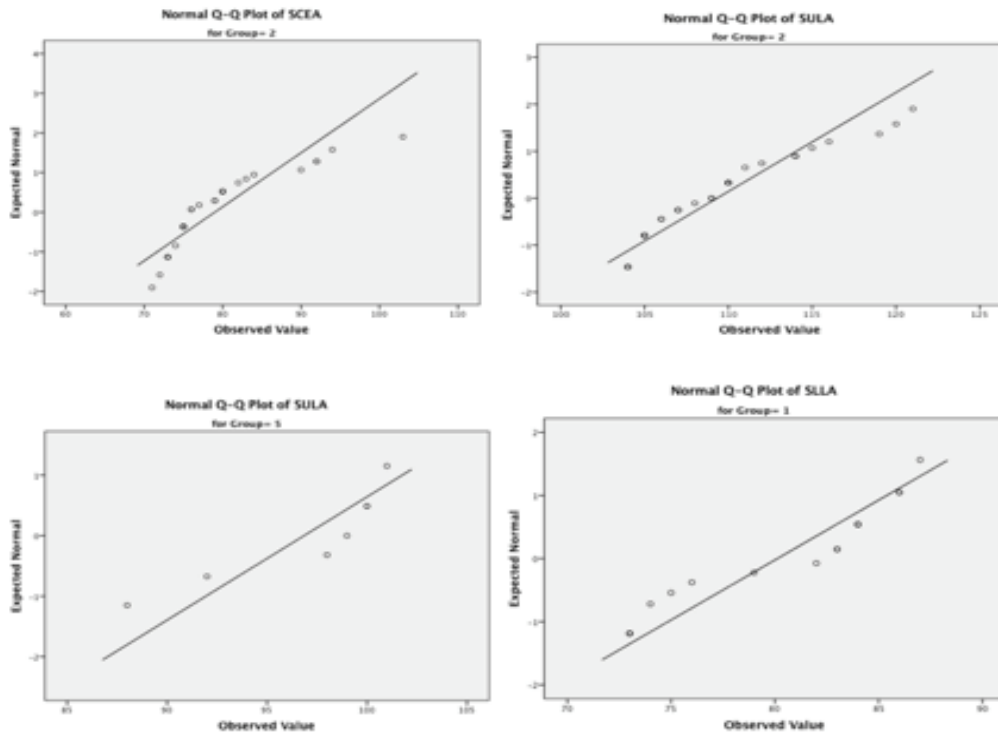
Descriptive Statistics

Group		N	Min.	Max.	Mean	Std. Deviation
1	SCEA	16	62	77	70.06	4.479
	SUTA	16	68	79	72.87	3.263
	SLTA	16	94	110	103.00	4.227
	SULA	16	100	115	107.13	3.612
	SLLA	16	73	87	80.13	5.265
	Valid N (listwise)		16			
2	SCEA	34	71	103	79.00	7.340
	SUTA	34	73	99	85.53	7.183
	SLTA	34	104	120	111.79	4.154
	SULA	34	104	121	109.32	4.746
	SLLA	34	64	91	77.03	6.590
	Valid N (listwise)		34			
3	SCEA	23	66	90	79.91	6.895
	SUTA	23	80	101	88.13	5.039
	SLTA	23	89	110	100.35	5.382
	SULA	23	96	109	102.70	3.125
	SLLA	23	70	89	77.22	4.472
	Valid N (listwise)		23			
4	SCEA	7	68	83	76.86	5.305
	SUTA	7	77	84	80.86	2.854
	SLTA	7	85	100	93.57	5.623
	SULA	7	85	105	97.71	6.676
	SLLA	7	69	80	76.14	3.805
	Valid N (listwise)		7			
5	SCEA	7	61	76	70.86	5.429
	SUTA	7	75	84	79.57	3.155
	SLTA	7	100	115	107.57	4.650
	SULA	7	88	101	96.86	4.914
	SLLA	7	64	76	68.43	4.036
	Valid N (listwise)		7			
6	SCEA	9	60	83	72.11	8.192
	SUTA	9	76	90	82.67	3.808
	SLTA	9	96	111	104.56	4.586
	SULA	9	89	106	96.33	4.610
	SLLA	9	45	65	55.67	5.612
	Valid N (listwise)		9			
7	SCEA	4	75	91	84.75	7.136
	SUTA	4	89	101	95.00	6.377
	SLTA	4	104	109	105.50	2.380
	SULA	4	94	96	95.25	.957
	SLLA	4	55	75	63.50	8.505
	Valid N (listwise)		4			

Tests of Normality							
	Group	Kolmogorov-Smirnov <sup>a</sup>			Shapiro-Wilk		
		Statistic	df	Sig.	Statistic	df	Sig.
SCEA	1	.130	16	.200*	.955	16	.568
	2	.217	34	.000	.801	34	.000
	3	.118	23	.200*	.959	23	.453
	4	.295	7	.067	.898	7	.320
	5	.172	7	.200*	.903	7	.350
	6	.217	9	.200*	.912	9	.331
	7	.224	4	.	.916	4	.514
SUTA	1	.155	16	.200*	.952	16	.515
	2	.118	34	.200*	.960	34	.245
	3	.138	23	.200*	.960	23	.472
	4	.202	7	.200*	.892	7	.288
	5	.268	7	.137	.924	7	.497
	6	.159	9	.200*	.960	9	.798
	7	.283	4	.	.805	4	.112
SLTA	1	.156	16	.200*	.960	16	.667
	2	.143	34	.074	.966	34	.372
	3	.170	23	.084	.962	23	.495
	4	.239	7	.200*	.922	7	.483
	5	.158	7	.200*	.982	7	.968
	6	.145	9	.200*	.964	9	.835
	7	.333	4	.	.763	4	.051
SULA	1	.131	16	.200*	.965	16	.758
	2	.179	34	.008	.890	34	.003
	3	.161	23	.127	.945	23	.226
	4	.199	7	.200*	.911	7	.406
	5	.306	7	.046	.806	7	.047
	6	.307	9	.015	.882	9	.166
	7	.283	4	.	.863	4	.272
SLLA	1	.207	16	.064	.862	16	.021
	2	.090	34	.200*	.981	34	.808
	3	.126	23	.200*	.945	23	.235
	4	.202	7	.200*	.890	7	.275
	5	.206	7	.200*	.907	7	.378
	6	.231	9	.184	.939	9	.570
	7	.227	4	.	.957	4	.760

\*. This is a lower bound of the true significance.

a. Lilliefors Significance Correction



First, Independent-Samples T tests were performed to compare the types of sagittal patterns defined with Type 1, which is the least flattened spinal alignment. Non-parametric Two-Independent Samples tests (Mann-Whitney tests) were also performed. As shown in the following, the results of the both tests are the same.

**T-TEST GROUPS=Group (Type 1, Type 2)**  
 /VARIABLES=SCEA SUTA SLTA SULA SLLA  
 /CRITERIA=CI (.95).

		Levene's Test for Equality of Variances		t-test for Equality of Means				
		F	Sig.	t	df	Sig. (2-tailed)	Mean Difference	Std. Error Difference
SCEA	Equal variances assumed	1.570	.216	-4.480	48	.000	-8.938	1.995
	Equal variances not assumed			-5.305	44.538	.000	-8.938	1.685
SUTA	Equal variances assumed	10.310	.002	-6.701	48	.000	-12.654	1.888
	Equal variances not assumed			-8.565	47.987	.000	-12.654	1.477
SLTA	Equal variances assumed	.006	.939	-6.944	48	.000	-8.794	1.266
	Equal variances not assumed			-6.900	29.012	.000	-8.794	1.274
SULA	Equal variances assumed	1.026	.316	-1.639	48	.108	-2.199	1.341
	Equal variances not assumed			-1.808	37.901	.079	-2.199	1.216
SLLA	Equal variances assumed	.155	.695	1.645	48	.106	3.096	1.881
	Equal variances not assumed			1.784	36.302	.083	3.096	1.735

**MANN-WHITNEY TEST, Group (Type 1, Type 2)**

**Test Statistics**

	SCEA	SUTA	SLTA	SULA	SLLA
Mann-Whitney U	65.500	23.500	32.000	208.000	193.000
Wilcoxon W	201.500	159.500	168.000	344.000	788.000
Z	-4.339	-5.176	-5.009	-1.342	-1.646
Asymp. Sig. (2-tailed)	.000	.000	.000	.180	.100

a. Grouping Variable: Group

**T-TEST GROUPS=Group (Type1, Type 3)**

/VARIABLES=SCEA SUTA SLTA SULA SLLA

/CRITERIA=CI (.95).

**Independent Samples Test**

		Levene's Test for Equality of Variances		t-test for Equality of Means				
		F	Sig.	t	df	Sig. (2-tailed)	Mean Difference	Std. Error Difference
SCEA	Equal variances assumed	3.093	.087	-5.015	37	.000	-9.851	1.964
	Equal variances not assumed			-5.406	36.882	.000	-9.851	1.822
SUTA	Equal variances assumed	2.112	.155	-10.635	37	.000	-15.255	1.434
	Equal variances not assumed			-11.468	36.869	.000	-15.255	1.330
SLTA	Equal variances assumed	.660	.422	1.647	37	.108	2.652	1.610
	Equal variances not assumed			1.721	36.371	.094	2.652	1.541
SULA	Equal variances assumed	.336	.566	4.084	37	.000	4.429	1.084
	Equal variances not assumed			3.977	29.275	.000	4.429	1.114
SLLA	Equal variances assumed	2.551	.119	1.857	37	.071	2.908	1.566
	Equal variances not assumed			1.803	28.875	.082	2.908	1.613

**MANN-WHITNEY TEST, Group (Type 1, Type 3)**

**Test Statistics**

	SCEA	SUTA	SLTA	SULA	SLLA
Mann-Whitney U	42.500	.000	130.500	66.000	127.500
Wilcoxon W	178.500	136.000	406.500	342.000	403.500
Z	-4.047	-5.262	-1.533	-3.397	-1.618
Asymp. Sig. (2-tailed)	.000	.000	.125	.001	.106
Exact Sig. [2*(1-tailed Sig.)]	.000 <sup>b</sup>	.000 <sup>b</sup>	.128 <sup>b</sup>	.000 <sup>b</sup>	.107 <sup>b</sup>

a. Grouping Variable: Group

b. Not corrected for ties.

**T-TEST GROUPS=Group (Type 1, Type 4)**  
 /VARIABLES=SCEA SUTA SLTA SULA SLLA  
 /CRITERIA=CI (.95).

		Independent Samples Test						
		Levene's Test for Equality of Variances			t-test for Equality of Means			
		F	Sig.	t	df	Sig. (2-tailed)	Mean Difference	Std. Error Difference
SCEA	Equal variances assumed	.420	.524	-3.170	21	.005	-6.795	2.143
	Equal variances not assumed			-2.959	9.940	.014	-6.795	2.297
SUTA	Equal variances assumed	.254	.619	-5.589	21	.000	-7.982	1.428
	Equal variances not assumed			-5.902	13.114	.000	-7.982	1.352
SLTA	Equal variances assumed	1.732	.202	4.457	21	.000	9.429	2.116
	Equal variances not assumed			3.972	9.111	.003	9.429	2.374
SULA	Equal variances assumed	1.696	.207	4.422	21	.000	9.411	2.128
	Equal variances not assumed			3.511	7.586	.009	9.411	2.680
SLLA	Equal variances assumed	4.463	.047	1.796	21	.087	3.982	2.217
	Equal variances not assumed			2.043	15.821	.058	3.982	1.949

**MANN-WHITNEY TEST, (Type 1, Type 4)**

**Test Statistics**

	SCEA	SUTA	SLTA	SULA	SLLA
Mann-Whitney U	19.500	3.500	10.000	8.000	34.500
Wilcoxon W	155.500	139.500	38.000	36.000	62.500
Z	-2.450	-3.518	-3.081	-3.226	-1.443
Asymp. Sig. (2-tailed)	.014	.000	.002	.001	.149
Exact Sig. [2*(1-tailed Sig.)]	.012 <sup>b</sup>	.000 <sup>b</sup>	.001 <sup>b</sup>	.001 <sup>b</sup>	.154 <sup>b</sup>

a. Grouping Variable: Group

b. Not corrected for ties.

**T-TEST GROUPS=Group (Type 1, Type 5)**  
 /VARIABLES=SCEA SUTA SLTA SULA SLLA  
 /CRITERIA=CI (.95).

		Independent Samples Test						
		Levene's Test for Equality of Variances			t-test for Equality of Means			
		F	Sig.	t	df	Sig. (2-tailed)	Mean Difference	Std. Error Difference
SCEA	Equal variances assumed	.102	.753	-.368	21	.717	-.795	2.162
	Equal variances not assumed			-.340	9.759	.741	-.795	2.338
SUTA	Equal variances assumed	.303	.588	-4.571	21	.000	-6.696	1.465
	Equal variances not assumed			-4.635	11.891	.001	-6.696	1.445
SLTA	Equal variances assumed	.001	.981	-2.318	21	.031	-4.571	1.972
	Equal variances not assumed			-2.229	10.570	.049	-4.571	2.051
SULA	Equal variances assumed	1.103	.305	5.626	21	.000	10.268	1.825
	Equal variances not assumed			4.972	8.973	.001	10.268	2.065
SLLA	Equal variances assumed	3.493	.076	5.220	21	.000	11.696	2.241
	Equal variances not assumed			5.806	14.947	.000	11.696	2.015

**MANN-WHITNEY TEST, (Type 1, Type 5)**

**Test Statistics**

	SCEA	SUTA	SLTA	SULA	SLLA
Mann-Whitney U	47.500	7.000	24.000	2.000	5.500
Wilcoxon W	183.500	143.000	160.000	30.000	33.500
Z	-.570	-3.290	-2.148	-3.624	-3.384
Asymp. Sig. (2-tailed)	.569	.001	.032	.000	.001
Exact Sig. [2*(1-tailed Sig.)]	.579 <sup>b</sup>	.000 <sup>b</sup>	.033 <sup>b</sup>	.000 <sup>b</sup>	.000 <sup>b</sup>

a. Grouping Variable: Group

b. Not corrected for ties.

**T-TEST GROUPS=Group (Type 1, Type 6)**

/VARIABLES=SCEA SUTA SLTA SULA SLLA

/CRITERIA=CI (.95).

**Independent Samples Test**

		Levene's Test for Equality of Variances		t-test for Equality of Means				
		F	Sig.	t	df	Sig. (2-tailed)	Mean Difference	Std. Error Difference
SCEA	Equal variances assumed	11.127	.003	-.815	23	.424	-2.049	2.515
	Equal variances not assumed			-.694	10.755	.502	-2.049	2.951
SUTA	Equal variances assumed	.035	.854	-6.787	23	.000	-9.792	1.443
	Equal variances not assumed			-6.489	14.643	.000	-9.792	1.509
SLTA	Equal variances assumed	.000	.994	-.857	23	.400	-1.556	1.815
	Equal variances not assumed			-.837	15.577	.415	-1.556	1.858
SULA	Equal variances assumed	.007	.936	6.495	23	.000	10.792	1.662
	Equal variances not assumed			6.055	13.615	.000	10.792	1.782
SLLA	Equal variances assumed	.671	.421	10.894	23	.000	24.458	2.245
	Equal variances not assumed			10.693	15.813	.000	24.458	2.287

**MANN-WHITNEY TEST, (Type 1, Type 6)**

**Test Statistics**

	SCEA	SUTA	SLTA	SULA	SLLA
Mann-Whitney U	60.000	2.500	59.500	7.500	.000
Wilcoxon W	196.000	138.500	195.500	52.500	45.000
Z	-.682	-3.943	-.711	-3.668	-4.085
Asymp. Sig. (2-tailed)	.495	.000	.477	.000	.000
Exact Sig. [2*(1-tailed Sig.)]	.522 <sup>b</sup>	.000 <sup>b</sup>	.487 <sup>b</sup>	.000 <sup>b</sup>	.000 <sup>b</sup>

a. Grouping Variable: Group

b. Not corrected for ties.

**T-TEST GROUPS=Group (Type 1, Type 7)**  
 /VARIABLES=SCEA SUTA SLTA SULA SLLA  
 /CRITERIA=CI (.95).

**Independent Samples Test**

		Levene's Test for Equality of Variances		t-test for Equality of Means				
		F	Sig.	t	df	Sig. (2-tailed)	Mean Difference	Std. Error Difference
SCEA	Equal variances assumed	1.074	.314	-5.233	18	.000	-14.688	2.807
	Equal variances not assumed			-3.928	3.613	.021	-14.688	3.739
SUTA	Equal variances assumed	10.958	.004	-10.004	18	.000	-22.125	2.212
	Equal variances not assumed			-6.722	3.403	.004	-22.125	3.291
SLTA	Equal variances assumed	1.681	.211	-1.124	18	.276	-2.500	2.224
	Equal variances not assumed			-1.571	8.533	.153	-2.500	1.592
SULA	Equal variances assumed	4.064	.059	6.397	18	.000	11.875	1.856
	Equal variances not assumed			11.618	17.647	.000	11.875	1.022
SLLA	Equal variances assumed	.709	.411	5.016	18	.000	16.625	3.314
	Equal variances not assumed			3.735	3.596	.024	16.625	4.451

**MANN-WHITNEY TEST, (Type 1, Type 7)**

**Test Statistics**

	SCEA	SUTA	SLTA	SULA	SLLA
Mann-Whitney U	2.500	.000	23.000	.000	4.500
Wilcoxon W	138.500	136.000	159.000	10.000	14.500
Z	-2.804	-3.034	-.857	-3.041	-2.609
Asymp. Sig. (2-tailed)	.005	.002	.392	.002	.009
Exact Sig. [2*(1-tailed Sig.)]	.002 <sup>b</sup>	.000 <sup>b</sup>	.437 <sup>b</sup>	.000 <sup>b</sup>	.005 <sup>b</sup>

a. Grouping Variable: Group

b. Not corrected for ties.

**Appendix 5.3** Descriptive statistics for 7 sagittal misalignment patterns classified by the apex location of coronal curves

Descriptive Statistics

Group	N	Min.	Max.	Mean	Std. Deviation
1.2	SCEA 6	74	82	79.00	2.683
	SUTA 6	82	94	88.67	4.967
	SLTA 6	104	116	109.83	4.167
	SULA 6	104	110	106.00	2.280
	SLLA 6	74	90	81.50	5.541
	Valid N (listwise)	6			
1.3	SCEA 8	68	90	79.13	8.008
	SUTA 8	85	96	90.00	3.546
	SLTA 8	90	107	98.50	6.211
	SULA 8	100	109	103.88	2.949
	SLLA 8	70	89	78.88	6.105
	Valid N (listwise)	8			
1.4	SCEA 2	68	83	75.50	10.607
	SUTA 2	80	83	81.50	2.121
	SLTA 2	85	96	90.50	7.778
	SULA 2	85	95	90.00	7.071
	SLLA 2	76	79	77.50	2.121
	Valid N (listwise)	2			
1.7	SCEA 3	75	89	82.67	7.095
	SUTA 3	89	100	93.00	6.083
	SLTA 3	104	109	105.67	2.887
	SULA 3	95	96	95.67	.577
	SLLA 3	60	75	66.33	7.767
	Valid N (listwise)	3			
2.2	SCEA 2	72	76	74.00	2.828
	SUTA 2	77	79	78.00	1.414
	SLTA 2	109	110	109.50	.707
	SULA 2	105	109	107.00	2.828
	SLLA 2	76	79	77.50	2.121
	Valid N (listwise)	2			
2.6	SCEA 2	60	66	63.00	4.243
	SUTA 2	80	82	81.00	1.414
	SLTA 2	101	103	102.00	1.414
	SULA 2	94	106	100.00	8.485
	SLLA 2	58	59	58.50	.707
	Valid N (listwise)	2			
3.1	SCEA 3	69	73	71.00	2.000
	SUTA 3	69	75	71.67	3.055
	SLTA 3	98	105	100.33	4.041
	SULA 3	100	105	103.00	2.646
	SLLA 3	73	83	77.33	5.132
	Valid N (listwise)	3			
3.2	SCEA 11	71	84	76.73	4.027

	SUTA 11	73	95	80.64	6.169
	SLTA 11	106	120	111.64	4.154
	SULA 11	105	121	110.64	4.945
	SLLA 11	64	91	73.45	6.788
	Valid N (listwise)		11		
3.3	SCEA 2	79	89	84.00	7.071
	SUTA 2	85	92	88.50	4.950
	SLTA 2	89	100	94.50	7.778
	SULA 2	97	98	97.50	.707
	SLLA 2	80	81	80.50	.707
	Valid N (listwise)		2		
3.5	SCEA 2	61	76	68.50	10.607
	SUTA 2	80	84	82.00	2.828
	SLTA 2	110	115	112.50	3.536
	SULA 2	100	100	100.00	.000
	SLLA 2	65	66	65.50	.707
	Valid N (listwise)		2		
3.6	SCEA 1	65	65	65.00	.
	SUTA 1	85	85	85.00	.
	SLTA 1	105	105	105.00	.
	SULA 1	89	89	89.00	.
	SLLA 1	55	55	55.00	.
	Valid N (listwise)		1		
4.6	SCEA 3	65	83	74.67	9.074
	SUTA 3	76	83	80.00	3.606
	SLTA 3	105	111	107.67	3.055
	SULA 3	95	96	95.67	.577
	SLLA 3	45	57	50.67	6.028
	Valid N (listwise)		3		
5.2	SCEA 1	75	75	75.00	.
	SUTA 1	84	84	84.00	.
	SLTA 1	111	111	111.00	.
	SULA 1	104	104	104.00	.
	SLLA 1	70	70	70.00	.
	Valid N (listwise)		1		
5.3	SCEA 1	79	79	79.00	.
	SUTA 1	85	85	85.00	.
	SLTA 1	100	100	100.00	.
	SULA 1	105	105	105.00	.
	SLLA 1	72	72	72.00	.
	Valid N (listwise)		1		
6.1	SCEA 8	66	77	70.38	4.438
	SUTA 8	68	76	72.12	2.800
	SLTA 8	94	110	103.25	5.312
	SULA 8	104	111	108.13	2.295
	SLLA 8	73	86	79.75	5.751
	Valid N (listwise)		8		
6.2	SCEA 3	75	103	86.00	14.933

	SUTA 3	95	99	96.33	2.309
	SLTA 3	110	119	114.33	4.509
	SULA 3	108	120	112.33	6.658
	SLLA 3	73	84	79.67	5.859
	Valid N (listwise)		3		
6.3	SCEA 5	73	87	81.60	5.595
	SUTA 5	84	90	86.80	2.775
	SLTA 5	96	104	99.60	2.966
	SULA 5	96	105	102.00	3.937
	SLLA 5	73	78	75.60	2.074
	Valid N (listwise)		5		
6.4	SCEA 4	73	80	76.75	3.775
	SUTA 4	77	84	79.75	3.096
	SLTA 4	90	100	96.25	4.500
	SULA 4	97	105	101.50	3.697
	SLLA 4	69	79	74.50	4.203
	Valid N (listwise)		4		
6.5	SCEA 1	72	72	72.00	.
	SUTA 1	82	82	82.00	.
	SLTA 1	109	109	109.00	.
	SULA 1	92	92	92.00	.
	SLLA 1	76	76	76.00	.
	Valid N (listwise)		1		
7.1	SCEA 4	62	75	67.50	5.802
	SUTA 4	70	79	74.00	3.916
	SLTA 4	104	106	104.75	.957
	SULA 4	104	115	108.50	5.066
	SLLA 4	82	87	84.25	2.062
	Valid N (listwise)		4		
7.2	SCEA 8	73	94	78.50	8.452
	SUTA 8	77	90	85.25	4.652
	SLTA 8	107	116	112.88	3.227
	SULA 8	104	119	110.00	5.451
	SLLA 8	66	89	79.00	7.031
	Valid N (listwise)		8		
7.3	SCEA 6	66	90	78.83	8.400
	SUTA 6	80	93	85.00	5.367
	SLTA 6	102	110	105.00	2.683
	SULA 6	101	105	103.33	1.633
	SLLA 6	73	83	76.67	3.615
	Valid N (listwise)		6		
7.4	SCEA 1	80	80	80.00	.
	SUTA 1	84	84	84.00	.
	SLTA 1	89	89	89.00	.
	SULA 1	98	98	98.00	.
	SLLA 1	80	80	80.00	.
	Valid N (listwise)		1		
7.5	SCEA 3	67	74	70.33	3.512

	SUTA	3	75	80	77.00	2.646
	SLTA	3	105	108	106.33	1.528
	SULA	3	98	101	99.33	1.528
	SLLA	3	64	69	67.33	2.887
	Valid N (listwise)		3			
7.6	SCEA	3	75	80	78.00	2.646
	SUTA	3	83	90	85.67	3.786
	SLTA	3	96	110	103.00	7.000
	SULA	3	95	100	97.00	2.646
	SLLA	3	56	65	59.00	5.196
	Valid N (listwise)		3			
7.7	SCEA	1	91	91	91.00	.
	SUTA	1	101	101	101.00	.
	SLTA	1	105	105	105.00	.
	SULA	1	94	94	94.00	.
	SLLA	1	55	55	55.00	.
	Valid N (listwise)		1			
8.1	SCEA	1	75	75	75.00	.
	SUTA	1	78	78	78.00	.
	SLTA	1	102	102	102.00	.
	SULA	1	106	106	106.00	.
	SLLA	1	75	75	75.00	.
	Valid N (listwise)		1			
8.2	SCEA	3	75	92	86.33	9.815
	SUTA	3	85	98	92.67	6.807
	SLTA	3	104	120	112.67	8.083
	SULA	3	107	112	109.67	2.517
	SLLA	3	71	78	75.33	3.786
	Valid N (listwise)		3			
8.3	SCEA	1	77	77	77.00	.
	SUTA	1	101	101	101.00	.
	SLTA	1	103	103	103.00	.
	SULA	1	101	101	101.00	.
	SLLA	1	74	74	74.00	.
	Valid N (listwise)		1			
8.5	SCEA	1	76	76	76.00	.
	SUTA	1	80	80	80.00	.
	SLTA	1	100	100	100.00	.
	SULA	1	88	88	88.00	.
	SLLA	1	70	70	70.00	.
	Valid N (listwise)		1			

**Appendix 5.4** Descriptive statistics for 7 sagittal misalignment patterns classified by the apex location of coronal curves

Descriptive Statistics

Group	N	Min.	Max.	Mean	Std. Deviation
-------	---	------	------	------	----------------

1	SCEA 19	68	90	79.26	6.505
	SUTA 19	80	100	89.16	5.047
	SLTA 19	85	116	102.37	8.173
	SULA 19	85	110	101.79	6.097
	SLLA 19	60	90	77.58	7.545
	Valid N (listwise)		19		
2	SCEA 4	60	76	68.50	7.000
	SUTA 4	77	82	79.50	2.082
	SLTA 4	101	110	105.75	4.425
	SULA 4	94	109	103.50	6.557
	SLLA 4	58	79	68.00	11.045
	Valid N (listwise)		4		
3	SCEA 19	61	89	75.11	6.497
	SUTA 19	69	95	80.42	6.744
	SLTA 19	89	120	107.79	7.502
	SULA 19	89	121	105.79	7.554
	SLLA 19	55	91	73.00	7.895
	Valid N (listwise)		19		
4	SCEA 3	65	83	74.67	9.074
	SUTA 3	76	83	80.00	3.606
	SLTA 3	105	111	107.67	3.055
	SULA 3	95	96	95.67	.577
	SLLA 3	45	57	50.67	6.028
	Valid N (listwise)		3		
5	SCEA 2	75	79	77.00	2.828
	SUTA 2	84	85	84.50	.707
	SLTA 2	100	111	105.50	7.778
	SULA 2	104	105	104.50	.707
	SLLA 2	70	72	71.00	1.414
	Valid N (listwise)		2		
6	SCEA 21	66	103	76.57	8.582
	SUTA 21	68	99	81.00	9.044
	SLTA 21	90	119	102.90	7.056
	SULA 21	92	120	105.24	6.041
	SLLA 21	69	86	77.57	4.905
	Valid N (listwise)		21		
7	SCEA 26	62	94	76.42	8.305
	SUTA 26	70	101	83.12	7.005
	SLTA 26	89	116	106.69	6.032
	SULA 26	94	119	104.42	6.426
	SLLA 26	55	89	74.73	9.694
	Valid N (listwise)		26		
8	SCEA 6	75	92	81.17	8.424
	SUTA 6	78	101	89.50	9.772
	SLTA 6	100	120	107.17	7.960
	SULA 6	88	112	104.00	8.695
	SLLA 6	70	78	74.17	3.189
	Valid N (listwise)		6		

**Appendix 6.1** Descriptive Statistics and Normality Plots

		Descriptive	Statistic	Std. Error
CCEA	Mean		90.8462	.79135
Anatomical Landmarks	95% Confidence Interval for Mean	Lower Bound	89.1220	
		Upper Bound	92.5704	
	5% Trimmed Mean		90.9402	
	Median		90.0000	
	Variance		8.141	
	Std. Deviation		2.85325	
	Minimum		85.00	
	Maximum		95.00	
	Range		10.00	
	Interquartile Range		4.00	
	Skewness		-.199	.616
	Kurtosis		.157	1.191
CCEA Metal balls	Mean		91.0769	.83560
	95% Confidence Interval for Mean	Lower Bound	89.2563	
		Upper Bound	92.8975	
	5% Trimmed Mean		91.1966	
	Median		91.0000	
	Variance		9.077	
	Std. Deviation		3.01279	
	Minimum		85.00	
	Maximum		95.00	
	Range		10.00	
	Interquartile Range		5.00	
	Skewness		-.346	.616
	Kurtosis		-.127	1.191
CUTA	Mean		97.8462	2.09348
Anatomical Landmarks	95% Confidence Interval for Mean	Lower Bound	93.2849	
		Upper Bound	102.4074	
	5% Trimmed Mean		98.1068	
	Median		97.0000	
	Variance		56.974	
	Std. Deviation		7.54814	
	Minimum		83.00	
	Maximum		108.00	
	Range		25.00	
	Interquartile Range		11.00	
	Skewness		-.622	.616
	Kurtosis		-.134	1.191
CUTA Metal balls	Mean		93.6154	1.14656
		Lower Bound	91.1172	

	95% Confidence Interval for Mean	Upper Bound	96.1135	
	5% Trimmed Mean		93.6838	
	Median		94.0000	
	Variance		17.090	
	Std. Deviation		4.13397	
	Minimum		86.00	
	Maximum		100.00	
	Range		14.00	
	Interquartile Range		6.00	
	Skewness		-.245	.616
	Kurtosis		-.406	1.191
CLTA	Mean		80.5385	1.93024
Anatomical Landmarks	95% Confidence Interval for Mean	Lower Bound	76.3328	
		Upper Bound	84.7441	
	5% Trimmed Mean		80.7650	
	Median		81.0000	
	Variance		48.436	
	Std. Deviation		6.95959	
	Minimum		65.00	
	Maximum		92.00	
	Range		27.00	
	Interquartile Range		8.00	
	Skewness		-.653	.616
	Kurtosis		1.144	1.191
CLTA Metal balls	Mean		84.6923	1.31259
	95% Confidence Interval for Mean	Lower Bound	81.8324	
		Upper Bound	87.5522	
	5% Trimmed Mean		84.9359	
	Median		86.0000	
	Variance		22.397	
	Std. Deviation		4.73259	
	Minimum		75.00	
	Maximum		90.00	
	Range		15.00	
	Interquartile Range		6.50	
	Skewness		-.877	.616
	Kurtosis		.186	1.191
CULA	Mean		85.0000	2.45733
Anatomical Landmarks	95% Confidence Interval for Mean	Lower Bound	79.6459	
		Upper Bound	90.3541	
	5% Trimmed Mean		85.1111	
	Median		86.0000	
	Variance		78.500	
	Std. Deviation		8.86002	

	Minimum		68.00	
	Maximum		100.00	
	Range		32.00	
	Interquartile Range		14.00	
	Skewness		-.113	.616
	Kurtosis		-.270	1.191
CULA Metal	Mean		87.4615	1.85229
balls	95% Confidence Interval for	Lower Bound	83.4258	
	Mean	Upper Bound	91.4973	
	5% Trimmed Mean		87.7906	
	Median		90.0000	
	Variance		44.603	
	Std. Deviation		6.67852	
	Minimum		74.00	
	Maximum		95.00	
	Range		21.00	
	Interquartile Range		11.50	
	Skewness		-.892	.616
	Kurtosis		-.391	1.191
CLLA	Mean		99.6923	2.25714
Anatomical	95% Confidence Interval for	Lower Bound	94.7744	
Landmarks	Mean	Upper Bound	104.6102	
	5% Trimmed Mean		100.0470	
	Median		99.0000	
	Variance		66.231	
	Std. Deviation		8.13823	
	Minimum		80.00	
	Maximum		113.00	
	Range		33.00	
	Interquartile Range		8.50	
	Skewness		-.760	.616
	Kurtosis		2.233	1.191
CLLA Metal	Mean		94.1538	1.72034
balls	95% Confidence Interval for	Lower Bound	90.4055	
	Mean	Upper Bound	97.9021	
	5% Trimmed Mean		94.0043	
	Median		93.0000	
	Variance		38.474	
	Std. Deviation		6.20277	
	Minimum		83.00	
	Maximum		108.00	
	Range		25.00	
	Interquartile Range		6.50	
	Skewness		.616	.616
	Kurtosis		1.423	1.191

SCEA	Mean		86.7692	1.46390
Anatomical Landmarks	95% Confidence Interval for Mean	Lower Bound	83.5797	
		Upper Bound	89.9588	
	5% Trimmed Mean		86.8547	
	Median		86.0000	
	Variance		27.859	
	Std. Deviation		5.27816	
	Minimum		76.00	
	Maximum		96.00	
	Range		20.00	
	Interquartile Range		6.50	
	Skewness		-.084	.616
	Kurtosis		.512	1.191
	SCEA Metal balls	Mean		75.4615
	95% Confidence Interval for Mean	Lower Bound	72.4238	
		Upper Bound	78.4992	
	5% Trimmed Mean		75.5684	
	Median		76.0000	
	Variance		25.269	
	Std. Deviation		5.02685	
	Minimum		65.00	
	Maximum		84.00	
	Range		19.00	
	Interquartile Range		5.00	
	Skewness		-.252	.616
	Kurtosis		.794	1.191
	SUTA	Mean		89.0000
Anatomical Landmarks	95% Confidence Interval for Mean	Lower Bound	85.1306	
		Upper Bound	92.8694	
	5% Trimmed Mean		88.9444	
	Median		90.0000	
	Variance		41.000	
	Std. Deviation		6.40312	
	Minimum		77.00	
	Maximum		102.00	
	Range		25.00	
	Interquartile Range		7.00	
	Skewness		.308	.616
	Kurtosis		.842	1.191
	SUTA Metal balls	Mean		90.5385
	95% Confidence Interval for Mean	Lower Bound	87.3066	
		Upper Bound	93.7703	
	5% Trimmed Mean		90.3205	
	Median		92.0000	
	Variance		28.603	

	Std. Deviation		5.34814	
	Minimum		83.00	
	Maximum		102.00	
	Range		19.00	
	Interquartile Range		8.00	
	Skewness		.369	.616
	Kurtosis		.306	1.191
SLTA	Mean		103.3077	1.40231
Anatomical Landmarks	95% Confidence Interval for Mean	Lower Bound	100.2523	
		Upper Bound	106.3631	
	5% Trimmed Mean		103.1752	
	Median		103.0000	
	Variance		25.564	
	Std. Deviation		5.05610	
	Minimum		95.00	
	Maximum		114.00	
	Range		19.00	
	Interquartile Range		6.50	
	Skewness		.436	.616
	Kurtosis		.499	1.191
SLTA Metal balls	Mean		102.5385	1.21220
	95% Confidence Interval for Mean	Lower Bound	99.8973	
		Upper Bound	105.1796	
	5% Trimmed Mean		102.5427	
	Median		102.0000	
	Variance		19.103	
	Std. Deviation		4.37065	
	Minimum		95.00	
	Maximum		110.00	
	Range		15.00	
	Interquartile Range		5.00	
	Skewness		.284	.616
	Kurtosis		.080	1.191
SULA	Mean		100.5385	1.84188
Anatomical Landmarks	95% Confidence Interval for Mean	Lower Bound	96.5254	
		Upper Bound	104.5516	
	5% Trimmed Mean		100.9316	
	Median		101.0000	
	Variance		44.103	
	Std. Deviation		6.64098	
	Minimum		87.00	
	Maximum		107.00	
	Range		20.00	
	Interquartile Range		8.50	
	Skewness		-1.127	.616

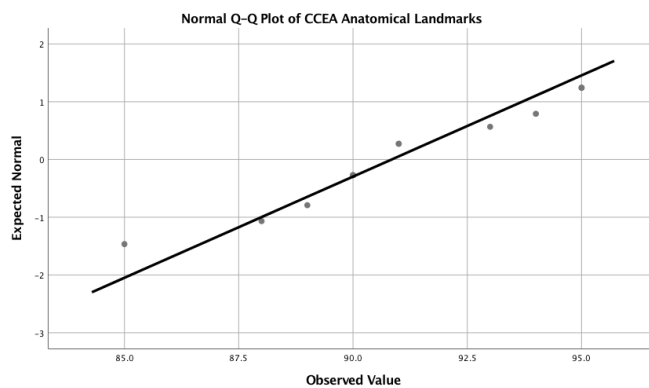
	Kurtosis		.714	1.191
SULA Metal	Mean		96.7692	2.14283
balls	95% Confidence Interval for Mean	Lower Bound	92.1004	
		Upper Bound	101.4381	
	5% Trimmed Mean		96.9103	
	Median		100.0000	
	Variance		59.692	
	Std. Deviation		7.72608	
	Minimum		83.00	
	Maximum		108.00	
	Range		25.00	
	Interquartile Range		13.00	
	Skewness		-.383	.616
	Kurtosis		-.855	1.191
SLLA	Mean		77.2308	3.21884
Anatomical Landmarks	95% Confidence Interval for Mean	Lower Bound	70.2175	
		Upper Bound	84.2440	
	5% Trimmed Mean		77.3675	
	Median		80.0000	
	Variance		134.692	
	Std. Deviation		11.60570	
	Minimum		57.00	
	Maximum		95.00	
	Range		38.00	
	Interquartile Range		19.00	
	Skewness		-.437	.616
	Kurtosis		-.771	1.191
SLLA Metal	Mean		78.8462	2.86412
balls	95% Confidence Interval for Mean	Lower Bound	72.6058	
		Upper Bound	85.0865	
	5% Trimmed Mean		79.1068	
	Median		81.0000	
	Variance		106.641	
	Std. Deviation		10.32671	
	Minimum		62.00	
	Maximum		91.00	
	Range		29.00	
	Interquartile Range		19.50	
	Skewness		-.460	.616
	Kurtosis		-1.028	1.191

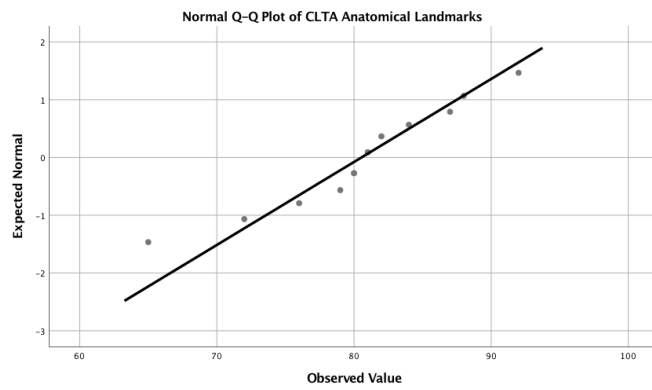
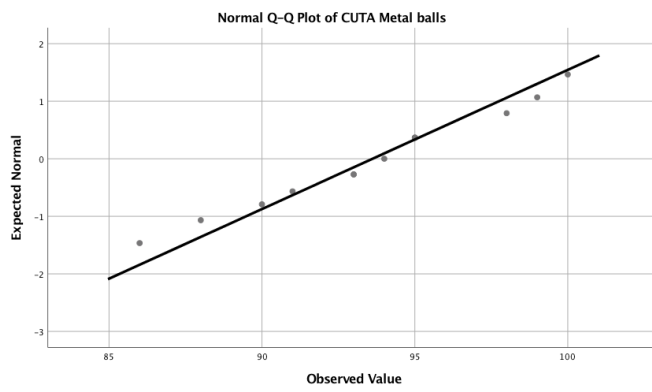
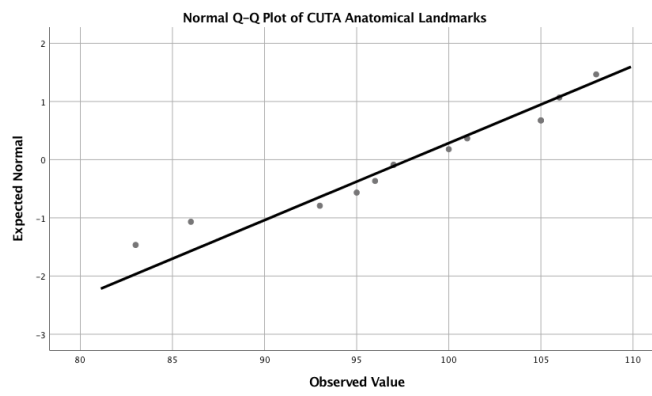
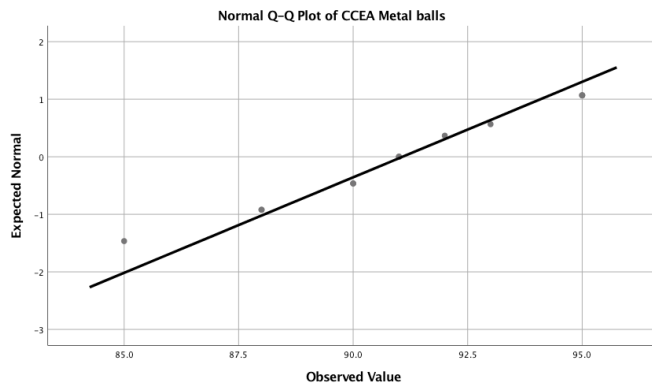
### Tests of Normality

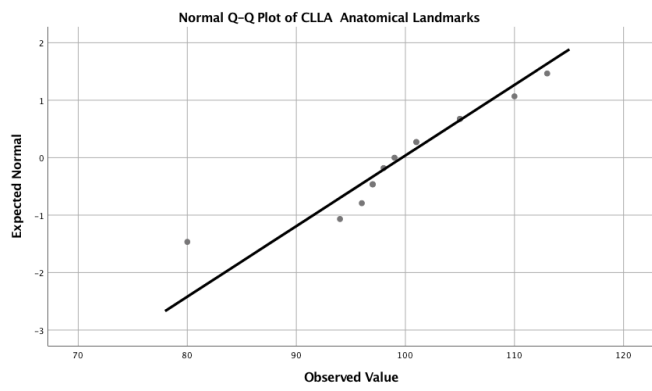
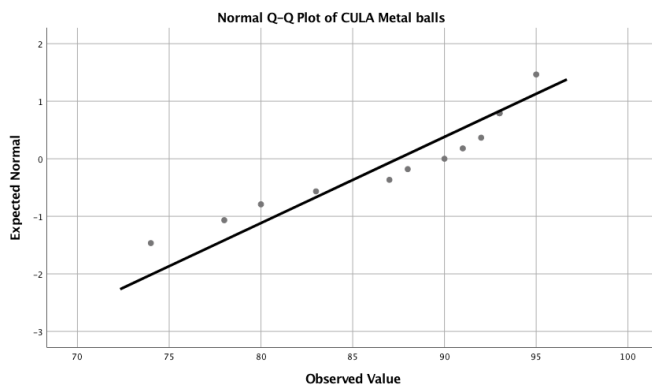
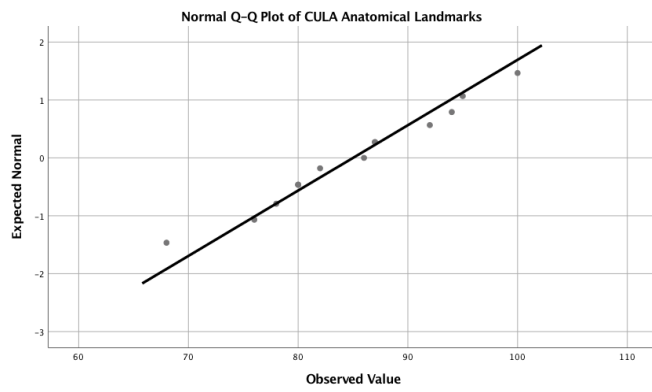
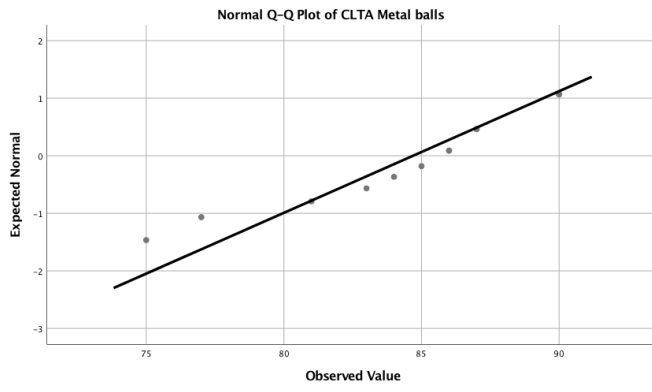
	Kolmogorov-Smirnov <sup>a</sup>			Shapiro-Wilk		
	Statistic	df	Sig.	Statistic	df	Sig.
CCEA Anatomical Landmarks	.171	13	.200*	.937	13	.420
CCEA Metal balls	.134	13	.200*	.938	13	.426
CUTA Anatomical Landmarks	.136	13	.200*	.941	13	.466
CUTA Metal balls	.138	13	.200*	.969	13	.886
CLTA Anatomical Landmarks	.182	13	.200*	.956	13	.685
CLTA Metal balls	.147	13	.200*	.905	13	.157
CULA Anatomical Landmarks	.103	13	.200*	.982	13	.987
CULA Metal balls	.187	13	.200*	.887	13	.090
CLLA Anatomical Landmarks	.171	13	.200*	.927	13	.310
CLLA Metal balls	.169	13	.200*	.953	13	.649
SCEA Anatomical Landmarks	.177	13	.200*	.969	13	.881
SCEA Metal balls	.156	13	.200*	.951	13	.607
SUTA Anatomical Landmarks	.166	13	.200*	.964	13	.810
SUTA Metal balls	.169	13	.200*	.924	13	.281
SLTA Anatomical Landmarks	.140	13	.200*	.978	13	.970
SLTA Metal balls	.150	13	.200*	.951	13	.613
SULA Anatomical Landmarks	.197	13	.176	.834	13	.018
SULA Metal balls	.201	13	.158	.950	13	.597
SLLA Anatomical Landmarks	.176	13	.200*	.952	13	.634
SLLA Metal balls	.145	13	.200*	.908	13	.171

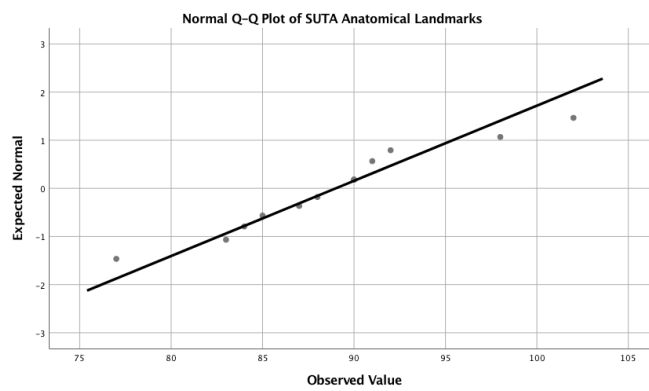
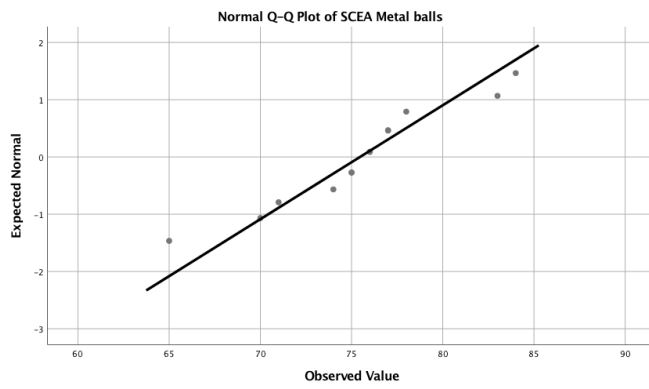
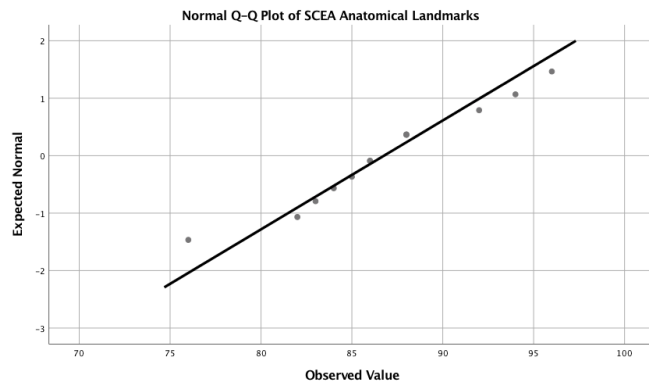
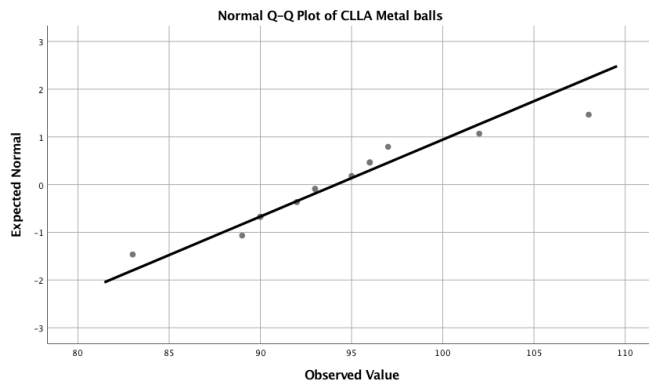
\*. This is a lower bound of the true significance.

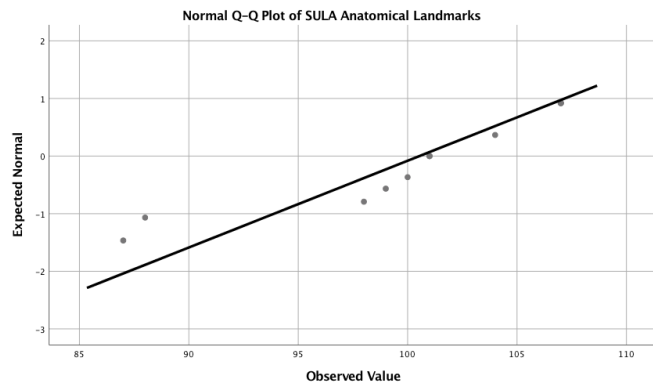
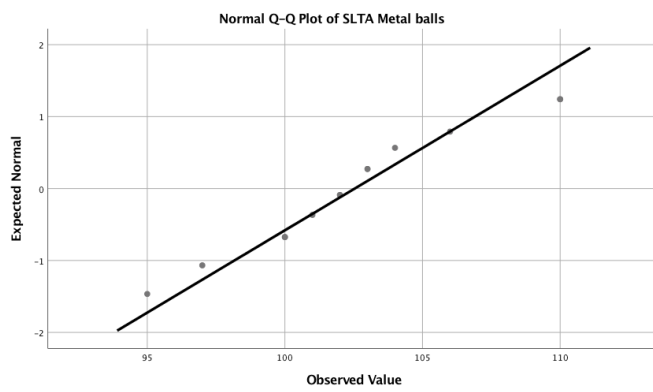
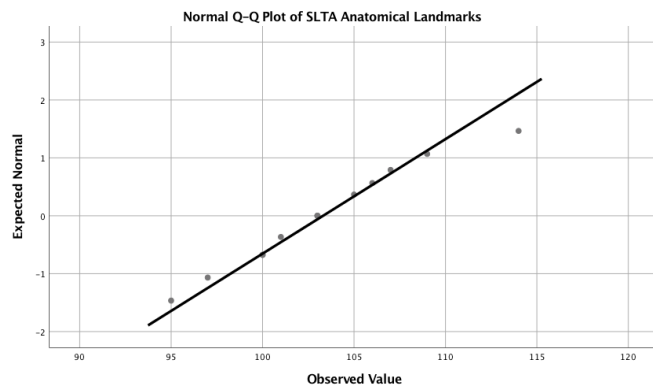
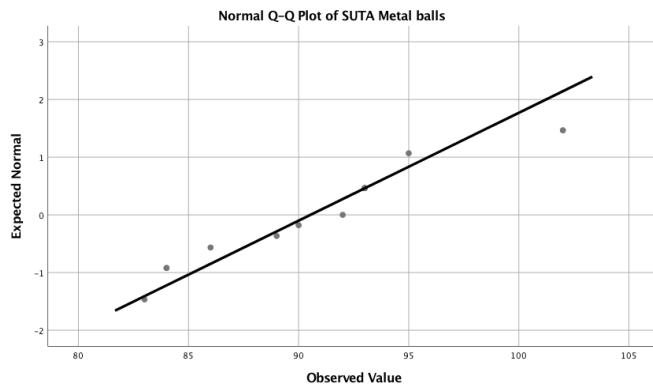
a. Lilliefors Significance Correction

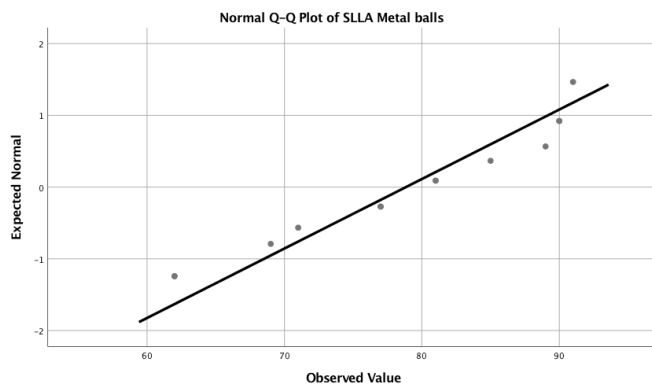
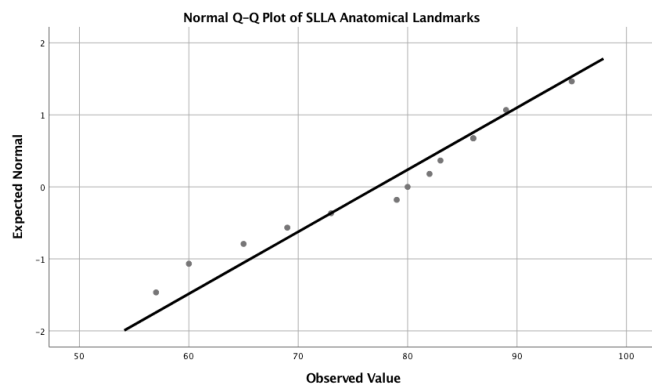
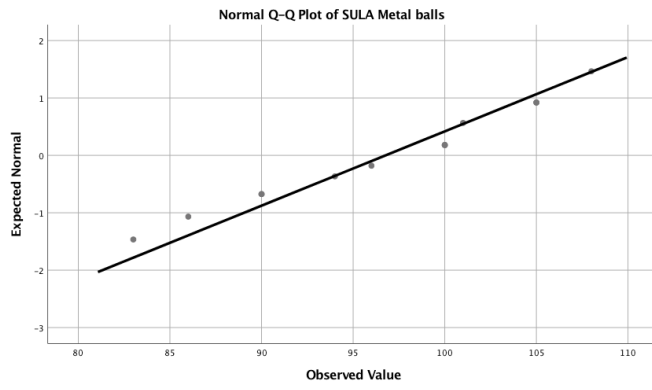












**Appendix 6.2** Test Statistics for Pearson's Correlation Coefficient

**Correlations**

		CCEA Anatomical Landmarks	CCEA Metal balls
CCEA Anatomical Landmarks	Pearson Correlation	1	.952**
	Sig. (2-tailed)		.000
	N	13	13
CCEA Metal balls	Pearson Correlation	.952**	1
	Sig. (2-tailed)	.000	
	N	13	13

\*\* . Correlation is significant at the 0.01 level (2-tailed).

		CUTA Anatomical Landmarks	CUTA Metal balls
CUTA Anatomical Landmarks	Pearson Correlation	1	.871**
	Sig. (2-tailed)		.000
	N	13	13
CUTA Metal balls	Pearson Correlation	.871**	1
	Sig. (2-tailed)	.000	
	N	13	13

\*\* . Correlation is significant at the 0.01 level (2-tailed).

		CLTA Anatomical Landmarks	CLTA Metal balls
CLTA Anatomical Landmarks	Pearson Correlation	1	.787**
	Sig. (2-tailed)		.001
	N	13	13
CLTA Metal balls	Pearson Correlation	.787**	1
	Sig. (2-tailed)	.001	
	N	13	13

\*\* . Correlation is significant at the 0.01 level (2-tailed).

		CULA Anatomical Landmarks	CULA Metal balls
CULA Anatomical Landmarks	Pearson Correlation	1	.814**
	Sig. (2-tailed)		.001
	N	13	13
CULA Metal balls	Pearson Correlation	.814**	1
	Sig. (2-tailed)	.001	
	N	13	13

\*\* . Correlation is significant at the 0.01 level (2-tailed).

		CLLA Anatomical Landmarks	CLLA Metal balls
CLLA Anatomical Landmarks	Pearson Correlation	1	.699**
	Sig. (2-tailed)		.008
	N	13	13
CLLA Metal balls	Pearson Correlation	.699**	1
	Sig. (2-tailed)	.008	
	N	13	13

\*\* . Correlation is significant at the 0.01 level (2-tailed).

		SCEA Anatomical Landmarks	SCEA Metal balls
SCEA Anatomical Landmarks	Pearson Correlation	1	.692**
	Sig. (2-tailed)		.009
	N	13	13
SCEA Metal balls	Pearson Correlation	.692**	1
	Sig. (2-tailed)	.009	
	N	13	13

\*\* . Correlation is significant at the 0.01 level (2-tailed).

		SUTA Anatomical Landmarks	SUTA Metal balls
SUTA Anatomical Landmarks	Pearson Correlation	1	.917**
	Sig. (2-tailed)		.000
	N	13	13
SUTA Metal balls	Pearson Correlation	.917**	1
	Sig. (2-tailed)	.000	
	N	13	13

\*\* . Correlation is significant at the 0.01 level (2-tailed).

		SLTA Anatomical Landmarks	SLTA Metal balls
SLTA Anatomical Landmarks	Pearson Correlation	1	.961**
	Sig. (2-tailed)		.000
	N	13	13
SLTA Metal balls	Pearson Correlation	.961**	1
	Sig. (2-tailed)	.000	
	N	13	13

\*\* . Correlation is significant at the 0.01 level (2-tailed).

		SULA Anatomical Landmarks	SULA Metal balls
SULA Anatomical Landmarks	Pearson Correlation	1	.888**
	Sig. (2-tailed)		.000
	N	13	13
SULA Metal balls	Pearson Correlation	.888**	1
	Sig. (2-tailed)	.000	
	N	13	13

\*\* . Correlation is significant at the 0.01 level (2-tailed).

		SLLA Anatomical Landmarks	SLLA Metal balls
SLLA Anatomical Landmarks	Pearson Correlation	1	.826**
	Sig. (2-tailed)		.000
	N	13	13
SLLA Metal balls	Pearson Correlation	.826**	1
	Sig. (2-tailed)	.000	
	N	13	13

\*\* . Correlation is significant at the 0.01 level (2-tailed).

### Appendix 7.1 A and B for Each Load Cell

Y=AX+B	Y <sub>0</sub> =B	Y <sub>m</sub>	A= (Y <sub>m</sub> -Y <sub>0</sub> )/ (4.095*9.81)
Force10	282	376	2.3399
11	149	242	2.3150
12	271	364	2.3150
13	206	301	2.3648
20	134	218	2.0910
21	108	192	2.0910
22	278	371	2.3150
23	261	357	2.3897
30	201	123	-1.9417
31	172	261	2.2155
32	204	299	2.3648
33	140	232	2.2902
X <sub>m</sub> = 4.095kg = 40.17195N	=		X=Y-B/A

## Appendix 8.1 Descriptive Statistics

Descriptive			Statistic	Std. Error
3CEA/SCEA	Mean		60.77530	2.10916
	95% Confidence Interval for Mean	Lower Bound	56.36078	
		Upper Bound	65.18983	
	5% Trimmed Mean		60.52068	
	Median		60.63986	
	Variance		88.97113	
	Std. Deviation		9.43245	
	Minimum		41.85089	
	Maximum		84.28301	
	Range		42.43212	
	Interquartile Range		8.90080	
	Skewness		0.57224	0.51210
	Kurtosis		1.35451	0.99238
CCEA	Mean		89.57513	0.37225
	95% Confidence Interval for Mean	Lower Bound	88.79599	
		Upper Bound	90.35426	
	5% Trimmed Mean		89.61463	
	Median		89.66708	
	Variance		2.771	
	Std. Deviation		1.664768	
	Minimum		86.18826	
	Maximum		92.25101	
	Range		6.062751	
	Interquartile Range		2.149112	
	Skewness		-0.067	0.512
	Kurtosis		-0.295	0.992

3UTA	Mean		77.61021	1.19042
	95% Confidence Interval for Mean	Lower Bound	75.11862	
		Upper Bound	80.10179	
	5% Trimmed Mean		77.54804	
	Median		77.30368	
	Variance		28.34221	
	Std. Deviation		5.32374	
	Minimum		68.01273	
	Maximum		88.32657	
	Range		20.31383	
	Interquartile Range		6.97633	
	Skewness		0.50481	0.51210
	Kurtosis		0.05899	0.99238
CUTA	Mean		90.08284	0.43984
	95% Confidence Interval for Mean	Lower Bound	89.16223	
		Upper Bound	91.00344	
	5% Trimmed Mean		90.12479	
	Median		90.52880	
	Variance		3.86926	
	Std. Deviation		1.96704	
	Minimum		85.92088	
	Maximum		93.48964	
	Range		7.56876	
	Interquartile Range		2.41098	
	Skewness		-0.62096	0.51210
	Kurtosis		0.22854	0.99238
SUTA	Mean		77.78605	1.21040

	95% Confidence Interval for Mean	Lower Bound	75.25265	
		Upper Bound	80.31945	
	5% Trimmed Mean		77.69560	
	Median		77.35179	
	Variance		29.30147	
	Std. Deviation		5.41308	
	Minimum		68.01539	
	Maximum		89.18485	
	Range		21.16946	
	Interquartile Range		6.98460	
	Skewness		0.53162	0.51210
	Kurtosis		0.13989	0.99238
3LTA	Mean		99.99610	1.45161
	95% Confidence Interval for Mean	Lower Bound	96.95783	
		Upper Bound	103.0344	
	5% Trimmed Mean		99.75208	
	Median		97.80103	
	Variance		42.14368	
	Std. Deviation		6.49182	
	Minimum		90.67875	
	Maximum		113.7057	
	Range		23.02696	
	Interquartile Range		8.39142	
	Skewness		0.68452	0.51210
	Kurtosis		-0.30244	0.99238
CLTA	Mean		89.51065	0.48080
	95% Confidence Interval for Mean	Lower Bound	88.50434	
		Upper Bound	90.51697	
	5% Trimmed Mean		89.45561	
	Median		89.41440	

	Variance		4.62331	
	Std. Deviation		2.15019	
	Minimum		85.98169	
	Maximum		94.03035	
	Range		8.04866	
	Interquartile Range		3.52917	
	Skewness		0.18652	0.51210
	Kurtosis		-0.37945	0.99238
SLTA	Mean		99.70240	1.47803
	95% Confidence Interval for Mean	Lower Bound	96.60885	
		Upper Bound	102.7959	
	5% Trimmed Mean		99.43379	
	Median		97.51142	
	Variance		43.69131	
	Std. Deviation		6.60994	
	Minimum		90.62191	
	Maximum		113.61788	
	Range		22.99597	
	Interquartile Range		8.10616	
	Skewness		0.65971	0.51210
	Kurtosis		-0.33117	0.99238
3ULA	Mean		98.10499	1.01630
	95% Confidence Interval for Mean	Lower Bound	95.97786	
		Upper Bound	100.23213	
	5% Trimmed Mean		98.00965	
	Median		98.08535	
	Variance		20.65720	
	Std. Deviation		4.54502	
	Minimum		91.25419	
	Maximum		106.67198	

	Range		15.41778	
	Interquartile Range		7.07238	
	Skewness		0.40149	0.51210
	Kurtosis		-0.91734	0.99238
CULA	Mean		89.38517	0.48247
	95% Confidence Interval for Mean	Lower Bound	88.37536	
		Upper Bound	90.39499	
	5% Trimmed Mean		89.43173	
	Median		89.79064	
	Variance		4.65548	
	Std. Deviation		2.15766	
	Minimum		84.79889	
	Maximum		93.13336	
	Range		8.33447	
	Interquartile Range		3.32150	
	Skewness		-0.41403	0.51210
	Kurtosis		-0.27525	0.99238
SULA	Mean		97.73541	1.04678
	95% Confidence Interval for Mean	Lower Bound	95.54448	
		Upper Bound	99.92634	
	5% Trimmed Mean		97.60224	
	Median		97.74261	
	Variance		21.91482	
	Std. Deviation		4.68133	
	Minimum		91.24371	
	Maximum		106.62415	
	Range		15.38044	
	Interquartile Range		6.44367	
	Skewness		0.41880	0.51210
	Kurtosis		-0.82502	0.99238

3LLA	Mean		76.10121	1.80383
	95% Confidence Interval for Mean	Lower Bound	72.32575	
		Upper Bound	79.87666	
	5% Trimmed Mean		76.20026	
	Median		77.40287	
	Variance		65.07595	
	Std. Deviation		8.06697	
	Minimum		62.31821	
	Maximum		88.10122	
	Range		25.78301	
	Interquartile Range		14.47510	
	Skewness		-0.36318	0.51210
	Kurtosis		-1.00803	0.99238
CLLA	Mean		89.15740	0.42545
	95% Confidence Interval for Mean	Lower Bound	88.26692	
		Upper Bound	90.04787	
	5% Trimmed Mean		89.14015	
	Median		89.17525	
	Variance		3.62017	
	Std. Deviation		1.90268	
	Minimum		85.68259	
	Maximum		92.94263	
	Range		7.26004	
	Interquartile Range		2.87931	
	Skewness		0.08441	0.51210
	Kurtosis		-0.56337	0.99238
SLLA	Mean		76.31852	1.83522
	95% Confidence Interval for Mean	Lower Bound	72.47737	
		Upper Bound	80.15968	
	5% Trimmed Mean		76.41362	

	Median		77.44850	
	Variance		67.36037	
	Std. Deviation		8.20734	
	Minimum		62.32000	
	Maximum		88.60538	
	Range		26.28538	
	Interquartile Range		14.61898	
	Skewness		-0.35373	0.51210
	Kurtosis		-1.02438	0.99238
3SCA/SSCA	Mean		60.51974	1.05332
	95% Confidence Interval for Mean	Lower Bound	58.31511	
		Upper Bound	62.72438	
	5% Trimmed Mean		60.55416	
	Median		61.02576	
	Variance		22.18985	
	Std. Deviation		4.71061	
	Minimum		49.90303	
	Maximum		70.51684	
	Range		20.61381	
	Interquartile Range		6.73379	
	Skewness		-0.12820	0.51210
	Kurtosis		0.43786	0.99238
TRA	Mean		-1.54335	0.78788
	95% Confidence Interval for Mean	Lower Bound	-3.19240	
		Upper Bound	0.10570	
	5% Trimmed Mean		-1.59029	
	Median		-1.60694	
	Variance		12.41507	
	Std. Deviation		3.52350	
	Minimum		-8.41116	

	Maximum		6.16938	
	Range		14.58054	
	Interquartile Range		4.86945	
	Skewness		0.28599	0.51210
	Kurtosis		0.06561	0.99238
LRA	Mean		-0.46195	0.78965
	95% Confidence Interval for Mean	Lower Bound	-2.11470	
		Upper Bound	1.19081	
	5% Trimmed Mean		-0.42672	
	Median		-0.56099	
	Variance		12.47086	
	Std. Deviation		3.53141	
	Minimum		-8.22167	
	Maximum		6.66375	
	Range		14.88541	
	Interquartile Range		3.58934	
	Skewness		-0.57659	0.51210
	Kurtosis		1.29710	0.99238
PTA	Mean		11.40560	1.22502
	95% Confidence Interval for Mean	Lower Bound	8.84160	
		Upper Bound	13.96960	
	5% Trimmed Mean		11.22645	
	Median		11.55357	
	Variance		30.01362	
	Std. Deviation		5.47847	
	Minimum		2.82840	
	Maximum		23.20747	
	Range		20.37907	
	Interquartile Range		7.88602	
	Skewness		0.35769	0.51210

	Kurtosis		-0.23728	0.99238
C5A	Mean		5.45174	0.75403
	95% Confidence Interval for Mean	Lower Bound	3.87355	
		Upper Bound	7.02993	
	5% Trimmed Mean		5.27611	
	Median		5.17205	
	Variance		11.37108	
	Std. Deviation		3.37210	
	Minimum		0.81191	
	Maximum		13.25282	
	Range		12.44091	
	Interquartile Range		4.29875	
	Skewness		0.87473	0.51210
	Kurtosis		0.26713	0.99238
SSA	Mean		21.73575	1.70552
	95% Confidence Interval for Mean	Lower Bound	18.16605	
		Upper Bound	25.30546	
	5% Trimmed Mean		21.58150	
	Median		20.50942	
	Variance		58.17627	
	Std. Deviation		7.62734	
	Minimum		11.21430	
	Maximum		35.03370	
	Range		23.81940	
	Interquartile Range		14.37961	
	Skewness		0.379	0.512
	Kurtosis		-1.300	0.992

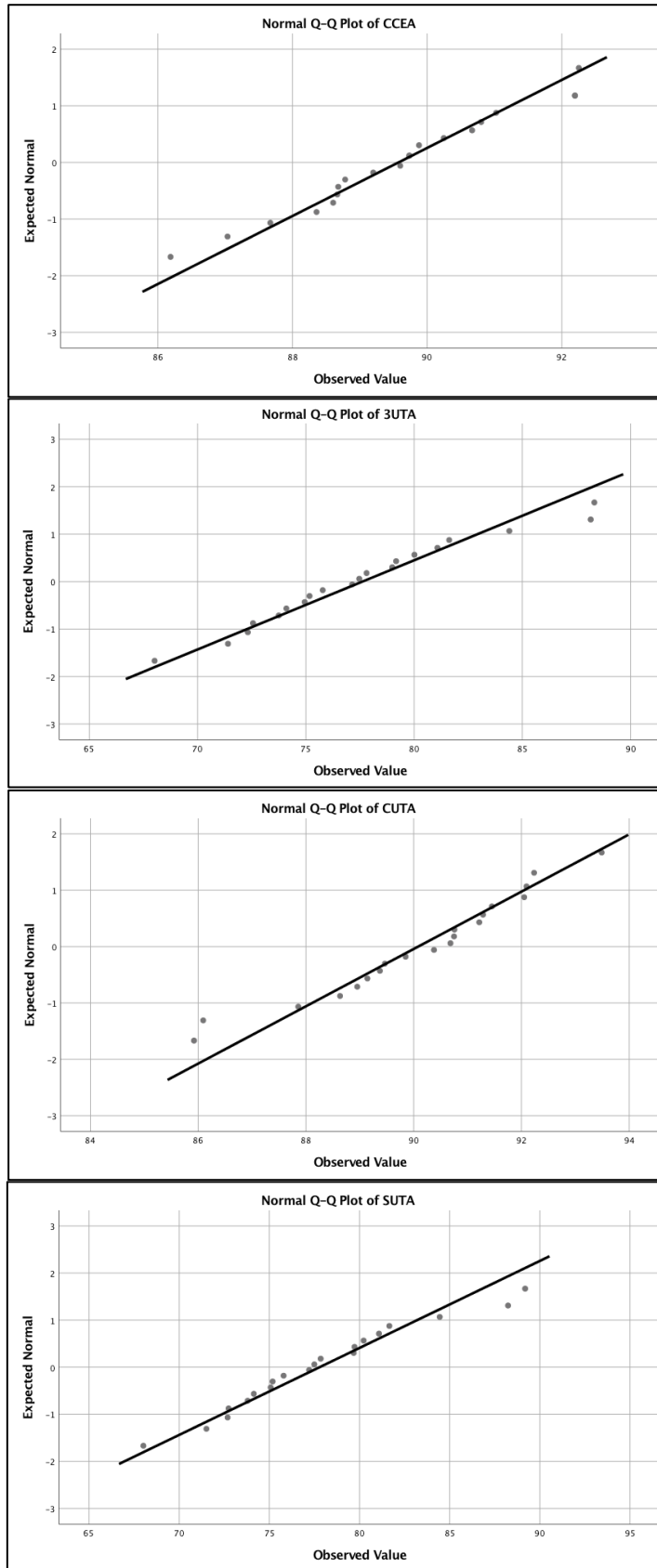
## Appendix 8.2 Tests of Normality

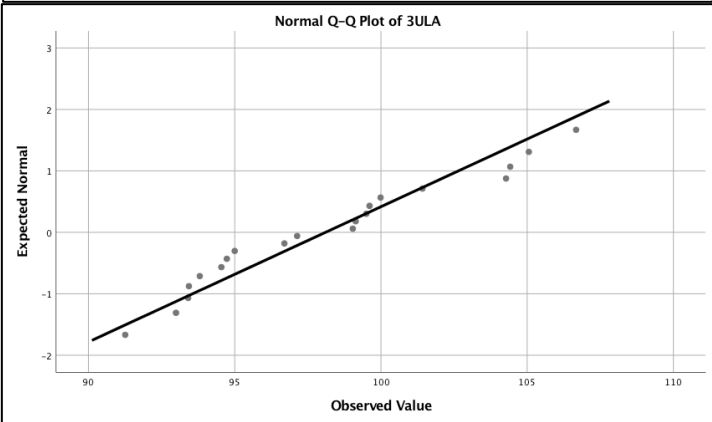
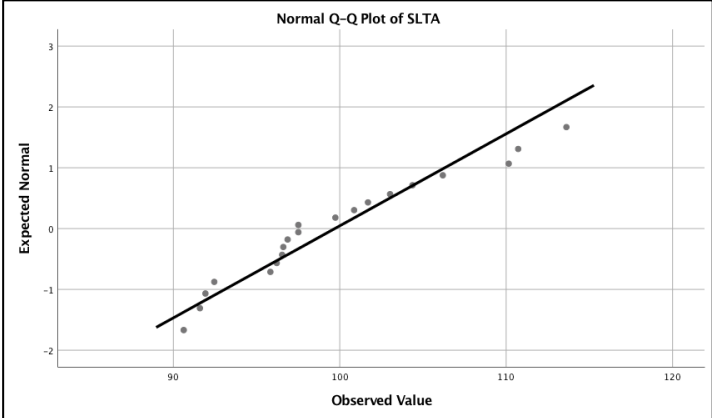
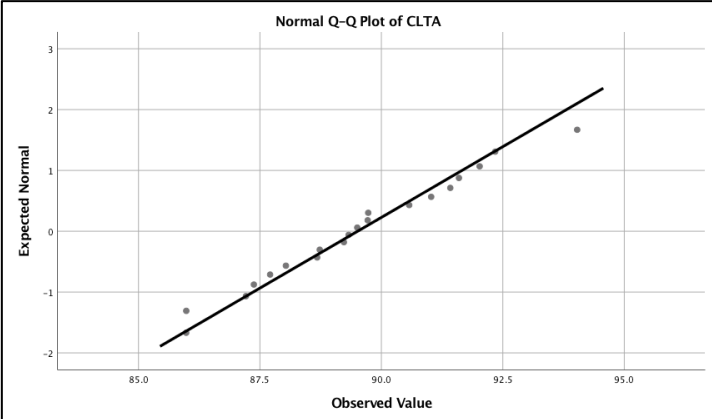
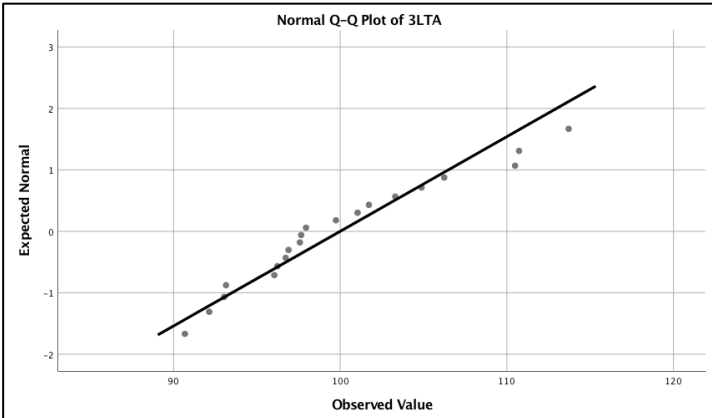
Tests of Normality						
	Kolmogorov-Smirnov <sup>a</sup>			Shapiro-Wilk		
	Statistic	df	Sig.	Statistic	df	Sig.
3CEA/SCEA	0.153	20	.200*	0.960	20	0.540
CCEA	0.92	20	.200*	0.960	20	0.729
3UTA	0.085	20	.200*	0.965	20	0.656
CUTA	0.120	20	.200*	0.956	20	0.471
SUTA	0.095	20	.200*	0.966	20	0.671
3LTA	0.174	20	0.115	0.938	20	0.219
CLTA	0.110	20	.200*	0.980	20	0.931
SLTA	0.180	20	0.089	0.935	20	0.192
3ULA	0.153	20	.200*	0.940	20	0.244
CULA	0.116	20	.200*	0.974	20	0.842
SULA	0.138	20	.200*	0.938	20	0.218
3LLA	0.153	20	.200*	0.937	20	0.211
CLLA	0.098	20	.200*	0.984	20	0.972
SLLA	0.157	20	.200*	0.940	20	0.235
3SCA/SSCA	0.094	20	.200*	0.984	20	0.972
TRA	0.091	20	.200*	0.987	20	0.991
LRA	0.144	20	.200*	0.937	20	0.211
PTA	0.106	20	.200*	0.975	20	0.858
C5A	0.138	20	.200*	0.933	20	0.173
SSA	0.165	20	0.160	0.918	20	0.090

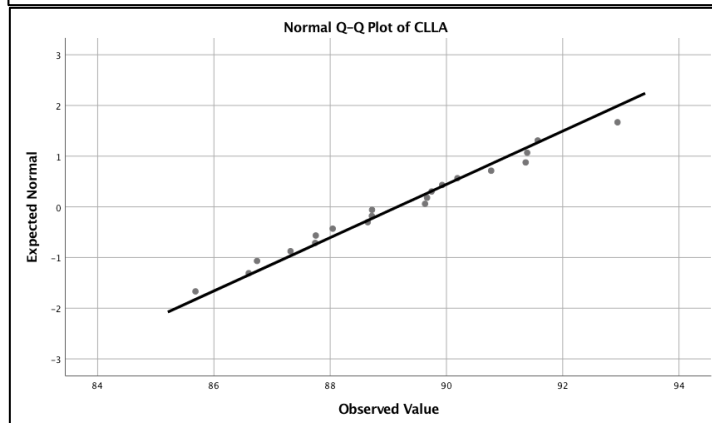
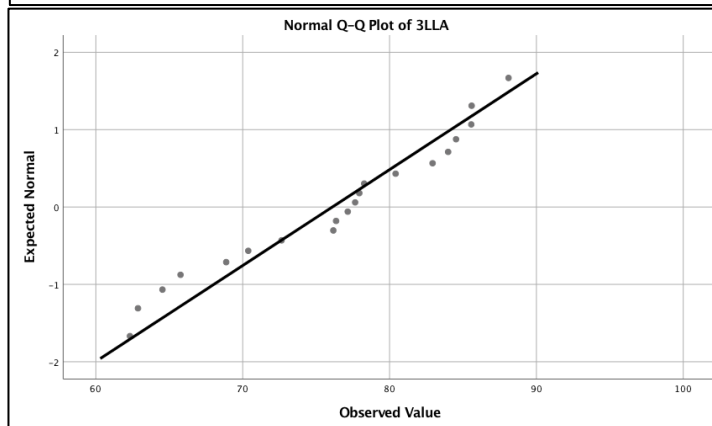
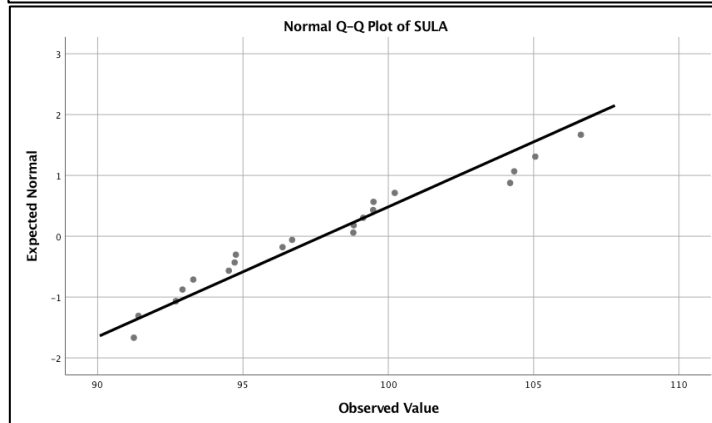
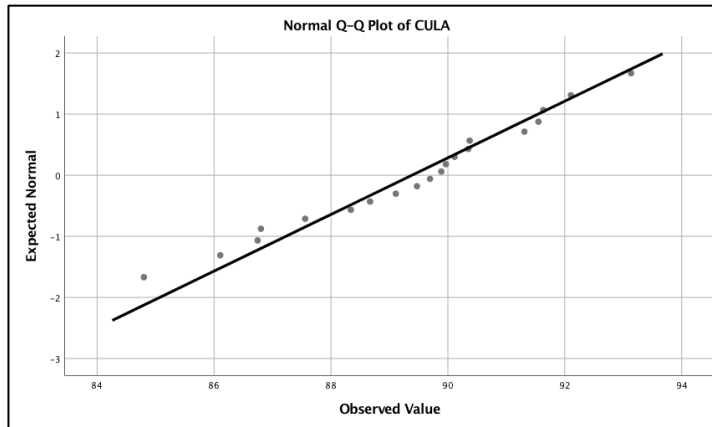
\*. This is a lower bound of the true significance.

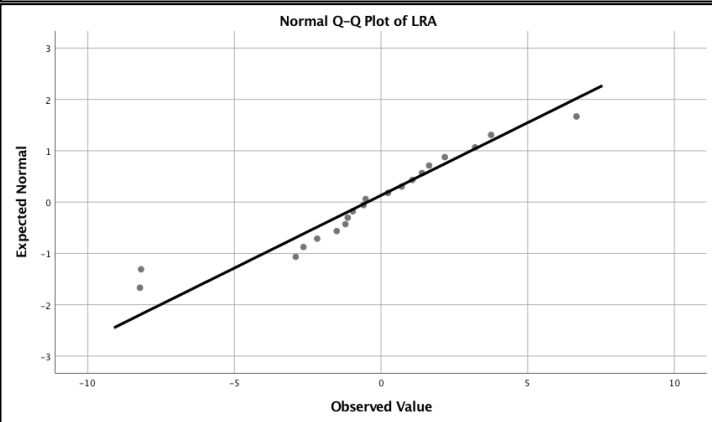
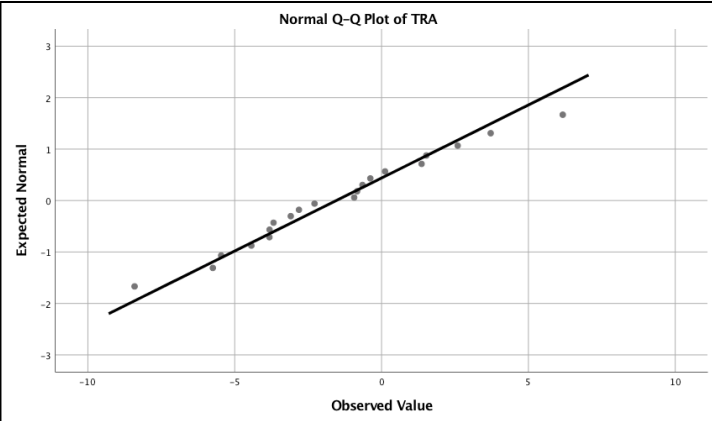
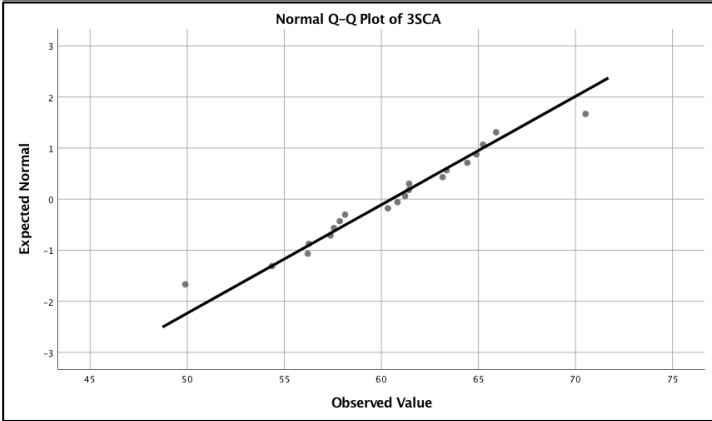
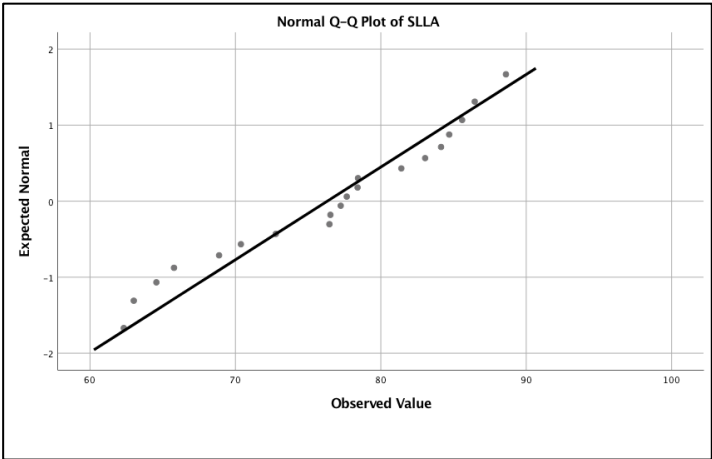
a. Lilliefors Significance Correction

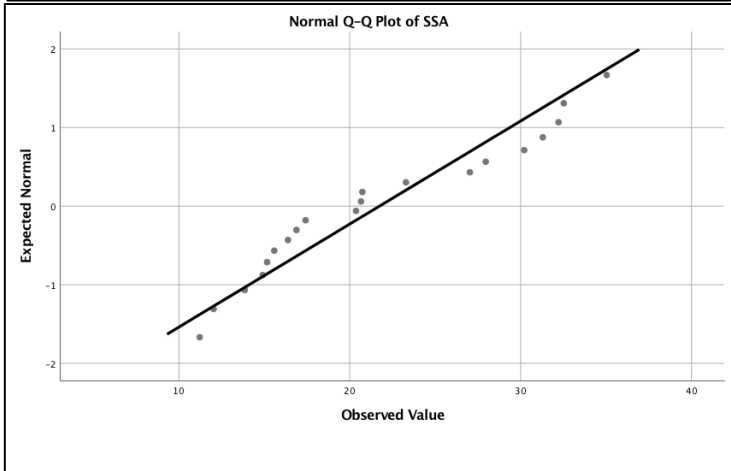
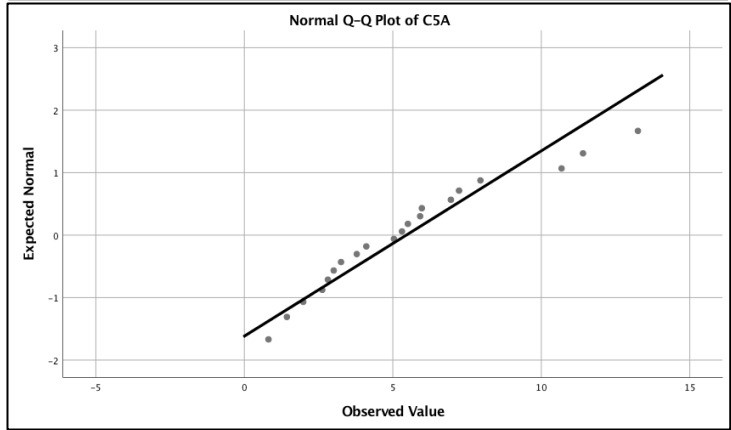
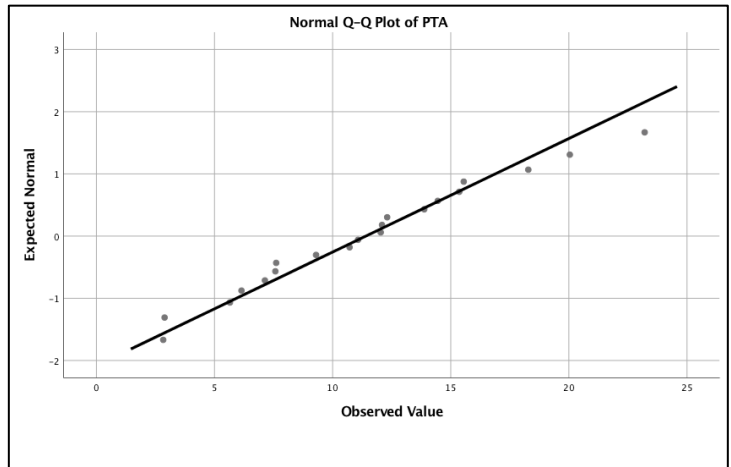
### Appendix 8.3 Normal Probability Q-Q Plots











**Appendix 9.1** The Descriptive Statistics and the Results of the Performed Test Statistics

	Group	N	Group Statistics		
			Mean	Std. Deviation	Std. Error Mean
C3EA	1	5	67.95200000000000	10.380947451942907	4.642500834679515
	2	20	60.775303650000010	9.432450844447173	2.109160128260917
U3TA	1	5	88.80400000000000	.664401986751994	.297129601352674
	2	20	77.610205316590900	5.323740653030489	1.190424599475530
L3TA	1	5	90.49199999999999	.618320305343435	.276521246923269
	2	20	99.996098023409090	6.491816527082138	1.451614305201227
U3LA	1	5	105.68400000000000	2.346493128053013	1.049383628612531
	2	20	98.104991757954540	4.545018904973744	1.016297123054295
L3LA	1	5	74.66200000000000	8.727761454118694	3.903173580562362
	2	20	76.101207836818190	8.066966767680219	1.803828606476472
SCA	1	5	68.40200000000000	9.047031004699827	4.045955264211406
	2	20	60.519741864090930	4.710610205209036	1.053324463435164
TRA	1	5	21.773999999999997	27.301584752537718	12.209639880029222
	2	20	-1.543353890000000	3.523503107896137	.787879246818754
LRA	1	5	20.37200000000000	17.395696881700370	7.779592148692630
	2	20	-.461945139242424	3.531410174183445	.789647320590856
PTA	1	5	15.081999999999999	7.096342015433022	3.173580627619220
	2	20	11.405602048409092	5.478468832611664	1.225022872233360
C5A	1	5	19.73400000000000	17.708377396023610	7.919427125745902
	2	20	5.451738590000001	3.372103825474101	.754025338094718
SSA	1	5	21.862000000000002	18.361845495483294	8.211666944049790
	2	20	21.735754755227270	7.627336984329206	1.705524398425835

**Mann-Whitney Test**  
**Ranks**

	Group	N	Mean Rank	Sum of Ranks
C3EA	1	5	17.40	87.00
	2	20	11.90	238.00
	Total	25		
U3TA	1	5	22.60	113.00
	2	20	10.60	212.00
	Total	25		
L3TA	1	5	3.40	17.00
	2	20	15.40	308.00
	Total	25		
U3LA	1	5	21.20	106.00
	2	20	10.95	219.00
	Total	25		
L3LA	1	5	12.00	60.00
	2	20	13.25	265.00
	Total	25		
SCA	1	5	19.80	99.00

	2	20	11.30	226.00
	Total	25		
TRA	1	5	22.60	113.00
	2	20	10.60	212.00
	Total	25		
LRA	1	5	21.60	108.00
	2	20	10.85	217.00
	Total	25		
PTA	1	5	15.80	79.00
	2	20	12.30	246.00
	Total	25		
C5A	1	5	19.20	96.00
	2	20	11.45	229.00
	Total	25		
SSA	1	5	14.00	70.00
	2	20	12.75	255.00
	Total	25		

#### Test Statistics<sup>a</sup>

	C3EA	U3TA	L3TA	U3LA	L3LA	SCA	TRA	LRA
Mann-Whitney U	28.000	2.000	2.000	9.000	45.000	16.000	2.000	7.000
Wilcoxon W	238.000	212.000	17.000	219.000	60.000	226.000	212.000	217.000
Z	-1.495	-3.261	-3.262	-2.785	-.340	-2.310	-3.261	-2.921
Asymp. Sig. (2-tailed)	.135	.001	.001	.005	.734	.021	.001	.003
Exact Sig. [2*(1-tailed Sig.)]	.148 <sup>b</sup>	.000 <sup>b</sup>	.000 <sup>b</sup>	.003 <sup>b</sup>	.767 <sup>b</sup>	.019 <sup>b</sup>	.000 <sup>b</sup>	.002 <sup>b</sup>

	PTA	C5A	SSA
Mann-Whitney U	36.000	19.000	45.000
Wilcoxon W	246.000	229.000	255.000
Z	-.951	-2.106	-.340
Asymp. Sig. (2-tailed)	.342	.035	.734
Exact Sig. [2*(1-tailed Sig.)]	.371 <sup>b</sup>	.035 <sup>b</sup>	.767 <sup>b</sup>

a. Grouping Variable: Group

b. Not corrected for ties.

## Appendix 10.1 Two Ethics Committee Approval Letters

# RESEARCH @ EMU

---

**UHSRC Determination:** EXPEDITED INITIAL APPROVAL

**Date:** July 26, 2017

**To:** Sun Hae Jang  
Eastern Michigan University

**Re:** UHSRC: # J20170721-1  
Category: Expedited Category 4  
Approval Date: July 26, 2017  
Expiration Date: July 25, 2018

**Title:** Corrective Biomechanical Analysis of Adolescent Idiopathic Scoliosis with a New Digital Calculating and Visualization System

Your research project, entitled **Corrective Biomechanical Analysis of Adolescent Idiopathic Scoliosis with a New Digital Calculating and Visualization System** has been approved in accordance with all applicable federal regulations.

This approval includes the following:

1. Enrollment of 20 subjects to participate in the approved protocol.
2. Use of the following stamped recruitment materials: *Recruitment Document/Letter; Recruitment flyer 1; Recruitment flyer 2*
3. Use of the stamped: *Parental Consent form; Child Assent form*

**Renewals:** This approval is valid for one year and expires on July 25, 2018. If you plan to continue your study beyond July 25, 2018, you must submit a Continuing Review Form by June 25, 2018 to ensure the approval does not lapse.

**Modifications:** All changes must be approved prior to implementation. If you plan to make any minor changes, you must submit a **Minor Modification Form**. For any changes that alter study design or any study instruments, you must submit a **Human Subjects Approval Request Form**.

**Problems:** All major deviations from the reviewed protocol, unanticipated problems, adverse events, subject complaints, or other problems that may increase the risk to human subjects or change the category of review must be reported to the UHSRC via an **Event Report** form.

**Follow-up:** If your Expedited research project is not completed and closed after **three years**, the UHSRC office requires a new **Human Subjects Approval Request Form** prior to approving a continuation beyond three years.

Please use the UHSRC number listed above on any forms submitted that relate to this project, or on any correspondence with the UHSRC office.

Good luck in your research. If we can be of further assistance, please contact us at 734-487-3090 or via e-mail at [human.subjects@emich.edu](mailto:human.subjects@emich.edu). Thank you for your cooperation.

---

University Human Subjects Review Committee · Eastern Michigan University · 200 Boone Hall  
Ypsilanti, Michigan 48197  
Phone: 734.487.3090  
E-mail: [human.subjects@emich.edu](mailto:human.subjects@emich.edu)  
[www.emich.edu/ord](http://www.emich.edu/ord) (see Research Compliance)

The EMU UHSRC complies with the Title 45 Code of Federal Regulations part 46 (45 CFR 46) under FWA00000050.

# RESEARCH @ EMU

---

Sincerely,

Jennifer Kellman Fritz, PhD  
Chair  
University Human Subjects Review Committee

## RESEARCH @ EMU

---

**UHSRC Determination:** EXPEDITED MODIFICATION APPROVAL

**Date:** August 15, 2017

**To:** Sun Hae Jang  
Eastern Michigan University

**Re:** UHSRC: # 20170721-2  
Category: Expedited category 4  
Approval Date: August 15, 2017  
Expiration Date: July 25, 2018

**Title:** Corrective Biomechanical Analysis of Adolescent Idiopathic Scoliosis with a New Digital Calculating and Visualization System

Your requested modifications have been approved in accordance with all applicable federal regulations.

This approval includes the following:

- (1) If patients are interested in this study, the recruitment clinic sites will have them sign a medical record release form and allow them to take the required medical records. Each participant must bring the medical records to EMU for their visits or send them to the PI prior to the visits.
- (2) Use of the modified parental consent form.

**Renewals:** This approval does not change the original expiration date. This study expires on **July 25, 2018**. If you plan to continue your study beyond **June 25, 2018**, you must submit a Continuing Review Form by **June 25, 2018** to ensure the approval does not lapse.

**Modifications:** All additional changes must be approved prior to implementation. If you plan to make any minor changes, you must submit a **Minor Modification Form**. For any changes that alter study design or any study instruments, you must submit a **Human Subjects Approval Request Form**.

**Problems:** All major deviations from the reviewed protocol, unanticipated problems, adverse events, subject complaints, or other problems that may increase the risk to human subjects **or** change the category of review must be reported to the UHSRC via an **Event Report** form.

**Follow-up:** If your Expedited research project is not completed and closed after **three years**, the UHSRC office requires a new **Human Subjects Approval Request Form** prior to approving a continuation beyond three years.

Please use the UHSRC number listed above on any forms submitted that relate to this project, or on any correspondence with the UHSRC office.

Good luck in your research. If we can be of further assistance, please contact us at 734-487-3090 or via e-mail at [human.subjects@emich.edu](mailto:human.subjects@emich.edu). Thank you for your cooperation.

Sincerely,

---

University Human Subjects Review Committee - Eastern Michigan University - 200 Boone Hall  
Ypsilanti, Michigan 48197  
Phone: 734.487.3090  
E-mail: [human.subjects@emich.edu](mailto:human.subjects@emich.edu)  
[www.emich.edu/ord](http://www.emich.edu/ord) (see Research Compliance)

The EMU UHSRC complies with the Title 45 Code of Federal Regulations part 46 (45 CFR 46) under FWA00000050.

## RESEARCH @ EMU

---

April M Gravit, MS  
Research Compliance Analyst  
University Human Subjects Review Committee